INSTITUTO TECNOLÓGICO Y DE ESTUDIOS
SUPERIORES DE MONTERREY

CAMPUS MONTERREY

GRADUATE PROGRAM IN ELECTRONICS,
COMPUTER SCIENCE, INFORMATION AND COMMUNICATIONS

CONFIGURATION OF AN AUTONOMOUS VEHICLE: A SYSTEMATIC FRAMEWORK

THESIS

PRESENTED IN PARTIAL FULFILLMENT OF THE
REQUIREMENTS FOR THE ACADEMIC DEGREE OF:

DOCTOR OF PHILOSOPHY IN
ARTIFICIAL INTELLIGENCE

BY

JOAQUÍN GUTIÉRREZ JAGÜEY

Monterrey, N.L. December 2004

INSTITUTO TECNOLÓGICO Y DE ESTUDIOS SUPERIORES DE MONTERREY

SUPERVISORY COMMITTEE APPROVAL

of a dissertation submitted by

Joaquín Gutiérrez Jagüey

This dissertation has been read by each member of the following supervisory committee and by majority vote has been found to be satisfactory.

Chair: José Luis Gordillo Moscoso, Ph.D.

Dimitrios Apostolopoulos, Ph.D.

Noel León Rovira, Ph.D.

Horacio Martínez Alfaro, Ph.D.

Ricardo A. Ramírez Mendoza, Ph.D.

INSTITUTO TECNOLÓGICO Y DE ESTUDIOS SUPERIORES DE MONTERREY

FINAL READING APPROVAL

To the Graduate Program of the Tecnológico de Monterrey:

I have read the dissertation of Joaquín Gutiérrez Jagüey in its final form and have found that (1) its format, citations, and bibliographic style are consistent and acceptable; (2) its illustrative materials including figures, tables, and charts are in place; and (3) the final manuscript is satisfactory to the Supervisory Committee and is ready for submission to The Graduate Program.

Date

José Luis Gordillo Moscoso, Ph.D.
Chair: Supervisory Committee

Approved for the Center for Intelligent Systems

Rogelio Soto Rodríguez, Ph.D.
Chair/Director

Approved for the Graduate Council

David Garza Salazar, Ph.D.
Dean of The Graduate Program

CONFIGURATION OF AN AUTONOMOUS VEHICLE: A SYSTEMATIC FRAMEWORK

by

Joaquín Gutiérrez Jagüey

A dissertation presented to the Graduate Program in
Electronics, Computer Science, Information and Communications of
Tecnológico de Monterrey
in partial fulfillment of the requirements for the degree of

Doctor of Philosophy

in

Artificial Intelligence

Center for Intelligent Systems

TECNOLÓGICO
DE MONTERREY

December 2004

Contents

To...

Acknowledgements

I would like to express my first and foremost gratitude to my thesis advisor Dr. José Luis Gordillo, for his invaluable technical advice and wisdom guidance, and most importantly the opportunity to work in his research group. The years that I spent on the autonomous vehicle project, will always be deeply remembered for many years to come.

I also want to thank my other thesis co-advisors, Drs. Dimitrios Apostolopoulos, Noel León, Horacio Martínez, and Ricardo A. Ramírez, whose suggestions, insights and critique proved to be invaluable to my dissertation work.

Special thanks to Dr. Apostolopoulos for the experiences during my doctoral stay in the Robotics Institute. Apostolopoulos' support in providing creative solutions to problem still continue to awe me, I have learnt and benefited so much from his unrivalled expertise and profound knowledge in the field of robotic vehicles.

I would like to thank the members of the Vision and Autonomous Vehicle groups, the weekly meetings with the groups have proved to be one of my best learning experiences at Center for Intelligent Systems. I would like to specifically acknowledge Carlos Albores, Fernando Von Borstel, and Hugo Ortega for their help. My stay in the Robotics Institute would not be as enjoyable without the friendship of Paul Tompkins, Michael Wagner, Christoper Urmson, and Octavio Juárez. A special thanks to Elizabeth Villegas for her invaluable support and friendship, in truth appreciated.

I also wish to show my appreciation to Drs. Rogelio Soto and Hugo Terashima for the interest that they have shown in my Ph.D. career. Thanks also go to Doris Juárez and her staff, for the administrative help they rendered in all these years.

Last but not least, my ever supportive family for all their love and the understanding, I cannot imagine how things would be without their faith and care, for which I feel exceedingly indebted.

This research was supported in part by the Consejo Nacional de Ciencia y Tecnología (CONACYT) grant 35396 and by the Tecnológico de Monterrey; special gratitude to the Centro de Investigaciones Biológicas del Noroeste, S.C. (CIBNOR). Their support is gratefully acknowledged.

Abstract

Autonomous Vehicles have generated an emerging interest in demanding applications due to their great potential to move toward a particular site and perform some specialized work (such as goods transportation, exploration, and work tool manipulation), especially in remote environments which can be dangerous, unsuitable, and inaccessible for humans. Despite the great potential of Autonomous Vehicles, including safety and productivity, their use is not widespread because of the complexity to define the robotic vehicle configuration. Besides, current design processes rely on the designer's experience, require long periods of time and signify high investments. Thus, practical approaches for their configuration are needed.

This thesis focuses on the development of a method for the synthesis of an Autonomous Vehicle configuration, based on the analysis of both the task and the environment. The method assists to determine a suitable configuration to that serves as a comprehensive foundation in the building of the robotic vehicle. The configuration is expressed as a hierarchical and modular structure of interlinked components that fulfill the requirements to perform a given task under the constraints of a certain environment. The components implement the functionality of a composition of motions that solve the task. This composition is selected through a preliminary analysis, in which a geometric description of the task and the environment is used to combine motions and to find viable compositions (possible solutions). Each motion of the selected composition becomes a component or component set into the vehicle structure. To select the components, the method uses criteria of Robotics and engineering principles for providing of autonomy to the configuration, as a function that correlates the perception, the control, the positioning, and the geometry of the robotic vehicle.

The definition of the requirements, the geometric description, the combination of motions, the selection of the fundamental composition, and the gradual fulfillment of the configuration with the proper components are derived through this systematic framework, exploiting the vast inventory of technologies and products developed by decades of engineering and robotic research.

The implementation of this method is illustrated through a real request for the underground mining domain. The major result of this research work has been the formulation and validation of the proposed framework as a suitable approach to systematically determine the Autonomous Vehicle configuration.

Chapter 1

Introduction

Robots are an integration of mechanics with electronics and information technology into a proper configuration to perform tasks in diverse domains, e.g., manipulators or mobile robots equipped with actuators, sensors, and tools under control systems. Many tasks require for mobile robots that must move toward a particular site and then perform some kind of work involving manipulation of tools. Autonomous Vehicles (AVs) have this great potential to navigate and perform tasks in remote environments where humans hardly can accede and there exist hazardous conditions of operation.

Robotic practitioners have developed robotic vehicles for several decades, beginning the building of mobile robots for scientific research and indoor applications. Despite the significance of this research work, almost of these mobile robots are confined to laboratories and limited for experimental applications, i.e., these mobile robots are restricted to perform tasks that have to cover a large workspace or for supporting a significant payload. Recent research efforts have addressed to develop the technology and components for building of AVs in outdoor applications, involving the configuration of robotic vehicles from the automation of an existing vehicle (such as conventional farming vehicles) to an innovative vehicle design (such as planetary rovers).

The AV scope includes land applications such as agriculture, construction and mining; in marine applications such as search and rescue, underwater exploration, and environment monitoring; in air applications such as mineral exploration, meteorology, and military reconnaissance; and in space applications such as planetary exploration. This diversity of tasks and environments results in a wide variety of robot configurations. A configuration depends on the appropriate components that must fulfill the requirements of the task and the environment. Configuration is hence the foundation to built and deploy of an operational AV that performs the assigned task in the expected environment.

Despite its implication, the process for systemizing of AV configuration has not been addressed. In fact, current configuration processes to implement AVs are performed in an *ad hoc* manner, relying on designer's experience and intuition. To make practical the configuration and construction of a robotic vehicle, this thesis proposes a method to systematize the synthesis process of the AV configuration, by means of an analysis of the required task and the environment to identify the components that perform the task. The approach suggests that the components could be selected and assembled to rapidly and cost-effectively construction of the AV, exploiting the universality of the conventional vehicles reserved for a particular purpose, such as mining, construction or agriculture, and using the inventory of products and technologies that have been developed during decades of robotics research and engineering.

The method focuses on the configuration of a wheeled robotic vehicle to perform autonomously an underground mining task. The configuration definition involves the identification of the necessary motions to achieve the task in this confined environment and the selection of the components (e.g., actuators, sensors, tools, and the wheeled vehicle) that implement such motions. The systematic analysis investigates the vehicle dimensions (e.g., wheelbase, wheel diameter), the vehicle kinematics (e.g. steering mechanism), and sensor requirements (e.g., sensor range) to improve the level of autonomy required for the positioning estimation, control, and perception performance, using parametric comparison of components under the expected conditions of operation (e.g., tunnel dimension, terrain properties). The solution representing the AV configuration is a tree structure that serves as a comprehensive layout to pursue the implementation of the robotic vehicle, which should be supported by a detailed process for the electromechanic adaptation of the selected components. The formulation of such process of adapting goes beyond of the scope of this thesis.

This chapter describes a general overview of this research work, reviewing the proposed method that has been formulated under the aforementioned context. The research motivation is presented, as well as the thesis problem, the thesis statement, and the investigation scope are introduced. A summary of the approach for synthesis of AV configuration is presented in this section; Chapter 3 constitutes a more complete description of the proposed method. Finally, an outline of the thesis and a brief description on the contents of each chapter are also presented.

1.1 Motivation

The emerging applications of the AVs call for pragmatic approaches to assist their synthesis process. Several tasks are well suited for automation through such robotic vehicles. These Autonomous Vehicles are composed of interlinked components with multiple choices for each of them; thus, a systematic framework can assist the designer in identifying for an effective configuration to lead the selection of the components.

Since AV applications are so different, prototyping an operational AV can become an expensive process, requiring several prototype iterations; hence it is practical to design the robotic vehicle apriori through a configuration that facilitates its implementation. Moreover, the synthesis is a complex assignment in which are involved an ample number of components of diverse engineering (such as mechanical, electronic, and programming). Consequently, the development of robotic vehicle is an extensive integration process of conventional and robotic components.

These observations motivated this research. The identified lack, in the state-of-practice, is for a practical framework to direct the AV synthesis development. This thesis formulates such a systematic framework in which the implementation of an AV can be facilitated by defining the suitable configuration and by exploiting the vast inventory of components developed by the broad disciplines that converge in Robotics.

1.2 Problem Statement

A fundamental potential of Autonomous Vehicles is to increase the human abilities to perform diverse tasks especially in hostile and remote environments, in addition to the improvement of the safety and productivity issues. Despite these advantages of AVs, their use is not widespread due to the complexity to define the robotic vehicle configuration. Moreover, there exists no theory or methods for the systematic translating the requirements of a task within an expected environment into an AV configuration. Instead, the current design processes rely on design team experience and intuition (such as traditional brainstorm), and require long times and high investments.

Although, the state-of-the-practice has experimented significant advances in the automatization of many tasks in diverse applications, such as mechanical assembles and machining of products. Further reflections on tasks executed in unstructured environments, indicate the absence of these systematic efforts for the specification of such tasks and their automatization into the appropriate definition of the robotic vehicle configuration. In this context, different tasks that could be automated, such as the intensive labours in the underground mining domain, must be made manually, even though in the engineering the necessary components exist to the achievement of these tasks autonomously (i.e., sensors, actuators, control schemes, and mobile platforms). Thus, pragmatic approaches for synthesis of AV configuration are needed in order to reduce the design process complexity and to extend the AV use in a wide variety of emerging applications.

1.3 Thesis: Synthesis of an AV Configuration

The thesis is focused on the development of a method to create a rational AV configurations from concept to implementation, based on a geometrical analysis of both the

task and the environment, also with an analytical process of the vehicle kinematics. The objective of this research is to formulate and implement a systematic framework to find the appropriate candidate configuration that serves as foundation in the building of a robotic vehicle to perform a required task with certain level of autonomy in a finite environment. This research work addresses to validate and prove the thesis that:

> The geometric abstraction of both the task and the environment, and the analytical relation among their specifications and constraints are fundamental elements to synthesize Autonomous Vehicles. This synthesis depends on a structured model description, and a method based on these elements to systematically transform the task and the environment requirements into components of the model.

1.4 Thesis Scope

Throughout this thesis, an AV is a well configured system that can be represented by a structured model. It is a hierarchical structure of interlinked subsystems and modules, which must be instanced with the proper components that fulfill the specifications to perform a task under the constraints of a certain environment. Thus, the challenge of this approach is the identification of the entire subsystems and their hierarchical interaction for the fulfillment of each module with the proper components. Moreover, the thesis implicitly considers the AV controller to be embedded in the hierarchical architecture in which the higher layers provide a series of actions to the lower layers. The lower controllers deal with the basic issue of converting actions into execution commands.

The configuration of the AV system aims at a fundamental hypothesis, it is that the necessary components to develop an operational AV already exist. These components include sensors, actuators, mobile platforms, and algorithms that must improve the robotic vehicle performance by allowing the successful completion of the assigned task. This thesis assumes a reliable degree of autonomy where the vehicle is controlled by itself without the aid of a human operator exclusively during the execution of the task. To this end, the autonomous behavior implicates the estimation of the vehicle state to provide safe and effective control of its actions as perceived by its sensors. Thus, the definition of the configuration concerns an analysis of autonomy that takes into account the positioning, control, and perception performance against the suitable vehicle kinematics, rather than being regarded by intelligence and learning capabilities, such subjects are beyond of this research.

Besides, the robustness of the AV prototype emerges out through the distribution of the functionality and the interaction between subsystems, involving the individual robustness of every component. This robust performance is assumed in the scope of well-defined functions and conditions of operation derived by the framework for each

subsystem and component, respectively. In this context, the thesis does not attempt to investigate the mechanisms of detecting faults, assessing the impact of subsystem failure, and redundancy resolution to maintain fault tolerance, if one of the selected components fail or is immobilized.

The systematic framework assumption is that the Autonomous Vehicle objective is to perform a specific task, using suitable components, under three essential functions: 1) mobility around its workspace to navigate and carry on the rest of components, 2) capability to reach a particular position and orientation, and 3) the actuation of tools for the achievement the required task. These three functions are placed into the context of the mining vehicle example. The goal of the synthesis process is to define in detail these essential functions into the configuration, which is identified as the best composition of basic motions in terms of their functionality to perform the task, by then select, of an inventory, the components that implement the function of every motion within the basic composition.

This process implies a design philosophy in which the Autonomous Vehicle, to be designed and built, is composed of individual components that are configured separately and finally integrated into the structured model to reduce the complexity. Only in this way the robotic system can be designed and analyzed efficiently and comprehensively. Thus, the implicit decomposition, normally driven by the idea one function-one module, leads to modular (horizontal) designs over hierarchical level (vertical), forming the generic tree structure to express the AV configuration. In this engineering perspective, such philosophy has enormous advantages, since modularization is one of the essential virtues for the design of systems; modules can be tested independently of one another and combined in larger systems under rational way.

The configuration process may be formally defined as the creation of a synthesized solution in the form of the hierarchical and modular structure, afterward the mapping of the requirements of the functional domain into the physical domain of the robotic vehicle. In this perspective, the method centers on the requirements of a definite task in a finite environment, to pursue the identification of the specifications and boundaries the components for the correct and efficient achievement of AV task, including its own safety.

The configuration for an underground mining application is a case of implementation and evaluation for the proposed method. The framework will be used to configure an Autonomous Vehicle as the prototype for surveying the tunnel profile under the tough constraints of an active underground mine, a challenging real-world task requested explicitly by a mining company. Addressing issues of synthesis for such AV configuration would gain a significant amount of aware for other realistic applications, such as agriculture, construction, forestry, and transportation, where the framework can be employed and its formulation has been focused.

1.5 Approach

When not having a predefined or an arbitrary configuration, this systematic framework is distinct from existing design methods and those that use creative brainstorming to generate possible solutions. The configuration is expressed in a structure of components that should fulfill the specifications to perform a given task under the constraints of a certain environment. The components embody the functionality of a composition of motions that solve the task. The composition is selected through a geometric analysis of the task and the environment to combine motions and to find viable compositions. Each motion of the selected composition is mapped as a component or components, which correlate the operation parameters of the motion concerning the task specifications and environment constraints.

Emphasis is placed on autonomy analysis during the selection of components, using robotic criteria and engineering principles through mathematical expressions that relate the task requirements to the component features. A reliable degree of autonomy requires that the vehicle be controlled by itself to navigate, following a given path and avoiding obstacles. Key to mobile robot autonomous performance is accurate positioning, which implicates that the vehicle positioning must be estimated to provide safe and effective control. In this analysis, the configuration is discussed to improve positioning, control and perception from robotic vehicle kinematics.

The Figure 1.1 shows the method for synthesis of AVs, which follows a general systematic procedure of first defining the task; second, finding possible solutions; and third, implementing the basic configuration that ensures a suitable robotic system through of the System Abstraction, System Analysis, and System Design phases. The model representing the robotic vehicle configuration is integrated gradually with the results provided by the method into the AV structure, a layout that contains enough information to pursue the implementation of the robotic vehicle prototype.

In the System Abstraction phase, the information of the task and the environment is converted into the Configuration Requirements, defining the Geometric Description, which is generated from a geometrical analysis to describe what and where the task is to be accomplished. These outputs are reviewed and used in the subsequent phases to generate possible solutions and to define the AV configuration. In the System Analysis phase, the functional relation of the configuration is characterized as a set of subsystems that are defined from the required motions to perform the task inside the Geometric Description. A feasible composition of motions is a chain of fundamental motions, which are adjusted property and constrained by the rest of attached motions. The compositions are considered as templates to define the functionality of the vehicle. Then, each composition is evaluated to select the most appropriate template, using simplicity and uniformity criteria in its configuration space, producing the Configuration Parameters of the Basic Configuration, such as range, execution order, and constraints.

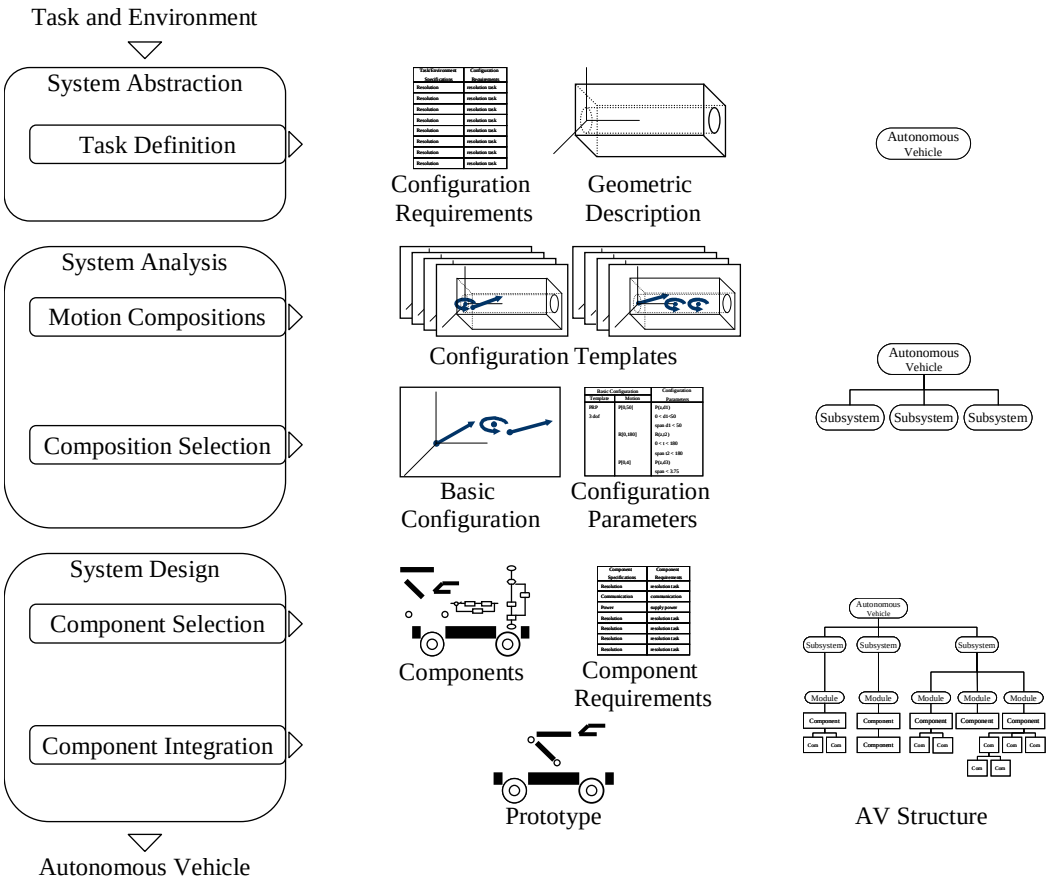

Figure 1.1: **Proposed framework for synthesis of AV configurations.**

Both Configuration Requirements and Configuration Parameters are used in the System Design phase as technical specifications and metrics to select each component, involving mathematical expressions that relate these values and the component features. In this phase, the method uses an inventory of actuators, sensors, control elements, and mobile platforms. The selected components generate their Component Requirements, which are actuation-sensing specifications and constraints that also are analyzed to avoid propagation of conflicts or technical contradictions.

A feasible solution is defined when the Configuration Requirements, the Configuration Parameters, and the Component Requirements have been satisfied and the Basic Configuration is transformed into a complete structure of subsystems and modules that integrate the physical and logical components synthesizing the AV configuration. The System Design phase ends with the integration of the selected components into the AV structure, which should serve as guide to conduct and facilitate the implementation of the robotic vehicle prototype.

The implementation of the geometrical analyses, the analytical equations, and the simulations are encoded in computational procedures, which are structured independently to carry out systematically the various analytical studies and allow the incorporation of additional processes. The procedures produce both numerical data and parametric graphs that allow a comprehensive interpretation of the quantitative relation among the robotic vehicle performance, the component features, and the environment properties. In this context, the designer must compile all the information and the numerical results in spreadsheets and tables that serve as input and output interfaces (e.g., Configuration Requirements and Configuration Parameters) to interact with the computational procedures and to fulfill the AV structure. Thus, designer's intervention is implicated to manipulate the current instantiation of the framework, and to evaluate the parametric results that serve as trade-offs to support the design decision for synthesis of the AV configuration.

It is important to make note that the intention of this systematic framework is addressed neither to automate the synthesis process nor to relieve the designer; instead, the framework assists the user in developing the design processes to define a viable AV configuration. The core of this research is to validate the proposed method, apply it to obtain an AV configuration in the underground mining domain, and to illustrate its fundamental contribution issues:

- Formulation of a systematic framework to synthesize an AV configuration, from the task and environment requirements to support the implementation of the operational robotic vehicle, based on the use and adaptation of conventional vehicles produced during decades of engineering.
- Definition of the configuration, consisting in a functional structure, through analytical and geometrical analysis, rather than designer experience.
- Integration of autonomy analysis to detail the robotic vehicle configuration, leading trade-offs to select the locomotion component and its actuation and sensing components.
- Introduction of analytical expressions derived from reformulated kinematic models of steering geometries to evaluate and compare their fundamental differences, in the expected positioning and control errors, and the estimated perception parameters.
- Introduction of a positioning uncertainty evaluation to relate the performance of an Ackermann vehicle to the expected sensor uncertainties, simulating the assigned task.
- Formulation of the analytical and geometrical processes in individual computational procedures, to maximize the parametric information from each analysis of the systematic framework. In addition of making this framework available as an analysis toolkit.

1.6 Document Outline

The derivation of the systematic framework is detailed in this thesis, developing the proposed framework for synthesis of an Autonomous Vehicle prototype, which is configured to perform a task of the underground mining domain. This thesis is composed of nine chapters and three appendices. This chapter serves as an introduction and overview of the work.

Chapter 2 summarizes relevant works that address the synthesis of robotic systems. Related literature is reviewed in this chapter, linking topics to the implementation of Autonomous Vehicles. Chapter 3 describes the proposed framework, and outlines the fundamental phases to generate the rational configuration.

From Chapter 4 to Chapter 8 is presented the development of the proposed framework applied to the underground mining task. A first synthesis experiment allows the implementation of an AV prototype to be rapidly deployed, as a viable solution of the tasks from the selected and available components, validating the proposed method. The geometrical and analytical process of this exercise is developed in the Chapter 4, whereas the integration and the implementation of the prototype are presented in Chapter 5.

A second configuration is formulated as a generalization of the previous exercise, but also by an analysis to configure an AV with certain degree of autonomy that correlates perception, control, positioning, and kinematics of the robotic vehicle. This later configuration is developed through the Chapter 6, Chapter 7, and Chapter 8.

Chapter 6 presents the autonomy analysis, related to the System Design phase, to identify the kinematics requirements that improve the position estimation, the control and the perception requirements, from a parametric comparison of different steering mechanisms, which are investigated under equal operation conditions, to select then the proper kinematics for the AV configuration. In this analysis, three steering mechanisms are examined: Ackermann Steering (AS), Articulated Steering (RS), and Explicit independent Steering (ES).

Chapter 7 addresses the analysis to investigate the quantitative sensor requirements for improved the position estimation of the selected kinematic vehicle. Simulation results are presented for estimated the degree of uncertainty in the odometry and absolute sensors by allowing the reliable achievement of the task.

Chapter 8 describes the integration of the complete configuration for the synthesis of the AV to perform the task. This configuration involves the results produced by the systematic framework.

Finally, the Chapter 9 summarizes the contributions of this thesis, presenting the conclusions and suggestions for future developments. The appendices to this thesis give detailed information on specific topics related to the work presented. Appendix A presents the detailed abstraction of the Geometric Description of the task. Appendix B presents the kinematic models of the Ackermann, Articulated, and Explicit independent vehicles. Appendix C presents a description of an Extended Kalman Filter (EKF) that is used for the position estimation.

Chapter 2

State of the Art

Autonomous Vehicles are composed by an appropriate configuration of electromechanical and information components, which provide the capability to perform the assigned task. The development of a method to determine this configuration is the purpose of this thesis which is motivated for the technological progress that has been made in AVs and their suitable potential that concern with diverse applications.

This chapter describes a general background related to the research focus with the topic of robot configuration. Research works on synthesizing robot configurations have been in the field of modular robots; most of these approaches have defined the configuration of a manipulator or a mobile robot. For example, the configuration of manipulators has been done with the combination of prefabricated links and joints [Tesar 89]. The use identical components has been also explored, in which the components can be combined to generate manipulative and locomotive configurations [Yim 02].

Other works have used different components that include mobile platforms, actuators, wheels, and power systems, to produce the robot configuration [Leger 98, Farritor 01]. These approaches have applied search techniques to automate the selection of the robot configuration, through the parametric optimization of pre-defined configurations. Whereas, the analytical approaches for synthesis of robotic systems have been limited to the comparison amount possible candidates and the definition of the configuration of a specific element of entire robotic vehicle, such as the locomotion subsystem of a wheeled robot. However, the successful development of robotic vehicles reported in the literature exhibit the feasibility to build operational of AVs. This is the case of the automation of conventional vehicles to perform tasks in or out of their original purpose.

The following sections, divided into modular approaches, automated approaches, analytical approaches, and Autonomous Vehicles sections, briefly describe the efforts most relevant and complimentary to this research.

2.1 Modular Approaches

The concept of modular robots has been of interest in Robotics since various decades. Several techniques for robotic prototypes have been developed during this effort. This kind of robotic systems consists of modular components to generate the configuration of manipulators and mobile robots through these techniques, where the selection of the type and number of modules are of concern studies on kinematics and dynamic.

2.1.1 Manipulators

Extensive indoor applications have motivated research in developing modules to built manipulators. These works include links and joints as modular components to generate automatically the Denavit-Hartenberg (DH) kinematic parameters from geometric description of various prefabricated modules, defining the forward and inverse kinematic models through a numerical method [Kelmar 88]. The goal is to define mechanical design of planar modular manipulator using the performance arm as criteria to meet the task requirements [Ambrose 94] and to find an optimal assembly robot configuration that is generated from a given topology and number of degrees-of-freedom (DOF). The motion equations are then derived using a matrix representation of the manipulator kinematics for a specific task [Chen 97].

Other approaches find kinematic shape, according to task specifications and predefine configurations for which optimal parameters must be chosen, using some search technique. In [Paredis 93] has been used the simulated annealing, assuming the existence of a methodology that accept the task requirements as input, to determinate the DH parameters of a manipulator which must reach specified positions and orientations. The minimum DOF and reachability of a trajectory are used as criteria through a modified evolutionary algorithm to define the kinematic parameters of a manipulator for space application [Kim 93].

[Chen 95] have employed prescribed robot topologies to define the assembly configuration of a manipulator, which is solved as an optimization problem that considers obstacle avoidance in a computational simulation. The best mechanism is chosen from a data base of possible configurations for following a trajectory [Chedmail 96], so as to determine the manipulator configuration and its base position [Paredis 96a]. Other approaches have used evolutionary techniques from random seed to define the manipulator configuration for a 3-D trajectory [Chocron 97], to determine the necessary robot configuration and then identify the optimal link length [Han 97], and to select several parameters for a manipulator, determining the type and the optimal parameters of shoulder and wrist joints [McCrea 97], and using only one type of link and joint [Matsumaru 95].

2.1.2 Mobile Robots

The designs of mobile robotic systems have been also explored, using modular components, in which identical modules can be combined to generate not only manipulation but also the capability of locomotion. The key of these approaches is the creation of more complex modules and configurations, which are built from simpler ones.

For instance, in [Hornby 01] have been produced 2-D locomotion configurations from predetermined modules through of language design and an evolutionary algorithm. For adapting to a task in a particular environment, [Pamecha 96] have used mechatronic modules that can connect and disconnect to provide self-reconfigurability. The new configuration is reached from initial configuration using simulated annealing to drive the motion plan of the reconfiguration. The control decentralized approach to reach the new configuration using identical modules is used in [Yoshida 97], in order to provide self-reconfiguration and self-repair, avoiding the deadlock of the modules.

In the case of 3-D locomotion configurations, a manipulator is composed in [Fukuda 90], by homogeneous modules; its configuration is defined through the allocation of each module, determining the module combinations and the length between those modules to form a specific degree of freedom or joint, in order to follow the trajectory of the assigned task. Several configurations have been proposed for legged or climbing robots [Kotay 97], with self-maintainability by rejecting faulty modules [Murata 98], that can change its shape according to the locomotion [Unsal 00], that can modify its locomotion gaits [Yim 00], employing in all these approaches identical modules, which consist of the mechanical, electronic, and software components to create an autonomous unit or autonomous modules.

The aforementioned research works illustrate the notable advance in robotic technology. The core of these researches is that the modularity in electromechanical and control design allows the design of a manipulator or of a mobile robot that is appropriate for a given task. Though, the area of robot design has been much prior work, using modular components; this review leads a fundamental observation. It is evident that these robotic systems are limited for tasks that require large workspace or support a significant payload, e.g., tools to achieve tasks in unstructured environments.

This feature of modularity, certainly also, leads to some dependency between the number of modular elements and the type and diversity of configured robots. Such dependence results in reduction of suitable robotic systems, especially, produced with identical modules.

2.2 Automated Approaches

Robotic research has expanded to works that use a set of different modules that include mobile platforms, actuators, wheels, and power components to produce useful robot systems, such as manipulators and legged robots. To identify robot configuration, these approaches use engineering filters to reduce the search space and then an adaptive search technique is applied to select a robot configuration and its motion plan [Farritor 96, Farritor 98]. The core of this approach is the hierarchical selection process from the task and environment description, through the prefabricated hardware and software modules.

To find the optimal combination of components for certain required locomotion, a genetic algorithm (GA) is used through a hierarchical evaluation from mathematical to full simulation [Chocron 99]. An intensive task simulation, for a population of possible robot configurations, generated from parameterized modules, uses an optimization algorithm based on genetic programming to reproduce individuals that optimize performance requirements [Leger 99].

These mentioned methods focus on optimization of multiple performance metrics and solution of constraints from predefined robot configurations, which are generated by designer experience, as well by means of a random combination of a finite set of modules. Thus the initial definition (form or topology) of the configuration is previously decided and implicitly synthesized as a legged robot or a manipulator. This is a lack in these approaches, since the definition must constitute a fundamental phase of synthesis process, in which a rational configuration of the robotic system is defined from concept to its implementation through the task and environment requirements.

In addition to the approaches outlined above that attempt to automate the configuration process, there are works that define a formal grammar for artifact description and its representation [Roston 94]. This language definition is completed with a computational environment for the automation of robot design synthesis and optimization [Katragadda 99]. The engineering designs are applied into diverse domains; efforts that are focused on formal methods, rather than *ad hoc* methods [Antonsson 01].

2.3 Analytical Approaches

The design processes, based on the derivation of parametric and analytical solutions, have received attention from the robotics community. [Bares 91] proposes a systematic approach to generate the configuration of walking robots in which have been used the locomotion kinematics of candidates including mechanisms that roll, walk, or combine rolling and walking. This effort proves an analysis on terrain surface as a criterion to select wheeled or legged robot configurations [Todd 85] and geometric evaluation of gaits to analyze the performance for the candidate walker robots.

The criterion regarding the property of terrain is also included in the work for synthesizing a locomotion system [Apostolopoulos 01], examining the detailed configuration of a planetary robotic system for exploration of barren terrain and finally implementing the analytical configuration of wheeled robots. The derivation of configuration equations is presented, involving the estimation and optimization of configuration parameters, also with the predictions of performance from analytical models, based on the all-terrain and conventional vehicle works [Bekker 69, Wong 93].

The synthesizing wheeled system is generated through the formulation of analytic expression or mathematical functions that relate the environmental and task parameters, with the configuration and performance parameters. Although this computational framework is only addressed to the configuration of robotic locomotion, this work and the previous [Apostolopoulos 96] have been a substantial foundation on the work of the thesis here presented.

2.4 Autonomous Vehicles

The major reason for considering the use of Autonomous Vehicles is their ability to move toward a particular location and to perform some kind of task automatically. Potential applications are in demanding situations and environments where it is not feasible or safety to send humans to achieve the work. Deep underwater exploration and an excavation labor in mines are examples of such tasks.

Mobile Robotics has faced the development of robotic vehicles for several decades. The early implementations attacked problems from indoor applications under structured environments. The first works served as platforms or testbeds for purely scientific research purposes, such as navigation and exploration using AI approaches. Although the mobile robots for indoor applications offered, and still offer, many interesting contributions and technological challenges, the implementation of Autonomous Vehicles for outdoor applications started to be required gradually. The effort has been in the development of robotic vehicles for diverse application sources, which involve from industrial or civil environments, originally driven to perform heavy and hazardous work, into hostile and remote environments. Within that context, the Robotics discipline has created the necessary technology to develop AVs [Gage 95, Everett 95, Meyrowitz 96, Borenstein 97, Durrant-Whyte 01, Stroupe 01].

In the impetus for the development of AVs, Robotics has taken different approaches when implementing the robotic system that carries onboard all the required components to the achievement of the assigned task, including locomotion mechanisms, actuators, and sensors. These approaches have been from innovative designs, passing by the designs based on the nature, to automate existing vehicles. For instance, this is the case for the AV development where a traditional ground vehicle, initially designed to be lead

by a human, is adapted to perform robust tasks. Tasks that can be not only agreed with its original definition, but also concerned with its universality of mobile platform, taking advantage of the enormous existing tradition in engineering associated to the design and construction of vehicles of all type, such as automobiles, trucks, and so on.

Projects for autonomous driving have had important and favorable results, using light trucks or buses [Thorpe 91b, Thorpe 91a, Thorpe 97]. AVs have been extensively carried out in the automation of land vehicles for agriculture [Pilarski 99], construction [Stentz 98, Cannon 99], utility [Trebi-Ollennu 99, Fong 03] and mining applications [Hurteau 92, Steele 93, Scheding 97, Stentz 99, Stentz 01, Thrun 03]. Also, the development in original designs for planetary exploration domain have demonstrated the potential of the AVs [Hayati 97, Rollins 98, Fiorini 00].

However, these works aim either the task automation of the vehicle for which it has been made or the development of a specific technology for scientific research purpose. Additionally in these works, the process of implementation is limited to a description of the wide range of deployed technologies, including sensors, actuators, electronics, and mechanics, but lack of a description of the deployed synthesis process for the configuration choice during the implementation of such robotic systems.

2.5 Summary

Through this review in the area of robot configuration, it is evident the absence of a theory or method to synthesize an Autonomous Vehicle from its concept to its implementation. Thus, systematic synthesis approaches for a practical use of AVs are required. This is intended with the proposed method in this thesis, a framework to systematize the configuration and construction of AVs. A synthesis framework that takes advantage of the inventory of products that has been developed during decades of robotics research and engineering. In particular, the extensive expertise on vehicle designs of traditional engineering, the concepts of the modularity, the task-environment oriented, and the derivation of analytical solutions to define the Autonomous Vehicle configuration.

Chapter 3

Systematic Framework

> Vehicle configuration can generally be defined in terms of form, size, weight, and power [Bekker 69].
>
> Selection of vehicle configuration is primarily based on mission and operational requirements and on the environment in which the vehicle is expected to operate. To define an optimum vehicle configuration for a given mission and environment, a systems analysis approach should therefore be adopted [Wong 93].

This chapter describes the systematic framework that is used throughout this thesis for the synthesis of an AV configuration. The configuration is expressed as a structure of components that fulfill the specifications to perform a given task under the constraints of a certain environment, allowing the construction of the robotic system. The components embody the functionality of a composition of motions that solve the task. The composition is selected through a preliminary analysis, in which a geometric analysis of the task and the environment is used to combine motions and find viable compositions. Each motion of the selected composition is mapped as a component or component set, which integrates a specific subsystem into the vehicle structure. The components are selected using criteria of Robotics and engineering to provide a suitable AV configuration that performs the given task with certain level of autonomy.

The definition of the requirements, the geometric analysis, the combination of motions, the selection of composition, and the fulfillment of the configuration with the components are derived through this proposed framework. The framework includes engineering and robotic principles, involved in analytical and geometrical processes, to configure the robotic vehicle. It is as a computational and practical framework that takes advantage of the technology developed by engineering and Robotics. The following sections address a more detailed description of the formulation and the composition of the systematic framework; whereas, its implementation will be developed in the next chapters.

3.1 Autonomous Vehicle Synthesis

The systematic framework leads the synthesis process and assists with all the analyses to determine viable Autonomous Vehicle configurations. The method represents the vehicle configuration as a tree structure of interlinked components. Such structure is integrated gradually with the results provided by the method from functional analysis and leads to analytical selection of components. The synthesis process follows a general systematic procedure of first defining the task; second, finding possible solutions; and third, implementing the basic solution that ensures a suitable robotic system.

Figure 3.1 depicts the method for synthesis of AV configurations; the left-hand branch overviews the three gradual phases that compose the systematic framework: System Abstraction, System Analysis, and System Design; the center branch overviews the results of every phase; whereas the right-hand branch shows the progressive fulfillment of the structure to define the AV configuration.

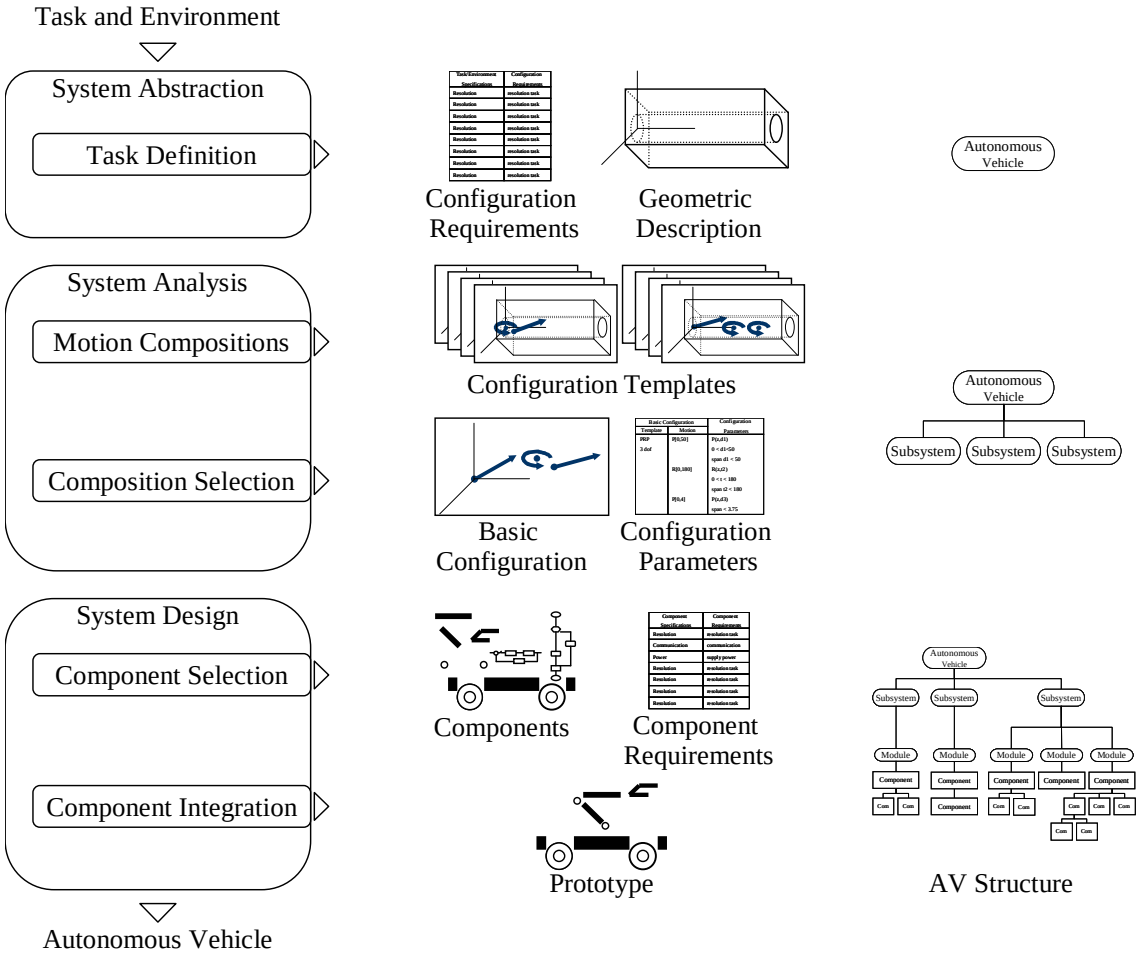

Figure 3.1: **Systematic Framework**

The systematic framework begins in the System Abstraction phase, in which all the information of the task and the environment is converted into Configuration Requirements and defined as a Geometric Description. These outputs are used in the subsequent phases to formulate and verify the functional features and the implementation of the robotic system.

In the System Analysis phase, the Basic Configuration is identified as the composition of fundamentals motions that cover the Geometric Description. This composition is considered as the most appropriate template to define the functionality of the robotic vehicle. All the motion parameters of the template are mapping into the Configuration Parameters.

A feasible solution to configure the vehicle is defined in the System Design phase, when the Configuration Requirements, the Configuration Parameters, and the Component Requirements have been satisfied. Then the Basic Configuration is transformed into a structure of subsystems that integrate the physical and logical components for synthesis of an Autonomous Vehicle. This phase ends with the implementation and the experimental verification of the vehicle Prototype. These phases combine geometrical and analytical procedures that relate the task specifications, the environment constraints, and the robotic vehicle requirements of autonomy.

The following sections present each one of the phases for the AV synthesis, involving a description the modules that compose every phase and specifying their inputs and outputs. Section 3.2 describes the phase to define the requirements of the task and the environment in qualitative, quantitative, and geometric terms. Section 3.3 presents the geometrical process to find possible solutions in terms of fundamental motions, i.e. the analysis of the robotic system. Section 3.4 describes the analytical process to select the components for the design of the robotic system, implementing the basic solution that is defined in the System Analysis phase.

3.2 System Abstraction Phase

The synthesis process develops a systematic transition from information about a task to concrete components. In the System Abstraction phase, the task and environment information, i.e., specifications and constraints, are used as input to define the Configuration Requirements and the Geometric Description. This abstraction refers with defining both specifications and constraints of the task and the environment, including the sort of task to be performed and its operational conditions, also with the geometric and the physical properties of the environment in which the AV is expected to operate.

Table 3.1: **Configuration Requirements**

Task & Environment Specifications	Configuration Requirements
Task resolution less than 1 cm	task_resolution $\leq$ 0.01 m
Run Operation greater than 2 hour	2 h $\leq$ run_time
Environmental Temperature between 10 °C and 40 °C	temperature $\leq$ 40 °C 10 °C $\leq$ temperature
Power: No fuel (combustible)	$\neg$fuel

3.2.1 Task Definition

The information is converted into Configuration Requirements, which consist in a requirement list that quantifies the features of the task and the environment and serves as metrics and criteria to detail the vehicle configuration [Apostolopoulos 96]. The Configuration Requirements are specified as algebraic expressions where a set of variables (quantifiers) relate to the different features of the robotic system.

These expressions denote the scope of the specifications and the constraints as inequalities that define the set of values which can be taken by quantifiers [Brooks 81], such as the conditions and properties of the environment or the required performance of task. For instance, to specify a resolution better than 10 cm for a given task, the configuration requirement is defined with the quantifier *task_resolution* and expressed as follows:

$$\text{task\_resolution} \quad \leq \quad 0.10\,\text{m}$$

All these collected requirements result into a table of Configuration Requirements, such as is shown in Table 3.1. The table is different from application to application, but it must detail the specifications and the constraints of the assigned task in the particular environment. The Configuration Requirements is a list that provides quantitative and qualitative metrics to be satisfied in the rest of phases.

The Geometric Description contains the functional relation of the task and the environment in the geometry of three-dimensional Euclidean space. This geometrical abstraction describes what and where the task is to be accomplished, rather than how it is to be accomplished. The Geometric Description is generated as a workspace, which consists of points, lines, area or volume that the vehicle should reach to perform the task in the specific environment.

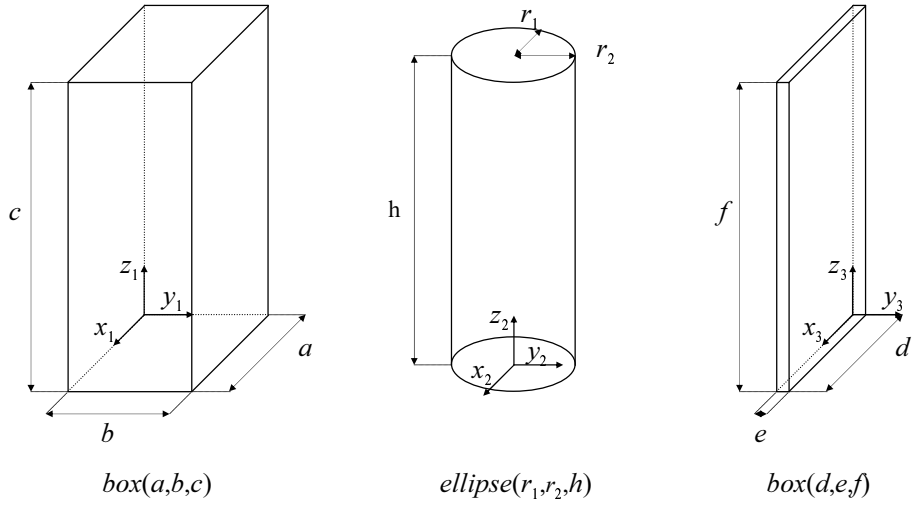

Figure 3.2: **Standard Primitives: Boxes and an ellipse.**

The workspace is constructed to describe either the collection of points or lines, or area, or the volume in space, using techniques for representing solids, such as constructive solid geometry (CSG) [Requicha 92]. In a CSG representation the workspace is connoted as a binary tree. Nonterminal nodes are operators, which may be either Boolean or transformation operations, whereas the terminal nodes are standard or general-sweep primitives [Huang 90a, Ulupinar 95], which are instantiated by the correspondent values of the Configuration Requirements.

For instance, to specify the task for determining the tunnel profile into a mine, the Geometric Description is defined by two box primitives and an ellipse primitive. These primitives are generic shapes associated to a local coordinate frame that must be instantiated by user with the quantifiers of the tunnel dimensions, which should be captured on the Configuration Requirements. Hence, the tunnel profile is an arrangement of two boxes of respective dimension $box(a, b, c)$, $box(d, e, f)$, and an ellipse of dimension $ellipse(r_1, r_2, h)$, that can specified as in Figure 3.2.

After instantiation, the primitive objects can be combined using regularized Boolean operations. The operations are the union, denoted $\cup^*$; intersection, denoted $\cap^*$; and difference, denoted $-^*$. Before the objects are intersected, united or differenced, they must be positioned appropriately with respect to each other. This is done by translation, rotation and scaling, as need. To make this positioning, a relationship among the local coordinate frames of the objects is identified with a single, universal coordinate frame. Thus, the tunnel results to subtract the ellipse of the first box and joined with the second box, with the respective transformations ($x\_translate$ and $y\_translate$, which are attached a common coordinate frame. The expression is conveniently represented as a tree, as shown in Figure 3.3.

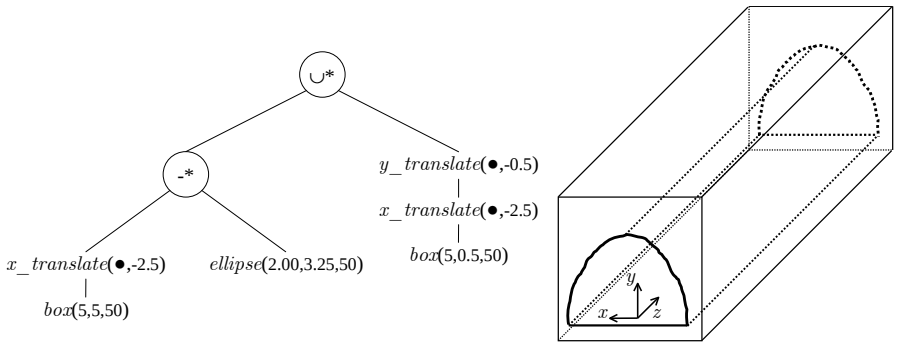

Figure 3.3: **Geometric abstraction of a generic shaft and its CSG tree.**

Both results of the System Abstraction phase, the Configuration Requirements and the Geometric Description, serve as references in the subsequent phases. The Geometric Description is a workspace on which are generated and analyzed possible solutions, whereas the Configuration Requirements are used as guidelines to define the AV configuration.

3.3 System Analysis Phase

The task and environment abstraction is followed by an analysis of possible solutions that depict a candidate configuration of the robotic vehicle. In the System Analysis phase, the vehicle configuration is characterized as a set of subsystems that are defined from the necessary motions to perform a given task. An examination of these motions serves to find out the nature and the functional interrelation of the subsystems that should form part of the AV configuration.

3.3.1 Motion Compositions

The vehicle functionality is referred to the minimum composition of motions, or degrees of freedom (DOF), that cover completely the Geometric Description of the task and the environment, considering the function of each motion and neglecting its physical and mechanical compound. Without loss of generality, the motions are considered as parametric entities that implement either a rotation or a translation displacement in particular direction and orientation within the Geometric Description, i.e., in the workspace. Each motion can be associated to a point of this three-dimensional Euclidean space to describe the magnitude correspondent of its movement with respect to the common coordinate frame.

A feasible composition is a combination of these fundamental motions: rotation and translation, forming a chain that keeps the order in which are aggregated. This order is denoted by a subscript i, whereas rotation is denoted by R and translation is expressed as P. For instance, a composition $P_1R_2P_3$ represents the combination of

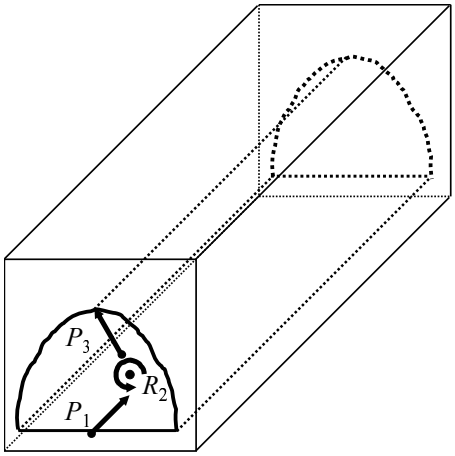

Figure 3.4: **Composition of motions $P_1R_2P_3$.**

a prismatic motion followed by a rotational and a translation. This notation makes ample use of the geometrical and mathematical concepts on which the robotics is based [Paul 81, Craig 86, Selig 00], such as the order in which compositions are constructed is important. Then in general, the final result of a composition R_2P_3 will be different to the composition P_2R_3.

In a composition, the motions are attached and could move relative to each other. To cover fully the workspace, the operation parameters of each motion, such as the magnitude of the movement, are adjusted property and constrained by the rest of attached motions, i.e., the position and orientation of the final chained motion depends on the predecessor motions, and the former motion chained depends on its initial location.

From the aforementioned composition $P_1R_2P_3$, the position and orientation of the motion R_2 depends on the motion P_1, which is situated on the origin of a correspondent Geometric Description, as shown in Figure 3.4. For example, the range of operation of the motion R_2 is from 0° to 180° to cover the ceiling of the tunnel, whereas the motion P_3 should have a magnitude equal to the range between $r_1$and r_2 of the ellipse.

The complexity of the task determines the numbers of motions required to create a composition [Paredis 96b]. Hence, the compositions are defined through a combination process that proposes a candidate minimum DOF for a given task based on the dimensionality of the Geometric Description. When this candidate fails to reach completely the workspace, the number of motions is increased by one. This process is repeated until diverse compositions satisfy the criterion of reachability of the Geometric Description. Then, all composition variants are specified as a Configuration Template table, since each composition is considered as a template to define the functionality of the vehicle, when adopting at a solution.

Table 3.2: **Configuration Template of the composition $P_1R_2P_3$.**

Template	Operating Range	Composition Specifications
$P_1R_2P_3$ 3 DOF	P_1 [0,h]	P_1 (z,d_1): $d_1 \leq h$ $0 \leq d_1$
	R_2 [0°,180°]	R_2 (z,θ_2): $\theta_2 \leq 180°$ $0° \leq \theta_2$
	P_2 [0,r_2]	P_3 (z,d_3): $d_3 \leq r_2$ $0 \leq d_3$

Table 3.2 shows the Configuration Template for the composition $P_1R_2P_3$, which describes its parameters that are expressed by quantifiers to form the specifications of the composition, such as the number of motions and range of operation for each motion. For instance, the quantifier d_3 specifies the operation range or magnitude required to perform the motion P_3, denoted as $0 \leq d_3$ and $d_3 \leq r_2$.

3.3.2 Composition Selection

The System Analysis phase carries out the aforementioned composition process to generate systematically alternatives of solution from the Geometric Description of the task and the environment. These alternatives solving the task are analyzed, to provide a rational AV configuration led by a geometrical and mathematical evaluation that includes the Configuration Space (C-space) [Lozano-Perez 83, Latombe 91, Joskowicz 94, McCarthy 00].

A configuration of the C-space is a specification of the position and orientation of every motion in a relative reference frame; hence, the C-space of a composition is a finite collection of position and orientation, achieved by the motions, to reach completely the Geometric Description of the task and the environment. A detail discussion of geometric and algebraic methods been applied to the C-space concept can be seen in the text [Latombe 91].

The C-space is used throughout this approach as a representational tool of the motion relation, i.e., to represent the motion specifications, making explicit the constraints on the motions. Thus, each composition is evaluated to select the most appropriate template, a suitable candidate configuration for the specific task, using simplicity and uniformity criteria in its C-space.

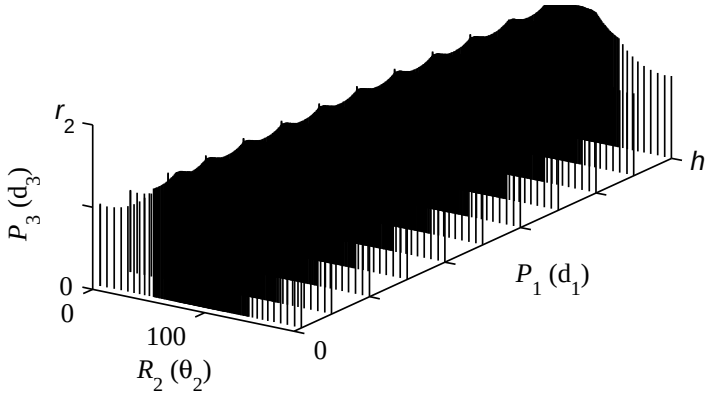

Figure 3.5: **Configuration space of the composition $P_1R_2P_3$.**

The parameterization of the C-space is obtained by representing every configuration through the quantifiers or variables associated to each motion. Figure 3.5 depicts the C-space of the composition $P_1R_2P_3$, where d_1, θ_2, and d_3 defines respectively all the position and orientation for this composition.

The analysis considers the number of DOF that involve each template as one criterion to evaluate every composition. The priority will be in those compositions that have minor number of degrees of freedom, since each motion represents a subsystem; thus, minimize actuated DOF is equal to minimal control and structural complexity of the configuration.

In addition, the framework considers also a C-space formulation as other element to analyze the candidate compositions. This formulation is a set of metric parameters for each transformation, which are expressed in quantitative forms to allow a comprehensive comparison among compositions, and finding out a fundamental composition based on its simplicity and uniformity. To this purpose, an approximation of all C-spaces is formulated by means polynomial functions, which can represent arbitrary shapes, such as B-spline [De-Boor 78, Hoschek 93]. The order of the C-space approximation is related to simplicity of the composition.

Furthermore, the distribution of the displacement on the C-space for every motion is analyzed; it is to investigate the practical span required of movement, which is considered as a histogram that shows the distribution of movements about the range of operation of the motion.

The selection aims a computation of these parameters, which are aggregated to the Configuration Template. A rational trade-off considers the composition of motions that presents more simplicity and uniformity based on the motion reachability of the Geometric Description.

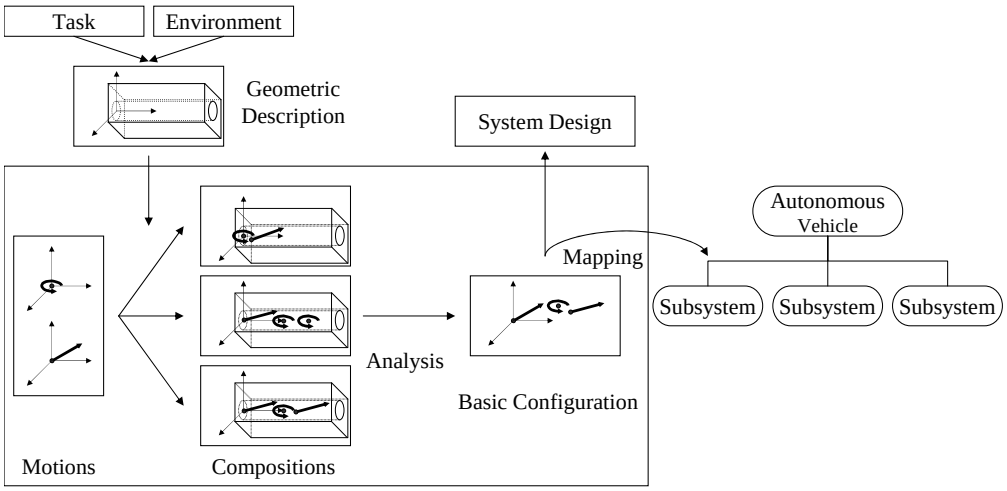

Figure 3.6: **System Analysis phase.**

The analysis involves the selection of the best candidate when defining the configuration of the AV. This selected composition becomes a Basic Configuration, where each one of motions is mapped as a subsystem into a hierarchical and modular structure. To define a suitable solution from this Basic Configuration a detailed synthesis of each one of the subsystems is required, i.e., a detailed system design. Figure 3.6 depicts the aforementioned process involved in the System Analysis phase.

All the information about the Basic Configuration is translated as a list of Configuration Parameters, such as the Configuration Requirements. These Configuration Parameters involve length, range, span, execution order, and constraints of each motion, which should be satisfied and considered during the phase of System Design, since the parameters are the requirements specifying how the task should be achieved. In this context, implicitly the execution order of the motions, from the Basic Configuration, can be seen as the basic strategy of operation for the robotic vehicle.

For instance, Table 3.3 shows the Configuration Parameters of the composition $P_1R_2P_3$. The first motion to execute is P_1, it also should carry the second and the third motion, then the second motion R_2 is executed, supporting the motion P_3, which is last to execute. Thus, there exists constraints where the capacity of payload for the motions P_1 and R_2 should be at least the weight of both motions R_2 and P_3, and the weight of the motion P_3, respectively.

At this stage of the method, a feasible candidate for AV configuration has been generated, i.e. the Basic Configuration. The AV system is structured into subsystems that are correlated, one by one with the motions, which should be substantiated by proper components.

Table 3.3: **Configuration Parameters of the composition $P_1R_2P_3$.**

Template	Operating Range	Configuration Parameters
$P_1R_2P_3$ 3 DOF	P_1 [0,h]	P_1 (z,d_1): $d_1 \leq h$ $0 \leq d_1$ $h \leq \text{span\_}d_1$
	R_2 [0°,180°]	R_2 (z,θ_2): $\theta_2 \leq 180°$ $0° \leq \theta_2$ $180° \leq \text{span\_}\theta_2$
	P_3 [0,r_2]	P_3 (z,d_3): $d_3 \leq r_2$ $0 \leq d_3$ $r_2 \leq \text{span\_}d_2$
		R_2_weight+P_3_weight $\leq$ P_1_payload P_3_weight $\leq$ R_2_payload

3.4 System Design Phase

The purpose of an AV is to move in a specified environment and to execute a particular task. Typical applications require a reliable degree of autonomy that allows the robotic vehicle be able to perform its actions in a controlled approach without human supervision. These actions and control should be implemented throughout the subsystems that embed the functionality of the Basic Configuration. Since the subsystems are integrated by components of mechanics with electronics and information technology; thus, the importance role of autonomy needs to be taken into account within the synthesis process to select such components, not only defined their physical and mechanical solutions for whole the robotic system.

3.4.1 Component Selection

In the System Design phase, both the Configuration Requirements and the Configuration Parameters are used as technical specifications and rationalized metrics to select each one of components, involving mathematical expressions that relate these values to the component features. The AV configuration has to be synthesize through the formulation and systematic evaluation of components that should integrate the AV structure.

This structure (see Figure 3.8) constitutes an abstraction of the functional relation of the subsystems that compose the robotic vehicle, as a hierarchical and modular (vertical and horizontal) representation of the component interaction to support the

conceptual and physical implementation of the AV. In this way the components are evaluated and the interactions with other new aggregated components can be analyzed. Thus, to establish the synthesis order, the existence of dependence and the constraint propagation among the motions should be identified at first; then, each motion is analyzed considering its functionality into the Basic Configuration.

In a practice context, the motions are mapped into a correspondent subsystem that provides either mobility, manipulation, or the appropriate action of the assigned task, based on the analysis of the Configuration Parameters and on engineering principles [Nordlund 96, Ulrich 00]. An AV can be constituted into Locomotion, Deployment, and Tool subsystems that also can be integrated by a synergy of tree parts: software, electronics and mechanics.

Tool subsystem: consists of a specific component, or a set of components, to perform expressly the sort of task beeing required. In general, the motions at the end of the Basic Configuration is mapped to this subsystem, since this motion becomes the last motion that reaches the workspace of the Geometric Description. Therefore, this motion abstracts the functionality of the expected task, so that the selection process to such component depends on the task functionality and it should embody appropriately this functionality.

The component not only must satisfy each one of the respective Configuration Parameters, but also have to meet the Configuration Requirements, which range from technical specifications in form of metrics (such as the parameters that are associated to an operation feature of the tool, physical principles of operation to match the span, measurement range, resolution, and rating needed, through mathematical equations that relate these properties) to constraints in form of guide to choose a tool. Recall that those constraints represent the environmental conditions in which the tool must operate that can be associated with powered by, construction material or digital result outs.

In the example of the configuration $P_1R_2P_3$, to explore the tunnel profile, the motion P_3 can be mapped as tool subsystem, operating as a distances sensor with a range of operation at least r_2 to embody the function to reach and cover the profile of the tunnel ceiling. For instance, a proper component to gather data can be implemented by a scanner, video camera, or *in situ* instrument for the measurement of physical variables of the environment. Whereas, a component to implement manipulation of items, it can be a worktool to drill, cut and transport.

Deployment subsystem: must implement the functionality of the motion that allows the manipulation of the Tool subsystem, consisting to hold and deploy the worktool in the specific position and orientation for performing the assigned task. This deployment of the tool must achieve conform to the identified motion of the Basic Configuration.

Thus, the component must satisfy the respective Configuration Parameters, involving the Configuration Requirements as the specifications and the constraints during the selection process. This subsystem can be implemented either by a linear or rotary motion mechanisms or robotic arms compose of several links and joints.

As in former subsystem, the selection is based on mathematical expressions that capture both the Configuration Parameters and requirements and the operation features of the components, with regard to robotic criteria (such as kinematic, stability, and performance analysis), but following the topology given for the Basic Configuration. For instance, a rotary mechanism such as an electric motor can be the component that embody the motion R_2 of the configuration $P_1R_2P_3$, allowing locate the distance sensor of the Tool subsystem towards the tunnel profile.

Locomotion subsystem: is the physical interface between an AV and its environment that allows the robotic vehicle moves to reach the desired site while carrying itself and the Deployment and Tool subsystems. Locomotion is mapped from the former motion of the Basic Configuration, which should have an extend parameters of operation as its environment. Because the locomotion is the foundation of the successful execution of the task, not only the locomotion must fulfill the above functions, but also it should perform such actions autonomously. This is a certain degree of autonomy that correlates to perception, control, and actions of the vehicle.

A reliable degree of autonomy requires that the vehicle be controlled by itself to navigate, following a given path and avoiding obstacles, based on the basic strategy. Key to mobile robot autonomous performance is accurate positioning, which implicates that the vehicle positioning must be estimated to provide safe and effective control. To configure the vehicle, selecting the adequate locomotion kinematics that minimizes the position estimation error is fundamental criterion in the synthesis process of autonomous vehicles, in addition the control and perception requirements.

Therefore, it is necessary to conduct a thorough analysis to identify the kinematic requirements of the vehicle locomotion that improve the position estimation, control and perception of the vehicle; since the kinematic model is derived propriety from locomotion subsystem which also is the physical interface between the environment and the vehicle or robot.

Figure 3.7 depicts the analysis for configuration of the robot by integration of basic aspects of autonomy. The analysis establishes as input the task and environment requirements that the robot must satisfy (i.e., Task model), it includes equations (i.e., Robot and Environment model) that capture the kinematic model and the positioning, the control and the perception parameters (i.e. Robot model), allowing compare different parameters of feasible vehicles, to then select the vehicle locomotion.

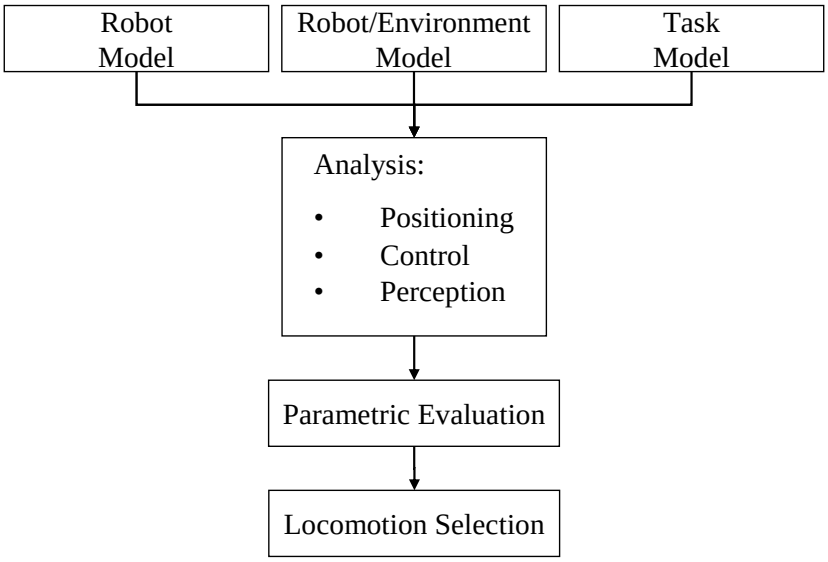

Figure 3.7: **Autonomy Analysis.**

The method works in the following steps:

1. The analysis uses simple steady-state models to estimate the generated error on vehicle positioning, considering the difference between a vehicle that navigates over ideal environment and other one that interacts with the expected environment. This calculated positioning error is used as a criterion for quantitative comparison of variant vehicles.

2. The method leads a similar analysis to compare the requirements of control and perception for the vehicle locomotion. The comparison is conducted under equal conditions of operation to evaluate the performance of different vehicles, regarding the tracking and heading errors and the estimated perception parameters.

3. The quantitative results allow the analytical understanding on the fundamental differences among different vehicles, to lead the definition of the components that integrate the locomotion subsystem, completing the vehicle configuration with the required degree of autonomy.

The synthesis of locomotion component involves the Configuration Parameters of the respective motion, and the Configuration Requirements. The analysis to choose the locomotion also involves from engineering criteria, such as basic mobility studies and principles to differentiate possible locomotion with respect to a confined environment, traditional analysis of interaction between mechanism and environment (i.e., air, ground, and underwater), and fundamental difference among types of locomotion as rolling and walking mechanisms to robotic criteria (such as an analysis of the traversability, positioning error, control, perception among different locomotion kinematics, e.g., Articulated and Ackermann steering).

The selection of the Locomotion subsystem involves the components that provide the positioning and consequently the control of the robotic vehicle in the specific environment. Therefore, a positioning uncertainty analysis is developed to investigate the positioning uncertainty evolution concerning the boundaries of sensor uncertainties, to provide a more predictable vehicle positioning while performing the assigned task.

Analytical expressions derived from kinematic model are used to relate the performance of the vehicle and the expected sensor uncertainties into the state estimate, using a technique filter such as the Kalman filter. The numerical results in simulation of the positioning uncertainty propagation yield the sensor requirements, such as the allowable sensor uncertainties and the number of landmarks, to reduce the positioning uncertainty.

In the example of the configuration $P_1R_2P_3$, the motion P_1 can be mapped as the Locomotion subsystem to move along the tunnel. For instance, a wheeled vehicle can be the component that develops this motion, allowing locate the Tool and Deployment subsystems into the corridors of the mine.

Through the aforementioned analysis carried out for synthesis the Tool, Deployment and Locomotion subsystem, the method defines quantitative results of suitable components for AV configuration, allowing the designer to make evaluation and trade-off decisions with regard these results to select the appropriate component for every subsystem.

The selected components are integrated into the AV structure, instancing each one the subsystems with all the components necessary to implement their functions. These components generate the Component Requirements, which are actuation specifications and constraints that imply the integration of mechanisms, electronics, and software such as computer, communication, and power components that will support the AV operation.

These Component Requirements are transformed as a list of quantifiers that determines the characteristics and necessary elements to operate each component. For instance, a selected tool can required a power supply with particular features, and a means of communication to receive commands and to send data. Thus a detailed analysis must integrate these Component Requirements to avoid propagation of conflicts or technical contradictions, in addition the Configuration Requirements and Configuration Parameters.

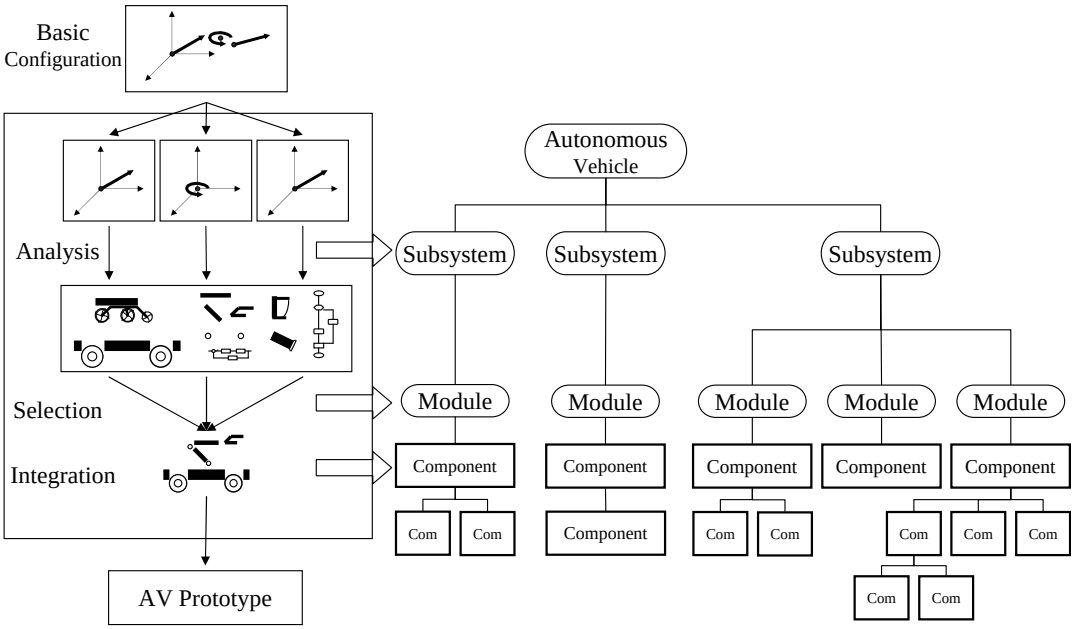

Figure 3.8: **System Design phase.**

3.4.2 Component Integration

A feasible solution to configure the vehicle is defined when the Configuration Requirements, the Configuration Parameters, and the Component Requirements have been satisfied and the Basic Configuration is transformed into a complete structure of subsystems that integrate the components for synthesis of the Autonomous Vehicle, as shown in Figure 3.8.

This modular and hierarchical configuration is a combination of hierarchical and modular components that contribute with their specific functions to perform the given task. On the top level is defined the function of the system (Autonomous Vehicle), i.e., the task of the robotic vehicle system. Function that should be developed by the different subsystems, forming the function subsystem level; each subsystem embodies the fundamental function of the motion defined by the Basic Configuration (e.g, Locomotion, Deployment, and Tool).

The implementation for each subsystem is made by the combination of modules that are combined to make up function module level (e.g., drive and steering modules). These modules are integrated by the lowest hierarchical level which include electronics (such as sensors, instruments and actuators), mechanics (such as actuators, and mechanical structures), and software (developed on information processing units, and communications), which are combined to form function component level. In this context, the AV configuration is a structure of proper components, interlinked by physical and logical interfaces, e.g., software through information processing devices that hold also the modular and hierarchical formation.

This structuring serves to the integration process. Individual modules can be built and tested separately to fulfill its functionality, which will provide faster and reliable prototyping of the particular subsystem. This structuring also is led during the aggregation of the subsystems since their combination support the function of the Autonomous Vehicle. This System Design phase ends with the implementation and the experimental verification of the vehicle Prototype, consisting of the assigned task execution in laboratory and then in the work environment to refine the vehicle configuration.

The operation of modules is ensured with the experimental testing process; if errors are found, they must be corrected until the module operates according to the required specifications. After that these modules are interlinked, the higher level entities into the structure are tested to reach their proper specifications of operation. Therefore the integration is an iterative procedure between testing and correction solutions deciding on the operationally of the robotic vehicle.

It is important to note that the integration of the selected components involves a detailed verification cycle, including system engineering, signal processing, electronic circuit board design, embedded microprocessor programming, and mechanical design (such as mounting and adaptation of components). Modeling the verification cycle is an extremely involved process that goes beyond the scope of this thesis. However, a reliable AV can be derived from the configuration defined by the systematic framework, assuming the implementation of such process in the construction of the Prototype.

3.5 Summary

The systematic framework assists the user to define a viable AV configuration that serves as foundation in the building of the robotic vehicle. The configuration is integrated gradually with the results provided by the framework, based on a general systematic procedure of defining the task and the environment in geometric terms, finding possible solutions in motion terms, and implementing the configuration with the component selection, in accordance with the following steps:

- Convert the task specifications and the environment conditions into a list of Configuration Requirements and define their Geometric Description, i.e., an abstraction of what and where the task is to be achieve.
- Combine fundamental motions to produce possible solutions, i.e., motion compositions that cover the Geometric Description workspace.
- Analyze the motion compositions, evaluating their parametric formulation and C-space uniformity to quantify the simplicity of every composition in the Configuration Templates.

- Compare the Configuration Templates to select the simplest composition and define the Basic Configuration to solve the task, converting its specifications into a list of Configuration Parameters and its execution sequence into the basic strategy to operate the robotic vehicle.

- Map the functionality of every motion to a subsystem into the robotic vehicle structure. The motions are analyzed as the Locomotion subsystem to move into the environment, as the Deployment subsystem to head the Tool subsystem, which is to achieve the assigned task.

- Analyze possible components to implement every subsystems, using the Configuration Parameters and Configuration Requirements as technical specifications and metrics to select the components. Employ analytical expressions that relate the operation features of components to the motion parameters, leading the selection of components to be the Tool and Deployment subsystems.

- For the Locomotion subsystem, analyze the and Configuration Requirements and the Configuration Parameter, using engineering principles to determine the type of mobile artifact for embodying the respective motion. Whereas, a geometric analysis investigates the stability pose of the vehicle to provide the vehicle dimensions.

- Identify the kinematics requirements to improve the positioning estimation, the control performance, and the perception parameters, using a parametric comparison of different steering mechanisms (e.g, the Ackermann and Articulated vehicles) under the expected conditions of operation.

- Define the sensor requirements to minimize the positioning uncertainty of the selected vehicle, keeping the uncertainty propagation within certain boundaries. Simulate the expected sensor uncertainty to determine the type and number of sensors and landmarks needed for the achievement of the task.

- Instantiate the subsystems and modules of the robotic vehicle configuration to implement the Basic Configuration with the selected components, whose technical specifications are mapped into the Component Requirements.

- Analyze the Components Requirements for the actuation and sensing of the selected components to complete the Autonomous Vehicle configuration.

- Integrate the entire components for the synthesis of the Autonomous Vehicle prototype that performs the assigned task with certain degree of autonomy.

Chapter 4

Development

Challenging applications for AVs are in demanding environments that involve from just scientific research to industrious tasks. In agriculture, construction, and mining applications, AVs are required to improve the operator skills and to increase the productivity and safety by removing these operators from hazardous conditions of work [Corke 99] [Gambao 02] [Pilarski 02]. This chapter addresses a survey of the systematic framework, developing the synthesis of an Autonomous Vehicle configuration to perform an underground mining task. This task was requested expressly by Industrias Peñoles, S.A. de C.V., an important mining company in Mexico [Peñoles 04]. In this chapter, the framework is applied from the abstraction of the assigned task and the mining environment to the analysis of components, providing a configuration with the sufficient specifications to build the robotic system. Since these results, two vehicle configurations are detailed and implemented in the next chapters. The first configuration, discussed in the chapter 5, is a viable solution using available components; whereas, the second solution is formulated in the chapter 8, with the results of the autonomy analysis developed in the chapters 6 and 7.

4.1 Study Case: The Tunnel-Profiling Task

The tunnel-profiling is a periodical task carried out in the underground mining from the construction of the tunnels. The task consists of determining the dimensions and contour (or three dimensional characteristics) of the tunnel profiling by the measurements of distances, directions, and elevations of their walls. In addition to this tunnel surveying, the task includes the processing of the information and its digital displaying. This information can be used for detect changes in tunnel geometry, estimation of extracted material, monitoring progress of excavation, and collection of drawings inventory, allowing the mining engineers settle down the actions for the work to be done. Thus, this mine survey must update permanently, not only for production reasons but also caution ones, since tunnels undergo continuous modifications by the material extraction and landslide.

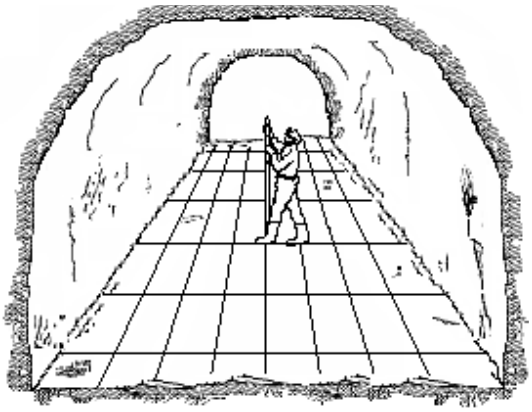

Figure 4.1: **Miner makes the Tunnel-Profiling Task**

Although there exist many different methods and instruments to acquire tunnel-profile data of structures such as tunnels, some more successfully than others, having different impact on speed, accuracy, range, and costs of operation [Bickel 82, Clarke 92, McCormac 99]. Actually in Peñoles mines, specialized miners make the operation manually utilizing traditional tools, such as level instrument, rules, steel or fiberglass tapes, compass, and in same case theodolites to collect data of the wall section of the tunnels.

The workers draw a grid over the corridor (a network of horizontal and vertical spaced lines at particular distances), the intersection of such lines provide coordinates for locating the elevation of wall such as is shown in Figure 4.1. Then, the miners measure and record the information on paper, which is introduced to a digital computer for generating the tunnel profiling. Thus, the miners are exposed to hard environmental conditions, such as extreme temperature, high relative humidity, toxic vapors, the possibility of rock fall, and so on [Potvin 01]. Moreover, using current way to perform the tunnel profiling it becomes a slow process and scarce accuracy, because of the human, instruments, and nature errors. To improve the current process for gathering data (both precise and accurate), a robust system that allows obtaining the profile of the mine with greater rapidity and safety is required.

4.2 Systematic Framework

The systematic framework is applied to synthesize the configuration of the robotic system that carries out the tunnel-profiling task. The robotic vehicle will become a specific Mining Autonomous Vehicle (MAV) that should be generated without a predefined configuration or an existing design. The following sections outline the synthesis process addressed to configure the MAV from well defined specifications of the task and the environment.

Task Specifications

Providing the profile of the tunnel walls is the objective of the task. The elevation of the walls must be obtained at least every 2 meters along of the tunnel corridors, with a resolution at least 10 centimeters among measurements on the walls. The data must be displayed and record digitally, e.g. by means of a computer. The time to achieve the task should be less than the miner's time, which is about 2 hours for a corridor so long as 50 meters.

Environment Specification

The type of mines where the task must be achieved is a network of tunnels at different level of deep connected by ramps to access the work places. The cross section of the tunnels is 3.5 m × 3.0 m, i.e. a small tunnel category; whereas the length of tunnel varies from 100 meters up to a pair of kilometers. The terrain is semi structured, since the mines are on active production, transporting the ore through heavy machines such as Load Haul Dump (LHD) vehicles that compact the floor. Beside the terrain is reinforced with a clay soil (called Tepetate). There is a distribution of rocks with an average height about 10 cm and holes with a depth less than 10 cm. The temperature into the tunnels varies from 10 °C to 40 °C, and a relative humidity between 60% and 85%.

4.3 System Abstraction

4.3.1 Configuration Requirements

The tunnel-profiling task (TPT) needs to make measurements of the tunnel distances, directions, and elevations through the MAV, a robotic system that must satisfy the list of quantitative and qualitative Task/Environment Specifications. All this information is mapped to Configuration Requirements (Table 4.1), which serves to relate the components that will integrate the configuration of the MAV, to be designed around these task and environment specifications, such as the task performance required and the environment dimensions.

The Configuration Requirements are expressed as free quantifiers of variables that can be filled with inequalities on algebraic expressions; for example, the values for the width dimension are expressed as:

$$\begin{aligned} \text{width\_tunnel} &\leq 4.0\,\text{m} \\ 3.0\,\text{m} &\leq \text{width\_tunnel} \end{aligned}$$

establishing a maximum value up to 4 m and a minimum value of 3 m for the width of the tunnel. Whereas, a constraint is related to the use of fuel, in this case ¬fuel which is read as No fuel, this is to avoid air contamination.

Table 4.1: **Configuration Requirements**

Task/Environment Specifications	**Configuration Requirements**
Task	
Measurement Accuracy less than ± 5 cm	accuracy_measured $\leq \pm$ 0.05 m $\Rightarrow$ accuracy_measured $\leq$ 0.05 m -0.05 m $\leq$ accuracy_measured
Measurement Resolution less than 1 cm	resolution_measured $\leq$ 0.01 m
Sampling Resolution less than 10 cm on the walls	sampling_resolution $\leq$ 0.10 m
Sampling Interval equal to 2 m along the tunnel	sampling_interval $\leq$ 2.00 m
Time Task less than 2 hours to cover 50 m of the tunnel length	task_time $\leq$ 2 h $\Rightarrow$ 2 h $\leq$ run_time sampling_time_interval $\leq$ 277 s
Environment	
Tunnel Height equal to 3.0 m ± 0.25 m irregularities	height_tunnel $\leq$ 3.00 m ± 0.25 m $\Rightarrow$ height_tunnel $\leq$ 3.25 m 2.75 m $\leq$ height_tunnel
Tunnel Width equal to 3.0 m ± 0.50 m irregularities	width_tunnel $\leq$ 3.5 m ± 0.5 m $\Rightarrow$ width_tunnel $\leq$ 4.00 m 3.00 m $\leq$ width_tunnel
Tunnel Length more than 50 m and less than 500 m	50 m $\leq$ length_tunnel $\leq$ 500 m $\Rightarrow$ length_tunnel $\leq$ 500 m 50 m $\leq$ length_tunnel
Ceiling Elevation from 1 m above the floor level	1 m $\leq$ elevation_ceiling
Terrain: Lean clay soil Muddy up to 22% Rock height up to 10 cm A concentration up to 3.7 rocks per square meter	 lean_clay moisture_soil $\leq$ 22 % height_rock $\leq$ 0.10 m distribution_rock $\leq$ 3.7 rocks/m^2 $\Rightarrow$ 0.10 m $\leq$ ground_clearance

Table 4.1: **(continued)**

Task/Environment Specifications	**Configuration Requirements**
Hole diameter and depth up to 10 cm A concentration up to 2.5 holes per square meter	height_hole $\leq$ 0.10 m depth_hole $\leq$ 0.10 m distribution_hole $\leq$ 2.5 holes/m^2 $\Rightarrow$ 0.10 m $\leq$ diameter_clearance
Slopes between 10° and 20°	slope $\leq$ 20 ° 10 ° $\leq$ slope
Environmental Temperature between 10 ° and 40 °C	temperature $\leq$ 40 °C 10 °C $\leq$ temperature
Environmental Relative Humidity between 60% and 85%	humidity $\leq$ 85% 60% $\leq$ humidity
Constraints	
Information computing (Acquisition and Manipulation)	digital
Power: No fuel (combustible)	$\neg$ fuel
Operation: Autonomous Control	autonomous
Communication: Wireless	wireless_link

These Configuration Requirements also allow the derivation of other requirements through an iterative procedure during the synthesis process of the MAV, the objective is to state Configuration Requirements in as much detail as is possible. For instance, the sampling time per each interval is computed by the time of task required to cover a distance equivalent to 50 m at interval of the sampling, which is as:

$$\begin{aligned} \text{intervals} &= \frac{50\text{ m}}{\text{sampling\_interval}} + 1 \\ \text{intervals} &= 26 \\ \text{sampling\_time\_interval} &= \frac{\text{task\_time}}{\text{intervals}} \\ \text{sampling\_time\_interval} &= 277\,\text{s} \end{aligned}$$

As a requirement from Peñoles, in this exercise only the tunnel walls has been considered until 1 meter over the floor; i.e., mainly the ceiling of the tunnel expressed as the quantifier elevation_ceiling.

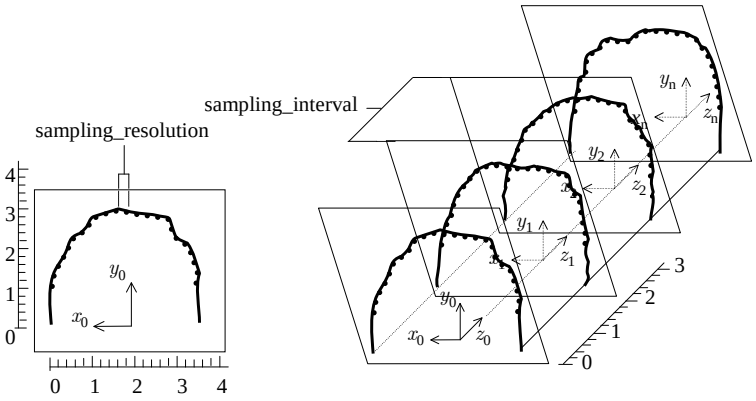

(a) Vertical plane xy (b) Vertical planes xy throughout z axis

Figure 4.2: **Tunnel-profiling task integrates a 3-D workspace generated by the vertical planes xy, a set of measured points at sampling_resolution on the wall (a), throughout a third z-axis along the tunnel at sampling_interval (b).**

4.3.2 Geometric Description

The TPT is physically interpreted as the dimensional estimation of the mine volume, determined by the measurements of distances, directions, and elevations. These measured data are expressed geometrically in a space of three dimensions (3-D). This 3-D space is described by means of a system of coordinates, in which vertical planes xy in two dimensions are integrated with a set of measured points over and around the wall as is shown in Figure 4.2a; i.e., the profile of the wall for a particular position of the tunnel. Then, the complete profile the tunnel is conformed by the generation of these planes xy throughout a third z-axis at regular distance intervals along it, which is illustrated in Figure 4.2b.

Therefore, the TPT is described as the construction of referenced vertical planes 2D into a coordinates system 3-D. This functional identification of the task is followed by a formal abstraction of the task and the environment formulated as a Geometric Description where compositions of motions must be generated and analyzed to perform the assigned task.

This Geometric Description is formulated through the CSG solid modeling technique, representing the physical shape of the TPT abstraction (Figure 4.2) as a generic mining tunnel, which is made through the Boolean operations and basic motion of instantiated standard primitives of respective dimensions such as box and ellipses. These dimensions are based on the Configuration Requirements.

Three standard primitives are needed to represent the generic tunnel, two boxes and one ellipse. The boxes and ellipse are specified as $box(5, 5, 50)$, $box(5, 0.5, 50)$, and $ellipse(2, 3.25, 50)$, these dimensions correspond to the minimum long of the tunnel (50 m $\leq$ length_tunnel), and a cross section that matches the maximum height and

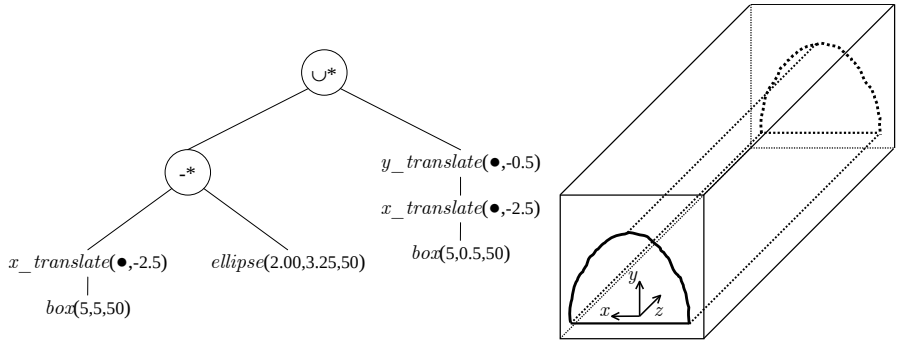

Figure 4.3: **Geometric Description for the tunnel-profile task. The generic tunnel representation includes the Boolean operations, basic motions, and the standard primitives with respect to a common coordinate frame.**

width of the tunnel (height_tunnel $\leq$ 3.25 m and width_tunnel $\leq$ 4.0 m, respectively). The Geometric Description of the tunnel is drawn as a tree, as shown in Figure 4.3.

The tree representation includes the set of operations and motions executed on each one of the instantiated primitives. The boxes only are used to limit the tunnel-profile task within 3-D space. Due to the real tunnel has no even walls is need to include this characteristic in its Geometric Description; therefore, the standard primitives are generated by Right Straight Homogeneous Generalized Cylinder RSHGC models. Towards this goal, a factor ε is introduced to the cross function for producing the variations on the solid superficies, which were included in the Configuration Requirements. This factor is generated randomly, and is added in the function of the cross section 2D area, which is swept along a linear path normal to the plane of the area to create the standard primitive. The representation of the tunnel is shown in Figure 4.4. The complete derivation of the Geometric Description is developed in the Appendix A.

4.4 System Analysis

4.4.1 Motion Compositions

This framework phase consists of the composition of possible configurations, considering exclusively the motions and their reachable configuration space, abstracting their physical or mechanical structure. The parameters to consider in this process are the number of DOF that depends strongly on the available knowledge to perform the task, which are captured as the abstraction of the task.

The TPT is obtained in a 3-D workspace. Thus, the analysis begins with the combination of three basic motions to reach each one of the points to measure and provide the tunnel profile. These motions could be prismatic (P) or rotational (R), each one of these motions is identified by a sub index i, according with its order into the composition. The following composition process addressed to formulate viable solutions.

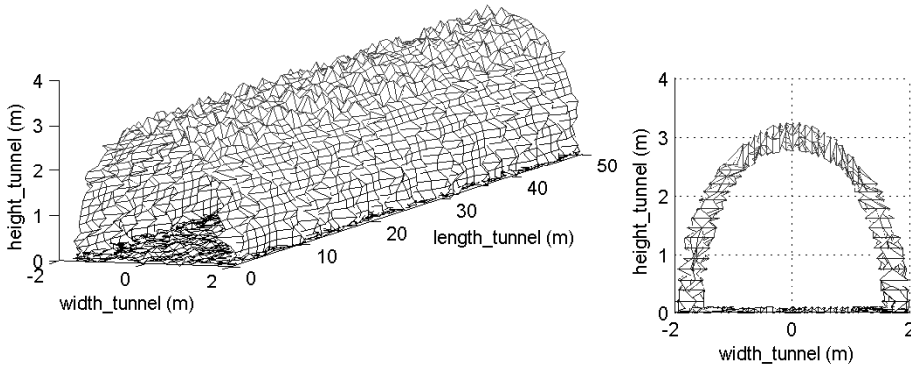

Figure 4.4: **Geometric Description of the tunnel with no even walls. This characteristics is generated by RSHGC technique, introducing an error factor ε equal to irregularities of the tunnel.**

Composition $P_1P_2P_3$:

The first composition considers three translational displacements PPP: The motion P_1 is horizontal to reach the tunnel interior, P_2 is also horizontal to cover the tunnel wide; motion P_3 is vertical to reach any point in the wall, according to the positions that keep previous displacements. The range that should reach P_1 is exactly the tunnel length, whereas the operation range of P_2 is the tunnel width and finally the range of P_3 is the tunnel height requirements. The array origin is the left-down extreme of the tunnel. In Figure 4.5 are shown the composition and its C-space that is generated on the Geometric Description of the tunnel with the Configuration Requirements as metric to relate the operation range of each one of the motions.

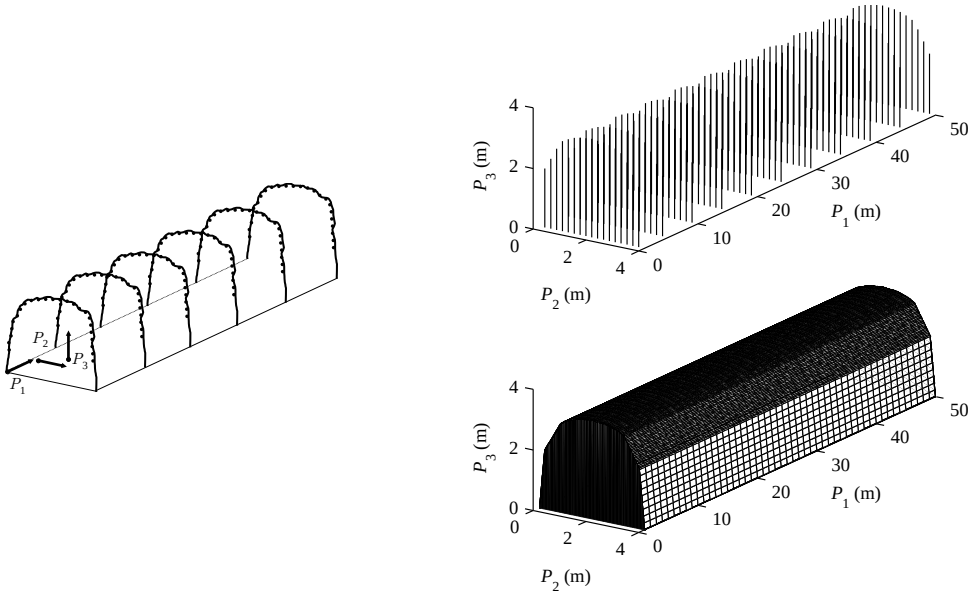

Figure 4.5: **Composition $P_1P_2P_3$, (left) the composition origin, (top) its discrete C-space, and (bottom) the continuous C-space.**

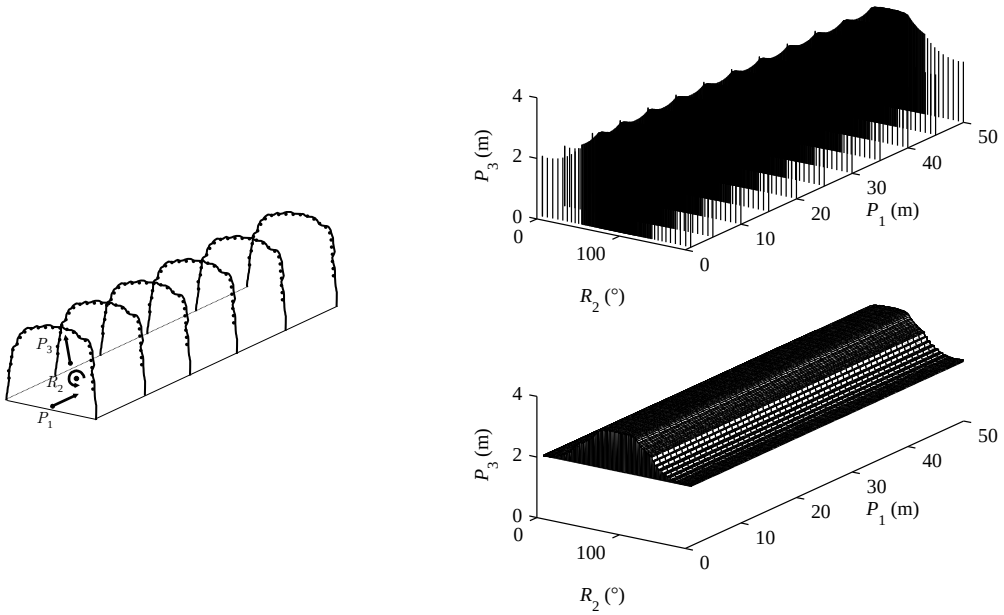

Figure 4.6: **Composition $P_1R_2P_3$, (left) the composition origin, (top) its discrete C-space, and (bottom) the continuous C-space.**

Composition $P_1R_2P_3$:

The second motions array to formulate is a PRP, which consists of a horizontal motion P_1 addressed towards the tunnel interior; followed by a rotational motion R_2 that serves to orient the last motion P_3, which is a linear displacement. This composition of motions has as its origin the middle of the tunnel width at floor level. The range that should reach P_1 is the tunnel length; the rotation operation range of motion R_2 is 180° to reach any point on the perimeter of the tunnel wall. Finally the range of P_3 is between the width half of the tunnel and its height. These motions and their C-space are shown in Figure 4.6.

Composition $R_1P_2P_3$:

The third composition consists of an array RPP. In this case, the origin of this composition is situated in middle of the tunnel for both its length and its width. The composition initiates with a rotary motion R_1, the second element is a prismatic motion P_2 to place the third motion towards the points of sampling. This latter motion is a linear displacement P_3. The range that should reach R_1 is a turn up to 180°. The second motion P_2 has an operation range about the tunnel half-length. The range for motion P_3 is between the tunnel half-width more a capacity to develop a forward displacement as well as a backward. The Figure 4.7 displays these motions and their respective C-space.

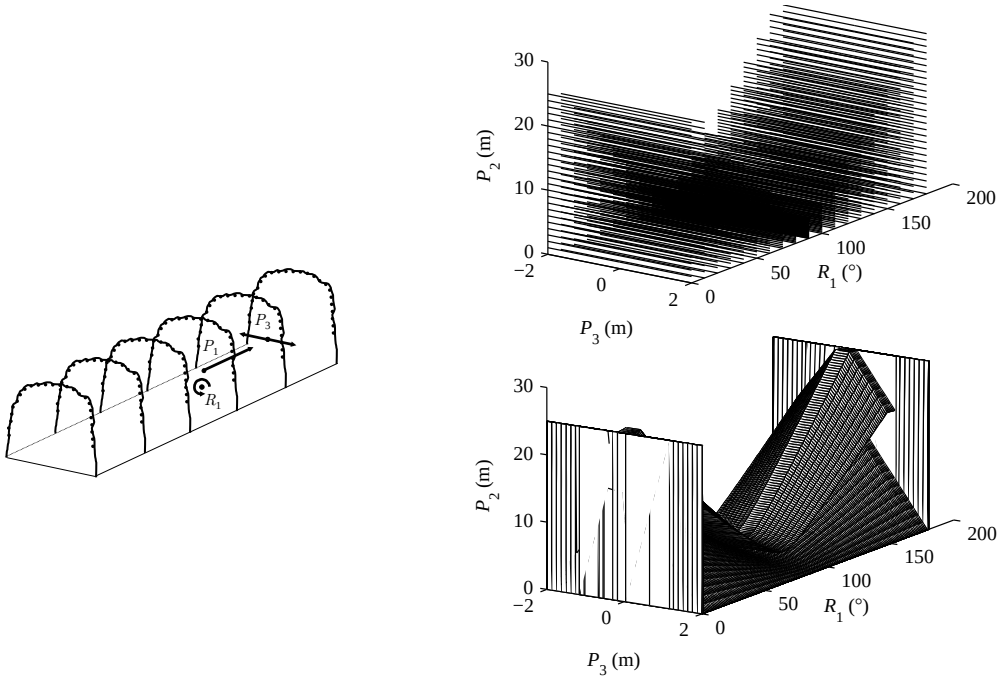

Figure 4.7: **Composition $R_1P_2P_3$, (left) the composition origin, (top) its discrete C-space, and (bottom) the continuous C-space.**

Composition $R_1R_2P_3$:

A fourth set of motions generates a composition RRP. The origin of this composition is located at middle of the tunnel (both length and width, similar as above composition $R_1P_2P_3$). The first motion R_1 is a rotational movement and its range should reach a turn up to 180°; in fact, it could be up to 360°. The second motion R_2 is also rotational to deployed the third motion, which should be oriented towards the sampling points through this prismatic motion P_3. The second motion R_2 has an operation range equivalent to 180°, but this motion requires a radius equal to the tunnel half-width. The P_3 range presents the identical characteristics that the motion P_3 in the composition $R_1R_2P_3$. The Figure 4.8 displays this composition and it's C-space.

Composition $R_1R_2R_3$:

This fifth alternative is formulated just by rotational motions; i.e. an array RRR. In this composition, its origin is situated in middle of the tunnel width on the tunnel enter. The motion R_1 together the motion R_2 are to place the third motion R_3 towards the sampling points. The range of the motion R_1 is 180°. The second motion R_2 also has an operation range of 180° and a link to cover a radius equal or less than tunnel half-width (in this analysis is 1.866 m). The range of motion R_3 is a full turn 360° with a link less than tunnel half-width (in this analysis is 0.7 m). In Figure 4.9 are shown the composition of these motions and their formed C-space.

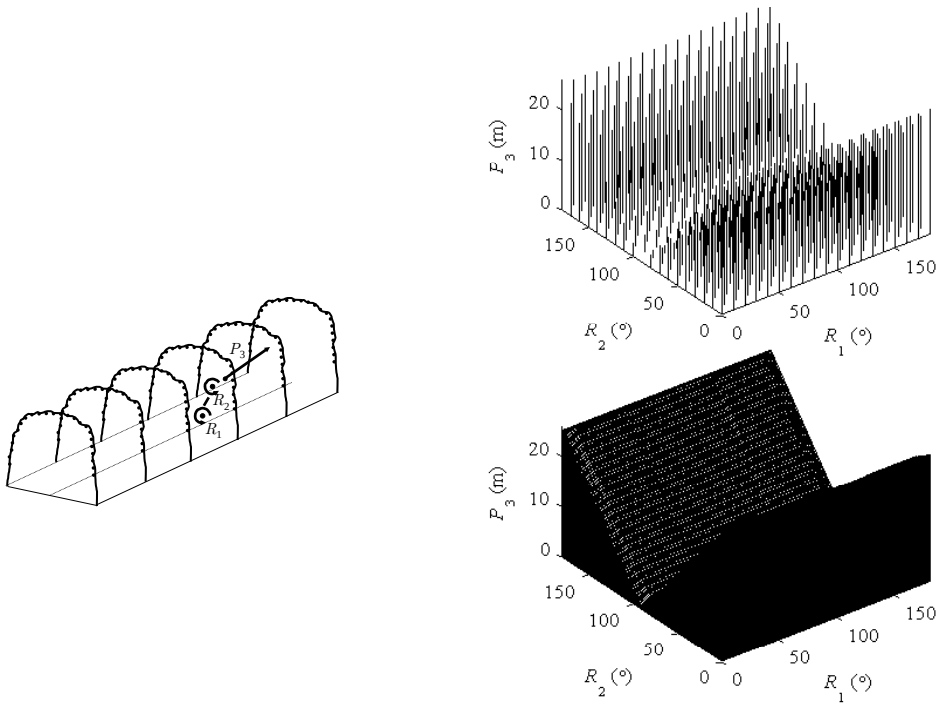

Figure 4.8: **Composition $R_1R_2P_3$, (left) the composition origin, (top) its discrete C-space, and (bottom) the continuous C-space.**

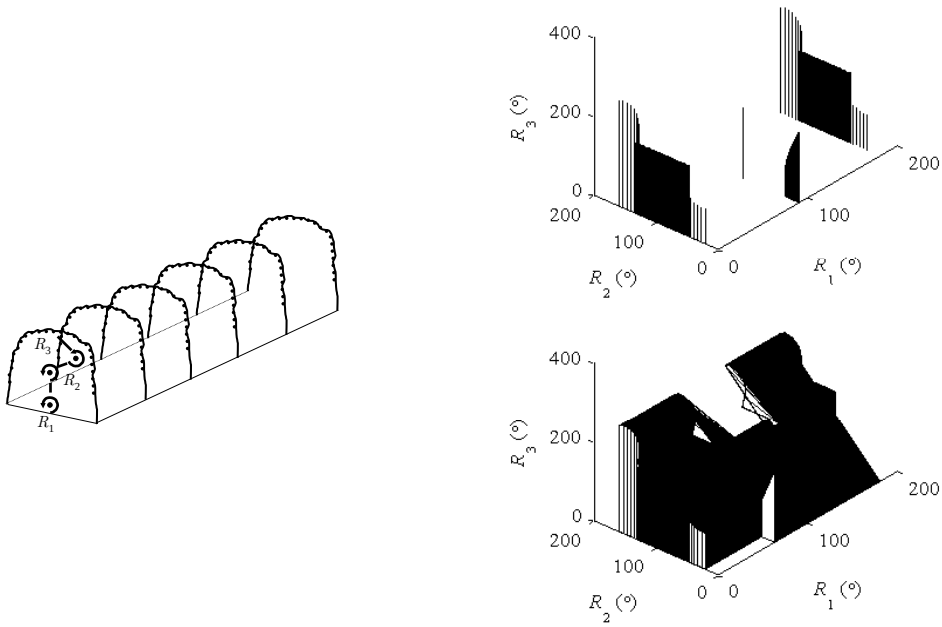

Figure 4.9: **Composition $R_1R_2R_3$, (left) the composition origin, (top) its discrete C-space, and (bottom) the continuous C-space.**

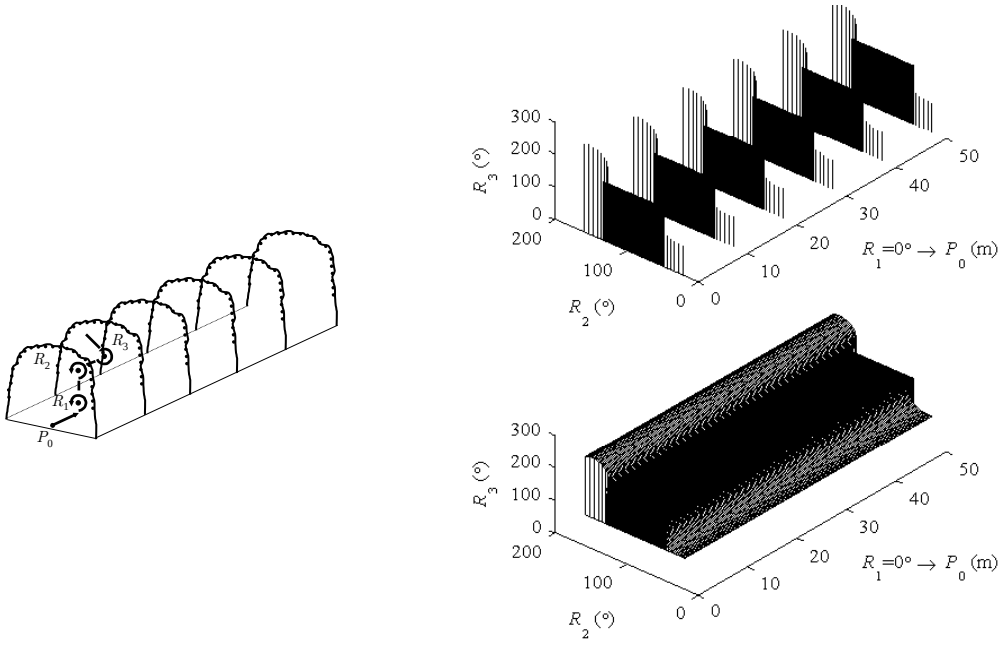

Figure 4.10: **Composition $P_0R_1R_2R_3$, (left) the composition origin, (top) its discrete C-space, and (bottom) the continuous C-space.**

Composition $P_0R_1R_2R_3$:

The sixth alternative generated is properly the composition $R_1R_2R_3$ attached to a prismatic motion P_0, which is located at beginning of the motions. Thus the transformation starts with this prismatic motion P_0 to reach complete the length of the corridor. From the second to fourth motion are $R_1R_2R_3$, such as above described. In this case, the origin of this composition is situated in middle of the tunnel width on the tunnel enter. The motion P_0 is horizontal to reach the tunnel interior, thus its operation range is exactly the tunnel length. The operation ranges of the motions R_2 and R_3 are as aforementioned; whereas the range of the motion R_1 is reduced to a value (0°). Figure 4.10 depicts this four-DOF composition and its C-space.

4.4.2 Configuration Templates

Each one of the identified compositions is one entrance for the Configuration Template, which is an evaluation table with the specifications of each composition generated. The following analysis addresses the fulfillment through a parametric decomposition of the primitive motions that build the composition. This examination includes the number of DOF, the metrics of operation range, technical specifications, constraints, and the C-space formulation. This analysis allows quantifying each composition and determining its ability to perform the task.

Composition $P_1P_2P_3$:

The composition $P_1P_2P_3$ is formulated by three prismatic motions; each one is developed on an axis whose order of application describes a Cartesian space. The first motion or DOF P_1 should move lineally from 0 m to 50 m and it should carry the rest of motions along this range. This is a parametric specification that is related to the operator of translation $P_1(z, d_1)$, i.e., the variable d_1 developed along of the z-axis. In addition, there exists a constraint with reference to the capacity of payload for this motion, denoted by $P_{1\_payload}$, to support the weight of the rest of motions, expressed as P_{2_weight} and P_{3_weight}. Thus, this constraint $P_{1\_payload}$ depends of the variables P_{2_weight} and P_{3_weight}. The both conditions operation range and constraint are mapped into the composition specification column of the Configuration Template (Table 4.2).

The second prismatic motion is adjusted to an operation range from 0 m to 4 m to reach the tunnel width, which is associated to the following translation operator $P_2(z, d_2)$. It should support the weight of the last motion P_{3_weight}; i.e., a constraint where $P_{3\_weight} \leq P_{2\_payload}$.

The motion P_3 is a lineal displacement to reach properly the points on the wall, and it requires an operation range between 0 m and 3.25 m under the translation operator $P_3(z, d_3)$. The latter motion has no a constraint with respect to its payload capacity. All these features are mapped to the composition specifications, respectively.

A parametric analysis over the effective displacement of each motion serves to define the span of operation required. This characteristic is addressed by the number of variants or instances that a motion develops to perform the task. It can be seen as the histogram in which the motion varies. Figure 4.11 depicts the operation spans for all the motions of the composition $P_1P_2P_3$. The results are included to the Composition Template.

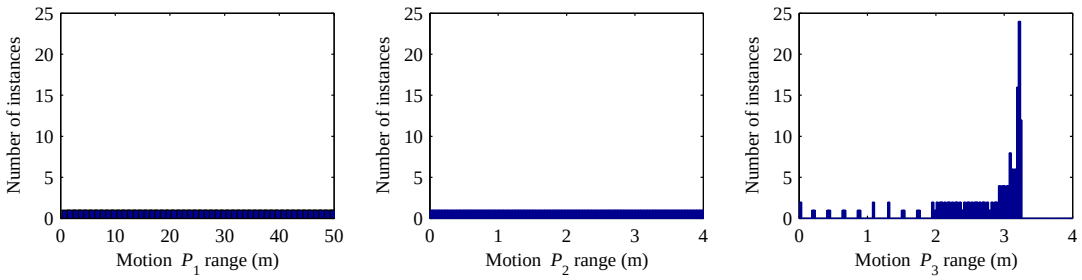

Figure 4.11: **Span histograms for the composition $P_1P_2P_3$. These histograms show the total displacement distribution in the composition to perform the task.**

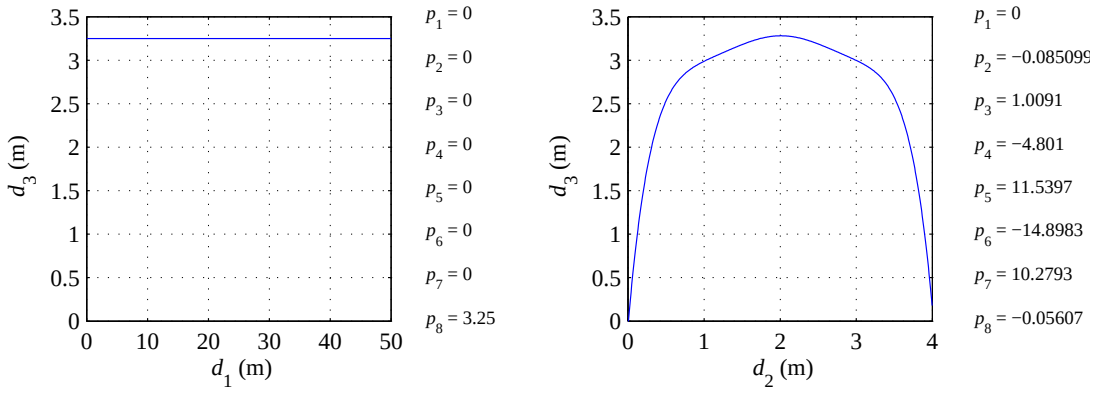

Figure 4.12: **Approximation functions $f(d_1,d_3)$ and $f(d_2,d_3)$ to formulate the composition $P_1P_2P_3$.**

The framework considers the C-space Formulation as another element to analyze the configuration. An analysis of the representative curves of this C-space is developed through a polynomial function to approximate the curves generated between the two motions.

This polynomial function $p(x)$ of degree n fits the data of the motions in a least-squares approximation, which is expressed as

$$p(x) \quad = \quad p_1 x^n + p_2 x^{n-1} + \cdots + p_n x + p_{n+1}$$

where p_i are the coefficients. The order of the powers is associated to the simplicity of the C-space; i.e., the simplicity of the composition.

In this case, the C-space of the composition $P_1P_2P_3$ can be formulated by the functions $f(d_1,d_3)$ and $f(d_2,d_3)$, that are the representative curves between the motions P_1 and P_3, and between P_2 and P_3. Figure 4.12 shows these curves and the coefficients found in an approximating polynomial of degree allowed $n = 7$. For the function $f(d_1,d_3)$, the formulation is a constant $p_8 = 3.25$ therefore the order is zero; whereas the formulation of the function $f(d_2,d_3)$ is approximated up to a power x^6 since the coefficient $p_2 = -0.08$.

To complete the geometric analysis of the C-space, the framework use a fourth order B-Spline approximation for the function $f(d_1,d_2,d_3)$, quantifying the coefficients as a metric of the simplicity for the composition to perform the task. The result is shown in the Figure 4.13.

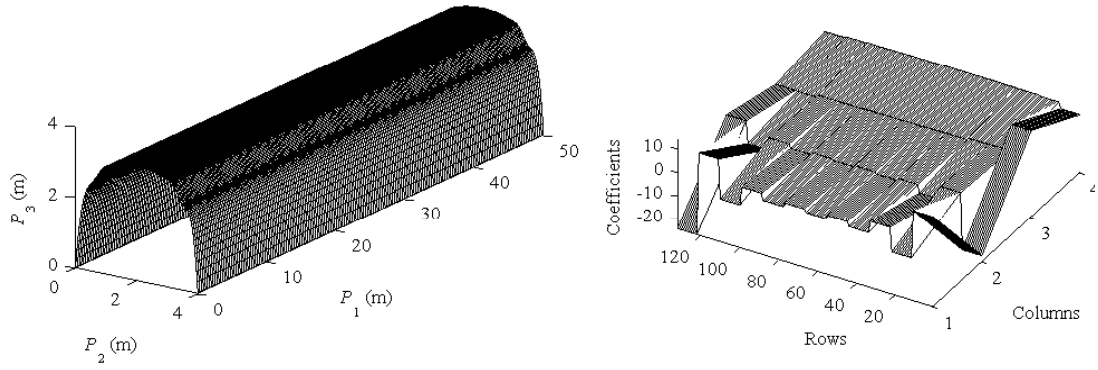

Figure 4.13: **Spline approximation functions $f(d_1,d_2,d_3)$ to formulate the composition $P_1P_2P_3$ (left) and its coefficients (right).**

Table 4.2: **Configuration Template $P_1P_2P_3$**

Template	Range	Specifications	C-space Formulation
$P_1P_2P_3$	P_1 [0,50]	P_1 (z,d_1):	
3 DOF		0 m $\leq d_1 \leq$ 50 m	$d_1 \leq$ 50 m
			0 m $\leq d_1$
			50 m $\leq$ span_d_1
		P_2_weight+P_3_weight $\leq$ P_1_payload	
	P_2 [0,4]	P_2 (z,d_2):	
		0 m $\leq d_2 \leq$ 4 m	$d_2 \leq$ 4 m
			0 m $\leq d_2$
			4 m $\leq$ span_d_2
		P_3_weight $\leq$ P_2_payload	
	P_3 [0,3.25]	P_3 (z,d_3):	
		0 m $\leq d_3 \leq$ 3.25 m	$d_3 \leq$ 3.25 m
			0 m $\leq d_3$
			3.25 m $\leq$ span_d_3
			f(d_1,d_3): 0
			f(d_2,d_3): 6
			f(d_1,d_2,d_3): Coefficients*

* Fig.4.13

Composition $P_1R_2P_3$:

The C-space described by the composition $P_1R_2P_3$ is cylindrical space. Its first motion P_1 should execute a operation range from 0 m to 50 m and it is constrained by the weight of the rest of motions R_{2_weight} and P_{3_weight}. The second motion R_2 develops an operation range from 0° to 180°, which is associated to the following rotational operator $R_2(z, \theta_2)$. It should support the weight of the last motion P_{3_weight}; i.e., a constraint where $R_{3\_weight} \leq P_{2\_payload}$. The third motion P_3 is to reach the points on the wall, requiring an operation range between 0 m and 3.25 m under the translation operator $P_3(z, d_3)$. This motion has no a constraint with respect to its payload capacity.

Figure 4.14 depicts the operation spans for all the motions of the composition $P_1R_2P_3$; whereas the approximation functions are shown in the Figure 4.15 and Figure 4.16. All the results are included to the Composition Template Table 4.3.

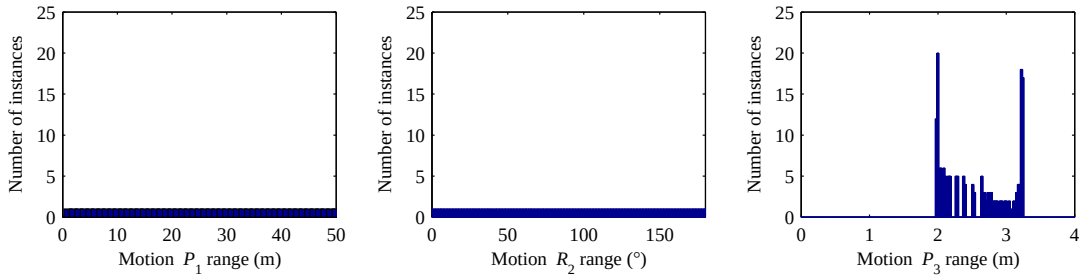

Figure 4.14: **Span histograms for the composition $P_1R_2P_3$. These histograms show the total displacement distribution in the composition to perform the task.**

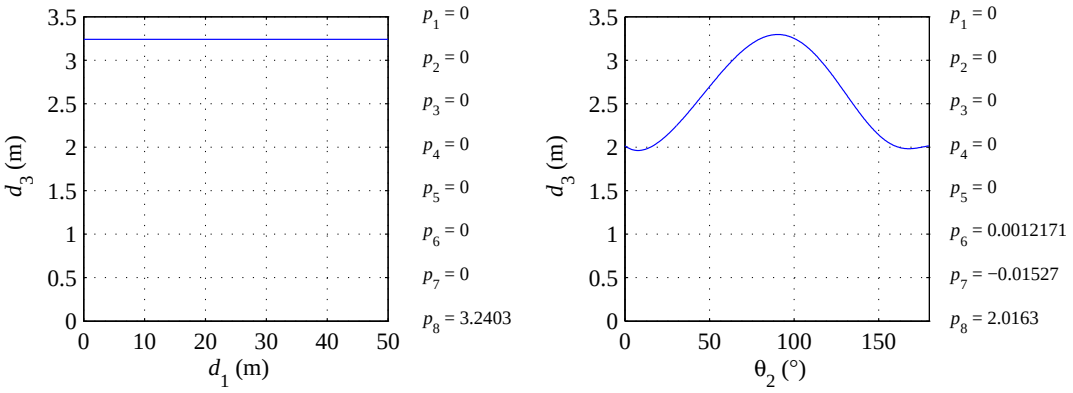

Figure 4.15: **Approximation functions $f(d_1,d_3)$ and $f(\theta_2,d_3)$ to formulate the composition $P_1R_2P_3$.**

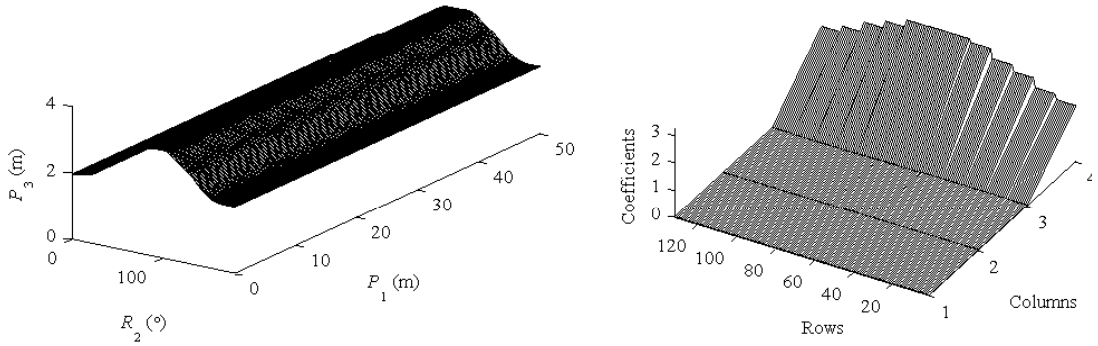

Figure 4.16: **Spline approximation functions $f(d_1,\theta_2,d_3)$ to formulate the composition $P_1R_2P_3$ (left) and its coefficients (right).**

Table 4.3: **Configuration Template $P_1R_2P_3$**

Template	Range	Specifications	C-space Formulation
$P_1R_2P_3$	P_1 [0,50]	P_1 (z,d_1):	
3 DOF		0 m $\leq d_1 \leq$ 50 m	$d_1 \leq$ 50 m
			0 m $\leq d_1$
			50 m $\leq$ span_d_1
		R_2_weight+P_3_weight $\leq$ P_1_payload	
	R_2 [0°,180°]	R_2 (z,θ_2):	
		0° $\leq \theta_2 \leq$ 180°	$\theta_2 \leq$ 180°
			0° $\leq \theta_2$
			180° $\leq$ span_θ_2
		P_3_weight $\leq$ R_2_payload	
	P_3 [0,3.25]	P_3 (z,d_3):	
		0 m $\leq d_3 \leq$ 3.25 m	$d_3 \leq$ 3.25 m
			2 m $\leq d_3$
			1.25 m $\leq$ span_d_3
			f(d_1,d_3): 0
			f(θ_2,d_3): 2
			f(d_1,θ_2,d_3): Coefficients*

* Fig.4.16

Composition $R_1P_2P_3$:

In the composition $R_1P_2P_3$, the first motion R_1 is associated by the following rotational operator $R_1(z, \theta_1)$. The quantifier θ_1 should execute a operation range from 0° to 180°; for this motion there exists a constraint because of the weight of the rest of motions P_{2_weight} and P_{3_weight}. The second motion P_2 should develop a range of operation from 0 m up to 25.2 m, which is associated to the following translational operator $P_2(z, d_2)$. It needs to support the weight of the last motion P_{3_weight}; i.e., a constraint where $P_{3\_weight} \leq P_{2\_payload}$. The third motion P_3 is to reach the points on the wall and requires an operation range between 0 m and 4 m. This range should be formed by a forward displacement and a backward displacement, thus the range can be ranged from -2 m to 2 m, under the translation operator $P_3(z, d_3)$. This latter motion has no a constraint with respect to its payload capacity.

Figure 4.17 depicts the motion spans of this composition; whereas the approximation functions are shown in the Figure 4.18 and Figure 4.19, respectively. The results are summarized in the Composition Template Table 4.4.

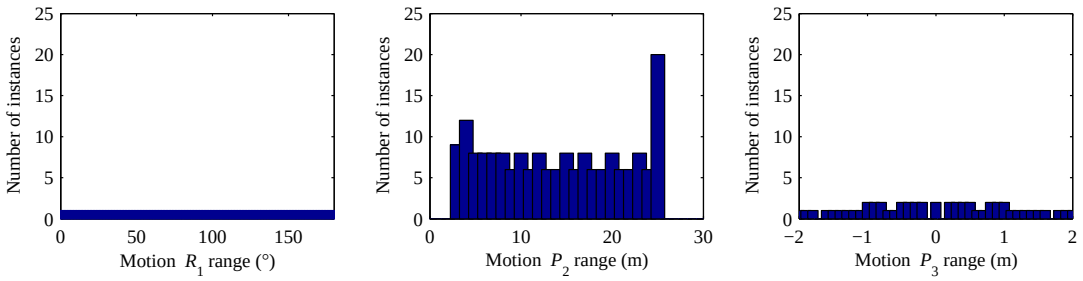

Figure 4.17: **Span histograms for the composition $R_1P_2P_3$. These histograms show the total displacement distribution in the composition to perform the task.**

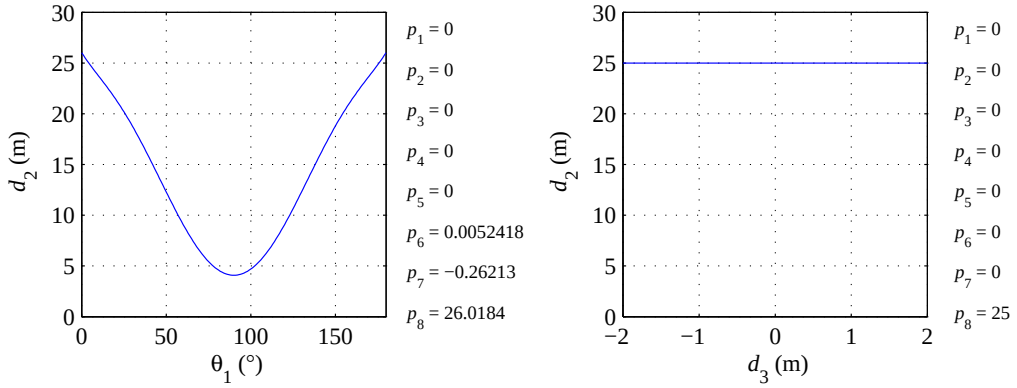

Figure 4.18: **Approximation functions $f(\theta_1,d_3)$ and $f(d_2,d_3)$ to formulate the composition $R_1P_2P_3$.**

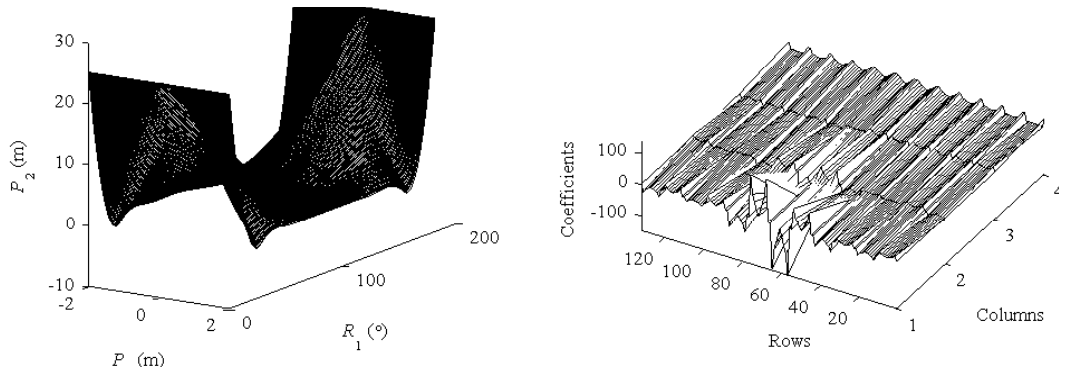

Figure 4.19: **Spline approximation functions $f(\theta_1,d_2,d_3)$ to formulate the composition $R_1P_2P_3$ (left) and its coefficients (right).**

Table 4.4: **Configuration Template $R_1P_2P_3$**

Template	Range	Specifications	C-space Formulation
$R_1P_2P_3$	R_1 [0°,180°]	R_1 (z,θ_1):	
3 DOF		$0° \leq \theta_1 \leq 180°$	$\theta_1 \leq 180°$
			$0° \leq \theta_1$
			$180° \leq$ span_θ_1
		P_2_weight+P_3_weight $\leq R_1$_payload	
	P_2 [0,25.5]	P_2 (z,d_2):	
		0 m $\leq d_2 \leq$ 25.5 m	$d_2 \leq$ 25.5 m
			0 m $\leq d_2$
			25.5 m $\leq$ span_d_1
		P_3_weight $\leq P_2$_payload	
	P_3 [0,4]	P_3 (z,d_3):	
		-2 m $\leq d_3 \leq$ 2 m	$d_3 \leq$ 2.0 m
			-2.0 m $\leq d_3$
			4.0 m $\leq$ span_d_3
			f(θ_1,d_2): 2
			f(d_2,d_3): 0
			f(θ_1,d_2,d_3): Coefficients*

* Fig.4.19

Composition $R_1R_2P_3$:

The composition $R_1R_2P_3$ includes as first motion R_1 a rotation that should turn a range from 0° to 180° and associated by the rotational operator $R_1(z, \theta_1)$. The constraint of this motion is denoted as $R_{2\_weight} + P_{3\_weight} \leq P_{3\_payload}$. The second motion R_2 also has to develop a rotation from 0° to 180°, and it is associated to the following operator $R_2(z, \theta_2)$. It requests a payload to support the weight of the last motion P_{3_weight}. The last motion P_3 involves an operation range about 25 m to reach the points on the wall. This motion is without constraint with respect to its payload capacity.

The plotted histograms of the motion spans are shown in Figure 4.20; the approximation functions are shown in the Figure 4.21 and Figure 4.22. The Composition Template Table 4.5 shows the results.

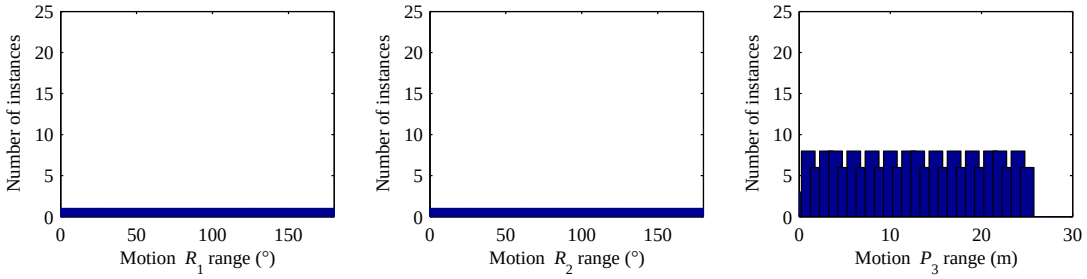

Figure 4.20: **Span histograms for the composition $R_1R_2P_3$. These histograms show the total displacement distribution in the composition to perform the task.**

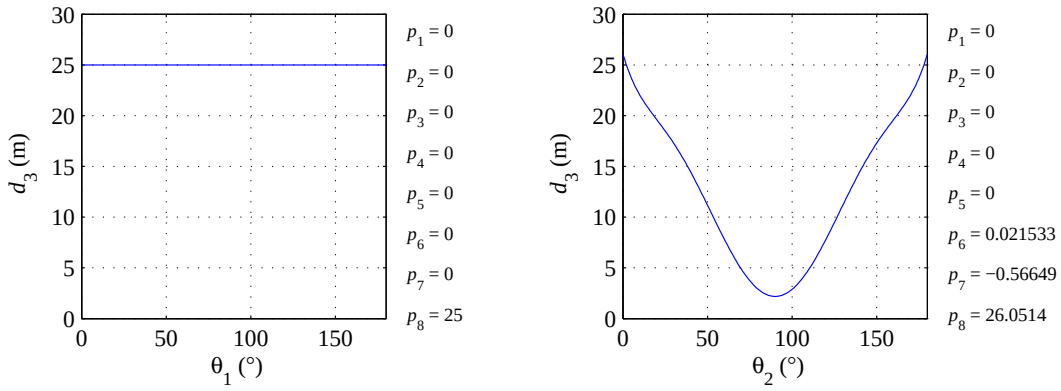

Figure 4.21: **Approximation functions $f(\theta_1,d_3)$ and $f(\theta_2,d_3)$ to formulate the composition $R_1R_2P_3$.**

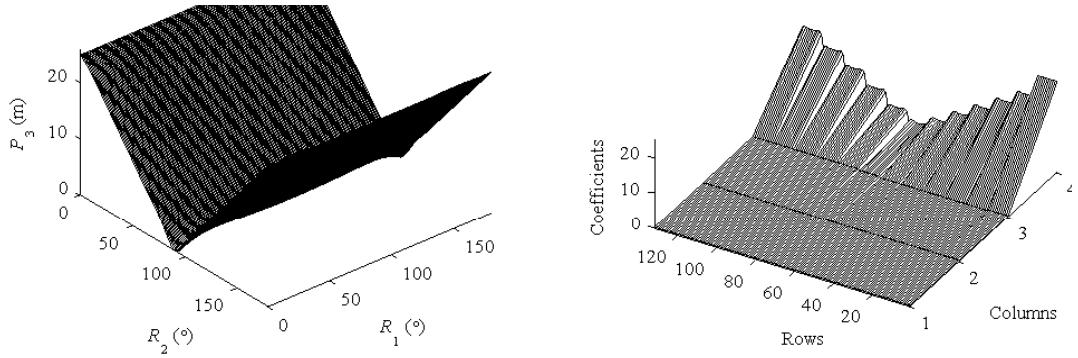

Figure 4.22: **Spline approximation functions $f(\theta_1,\theta_2,d_3)$ to formulate the composition $R_1R_2P_3$ (left) and its coefficients (right).**

Table 4.5: **Configuration Template $R_1R_2P_3$**

Template	Range	Specifications	C-space Formulation
$R_1R_2P_3$	R_1 [0°,180°]	R_1 (z,θ_1):	
3 DOF		$0° \leq \theta_1 \leq 180°$	$\theta_1 \leq 180°$
			$0° \leq \theta_1$
			$180° \leq$ span_θ_1
		R_2_weight+P_3_weight $\leq$ R_1_payload	
	R_2 [0°,180°]	R_2 (z,θ_2):	
		$0° \leq \theta_2 \leq 180°$	$\theta_2 \leq 180°$
			$0° \leq \theta_2$
			$180° \leq$ span_θ_2
		P_3_weight $\leq$ R_2_payload	
	P_3 [0,30]	P_3 (z,d_3):	
		0 m $\leq d_3 \leq$ 30 m	$d_3 \leq$ 25.2 m
			0 m $\leq d_3$
			25.2 m $\leq$ span_d_3
			f(θ_1,d_3): 0
			f(θ_2,d_3): 2
			f(θ_1,θ_2,d_3): Coefficients*

* Fig.4.22

Composition $R_1R_2R_3$:

The composition $R_1R_2R_3$ is constituted by three rotational motion. The first and second shows similar range between 0° and 180°. The farmer motion is associated to the rotational operator $R_1(z,\theta_1)$, whereas the latter motion to $R_2(z,\theta_2)$. The constraints for these motions are $R_{2\_weight} + R_{3\_weight} \leq R_{1\_payload}$ and $R_{3\_weight} \leq R_{2\_payload}$, respectively. The third motion R_3 develops a rotation from 0° up to 300°, and it is associated to the following operator $R_3(z,\theta_3)$. This motion is without constraint with respect to its payload capacity. To reach the points on the wall, according the Geometric Description, both the second and third motion should be attached with a link with a predefined length; in this analysis, the links are 1.85 m and 0.7 m, respectively.

The histograms are shown in Figure 4.23; the approximation functions are shown in the Figure 4.24. The Composition Template Table 4.6 shows the results. Since this motion is limited to reach completely the tunnel long, an approximation by means of B-splines is impracticable.

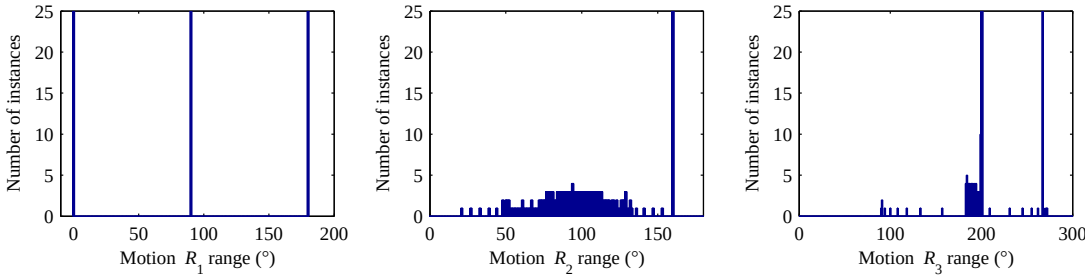

Figure 4.23: **Span histograms for the composition $R_1R_2R_3$. These histograms show the total displacement distribution in the composition to perform the task.**

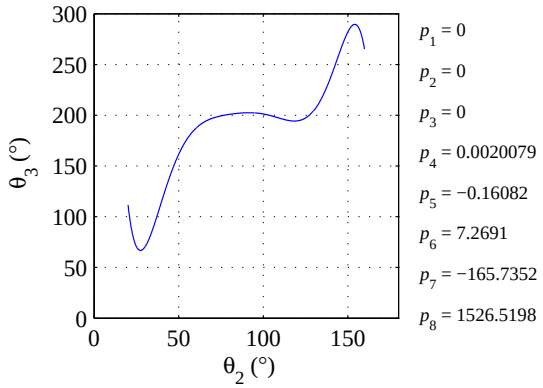

Figure 4.24: **Approximation functions $f(\theta_2,\theta_{32})$ to formulate the composition $R_1R_2R_3$.**

Table 4.6: **Configuration Template** $R_1R_2R_3$

Template	Range	Specifications	C-space Formulation
$R_1R_2R_3$	R_1 [0°,180°]	R_1 (z,θ_1):	
3 DOF		$0° \leq \theta_1 \leq 180°$	$\theta_1 \leq 180°$
			$0° \leq \theta_1$
			$180° \leq$ span_θ_1
		R_2_weight+R_3_weight $\leq$ R_1_payload	
	R_2 [0°,180°]	R_2 (z,θ_2):	
		$0° \leq \theta_2 \leq 180°$	$\theta_2 \leq 180°$
			$0° \leq \theta_2$
			$180° \leq$ span_θ_2
			1.85 m $\leq$ link_θ_2
		R_3_weight $\leq$ R_2_payload	
	R_3 [0°,360°]	R_3 (z,θ_3):	
		$0° \leq \theta_3 \leq 360°$	$\theta_3 \leq 300°$
			$0° \leq \theta_3$
			$180° \leq$ span_θ_3
			0.70 m $\leq$ link_θ_3
			f(θ_2,θ_3): 4

Composition $P_1R_2R_3$:

Due to the last composition $R_1R_2R_3$ is unfeasible to perform the task, the aggregation at beginning of a prismatic is the solution. This composition $P_0R_1R_2R_3$, where the first motion needs a range of operation from 0 m to 50 m, whereas that the motion R_1 is constrained to a value equal to 0°. Thus, this composition becomes properly the composition $P_1R_2R_3$. The second shows an operation range between 0° and 180°, and associated to the rotational operator $R_2(z, \theta_2)$. The motion R_3 is associated to the rotational operator $R_3(z, \theta_3)$, whereas its range is from 0° to 300°.

The constraints for these motions are included in the Composition Template Table 4.7. The histograms are shown in Figure 4.25. Whereas the Figure 4.26 and Figure 4.27 depict the approximation functions.

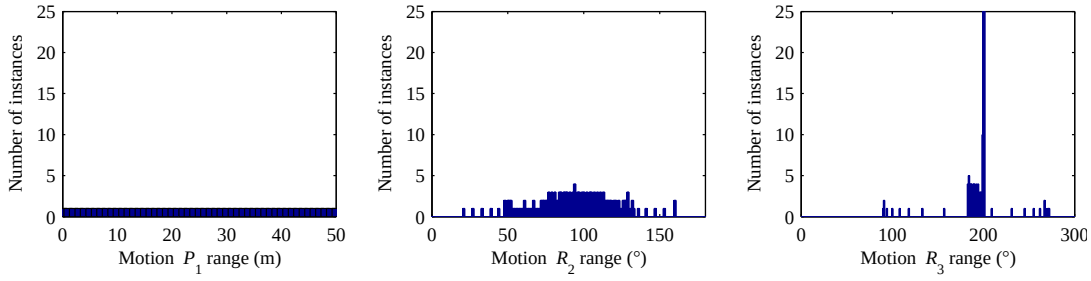

Figure 4.25: **Span histograms for the composition $P_1R_2R_3$. These histograms show the total displacement distribution in the composition to perform the task.**

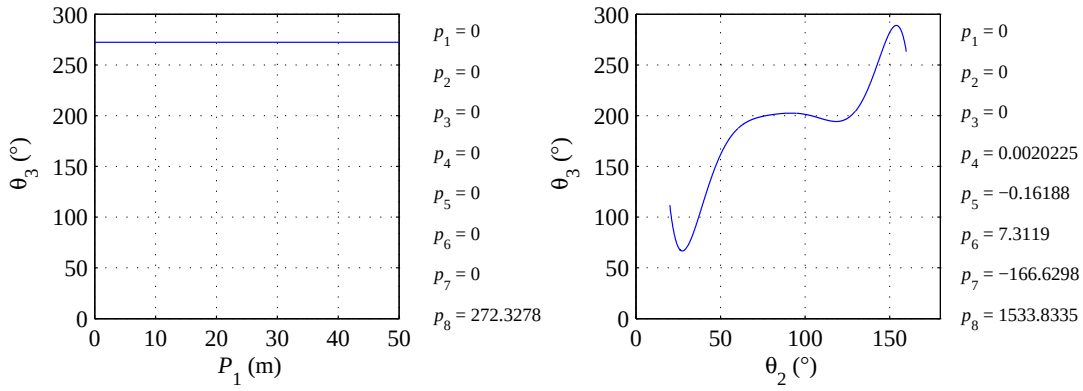

Figure 4.26: **Approximation functions $f(d_1,\theta_3)$ and $f(\theta_2,\theta_3)$ to formulate the composition $P_1R_2R_3$.**

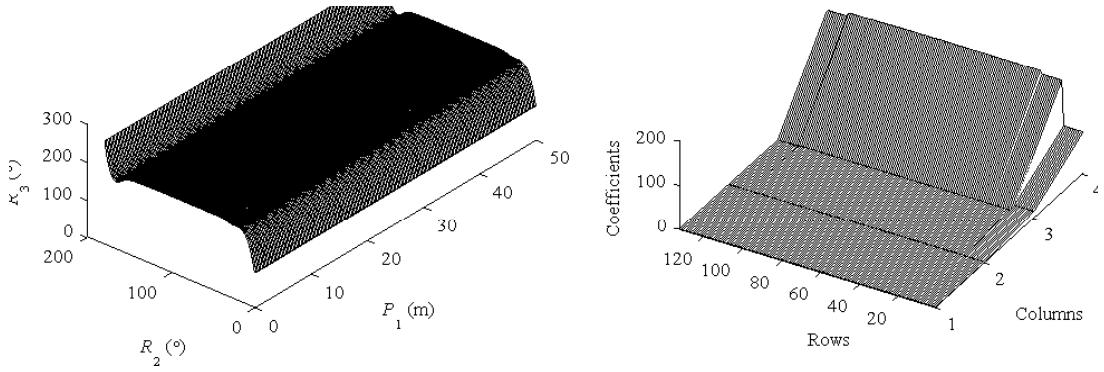

Figure 4.27: **Spline approximation functions $f(d_1,\theta_2,d_3)$ to formulate the composition $P_1R_2R_3$ (left) and its coefficients (right).**

Table 4.7: **Configuration Template $P_1R_2R_3$**

Template	Range	Specifications	C-space Formulation
$P_1R_2R_3$	P_1 [0,50]	P_1 (z,d_1):	
3 DOF		0 m $\leq d_1 \leq$ 50 m	$d_1 \leq$ 50 m
			0 m $\leq d_1$
			50 m $\leq$ span_d_1
		R_2_weight+R_3_weight $\leq P_1$_payload	
	R_2 [0°,180°]	R_2 (z,θ_2):	
		0° $\leq \theta_2 \leq$ 180°	$\theta_2 \leq$ 180°
			0° $\leq \theta_2$
			180° $\leq$ span_θ_2
			1.85 m $\leq$ link_θ_2
		R_3_weight $\leq R_2$_payload	
	R_3 [0°,360°]	R_3 (z,θ_3):	
		0° $\leq \theta_3 \leq$ 360°	$\theta_3 \leq$ 300°
			0° $\leq \theta_3$
			180° $\leq$ span_θ_3
			0.70 m $\leq$ link_θ_3
			f(d_1,θ_3): 0
			f(θ_2,θ_3): 4
			f(d_1,θ_2,θ_3): Coefficients*

* Fig.4.27

4.4.3 Basic Configuration

Criteria to evaluate the compositions are the DOF number involved and the simplicity to perform these motions, which is related to the C-space formulation order. In this analysis, the selection is based on the comparison of the Configuration Template information; referring to these results several observations are made:

- All the compositions are constituted by three basic motions at diverse order and combination. A same number of DOF, including the composition $P_0R_1R_2R_3$ that is transformed to the composition $P_1R_2R_3$.
- However, the result of the composition $R_1R_2R_3$ presents a disadvantage to complete the task, since the reachable workspace for this composition is limited to a vertical plane xy, only. The rest of compositions satisfy the total reachable workspace approached by the Geometric Description.
- The results of the C-space formulation show two clusters based on the power order of the approximation representative functions. The first cluster consists of an order equal to 2nd, whereas the other is equal to 4th order. In the former are the compositions $P_1R_2P_3$, $R_1P_2P_3$, and $R_1R_2P_3$, and in the latter cluster are $R_1R_2R_3$ and $P_1R_2R_3$. Whereas the composition $P_1P_2P_3$ shows the highest power equal to 6th order.
- The coefficients of the B-spline approximation indicate a more simplicity on the composition $P_1R_2P_3$, since these values are the smallest of the coefficients. The compositions $P_1R_2R_3$ and $R_1P_2P_3$ present the highest values. It can be seen that the compositions $P_1R_2P_3$, $R_1R_2P_3$, and $P_1R_2R_3$ show a behavior more homogeneous on these values.
- The operation ranges vary about 0 to 50 m to prismatic motions and from 0° to 180° on rotation motions. The lengthiest prismatic range corresponds properly to reach the total length of the tunnel, whereas the rotation range is to reach the semi-elliptic shape of the vertical planes xy.
- Although the aforementioned are the operation ranges, the span of each motion indicates the amplitude required to perform the task. For instance, the last motion P_3 in the composition $P_1R_2P_3$ needs a range between 0 m and 3.25 m, but a span equal to 1.25 m; i.e., 1.25 m of effective translational motion.

Under these observations and comparison, the analysis gives as result the selection of the fundamental composition $P_1R_2P_3$ to perform the task. The selection is based on, principally, its described C-space and its polynomial functions, which show the smallest power order and coefficients. Furthermore, this composition presents the minor ranges and spans on its motions.

For example, the composition $P_1P_2P_3$ and $P_1R_2P_3$ show, in common, same requirements for their first motion, but the second motion in the composition $P_1P_2P_3$ develops a translation up to 4 m, supporting the third motion. Thus, the component that embodies this motion has to be enough rigid to support the weight of the motion P_3 and to avoid instability. Both motions P_3, which reach the wall points, need similar operational range but the span of the composition selected is less. Besides, this motion P_3 in the composition $R_1P_2P_3$ implies a requirement to develops a forward and backward displacement. Additionally, the second motion impacts strongly the stability, even more than in the previous case, due to the required span is longer (25.2 m $\leq$ span_d_2).

Therefore, the election is on the composition $P_1R_2P_3$ since its uniformity and simplicity of the motions to perform the assigned task. This composition becomes the Basic Configuration that represents the template, which is used to lead the implementation of the robotic vehicle; i.e., the synthesis of the MAV.

All the specifications of the selected composition are mapped to the Configuration Parameters that should be fulfilled by the components selection. Table 4.8 shows the Configuration Parameters.

Table 4.8: **Basic Configuration** $P_1R_2P_3$

Configuration Parameters		
$P_1R_2P_3$ 3 DOF	P_1 [0,50]	P_1 (z,d_1): $d_1 \leq 50$ m 0 m $\leq d_1$ 50 m $\leq$ span_d_1 $\Delta d_1 \leq$ sampling_interval R_2_weight+P_3_weight $\leq P_1$_payload
	R_2 [0°,180°]	R_2 (z,θ_2): $\theta_2 \leq 180°$ $0° \leq \theta_2$ $180° \leq$ span_θ_2 $\Delta\theta_2 \leq 1.76°$ P_3_weight $\leq R_2$_payload
	P_3 [0,3.25]	P_3 (z,d_3): $d_3 \leq 3.25$ m 2 m $\leq d_3$ 1.25 m $\leq$ span_d_3

```
Start
Situate Basic Configuration
P1 = 0
    While P1 ≠ length_ tunnel
        For Execute R2 = 0° : Δθ2 :180°
            Execute P3
            Measure Distance
        Next R2
        Build Plane xy
        Advance P1 = P1 + Δd1
    End (while P1 )
Build tunnel profile
End
```

Figure 4.28: **Pseudo code of the basic strategy to perform the Basic Configuration.**

To perform the TPT, these motions of the Basic Configuration should be executed in such order of the selected composition. First, the prismatic motion is applied at intervals equal to the quantifier Δd_1 and defined by the requirement sampling_interval. Hence, this quantifier is given as

$$\begin{aligned} \Delta d_1 &\leq \text{sampling\_interval} \\ \Delta d_1 &\leq 2\,\text{m} \end{aligned}$$

This first motion is followed by the rotational motion at sampling interval quantifier $\Delta\theta_2$ which is derived from sampling_resolution and height_tunnel quantifiers, expressed by

$$\begin{aligned} \Delta\theta_2 &\leq \arctan \frac{\text{sampling\_resolution}}{\text{height\_tunnel}} \\ \Delta\theta_2 &\leq 1.76^\circ \end{aligned}$$

Finally, the third motion, a prismatic should be executed for reaching each one of the points in the tunnel space to generate the vertical planes xy along the tunnel (z-axis), defined by

$$\begin{aligned} d_3 &\leq 3.25\,\text{m} \\ 2\,\text{m} &\leq d_3 \end{aligned}$$

This sequence of execution is explicitly the basic strategy to achieve the TPT through the Basic Configuration; the pseudo-code of the strategy is shown in the Figure 4.28. The particular robotic system must be constituted with the correct components of hardware and software. Therefore, a process of matching the specifications with the characteristics of each component should be developed. The following sections outline this process.

4.5 System Design

The robotic system is built from this Basic Configuration, each motion must be mapped to a subsystem into the AV structure. This structure constitutes an abstraction of the functional relation among the motions, in which the subsystems should be composed by specific components that satisfy the Configuration Requirements and Parameters. These components will be interlinked in a hierarchical and modular approach to support the conceptual and physical implementation of the AV.

To establish the mapping and synthesis order, each motion is analyzed considering its functionality into the Basic Configuration and determining the dependence and constraint propagation among the motions.

4.5.1 Components

The mapping of the Basic Configuration to an Autonomous Vehicle includes three fundamental subsystems, in according to identical number of motions. The first motion P_1 is mapped to Locomotion subsystem, the second motion R_2 is to the Deployment subsystem, and the third motion P_3 is to the Tool subsystem. Figure 4.29 shows the mapped motions into the AV structure.

In the Basic Configuration (Table 4.8), there are constraints of the Configuration Parameters, which related to $P_{1\_payload}$ with the weight of the rest of the motions (R_{2_weight} and P_{3_weight}). Besides, the second motion R_2 is under the constraint $P_{3\_weight} \leq R_{2\_payload}$; i.e., these motion have dependence constraints. Finally, the last motion presents independency constraint; therefore, the analysis is developed following an order inverse or backtracking sequence to the execution of the motion into the composition.

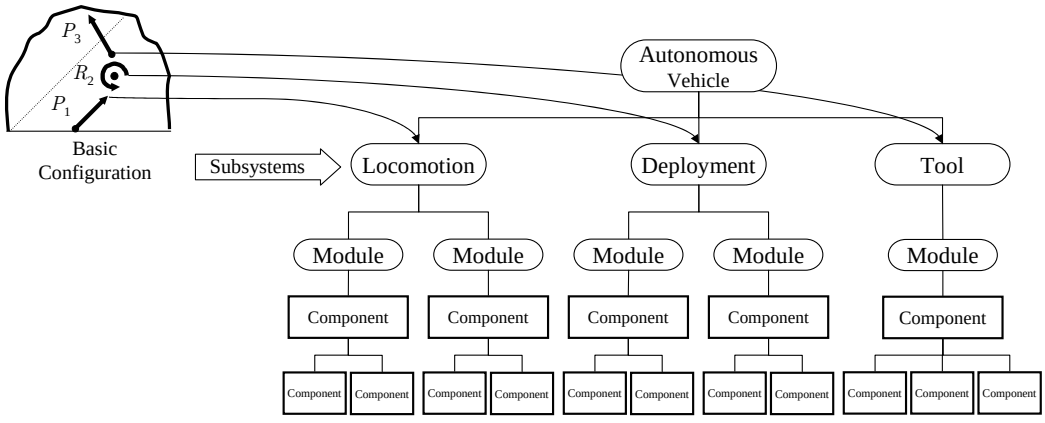

Figure 4.29: **Basic Configuration is mapped to functional subsystems in the hierarchical AV structure.**

4.5.2 Tool Subsystem

The motion P_3 is mapped to the Tool subsystem (Figure 4.29), since this motion is the measurement function of the wall points to form the vertical planes xy in conjunction with the motion R_2; such as was defined in the task abstraction phase. Thus, these measurements result of the prismatic displacements toward a particular point of the tunnel ceiling. It can be performed by a device used to measure the linear displacement of an object or a sensor to measure the distance o presence of a target, which must implement this characteristic (i.e., a prismatic motion under the specifications defined in the Configuration Parameters).

In contact and non-contact devices are classified the possible components to embody this motion. For instance, many moving mechanisms in robotics use a contact device-the end switch. This is an electrical switch that generates a signal as indication that the mechanism has the end position or target. An opposite principle is implemented in non-contact sensor that transmits some kind of signal and receives a reflected signal to detect the distance.

The constraint digital for the manipulation of the information to build the tunnel profiling in a computer, reduce the selection of the sensor into the electric device, rather the merely mechanical such as tape meter. For this kind of electric devices, there are alternatives such as stroke linear potentiometer implemented with end switch, ultrasonic distance meter, and laser ranger finder. In the process of selection there are implicated the following features and technical specifications, such as: resolution and accuracy of the measurements, range of operation, power, data I/O, the measured object or wall made from (metal, plastic, etc.), physical dimensions, and environmental conditions of operation, as well as cost. Such features of the component must satisfy whole the Configuration Requirements and the Configuration Parameters to be selected.

In the practice, a contact device can be used to measure linear displacement, which consist of front and rear bearings, metal housings, stainless steel shafts or stroke, and based on a resistive element and wiper assembly to provide the stroke's position (such as the Linear Potentiometer LP801-1200, manufactured by Omega, and the electro-hydraulic actuator Linear Potentiometer series 2HX-LRT by Parker). However, such devices have many drawbacks, for example, high mechanical load to reach the operation range required. Therefore the analysis is focused on non-contact devices.

Non-contact distance sensors are active instruments in which some kind of signal is transmitted and compute the distance from transit time of it. The transmitted energy may be in a form of any radiation such as optical, electromagnetic, and acoustic. Transmission and reception of the ultrasonic energy is a basis for popular ultrasonic range meter, and the electromagnetic for the laser range finder, using a common technique in Robotics the time-of-flight measurement (TOF).

Both classes of sensors have used wide in underground mining applications, under the rigorous demands of these harsh environments, which was reported by [Scheding 97]. Nevertheless, there exist differences due to the physical principles of operation and technical features of these sensors, which must be analyzed to lead the selection of the component.

Ultrasonic waves have a feature, they propagate with the speed of sound, which is slower than the light speed, thus time is much longer and making the measurements relatively simple. Laser ranger finders are electronic devices that operate by measuring the TOF of laser light pulses: a pulsed laser beam is emitted and reflected if it meets an object. There are with reflector and without reflector, obviously for this application are eliminated the finders with reflector, due to the necessary extra conditioning of the tunnels. Furthermore, there are instruments with an internal rotating mirror deflects the pulsed beam so that a fan-shaped scan is made of the surrounding area. In general, the data is available in real time for further evaluation via a serial interface.

Although, these devices satisfy the motion P_3 parameters, for the operation range (d_3) and the dynamic range (span_d_3), including environmental conditions of the Configuration Requirements such as temperature, humidity, and digital I/O interface. An analysis is developed to investigate the accuracy and the precision between sensors.

The ultrasonic sensor beamwidth is large and the energy is reflected in a diffuse manner, thus make it difficult to resolve the measurement in a particular point (punctual); therefore the results in the reflections is a poor that are both precise and accurate measurements.

The Figure 4.30 shows the spot diameter as a beamwidth function, which relates to accuracy and precision (Configuration Requirements), the operation frequency (component features), and the target range (Configuration Parameters). The footprint of the incident beam, at the target surface in term of this beam dispersion angle κ ([Everett 95]), is expressed as

$$d_s = 2\,R_t\,\tan\frac{\kappa}{2} \tag{4.1}$$

where d_s is the spot diameter and R_t denotes target range.

The beam dispersion depends on the transmission wavelength λ and the transducer diameter d_t, given as

$$\kappa = 1.22\,\frac{\lambda}{d_t} \tag{4.2}$$

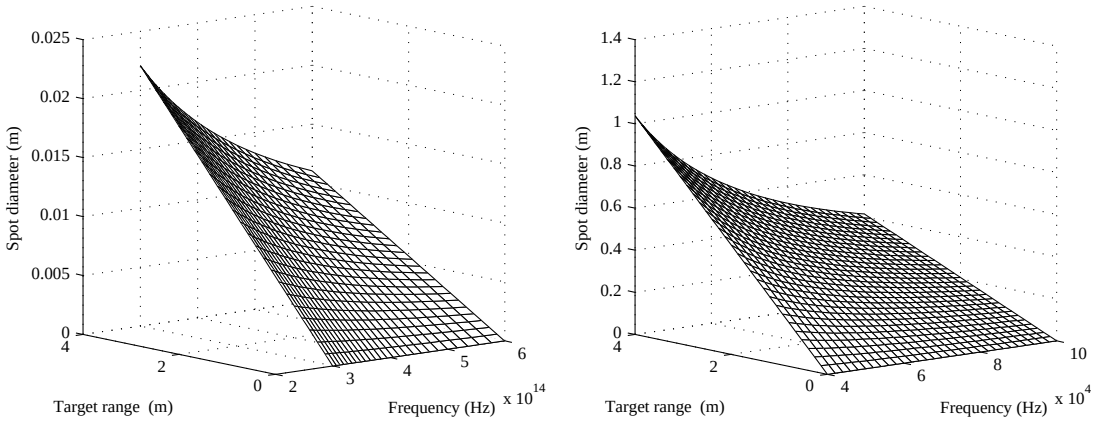

Figure 4.30: **Spot diameters for the laser (left) and ultrasonic (right) devices. The maximum spot diameter for laser sensor means that it is the best selection to achieve the motion P_3, satisfying and improving the accuracy and precision requirements.**

In the ultrasonic sensor the spot diameter reaches until 1.00 m, whereas in the laser telemeters the spot dimension is less than 0.02 m to reach 4.00 m of the target distance. The fundamental reason is the beamwidth, which is the order of degrees for the ultrasonic energy (e.g. 10°-20°), and with an order minor to half degree for light energy (e.g. 0.30°-0.10°).

This numerical comparison presents as the best component to a laser rangefinder, since it satisfies the Configuration Requirements and Parameters analyzed. Therefore, the motion P_3 will be implemented by a laser rangefinder, which should be instanced by a specific laser device together its actuation and sensing requirements. This component selection is mapped to the AV structure into the Tool subsystem.

4.5.3 Deployment Subsystem

The second motion R_2 is transformed to the Deployment subsystem. This motion is a rotational that allows deploying the motion P_3, i.e., the laser range finder toward the orientation required to reach the ceiling points and generate the series of measurements. The parameters are an operation range from 0° to 180° and a payload capacity to support the weight of the laser range finder. Therefore, it will be necessary to make a search of the component that satisfies these constraints, supported with the obtained results.

To perform a turn into this range, there are different items of common use, such as mechanical, hydraulic, pneumatic and electrical systems. The most widely used drive of this kind is an electromotor, among which there are DC motors, AC motors and stepper motors. The advantage of DC motor lies in the ease of speed control, whereas in AC motor requires the installation of sophisticated equipment, for example frequency transformers. For accurate positioning both DC and AC motors require feedbacks.

In contrast, stepper motors are suitable for accurate positioning and speed control. Such motor produces rotation through two independent coils that are controlled by impulses to move exactly a single step for forward and backward. These discrete steps are a size of certain angle per revolution, instead of a continuous motion in standard DC motors. The stepper motors are convenient for engagement with digital means (computer); hence, the alternative is a stepper motor or an arrangement as Pan Tilt Units (PTU).

The selection for a particular PTU depends on the component features of the previous motion. Therefore, the evaluation is based on the technical specifications generated by the laser and the Configuration Requirements and Parameters, such as the quantifiers sampling_resolution, resolution_measured, accuracy_measured, sampling_time_interval, and span_θ_2. However, a PTU is the component selected; hence, this component is mapped to the AV structure as the Deployment subsystem.

4.5.4 Locomotion Subsystem

Because the action of the motion P_3 is just to move throughout the tunnel, building, with its progression, the vertical planes xy along the z- axis. Thus, this motion is mapped to Locomotion subsystem, which must be selected with the Configuration Requirements and Parameters. In addition, the requirements for the second and third motion should be considered when these components will be instanced. However, the locomotion component is the physical device that must generate a linear displacement and support the payload, which are limited by the quantifiers 0 m $\leq d_1$, $d_1 \leq$ 50 m, and R_2_weight+P_3_weight $\leq P_1$_payload.

To cover this operation range, there are linear guide systems such as a steel bar, wires, electrical bands and rail track. The requirement of mobility for this motion should be at least 50 m, which involves infrastructure to build a guide system, implying the construction and modification of the tunnel environment to allocate this kind of components. Furthermore, the rails had long tradition to transport the ore in underground mining; nevertheless, the rail tracks became an obstacle for commuting in the mine and many mines actually use a variety of different equipments to the mineral transport. The aforementioned construction is an impractical solution, due to the tunnels suffer continually modifications, precisely by extracting the material; in addition there are another criteria should be considered, such as deflection system, supports, rigidity, actuator load capacity, and drive for such linear guide systems.

Therefore, this restriction may be solved using the engineering principles [Ivanov 94, Nordlund 96, Altshuller 01]. The principle of the segmentation to perform this long motion is negotiation by means of a mobile platform, a system that navigates into the tunnel carrying on the load of the Deployment and Tool subsystems.

There are a great variety of mobile platforms or vehicles, including ground, aerial, and underwater. For the kind of environment, the underwater and flying platforms are not analyzed for this effort. In particular, a flying vehicle such as a helicopter may resolve this situation; however its capacity of navigation is limited by the conditions and dimensions of the tunnel. Therefore, ground mobile platforms are analyzed to perform this motion; these system options can be wheeled and legged locomotion with different wheel and footpad geometries [Chun 87, Fiorini 00].

In both cases, the locomotion platform must support itself on the ground and generate traction to negotiate terrain for motion, avoiding be immobilized by the terrain. Comparative studies, based on soil mechanics, determine the differences between wheeled and legged vehicles; on a soft surface the ability of a legged locomotion is greater than a wheeled, whereas that it is equivalent on hard surface. Wheeled vehicles move in continuous contact with the terrain, producing a constant compaction and nonlinear energy losses in soft terrains; whereas legged vehicles suspend themselves over the terrain on only discrete contact points, conserving energy [Bekker 69, Todd 85, Song 88, Bares 91].

In comparison, wheeled vehicles have better speed mobility, and less weight, and legged vehicle only operate at low speed and are very complex. A typical wheeled vehicle only has 2 DOF whereas the simplest statically stable walker (6-legged frame walker) has 8 DOF; however these latter platforms possess other advantages that cannot be matched by the other systems [Waldron 85, Huang 90b, Waldron 95]. An important design criterion for locomotion selection is based on the geometrical characteristics of the terrain, such as topography, geometry and size of obstacles. [Bekker 56, Pettersson 98, Sukhatme 97]. Thus, the vehicle geometry must be designed to meet the operation range locomotion under the terrain soil type, slope, and rock size distribution. Table 4.9 shows the geophysical properties of the tunnel soil, which is a lean clay terrain (lean_clay). In comparison with the rest of tabulated soils, this soil is classified as hard terrain [Wong 93, Solleiro 02].

Table 4.9: **Terrain properties.**

Soil	Moisture	n	k_c	k_ϕ	c	ϕ
Dry sand	0%	1.10	0.10	3.90	0.15	28 °
Sandy loam	15%	0.70	5.27	3.90	0.15	28 °
Sandy loam	22%	0.20	7.00	3.00	0.20	38 °
Clay	38%	0.50	12.0	16.0	0.60	13 °
Heavy clay	40%	0.11	7.00	10.0	3.00	6 °
Lean clay*	22%	0.20	45.0	120	10.0	20 °
Snow	-	1.60	0.07	0.08	0.15	20 °

* Tunnel terrain

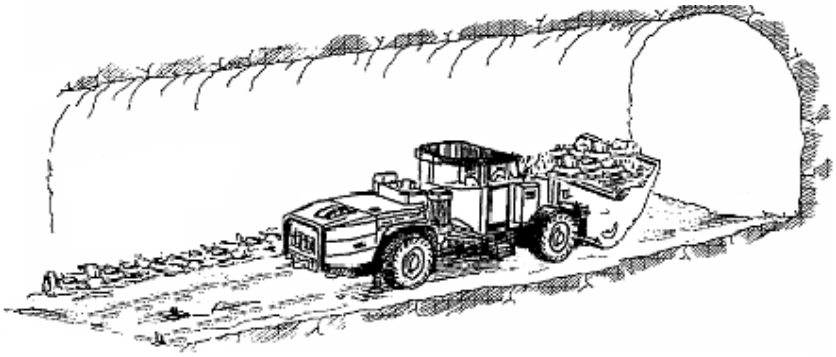

Figure 4.31: **Tunnel terrain is compacted by the heavy vehicles during the constant mineral transportation.**

Due to the continuous activity of heavy vehicles, the terrain is compacted by these vehicles, such as Loud Haul Dump loaders, while transporting the ore throughout the underground mine (Fig. 4.31). The geometrical characterization of tunnel terrain is shown in Figure 4.32.

The size-frequency distribution of rocks along the examined tunnel is plotted by the Fig. 4.33. This distribution is formulated by a power function used to describe rock population [Moore 89], which is expressed as

$$N(D) \;=\; K\,D^{-2.66} \tag{4.3}$$

where $N(D)$ is the cumulative number of rocks per square meter with diameter equal to D, and K_r is a constant determined from an estimation of the cumulative number of rocks equal to 0.10 m of the examined mine; for the tunnel site, K_r is 0.0081, i.e., a relation to 3.7 rocks/m^2 (distribution_rock).

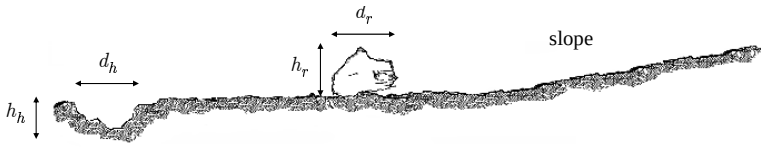

Holes:
Diameter d_h and depth h_h equal to 0.10 m
A distribution equal to 2.5 holes/m^2

Rocks:
Diameter d_r and height h_r equal to 0.10 m
A distribution equal to 3.7 rocks/m^2

Slopes:
Nominal slopes between 10° and 20°

Figure 4.32: **Geometrical characteristics of the tunnel terrain.**

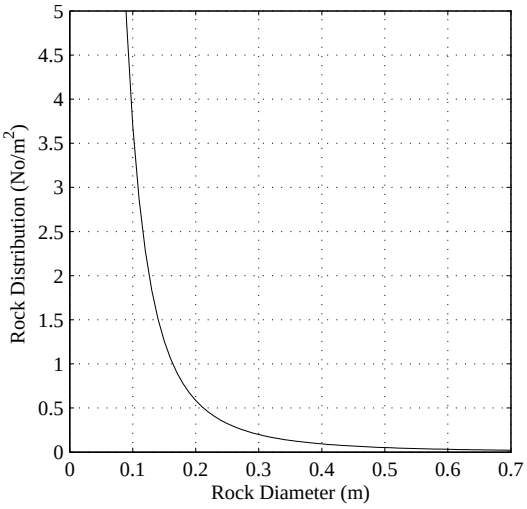

Figure 4.33: **Distribution of rocks for diameter greater than 0.10 m.**

However, the population of rocks presents different histograms at wide of the tunnel, Figure 4.34 shows these histograms for a size of rock equal to 10 cm, 15 cm, and 20 cm, respectively. This distribution is the result of the heavy vehicles, which push the rocks toward the sides of the tunnel while transporting the mineral.

Having a similarity, the hole distribution is estimated using the above Moore's expression, given by

$$N(D) \;=\; K_r\, D^{-2.66} \tag{4.4}$$

for this case, the K_h is 0.0055 since the distribution of hole with a diameter $d_h = 0.10$ m and depth $h_h = 0.10$ m is equal to 2.5 holes/m^2 (quantifier distribution_hole). Figure 4.35 depicts the hole distribution.

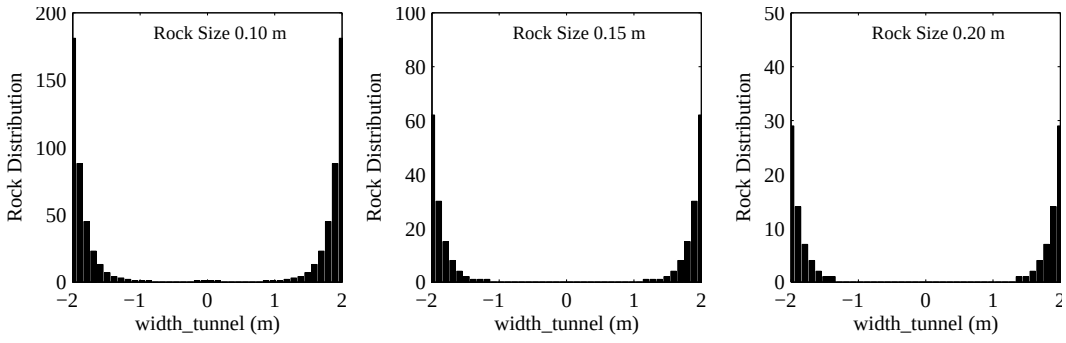

Figure 4.34: **Histograms showing number of rocks wide of the tunnel.**

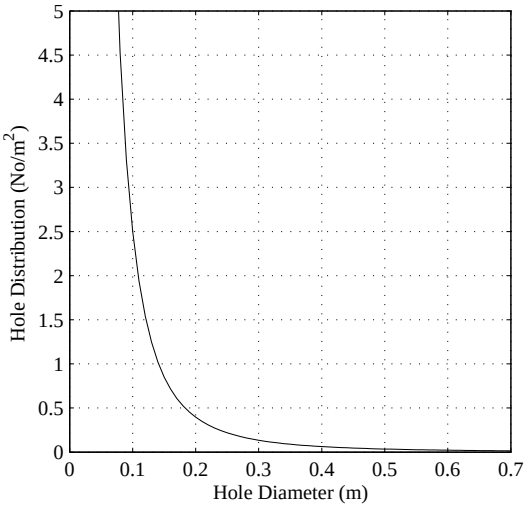

Figure 4.35: **Distribution of holes for diameter greater than 0.10 m and depth up to 0.10 m.**

Referring to these results the abovementioned differences, the selection is a wheeled vehicle to implement the motion P_1 instead of a legged vehicle, since the terrain consist of a hard soil with a distribution of rocks and holes that allow a continuous contact of the wheeled vehicle. Thus a wheeled vehicle is mapped to the AV structure as the Locomotion subsystem.

The AV structure is formulated by a wheeled vehicle to perform the motion along the tunnel, a stepper motor or PTU to orientate the tool mechanism, and a laser rangefinder to measure the tunnel profile, as shown in Figure 4.36.

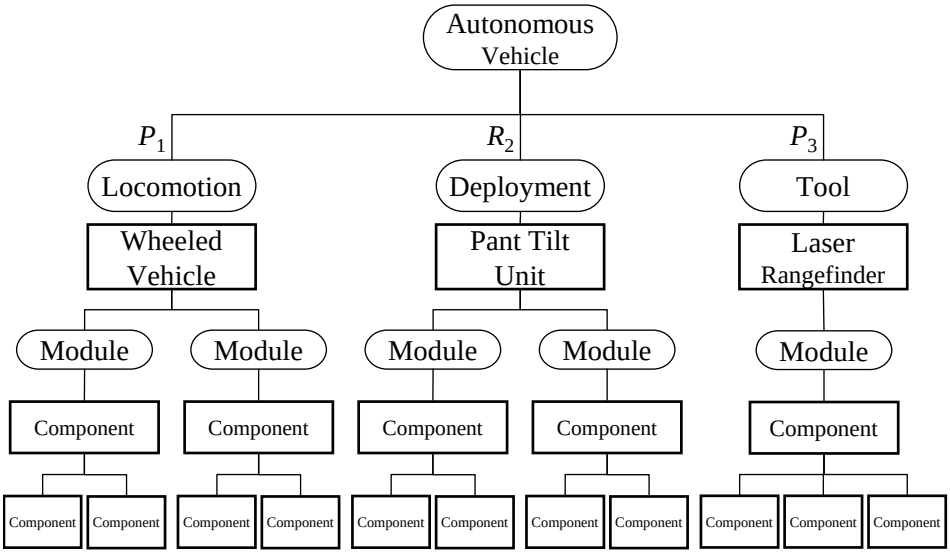

Figure 4.36: **Mining Autonomous Vehicle structure formulated by a wheeled vehicle, a pant tilt unit, and a laser rangefinder.**

A parametric analysis serves to select the proper components for each one the subsystems. This instantiation process uses the Configuration Requirements and Configuration Parameters relating to the particular technical features of the components. In this way the MAV configuration is detailed with the necessary components, including all the actuation and sensing requirements that the components require.

In the following chapters, two synthesized vehicle configurations are developed from the concentrated results in the robotic vehicle structure. The first synthesis allows the implementation of the MAV configuration, using available components to be rapidly deployed, and showing that the selected Basic Configuration is a viable solution to perform the tunnel profiling task. Chapter 5 addresses this MAV configuration.

For the second robotic vehicle, the MAV configuration is formulated not only from these results and the Basic Configuration, but also the System Design phase involves the autonomy analysis to identify the kinematics requirements that improve the position estimation, the control and the perception requirements, from a parametric comparison of different steering mechanisms under equal operation conditions to select then the proper Locomotion subsystem. Chapters 6 and 7 integrate the autonomy analysis in the synthesis process to detail the MAV configuration and define an operational MAV prototype.

List of Figures

List of Tables

Chapter 7

Vehicle Positioning

The definition of the Locomotion subsystem completes the MAV configuration, including the components that provide the positioning and consequently the control of the vehicle to execute the task in the specific environment. Therefore, the vehicle positioning is an essential requirement which is to be solved from the vehicle kinematics and the use of multiple sensors.

However, any sensor and method that can be implemented to provide the vehicle positioning suffers some lack, which leads to uncertainty and failures for the achievement of the given task [Borenstein 97]. For example, information of absolute sensors usually is unavailable at required rate to be used in the localization and control of the robotic vehicle or it may not be available for particular environments, such as Global Positioning System (GPS) for underground mining applications; whereas the relative sensors lead to the accumulation of errors, due to sensor noise, sensor limitations, and the interaction with the vehicle and the environment, which can be unpredictable.

One solution of overcoming this problem is to include data measured from relative sensors and to periodically reset using absolute sensors, which are incorporated into the state estimate using a technique filter to reduce errors, providing a more predictable vehicle positioning and vehicle control to perform its task. Figure 7.1 shows a generic architecture to estimate the vehicle positioning combined both relative and absolute sensors by mean of a filter.

This chapter develops an analysis to investigate the relation between errors present in sensor measurements, and the resultant uncertainty in computed vehicle positioning. Numerical results in simulation of the positioning uncertainty propagation yield the boundaries of the allowable sensor requirements, such as the sensor uncertainties and the number of landmarks, to achieve the targeted task. The following sections outline the uncertainty analysis, showing the simulation results that address the selection of components for computing the vehicle positioning to complete the MAV configuration.

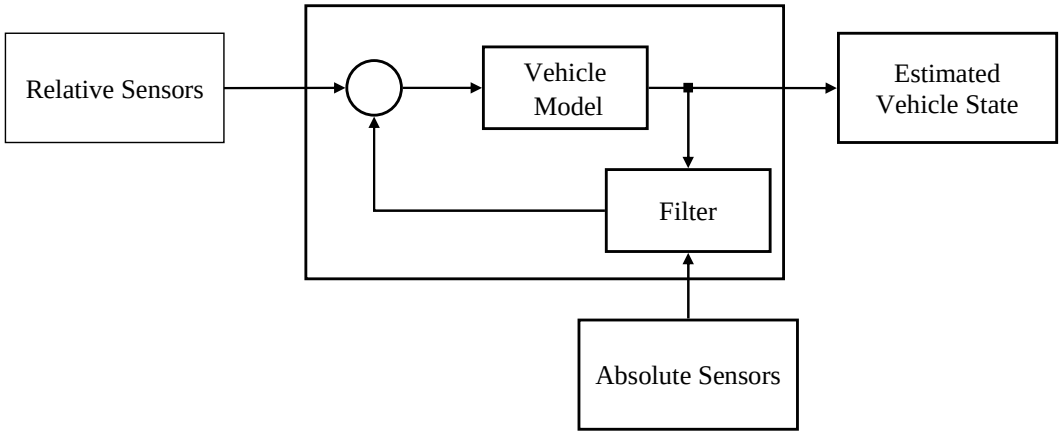

Figure 7.1: **Architecture for position and orientation estimation of a robotic vehicle using relative and absolute sensors through a filter.**

7.1 Analysis of Positioning Uncertainty

The section presents the uncertainty analysis on the Locomotion subsystem to provide the sensors that implement the vehicle positioning and complete the MAV configuration. For this purpose, the analysis examines the expected uncertainty in the positioning estimation that allows the robotic vehicle achieves successfully its assigned task. Such uncertainty becomes cumulative and unavoidable, due to the positioning estimation is subject to many different sources of error. Thus, the key issue addressed by the analysis is that the robotic vehicle has the ability to recover of this positioning uncertainty propagation from a set of sensors. Figure 7.2 shows the procedure of the uncertainty analysis to identify the requirements of such sensors.

The procedure is based on the mentioned architecture to estimate the vehicle state, applying a Kalman filtering technique to update periodically the vehicle positioning, provided by the information from odometry sensors, with respect to the data from an absolute sensor that observes landmarks. In this analysis, the vehicle positioning is computed considering the kinematic model of the vehicle under certain degree of uncertainty in such sensors. As a result, the vehicle performance is compared with respect to its positioning uncertainty evolution.

In particular, the uncertainty analysis, and the outline of the following sections, is as follows:

1. The kinematic model is derived from the vehicle parameters, in this case the Ackermann vehicle. The model also involves the uncertainties of the absolute and odometry sensors to estimate the position and orientation of the vehicle along a given path, which is defined by the task and environment requirements. The odometry sensors are defined from Ackermann geometry, as the required variables to control the vehicle.

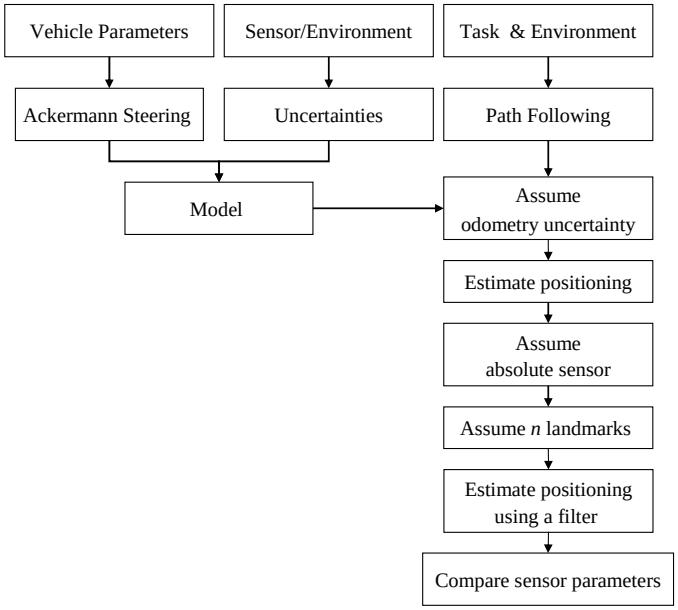

Figure 7.2: **Analysis of positioning uncertainty for AV configuration.**

2. The method leads the uncertainty evolution through the path following, considering only the odometry sensors. This simulation addresses the computation of the maximum traveled distance, after this distance the vehicle positioning is considered as ambiguous. Thus, this distance is the longest distance, in which the positioning must be reset using the absolute sensor information.

3. With this result, the locations and number of the landmarks are analyzed and the theoretical estimation of the positioning is developed from landmark to landmark, under the presence of the sensor uncertainties.

4. A quantitative comparison of the results allows the definition of the sensor requirements to the complete Locomotion subsystem. Minimize the number of landmarks and observations, and keep the sensor uncertainties within certain bounds are used as criteria.

7.1.1 Vehicle Model

The forward kinematic model of an Ackermann vehicle moving in a plane is replicated in Figure 7.3, where x and y denote the position of the centre of the rear axle relative to a reference frame and the angle θ denotes the orientation of the vehicle body with respect to the x axis. L is the vehicle wheelbase, the distance between the front axle and rear axle; whereas R is the turning radius. Hence, the inputs to control the vehicle are the linear velocity V at the centre of the rear axle and the steering angle γ. The motion equations at any time are derived from the control system shown in Table 6.1,

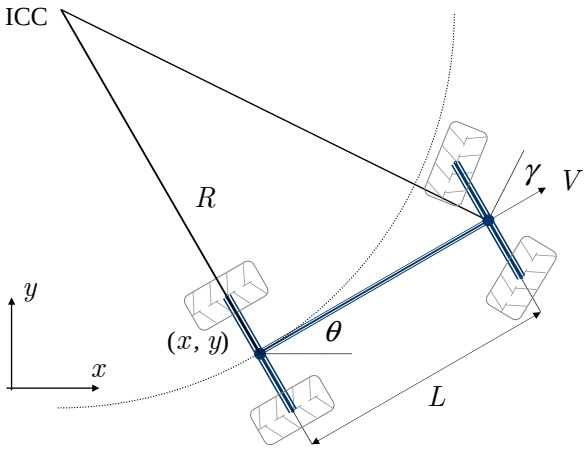

Figure 7.3: **Geometry of the Ackermann Steering: The vehicle positioning is defined by [x, y, θ], where (x,y) denote the position of the rear axle midpoint and θ denotes the vehicle orientation. L is the wheelbase, the distance between the front axle and rear axle, whereas R denotes the turning radius. The inputs to control the vehicle are the linear velocity V and the steering of the vehicle γ.**

$$\begin{aligned}
\dot{x}(t) &= V(t)\, cos(\theta(t)) \\
\dot{y}(t) &= V(t)\, sin(\theta(t)) \\
\dot{\theta}(t) &= \frac{V(t)\, tan(\gamma(t))}{L}
\end{aligned} \tag{7.1}$$

The continuous model is converted into discrete model, assuming that the control inputs are approximately constant over a sample period ΔT. There the motion model is given by state variables [x, y, θ] at the instant k,

$$\begin{aligned}
x(k+1) &= x(k) + \Delta T[V(k)\, cos(\theta(k))] \\
y(k+1) &= y(k) + \Delta T[V(k)\, sin(\theta(k))] \\
\theta(k+1) &= \theta(k) + \Delta T \left[\frac{V(k)\, tan(\gamma(k))}{L}\right]
\end{aligned} \tag{7.2}$$

7.1.2 Odemetry

For the Ackermann vehicle, the driving and steering variables are well suited inputs required for control purpose (controllability that has been demonstrated by [Laumond 93]). To control those variables two sensors are needed to estimate properly the vehicle positioning using dead reckoning technique, which is defined as odometry. This technique is able to approximate position and orientation by integrating the measured data from such sensors to the kinematic model of the vehicle:

Steering sensor: A sensor measures the angular displacement of the steering Ackermann mechanism, which is proportional to the steering angle γ, the average of the orientations of the two front wheels; hence the steering angle $\gamma(k)$ is related to the steering angle measured by the sensor $\gamma_s(k)$, it can be described as,

$$\gamma(k) = c_s\,\gamma_s(k)$$

where c_s is the gain of the sensor.

Velocity sensor: A wheel sensor measures the angular velocity $\omega(k)$ of a rear wheel, which is used to determinate the vehicle velocity $V_s(k) = r_w\,\omega(k)$, where r_w is the wheel radius. Thus the vehicle velocity $V(k)$ is related to the vehicle velocity measured by the sensor $V_s(k)$ which can be expressed as

$$V(k) = c_v\,V_s(k)$$

where c_s is the gain of the sensor.

7.1.3 Positioning Uncertainty

However the use of steering and velocity sensors is subject to errors which should be associated with measure of uncertainty; various source of uncertainty contribute to cumulative and unbounded uncertainty, which are practically present in rough-terrain applications. Thus, two sensor uncertainties are attached to vehicle velocity and steering measurements, the velocity uncertainty σ_v and the steering uncertainty σ_s, respectively. This leads to a reasonable assumption that the short unit of travel, the error is assumed to be zero mean, and white, i.e., uncorrelated with the previous $(k-1)$ or next $(k+1)$ unit of travel. Under this assumption, the vehicle positioning presents an uncertainty for both position (x,y) and orientation θ, propagating along a given path.

For the analysis of the uncertainty propagation, the concept of configuration uncertainty developed by [Fraichard 98] has been applied to investigate the odometry sensor parameters related to reach the task. In this concept, let u denotes the configuration uncertainty, which is the uncertainty associated the robotic vehicle positioning. This configuration uncertainty is characterized by two parameters,

$$u = (d, \delta\theta) \in \mathbb{R} \times S^1$$

where d represents the uncertainty on position of the vehicle, and $\delta\theta$ denotes the uncertainty on its orientation. Recall that a configuration of the vehicle is defined by the kinematic model as,

$$q = (x, y, \theta) \in \mathbb{R}^2 \times S^1$$

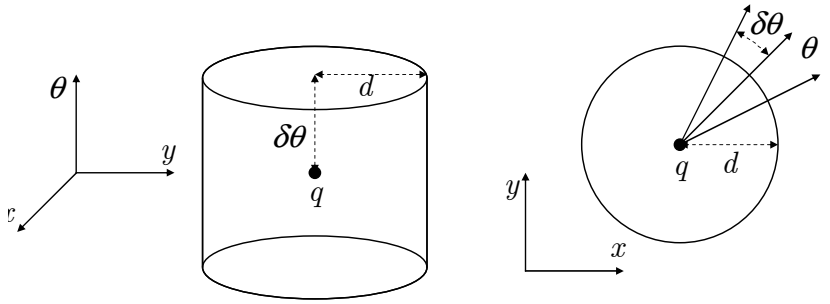

Figure 7.4: **Configuration of the uncertainty:** $\Delta(q, u)$ **represented in the configuration space of the vehicle and its representation in the plane** xy**.**

Hence, the set of possible configurations for the robotic vehicle, when its nominal configuration is q and its uncertainty is u, is represented as a cylindrical region in the space, whereas, its representation on the plane xy is a circle that bounds the position of the vehicle and an arc composed by the lines that bounds its orientation, as shown the Figure 7.4. These possible configurations are defined as,

$$\Delta(q, u) = \{q_c \,|\, dist(q, q_c) \,<\, d \, and \, |\theta \,-\, \theta_c| \,<\, \delta\theta\}$$

where $dist(q, q_c)$ is the Euclidean distance between the position components of q and q_c. To define the uncertainty propagation, the path is considered as sequence of elementary paths, which are defined as being either a straight segment or a circular arc. Therefore, it needs to compute the uncertainty evolution along every elementary path. Let $\Delta_E = (q, u, V, \gamma, \sigma_v, \sigma_s)$ denote the uncertainty of the vehicle at the end of an elementary path; i.e., a new configuration q' reached from the current configuration q, starting with an uncertainty u, and subject to the control parameters (the velocity V, the steering angle γ, and the associated uncertainties σ_v and σ_s, respectively).

As a result, the uncertainty evolution is defined as $\Delta_E = (d_E, \delta\theta_E)$; where d_E and $\delta\theta_E$ characterize the position and orientation uncertainty of the vehicle at end of the path. d_E denotes the maximum distance of the possible configuration q_c, it is the circle radius centered in the reached configuration q'; whereas $\delta\theta_E$ is the maximum unsigned difference between θ' and the orientation θ_c. Thus Δ_E can be expressed as,

$$d_E = max \, dist(q', q_c)$$

$$\delta\theta_E = max \, |\theta' \,-\, \theta_c|$$

Referenced to the vehicle kinematic model, which yields

$$\theta' = \theta \,+\, \left[\frac{V \, tan(\gamma)}{L}\right]$$

and,

$$\theta'_c = \theta_c + \left[\frac{V_c\, tan(\gamma_c)}{L}\right]$$

then $\delta\theta_E$ can be defined as,

$$\delta\theta_E = max \left| (\theta' - \theta_c) + (\left[\frac{V\, tan(\gamma)}{L}\right] - \left[\frac{V_c\, tan(\gamma_c)}{L}\right]) \right|$$

Using d_E and $\delta\theta_E$ expressions, it is possible to compute the uncertainty evolution along the given path. It can be observed that both d_E and $\delta\theta_E$ are monotonously and increasing functions, intrinsically related to the magnitudes of the steering uncertainty and the velocity uncertainty, which affect the accomplishment of the task. Thus an analysis is needed to identify the required parameters of the sensors to achieve successfully the task (i.e., the estimated uncertainty of the sensors).

The uncertainty propagation can be simulated using the discrete kinematic model and under the assumption of expected values for the velocity uncertainty σ_v and the steering uncertainty σ_s along a given path in a particular environment, as the Fig. 7.5 shows. In this analysis this evolution will be computed using maximum values for:

$$V_c \in [V - \sigma_v, V + \sigma_v]$$

$$\gamma_c \in [\gamma - \sigma_s, \gamma + \sigma_s]$$

$$(\theta - \theta_c) \in [-\delta\theta, \delta\theta]$$

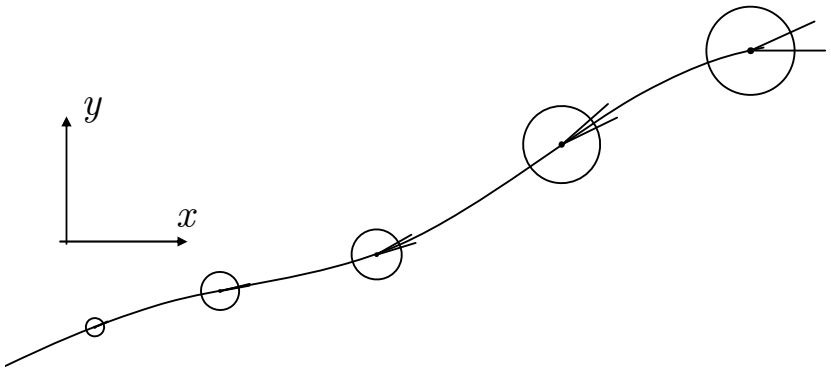

Figure 7.5: **Evolution of the positioning uncertainty along a given path.**

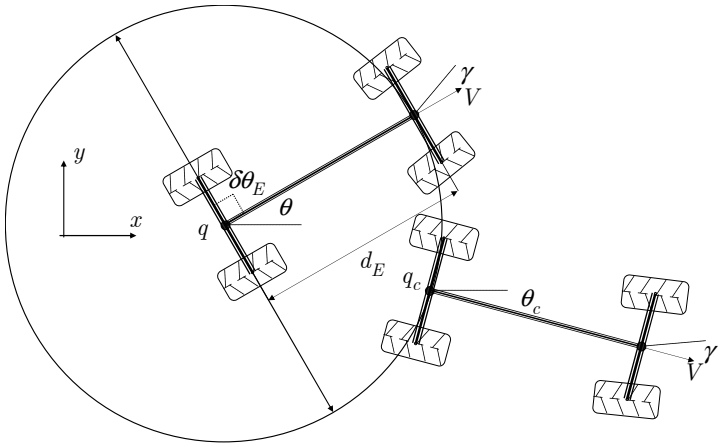

Figure 7.6: **Criterion for the positioning uncertainty.**

Based on dead reckoning, the autonomous vehicle may have a positioning failure due to the evolution of the positioning uncertainty, in which the vehicle is lost and it is unable to reach its task. This situation is assumed when the magnitude of the maximum distance d_E is greater than or equal to the wheelbase L ($d_E \geq L$) and/or the maximum orientation $\delta\theta_E$ is greater than or equal to a right angle $\frac{\pi}{2}$ ($\delta\theta_E \geq \frac{\pi}{2}$), as so this is shown by the Fig. 7.6. Throughout this analysis, the latter is assumed as a criterion to determinate the maximum traveled distance d_t for certain values of uncertainty in the velocity sensor and the steering sensor. After this distance d_t the vehicle positioning is ambiguous for both the position and the orientation.

7.1.4 Absolute Sensor

Relying on dead reckoning only, the autonomous vehicle will never be assured to reach its destination. Absolute localization is necessary to reduce the positioning uncertainty from time to time, preventing that the vehicle reaches the maximum traveled distance d_t without any update. To this end, the vehicle must have at least a sensor that allows the vehicle to recover its position and orientation; hence, the existence of an absolute sensor is required; landmarks are assumed in this analysis.

The landmarks must be located in the environment at fixed and known locations, which depend on maximum traveled distance d_t and the parameter set of the absolute sensor. The parameters of the absolute sensor are the sensor range r_{sensor}, the sensor scan rate $rate_{sensor}$, its intrinsic range uncertainty σ_r, and its bearing uncertainty σ_b. The absolute sensor provides information about the distance r_{Li} and the angle ϕ_{Li} to the landmark while the sensor observes it. Then, the vehicle can update its position and orientation with respect to the landmark coordinates (x_{Li}, y_{Li}). Figure 7.7 depicts the observation range and bearing (r_{Li}, ϕ_{Li}) made by the absolute sensor. To improve the result, a filter that accounts for the sensor uncertainties can be used.

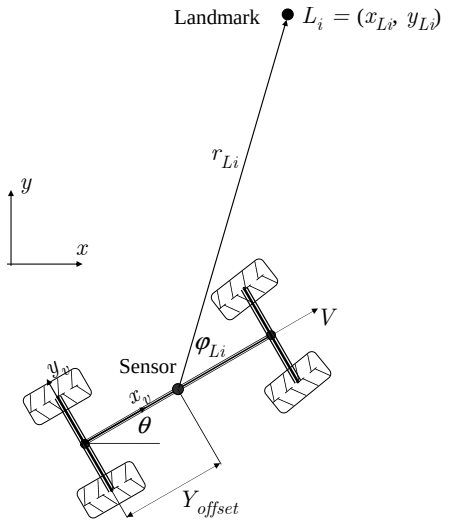

Figure 7.7: **Observation of landmarks to update the vehicle positioning, using the observed data (r_{Li}, ϕ_{Li}) under their uncertainties (σ_r, σ_b), respectively.**

An Extended Kalman Filter (EKF) uses all of the available information about the discrete-time controlled process to produce the best estimate of the vehicle positioning. The filtering procedure consists of two basic steps: prediction and correction. The estimated velocity and steering of the vehicle is used to predict its next position and orientation; this prediction is performed when absolute sensor information is unavailable. This prediction is then combined with the observation obtained from the landmark to update both the position and orientation and by consequence, the error is minimized statistically. The derivation of the EKF used for this analysis is found in the Appendix C. To compute the positioning uncertainty, the analysis assumes particular values of the sensor uncertainties. These estimated values are applied to the kinematic equations of the robotic vehicle to investigate the required sensor parameter, such as the number of landmarks to allow the achievement of the task.

7.2 Analysis for Selected Locomotion

The propagation analysis for the positioning uncertainty has been carried out using the selected locomotion: an Ackermann steering vehicle. In particular, and without loss of generality, the vehicle must reach and follow a geometric path avoiding the vehicle getting lost despite the expected uncertainty. The vehicle is equipped with two relative sensors (velocity sensor and steering sensor) and one absolute sensor (observation sensor); all the sensor information is integrated via the EKF. The wheelbase L is 1 m and the path following must be traced at constant velocity ($V = 1$ m/s) starting from an initial configuration as sketched in Figure 7.8; on the assumption that a planner provides a set of motion commands to a controller, which converts the commands into motion execution.

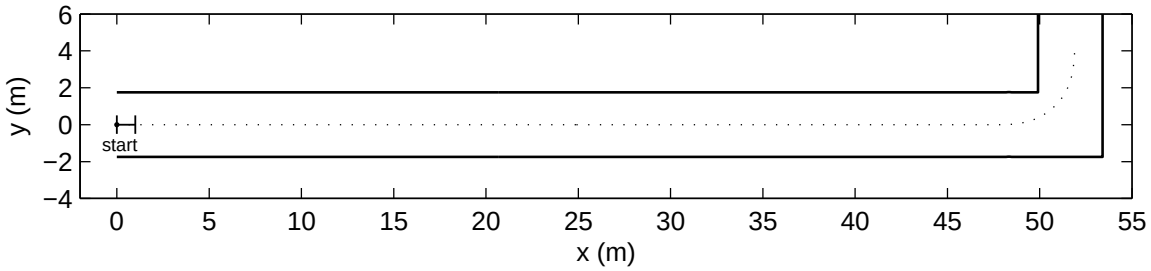

Figure 7.8: **Outline of the path (dashed line) to follow by the robotic vehicle in the tunnel-profiling task. The path keeps the middle of tunnel, limited by the walls (solid line), as proper criterion.**

7.2.1 Sensor Uncertainty

The sensor uncertainties depend on complex phenomena, regarding the interaction among sensors, vehicle, and environment, which are difficult to define in an accurate model; thus, the theoretical propagation of uncertainty is estimated from expected uncertainties. Such uncertainties are formulated by means of proportional relations that involve the vehicle parameters and the vehicle operation, such as steering and velocity. Henceforth, the associated sensor uncertainties are given by the following expressions:

Steering Uncertainty: proportional to maximum steering angle γ that the vehicle can perform (i.e., $\gamma \leq \gamma_{max}$). It can be described as,

$$\sigma_s = k_s \, \gamma_{max}$$

where $k_s \in (0, 1)$ is the constant of the steering uncertainty.

Velocity Uncertainty: proportional to the nominal velocity V of the vehicle during the path following. Thus, the velocity uncertainty σ_v is expressed by,

$$\sigma_v = k_v \, V$$

where k_v is the constant of the velocity uncertainty. This percentage is related to a maximum displacement allowed in terms of the sample period ΔT to the vehicle control; i.e, a ratio between the wheelbase and the sample period, which is defined by,

$$k_v = \frac{k_w \, L}{\Delta T}$$

with $k_w \in (0, 1)$ as the constant of the maximum displacement uncertainty.

Range Uncertainty: proportional to the maximum range r_{sensor} of the absolute sensor. This sensor uncertainty is given as,

$$\sigma_r = k_r \, r_{sensor}$$

where $k_r \in (0, 1)$ denotes the constant of the range uncertainty.

Bearing Uncertainty: related to the range uncertainty σ_r of the absolute sensor. Referring to the Figure 7.7 of observation model, the bearing uncertainty is expressed as

$$\sigma_b = atan(\frac{\sigma_r}{r_{sensor}})$$
$$\sigma_b = atan(k_r)$$

To compute the propagation uncertainty of the Ackermann steering mechanism, the uncertainty analysis assumes particular values for the constants derived in the above expressions. The percentage k_s is estimated as 10 % with respect to steering angle γ, as 10 % for the percentage k_w in terms of the ratio $frack_w \, L\Delta T$; whereas, the percentage k_r is estimated as 1 % with respect to the absolute sensor range r_{sensor}. These estimated values are applied to equations under a steering angle $\gamma_{max} = 35°$, a nominal velocity $V = 1.0$ m/s, a sampling step $\Delta T = 0.1$ s, and a sensor range $r_{sensor} = 10$ m. Table 7.1 shows the calculated uncertainties, as a reference to investigate the impact on the positioning estimation.

Table 7.1: **Sensor uncertainties**

Source	Constant	Uncertainty
Steering sensor	$k_s = 0.10$	$\sigma_s = 3.5°$
Velocity sensor	$k_v = 1.00$	$\sigma_v = 1.0$ m/s
Absolute sensor	$k_r = 0.01$	$\sigma_r = 0.1$ m
Absolute sensor	$k_r = 0.01$	$\sigma_b = 0.6°$

7.2.2 Positioning Estimation

The Ackermann vehicle positioning is computed to estimate the uncertainty propagation in odometry; i.e., dead reckoning from indications of velocity and steering sensors considering their respective uncertainty values (Table 7.1). In this simulation, the essential purpose is the derivation of the maximum traveled distance d_t, using the criterion of the positioning uncertainty. Figure 7.9 shows the resulting uncertainty evolution while the vehicle follows the given path; null uncertainty is assumed on the start position and the positioning uncertainty is associated with reference to the rear axle of the vehicle.

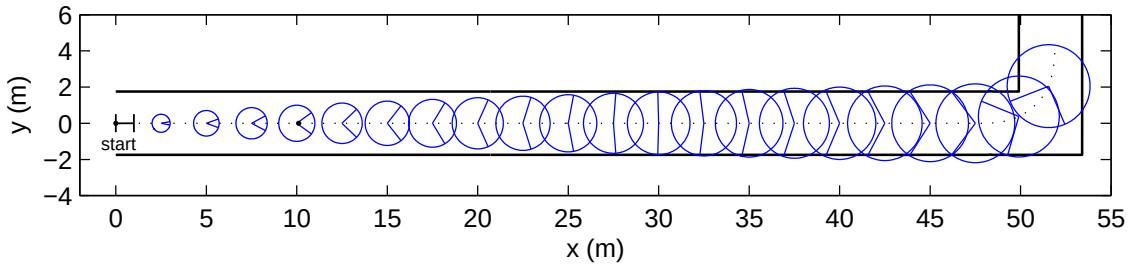

Figure 7.9: **Uncertainty propagation of the vehicle positioning along the path.**

The effect of the odometry sensor uncertainties is evident on the estimation of the vehicle positioning, and a significant inconvenience for the achievement of the task. In particular, the vehicle is limited to reach the end of the path; since the overall growth of the positioning uncertainty is more than the uncertainty criterion. Referring to this simulated propagation, the uncertainty criterion is reached by the vehicle at 10.1 m from the start setting, as shown the Figure 7.10. After this distance the vehicle will be lost, due to the magnitude of the maximum distance d_E that is greater than the wheelbase L ($d_E \geq L$); i.e., the vehicle positioning estimation presents ambiguity.

Hence, the maximum traveled distance d_t is equal to 10.1 m. Fig. 7.10 shows the estimated uncertainty at this distance, the centre of the circle is placed on the vehicle positioning references (x, y). The circle radius corresponds to position uncertainty d_E; whereas the orientation uncertainty $\delta\theta_E$ is the angle illustrated by the dashed lines with respect to the nominal orientation of the vehicle. To avoid that the vehicle reaches this situation and eventually lost, the traveled distance is scaled by a level of confidence. This confidence distance is the maximum or the longest distance, in which the position estimation must be update using the information from the absolute sensor and applying the nonlinear Kalman filter. Let k_c denotes the constant of confidence of 90%. Thus, this confidence distance d_c is equal to,

$$d_c = k_c\, d_t = 0.90(10.1) = 9.09m$$

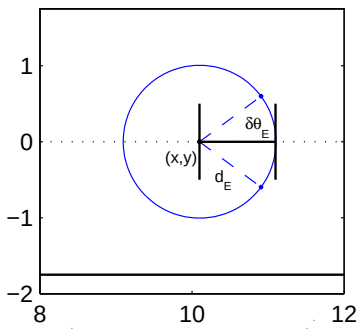

Figure 7.10: **Maximum traveled distance in odometry.**

Table 7.2: **Landmark location**

Landmark	Coordiante (x_{Li}, y_{Li})	Observations
L_1	$(19.99, 0.00)$	2
L_2	$(38.17, 0.00)$	2
L_3 *	$(51.41, 1.75)$	2

* corner landmark

7.2.3 Positioning Update

To recover the vehicle positioning, under the presence of these odometry uncertainties, the positioning estimation must be updated involving landmarks along the path. In this context, the landmark location depends on the confidence distance (d_c) and the range of the absolute sensor (r_{sensor}).

For computing the landmark locations, hereinafter it is assumed that landmarks are on the track of the given path; thus, the vehicle can only detect the landmark in its front field of view. It also is considered that on tight corner, such is the case of the given path (Figure 7.8), there must be a landmark defined as *corner landmark* that is visible. The location of absolute sensor is $Y_{sensor} = L$; this position is on the front axle and has been analyzed in the earlier Section 6.3, concerning with the perception analysis. Table 7.2 shows the computed landmark coordinates, considering an absolute sensor range $r_{sensor} = 10$ m and its respective uncertainty values (Table 7.1); whereas, the Figure 7.11 illustrates the locations of such landmarks.

In the following simulations, the EKF technique is used to investigate the requirements to minimize the positioning uncertainty. For such purpose, the evolution of the positioning uncertainty is computed, varying the number of landmarks and observations, as well as the range of the absolute sensor.

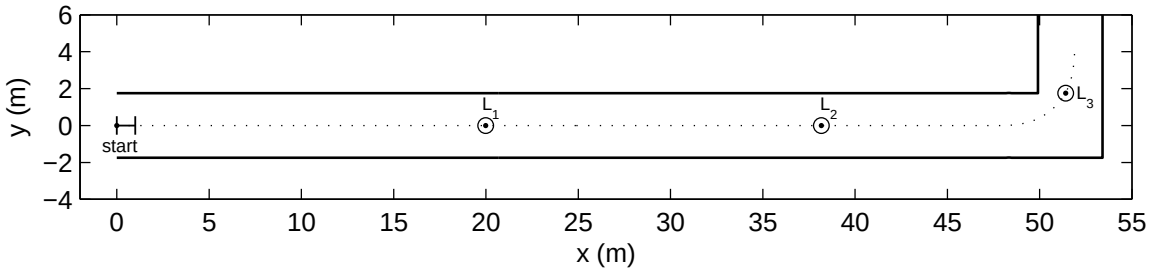

Figure 7.11: **Landmark placement along of the path.**

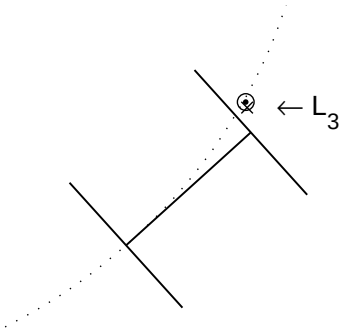

Figure 7.12: **Last observation of the corner landmark.**

Null uncertainty is assumed on the start position and the aforementioned odometry uncertainties. Furthermore, the absolute sensor must observate at least a landmark at the confidence distance d_c. It also is assumed that the vehicle must perform a last observation of the corner landmark, regardless of the amount the observations. This last observation is made at minimum distance, which is calculated based on the curvature of the path in the corner and the location of the corner landmark, as shown the Figure 7.12. In this exercise, the path presents a radius of the circle arc equal to 3.35 m, i.e. a constant curvature $c = \frac{1}{3.35}$.

Table 7.3 shows the distance of observation by which the vehicle is expected to observe a landmark. This distance of observation is given by $\frac{d_c}{Ratio}$; where the *Ratio* is the amount of observations made by the sensor inside of the confidence distance (d_c). It is important to note that the *Ratio* can be also expressed by $\frac{V\,Ratio}{d_c}$, as the rate of observations when the observations depend on time instead of the distance traveled. This may be interpreted as the scan rate of the absolute sensor.

Table 7.3: **Observation distance**

Ratio	Distance (m)	Scan rate (Hz)
1	9.09	0.11
2	4.54	0.22
3	3.03	0.33
4	2.27	0.44
5	1.82	0.55
10	0.91	1.10
20	0.45	2.20
100	0.09	11.00

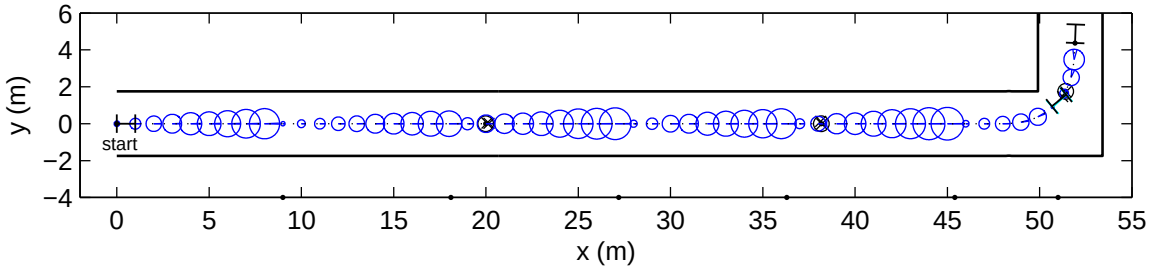

Figure 7.13: **Uncertainty propagation applying the EKF technique. The vehicle observes a landmark at intervals equal to confidence distance d_c.**

Figure 7.13 depicts the uncertainty evolution while the vehicle follows the given path. For this exercise, the absolute sensor must observe a landmark at intervals equal to the confidence distance d_c; i.e., a $Ratio = 1$ according to the Table 7.3. In such case, the vehicle can observe twice each landmark, the crosses show the estimated position of such landmarks, respectively; whereas, the distance where the absolute sensor observes a landmark is illustrated by black points over the x axis of the plot. In each observation, the absolute sensor measurement is converted into the range and the bearing observation referenced to the vehicle coordinate system. This observation is projected into base-coordinates, and then matched to the known landmark locations in the path (Table 7.2.). The matched landmark is transformed back into vehicle coordinate system, which is used to correct and to update the vehicle positioning, using the EKF technique.

It can be noted that the positioning uncertainty is minimized in every observation, allowing the vehicle reaches successfully the end of the path while moving from landmark to landmark, in spite of the sensor uncertainties. Thus, this behavior is analyzed for different amount of observations, according to the Table 7.3. Figure 7.14 shows the results of the estimated uncertainty evolution for the vehicle positioning, considering the same set of landmarks (Table 7.2.) and sensor uncertainties (Table 7.1).

Referring to these resulting propagations, it important to note that the uncertainty of the vehicle positioning decreases significantly while the absolute sensor performs a major number of observations; i.e., the reduction of the positioning uncertainty is proportional to the number of updates. In particular, when the number of observations and updates are close to the control frequency (the sample period ΔT), the positioning uncertainty may be negligible since it tends to be null, as shown the Figure 7.14 (e) that estimates the uncertainty evolution for a $Ratio = 100$ observations. However, in a realistic context, these frequent updates can result in excessive requirements for the absolute sensor, inclusive such information will be unavailable at required rates.

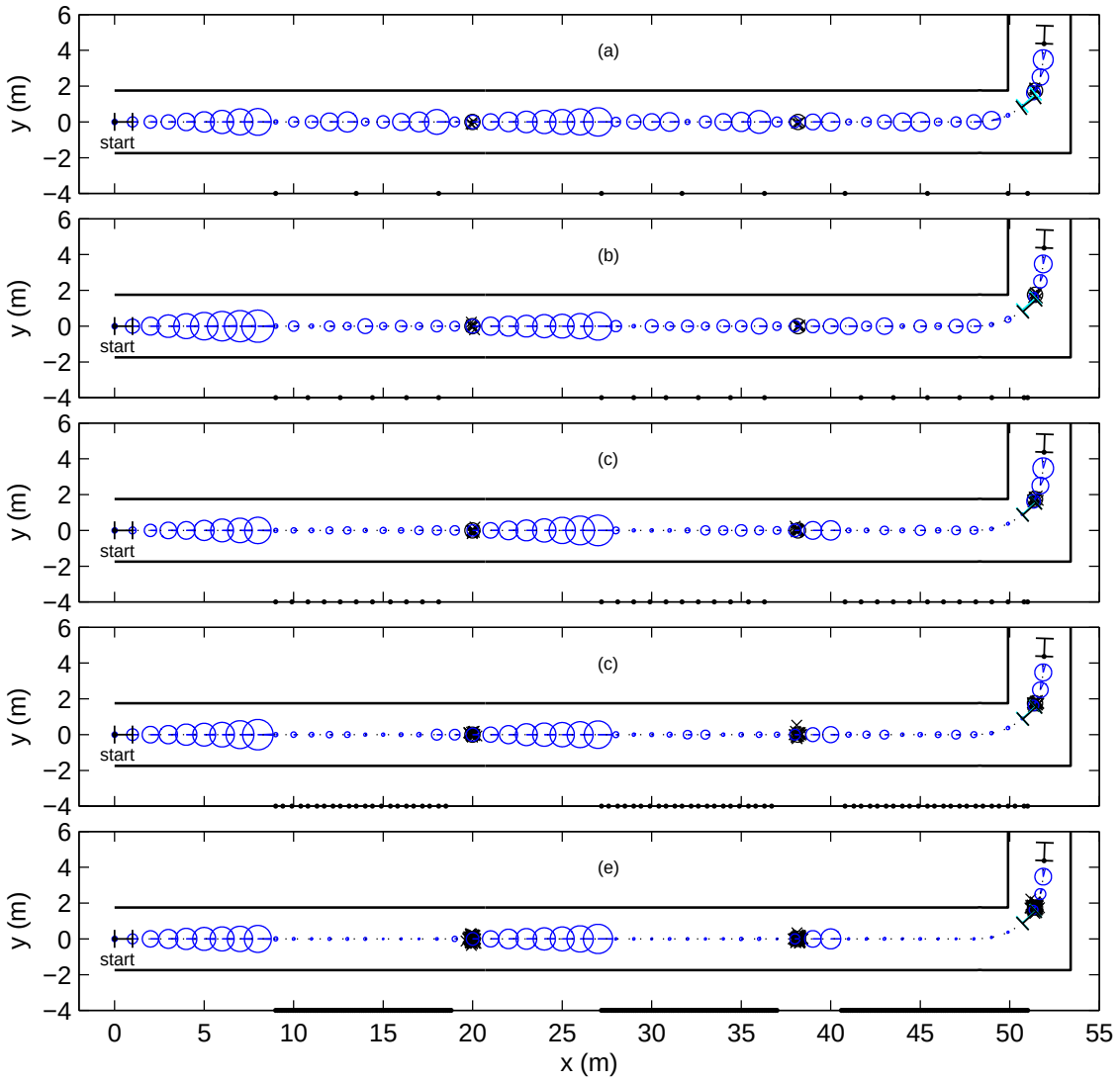

Figure 7.14: **Uncertainty evolution for a *Ratio*: a) 2, b) 5, c) 10, d) 20, and e) 100 observations.**

These results indicate a trade-off among the number of observations and the improvement of the vehicle positioning, under a certain sensor range (r_{sensor} = 10 m). To investigate the relation between the uncertainty propagation and the range of the absolute sensor, the vehicle positioning is simulated comparing diverse sensor ranges against the number of landmarks needed to reach the end of the path. Table 7.4 shows the calculated landmark number and locations for specific sensor ranges. Whereas, the Figure 7.15 presents the uncertainty evolution, assuming one observation per confidence distance ($Ratio = 1$). The case of minimal range ($r_{sensor} = 0$ m) is considered as direct and instant observations at the confidence distance.

Table 7.4: Landmark locations

Absolute sensor		r_{sensor} (m)		
0.0	6.0	10.0	20.0	50.0
(10.2,0.0)	(15.9,0.0)	(19.9,0.0)	(29.9,0.0)	(51.4,1.75)*
(19.3,0.0)	(25.1,0.0)	(38.1,0.0)	(51.4,1.75)*	
(28.4,0.0)	(34.2,0.0)	(51.4,1.75)*		
(37.4,0.0)	(43.2,0.0)			
(46.5,0.0)	(51.4,1.75)*			
(51.4,1.75)*				

* corner landmark

7.2.4 Discussion and Comparison

The uncertainty in the vehicle positioning has been estimated for the selected Ackermann vehicle. The uncertainty is calculated to investigate the vehicle performance in the context of its propagation along a given path. This theoretical evolution, developed in terms of the expected sensor uncertainties, absolute sensor range, quantity of updates, and number of landmarks, addresses the following observations:

1. The vehicle is limited to achieve the end of the path, using only dead reckoning from indications of velocity and steering sensors. The vehicle positioning uncertainty increases along of the path and consequently the vehicle is lost, as shown the Fig. 7.9.

2. Using the Kalman filter, integrated indications from an absolute sensor to estimate the vehicle positioning, the propagation of the uncertainty is minimized, at least in certain boundaries to complete the path. Thus, this architecture, composed by velocity, steering, and absolute sensors, is an essential component for the Locomotion subsystem.

3. The results indicate a trade-off in the number of observations to keep the uncertainty propagation within certain boundaries; i.e., under the uncertainty criterion defined in the Section 7.1.3. Such observation number depends on the availability of information for the absolute sensor, proportional to its frequency of operation or scan rate. Thus, it is a key parameter to select the absolute sensor, in addition to the criteria about computing and power cost.

4. Whereas, the trade-off in the number of landmarks to accomplish the path depends on the range of the absolute sensor and the environmental conditions. Since, the performance of the sensor is affected by the geometry of the tunnel that may set out of reach the landmarks. A minor reach of the absolute sensor increases the number of landmarks needed.

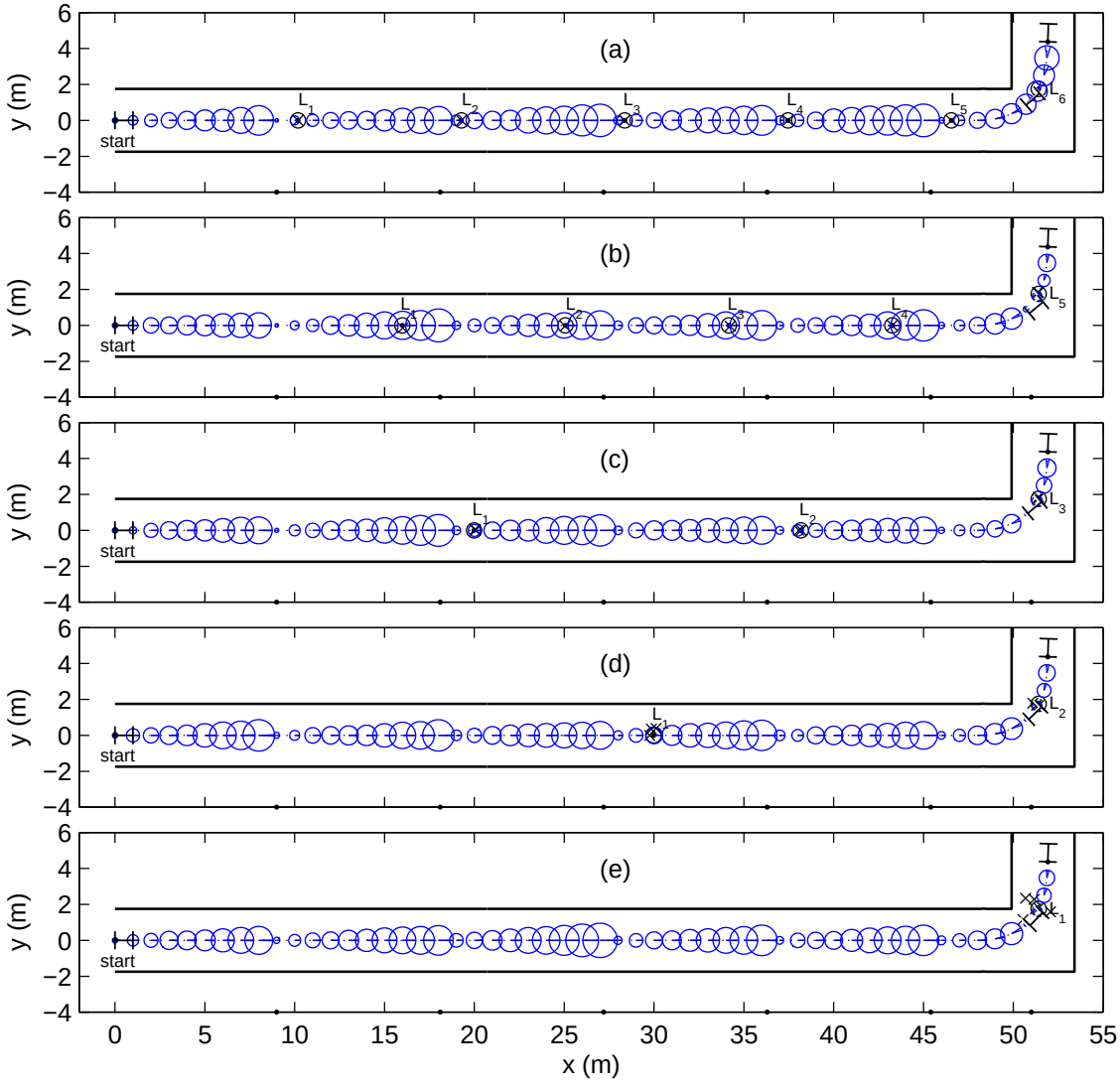

Figure 7.15: **Uncertainty evolution for r_{sensor}: a) 0, b) 6, c) 10, d) 20, e) 51.4 m.**

7.3 Locomotion Configuration

In order to complete the Locomotion subsystem, the uncertainty propagation in the vehicle positioning has been investigated. The uncertainty analysis is a comparison among the necessary sensor parameters to keep such uncertainty within boundaries along a given path. The theoretical results show that the parameters outlined in the Table 7.5 are a suitable solution to the uncertainty problem of the vehicle positioning for the tunnel-profiling task. Such solution is implemented through the filtering of observations of landmarks with odometry sensors in an Extended Kalman Filter to provide estimates of vehicle position and orientation, under certain uncertainty associated to the sensors.

Odometry is implemented by a steering sensor, limited by an allowable uncertainty less than 3.5 °, and a velocity sensors having an uncertainty less than 1.0 m/s; whereas the absolute sensor requires an associated uncertainty less than 0.1 m and 0.6 ° in its range and bearing, respectively. Under these parameters, three landmarks are needed to reach the end of the path; consequently, the relation between landmarks and observations is addressed by the sensor range $r_{sensor} = 10$ m of the absolute sensor, and a $Ratio = 1$, producing two observations to each one of these landmarks. Thus, the vehicle positioning is updated every 9.09 m (or a rate equal to 0.11 Hz) while the vehicle moves along the tunnel, as shown the Figure 7.13.

Therefore, this suitable solution must be included in the robotic vehicle configuration, which is mapped into the Mining Autonomous Vehicle structure as the module to estimate the vehicle positioning. Figure 7.16 shows such structure, which consists of the Locomotion, Deployment, and Tool subsystems to implement the Basic Configuration $P_1R_2P_3$ for performing the tunnel-profiling task.

The Locomotion subsystem includes the results of the autonomy and uncertainty analysis, which lead to identify an Ackermann vehicle and the positioning module. The Ackermann steering satisfies the kinematic requirements to improve the position estimation, the control and the perception requirements, identified by a parametric comparison of different steering mechanisms. Whereas, the positioning module implements the architecture to estimate the position and orientation of the Ackermann vehicle

Table 7.5: **Sensor parameters**

Sensors	Parameter
A Steering sensor	$\sigma_s \leq 3.5°$
A Velocity sensor	$\sigma_v \leq 1.0$ m/s
An Absolute sensor	$\sigma_r \leq 0.1$ m
	$\sigma_b \leq 0.6°$
	$r_{sensor} \geq 10.0$ m

Under the following values								
L (m)	γ_{max} (°)	V ($\frac{m}{s}$)	ΔT (s)	k_s	k_w	k_v	k_r	k_c
1.0	35	1.0	0.1	0.1	0.1	1.0	0.01	0.9

Landmark coordinates		
(19.99,0.0)	(38.17,0.0)	(51.41,1.75)*

Ratio	Observations	Distance	Rate
1	2	9.09 m	0.11 Hz

* corner landmark

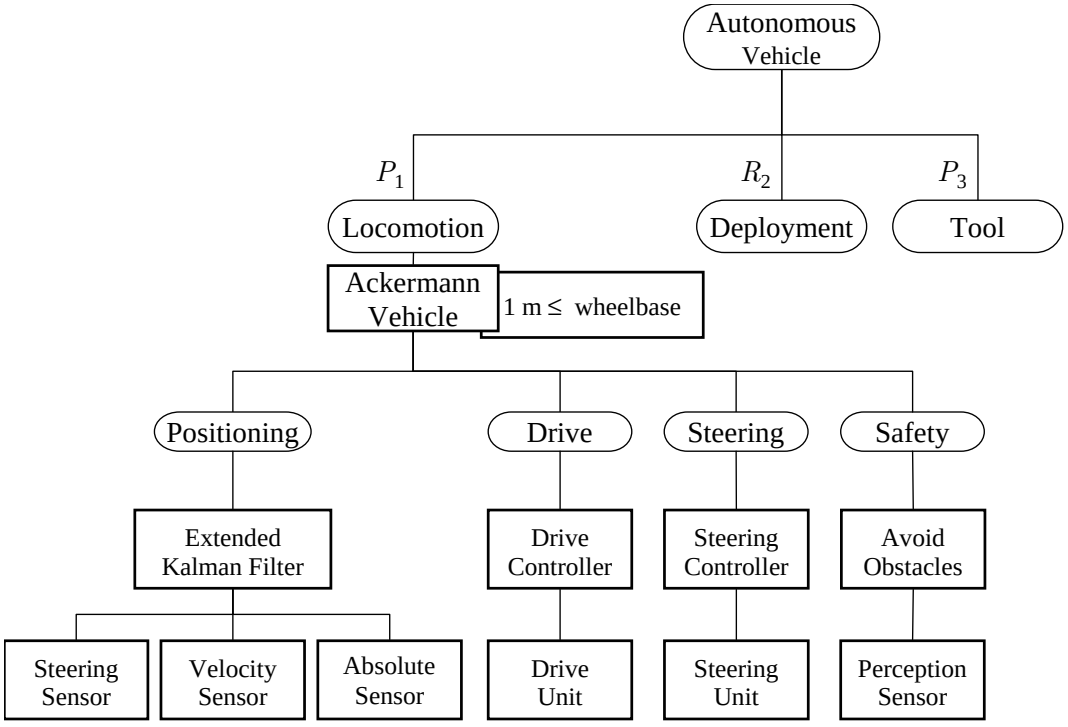

Figure 7.16: **Configuration of the MAV including the selected Locomotion subsystem that integrates the positioning, drive, steering and safety modules, referring to the results of the autonomy and uncertainty analysis.**

within acceptable levels of positioning uncertainty, integrating the measurements of the steering, velocity, and absolute sensors by means of an Extended Kalman Filter. The steering and velocity sensors should be connected with the drive and steering units of the Ackermann vehicle to provide available indications, via the drive and steering modules, respectively. Whereas, the absolute sensor keeps its location on the front axle of the Ackermann vehicle to observe the landmarks.

Based on this configuration, the synthesis of the robotic vehicle is developed in the following Chapter. The process of instantiation will be presented for every subsystem, recapturing the System Design phase of the systematic framework and selecting the correct component to provide the complete configuration of the Autonomous Vehicle that performs the tunnel-profiling task with certain degree of autonomy.

Chapter 8

Synthesis of MAV Configuration

This chapter addresses the systematic framework conclusion to complete the synthesis of the Mining Autonomous Vehicle configuration. To this purpose, every subsystem of the structure, derived by the autonomy analysis (Chapters 6 and 7), should be instantiated with proper components. This instantiation process provides a detailed structure of specific components to implement the Basic Configuration, based on the Configuration Requirements and Configuration Parameters to select each component; in regard to the technical specifications and constraints produced by the selected components.

In the following sections, the System Design phase is developed, from the component selection, to derive the complete and detailed MAV configuration, as the solution for synthesis of the robotic vehicle prototype to perform the tunnel-profiling task. Finally an outline of the integration process and observations are also presented.

8.1 Component Selection

The feasible solution is defined when the Configuration Requirements, the Configuration Parameters, and the Component Requirements have been satisfied and the Basic Configuration is transformed into a complete structure of subsystems, integrated by specific components to perform the given task. Thus, the instantiation implies the selection of such components for implementing the subsystem function defined by the motions of the Basic Configuration. Referring to the Figure 7.16 of the MAV structure, these subsystems are the Tool, Deployment, and Locomotion that must be instantiated by a laser rangefinder, a PTU or steeper motor, an Ackermann vehicle. The next sections present the selection procedure for each subsystem and involved modules, considering the order of analysis established in the Section 4.5.

8.1.1 Tool and Deployment Subsystems: Laser

Although the laser Sentinel 100 was selected for a previous example (Chapter 5), updating the component inventory and following both the Configuration Requirements

and the Configuration Parameters (Table 4.1 and 4.8, respectively), the laser LMS 221 presents a better fulfillment of the requirements and parameters for the motion P_3. In particular, this laser behaves the lowest spot diameter, having a diminution about 50 %, and a superior measurement rate, approximately 100 times faster than the laser Sentinel 100 (as is shown in the Table 5.2).

These specifications are related to an improvement in the measurement process, which is identified as the fundamental function of the Tool subsystem. Nevertheless, the necessary accuracy (accuracy_measured) in the Configuration Requirements should be relaxed by a threshold equal to ± 1 cm since the manufacturer reports an accuracy up to ± 6 cm, thus the requirement accuracy_measured is updated as,

$$\begin{aligned} \text{accuracy\_measured} &\leq 0.06 \text{ m} \\ \text{-0.06 m} &\leq \text{accuracy\_measured} \end{aligned}$$

In addition to the operation for measuring the time of flight of laser light pulses, the laser LMS 221 provides a rotational motion that matches the Configuration Parameters for the motion R_2, implementing the functionality of the Deployment subsystem to orientate the Tool subsystem (i.e., the laser beam). Since the laser beam is deflected by an internal rotating actuator up to 180° as maximum scanning range at three angular resolutions 0.25°/0.50°/1.00°/. This scanning motion satisfies the Configuration Parameters of the motion R_2, such as the range of operation (θ_2), the span necessary (span_θ_2), and the angular interval ($\Delta\theta_2 \leq 1.76°$). Thus, this laser is selected to instantiate both the Tool and Deployment subsystems. The pulses embodies the functionality of the prismatic motion P_3; whereas, the scanning motion embodies the functionality of the rotation motion R_2.

The technical specifications of the laser LMS 221 are mapped to a list of Component Requirements, which are actuation-sensing specifications and constraints. In this case, the laser is a non-contact measurement device that operates with a power supply 24 V DC and requires a data interface RS 232 for setting operation parameters and gathering the measured data. Thus, the necessary serial port for serial transmission and the power supply are denoted by the quantifiers port_serial and power_laser, respectively. Additionally, the features of the laser serve to instantiate certain parameters of the motions R_2 and P_3, such as the quantifier P_3_weight instantiated by the laser weight (i.e., P_3_weight $\leq$ 9.0 kg); whereas, the constraint R_2_payload is neglected, and the quantifier R_2_weight is updated as: R_2_weight $\leq$ 0. Table 8.1 shows these requirements that must be analyzed in order to avoid propagation of conflicts or technical contradictions with respect to rest of the components.

8.1.2 Locomotion Subsystem: Ackermann Vehicle

An initial configuration study that examined the Configuration Parameters of the motion P_1 determined that a wheeled vehicle was feasible to implement its functionality.

Table 8.1: **Laser Component Requirements**

Technical Specification	Component Requirements
LMS 221	
I/O Interface RS232	port_serial_laser ≤ 1
Power 24 VDC	power_laser $\leq$ 24 VDC
Weight 9.0 kg	P_3_weight $\leq$ 9.0 kg
	R_2_weight $\leq$ 0.0 kg
Dimension 352×195×266 (mm) (H×W×L)	height_laser $\leq$ 0.352 m
	width_laser $\leq$ 0.195 m
	length_laser $\leq$ 0.266 m

The selection has been leveraged by a four-wheel vehicle, to navigate under the geometry of the expected terrain while avoiding obstacles (such as rocks). The trade-offs in the vehicle dimensions has been determined by a geometric analysis based on equilibrium state to maintain a stability position through the tunnel. Consequently, the autonomy analysis, comparing different steering mechanisms, determined that an Ackermann vehicle with a wheelbase (1 m $\leq$ wheelbase) is the component to implement the Locomotion subsystem of the robotic vehicle configuration. Furthermore, the selected Locomotion subsystem must be completed with the positioning module derived by the uncertainty analysis for the achievement of tunnel-profiling task; in addition to the Configuration Requirements.

Therefore, these aforementioned results address to the selection of a four-wheeled Ackermann vehicle, such as motorcycles or compact utility vehicles. The vehicle model Super Truck made by Johnson Industries satisfies the Configuration Requirements and the Configuration Parameters (Table 4.1 and 4.8, respectively) for the Locomotion subsystem. This vehicle is steered by an Ackermann mechanism, according to the autonomy analysis, and driven by an electric motor, which fulfills the constraint $\neg$ fuel; whereas, its other technical specifications meet the rest of parameters and requirements, such as the required payload (P_1_payload), the vehicle dimensions (wheelbase_vehicle), and the ground clearance (ground_clearance), as shown the Table 8.2.

Table 8.3 shows the Component Requirements of the Super Truck vehicle; i.e., the list of the actuation-sensing specifications translated as requirements, which must be analyzed and satisfied to operate the Locomotion subsystem.

Table 8.2: **Super Truck Technical Specifications**

Specifications	Configuration Requirement/Parameters
Electric Motor 5 hp	¬ fuel
36 VDC	
Electric system:	
36 VDC	
six batteries 6 V/20 A	
Controller solid state 36 volt/ 400 amp	
Top Speed 20.5 m/s	
Run distance (single charge) upper 1 km	run_time
Transmission:	d_1
Forward/Reverse	span_d_1
Steering Ackermann	
commercial truck box w/ 6 turns	
lock-to-lock 1.49 m turn radius	
Payload Capacity 725 kg	P_1_payload
Empty Vehicle Weight 635 kg	wheel_loading
Ground Clearance 156 mm	ground_clearance
	height_rock
Tires 18-9.50-8 4	diameter_wheel
Diameter 459 mm Width 241 mm	width_wheel
Vehicle Dimension 980×1041×1250 mm (W×H×L)	wheelbase_vehicle
	width_vehicle
	height_tunnel
	width_tunnel
	length_tunnel

Table 8.3: **Ackermann Component Requirements**

Technical Specification	Component Requirements
Super Truck Vehicle	
Forward/Reverse Advance	control_drive
Steering	control_steering
Payload 725 kg	P_1_payload $\leq$ 725 kg
Power 36 VDC	power_vehicle $\leq$ 36 VDC
Weight 635 kg	P_1_weight $\leq$ 635 kg
	weight_vehicle $\leq$ 635 kg
Dimension 980×1041×1250 mm (W×H×L)	height_vehicle $\leq$ 1.041 m
	width_vehicle $\leq$ 0.980 m
	length_vehicle $\leq$ 1.250 m

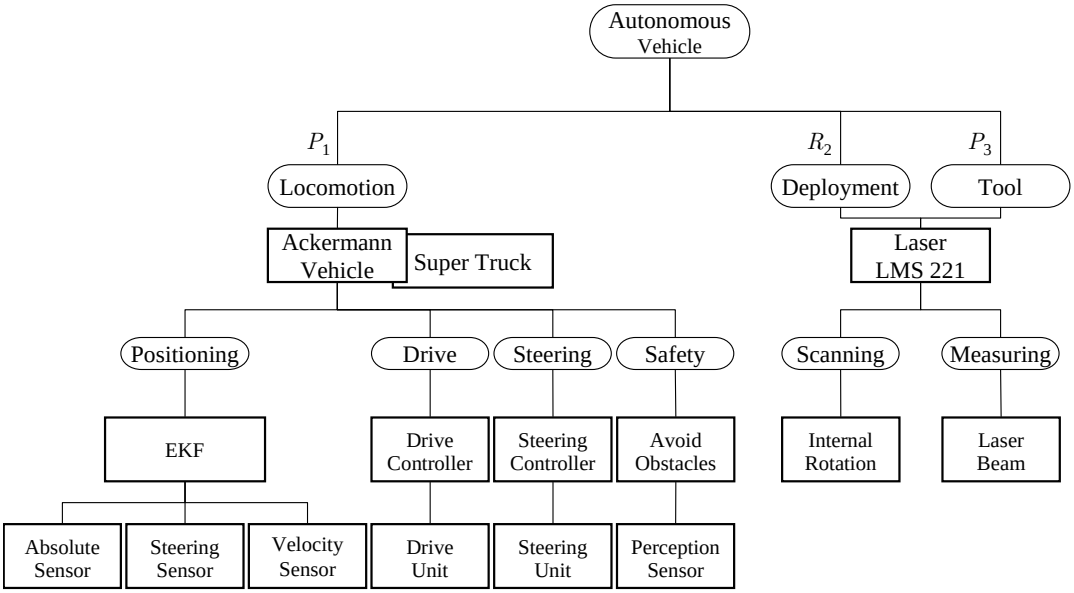

Figure 8.1: **MAV configuration formulated by the Ackermann vehicle Super Truck and the laser LMS 221.**

Therefore, the structure that represents the MAV configuration is instantiated with the selected components: the laser LMS 221 and the Ackermann vehicle Super Truck, as shown the Figure 8.1. The complete fulfillment of the MAV configuration must include each one of the defined modules to provide the controlling and sensing of every subsystem to perform the tunnel-profiling task.

8.2 Component Integration

An analysis of the Component Requirements completes the MAV configuration, under the constraints and specifications of the Configuration Requirements and Parameters. It is important to note that the integration of the selected components involves a detailed process, including system engineering, signal processing, electronic circuit board design, mechanical design (such as mounting and adaptation of components), and embedded microprocessor programming, which goes beyond the scope of this thesis. However, a feasible configuration can be derived from the requirements for actuation and sensing of the selected components, assuming the existence of such electromechanical and programming issues in the integration process.

8.2.1 Tool and Deployment Subsystems: Laser LMS 221

The laser LMS 221 is operated by its interface RS 232, to set the operation commands and to gather the measured data; i.e., both scanning and measuring functions are achieved via this interface. Moreover, an internal control leads to the sensing of these operations, for this reason no components of feedback are necessary. Therefore, an

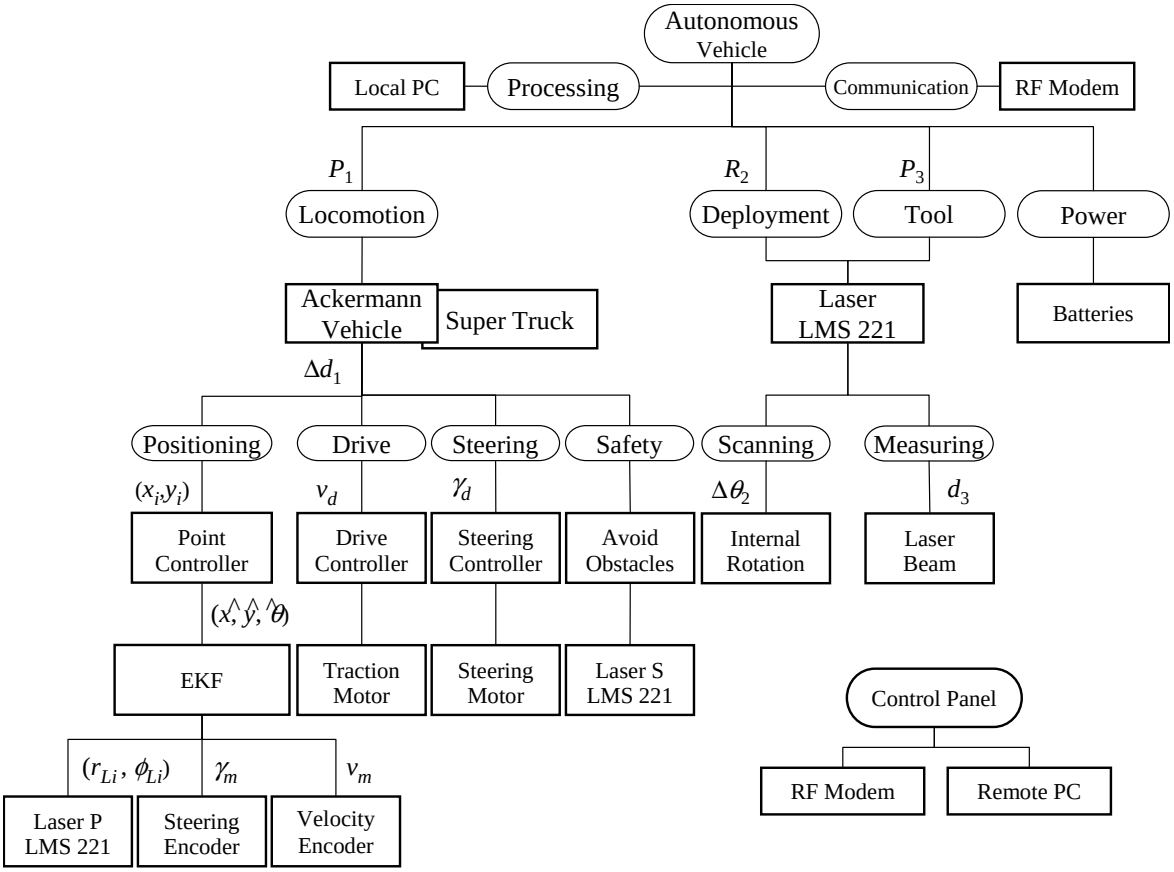

Figure 8.2: **Configuration of the Mining Autonomous Vehicle to perform the Tunnel Profiling Task.**

electronic and computing device that includes an interface RS 232 is required to control the laser, such as a personal computer (PC). This component is mapped to the MAV structure into the Processing Unit subsystem for operating the measuring and scanning modules. Whereas, the required power supply to support the operation of the laser is implemented by a commercial battery at 24 VDC, such battery is mapped into the Power Unit subsystem in the robotic vehicle structure, as shown the Figure 8.2.

8.2.2 Locomotion Subsystem: Super Truck Vehicle

The selected Ackermann vehicle should be adapted to navigate autonomously into the tunnel, implementing the motion P_1. Towards this goal, every module defined in the Locomotion subsystem has been analyzed to resolve the components that perform its controlled actuation. Such components are mapped into the structure of the Mining Autonomous Vehicle as shown in Figure 8.2.

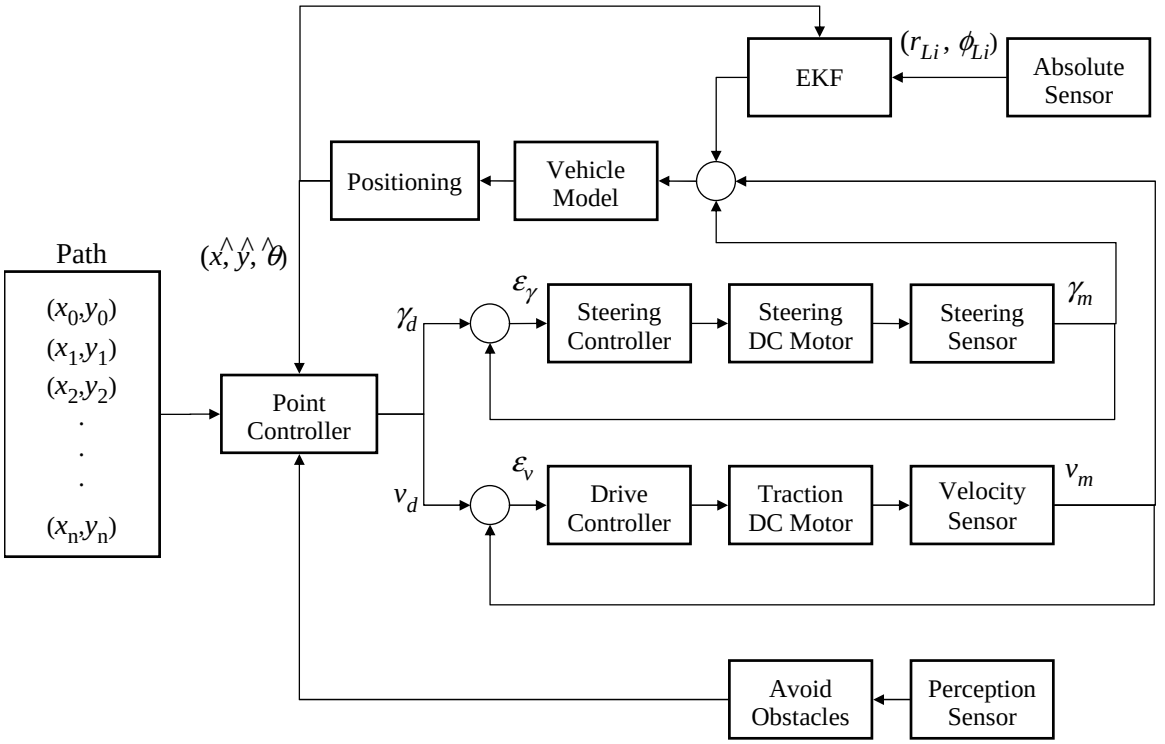

Figure 8.3: **MAV control formulated by the positioning estimation and the drive and steering controllers.**

The automation of the Locomotion subsystem implies that the vehicle navigation must be controlled with respect to a path. Such path is composed by a set of points on the plane; i.e., equidistant points at the sampling necessary according to the parameters of the motion P_1 and the Configuration Requirements (sampling_interval). Thus, the vehicle positioning must be estimated to provide the control of the vehicle to reach each one of these points; considering the positioning module and its interaction with the drive, steering, and safety modules, as shown the Figure 8.3.

Therefore, the vehicle control is implemented in this hierarchical and modular architecture; under the assumption, in which a higher-level planner develops the plan to follow, considering the nonholonomic constraints and obstacle avoidance [Latombe 91], and provides a series of points to the point controller [Palacios 00, Vazquez 02]. This controller addresses with the basic function of converting points into the desired values of actuation for both the drive and the steering controller, which deal with the generation of the lower-level commands to the respective actuator.

The following sections presents the components that implement this control architecture to instantiate the modules of the Locomotion subsystem, which are derived, not only from the kinematics of the Super Truck vehicle, but also from its physical and mechanical compound.

Referring to the geometry of the Ackermann vehicle, as shown the Figure 7.3, the kinematic model of the Super Truck vehicle is defined by the equation 7.1, which is rewritten as,

$$\begin{bmatrix} \dot{x} \\ \dot{y} \\ \dot{\theta} \\ \dot{\gamma} \end{bmatrix} = \begin{bmatrix} cos\,\theta \\ sin\,\theta \\ \frac{tan\,\gamma}{L} \\ 0 \end{bmatrix} v_1 + \begin{bmatrix} 0 \\ 0 \\ 0 \\ 1 \end{bmatrix} v_2 \tag{8.1}$$

where v_1 and v_2 correspond to the driving and the steering velocity inputs, which have been associated to the drive and steering controllers as the desired velocity (v_d) and the desired steering angle (γ_d) to operate the robotic vehicle via the point controller.

Drive Controller: The vehicle Super Truck is driven by an electric DC motor. This traction motor is powered by a supply of 36 VDC through a solid-state H-bridge circuit, provided by the manufacturer. Thus, the drive controller should be an interface that converts the forward and backward motion commands (i.e., the drive input v_d) to the electric signals for the H-bridge circuit.

This interface can be implemented by an embedded microprocessor unit to control the traction motor; in combination with electrical decoupled devices (e.g., optoisolators and a separate power supply) since this DC motor draws a significant power (up to 100 A). By varying the pulse width of the Pulse Width Modulation (PWM) in an algorithm software can be used to control the motor speed (v_d) via a conventional PID (proportional, integral, and derivative) controller that is used in the classical control theory such as [Ogata 02]. The control loop is closed by the velocity sensor, which is instantiated by an incremental encoder that must satisfy the specifications established in the uncertainty analysis and resumed in the Table 7.5.

Steering Controller: Whereas the steering operation of the vehicle Super Truck is developed by a manual wheel steering, which is attached directly to a commercial truck box with 6 turns lock-to-lock at 1.498 m turn radius referred to the Ackermann steering mechanism. A feasible solution to automate this manual wheel steering is to use a DC motor (called steering motor in the robotic vehicle structure) connected by a link to performs the steering actuation, such as a gear mechanism [Chironis 96, Norton 04]. The link transmits the motor motion towards the truck box under the constraint of the ratio between the output force and the input force applied to it.

Similar to the drive controller, the steering controller can be implemented by an embedded microprocessor unit to control the steering motor, with the control algorithm in software. In this case, a PD (proportional and derivative) controller is proposed to reach the equilibrium state faster [Ogata 02], and an absolute encoder to instantiate the steering sensor, closing the control loop for the steering angle (γ_d). This encoder must also fulfill the parameters defined in the Table 7.5.

Point Controller: To reach each one of the points (x_i, y_i), for $i = 0 \cdots n$, the point controller sets the desired velocity v_d and the desired steering angle γ_d for the drive and steering controller, respectively. In this context, the point controller uses the estimation of the vehicle positioning ($\hat{x}$, $\hat{y}$, $\hat{\theta}$) to close the control loop for the vehicle navigation, provided by the Extended Kalman Filter through the sensor measurements: measured velocity v_m, measured steering angle γ_m, and the measured range r_{Li} and bearing ϕ_{Li} from the absolute sensor, using the kinematic model (Equation 8.1) of the Ackermann vehicle.

This point controller is carried through an embedded microprocessor unit, which is implemented into this module of the vehicle structure. Similarly, the positioning estimation can be implemented in an embedded microprocessor unit to develop the Extend Kalman Filter. Whereas, the absolute sensor is embodied by the laser LMS 221, which has been identified in the uncertainty analysis (Chapter 7) and denoted as Laser P in the robotic vehicle structure. Additionally, the point controller received the information of the perception sensor to avoid obstacles and collisions; this sensor is instantiated by a laser LMS 221, since it fulfills the specifications defined in the Chapter 6 for the perception parameters. This component is denoted as Laser S in the structure of the robotic vehicle into the safety module (Figure 8.2).

These selected components are mapped into the Locomotion subsystem, according the Mining Autonomous Vehicle structure to implement the positioning, drive, steering, and safety modules, as shown the Figure 8.2. In addition to the Locomotion, Deployment, and Tool subsystems, there exist a local personal computer (PC) that is mapped as Processing Unit, and a Communication subsystem that provides the link between the robotic vehicle and its exterior. A remote PC is used to govern the vehicle; this component is mapped into the Control Panel where high-level commands will send via the communication link. Finally, there is a Power subsystem that concerts with the series of batteries necessary to supply the robotic vehicle.

Therefore, this complete structure expresses the Mining Autonomous Vehicle configuration to perform the tunnel-profiling task. The robotic vehicle configuration formulates the Basic Configuration and involves the kinematics and sensors requirements to the development of an operational MAV prototype. The synthesis of the configuration is presented in the following section.

8.3 Prototype

The current status of the MAV prototype is the integration of the selected components, as well as the acquisition of remaining components described by the MAV configuration. A concurrent prototyping and testing stages have been achieved, which are addressed to build the Mining Autonomous Vehicle from of the defined configuration, referred to the Figure 8.2. To drive with this challenge, a detailed performance evaluation and an adaptation process are in progress; under the results derived by the framework to solve the tunnel-profiling task in the expected underground mining environment.

In building the Autonomous Vehicle, the drive and steering have been automating to control the Super Truck vehicle [González 04]. In this phase the control architecture is implemented, two controllers have already been completed: Drive and Steering controllers, which must be evaluated, checking that the hardware adaptations are performing properly. These controllers have been implemented in separately embedded microprocessors, according the modular structure of the robotic vehicle and writing code to control the actuators (i.e., the traction and steering motors). In order to evaluate these modules various tests will undertake in a series of experiments to compare their performances. Figure 8.4 shows the robotic vehicle while following a closed path, controlled directly by the Drive and Steering Controllers.

Figure 8.4: **The robotic vehicle prototype while following a closed path to check the performance of the drive and steering controllers.**

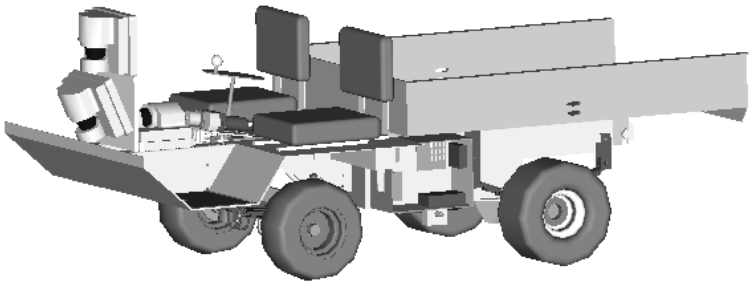

Figure 8.5: **Mining Autonomous Vehicle prototype to perform the tunnel-profiling task.**

The next stage of experiments will involve performing the tunnel-profiling task, but integrating gradually the rest of selected components. These experiments will test the ability of the prototype to achieve the given task. Figure 8.5 outlines a 3D model of the MAV prototype, involving the selected Ackermann vehicle to perform the motion P_1, and the laser LMS 221 to implement the motions R_2 and P_3. Moreover, the robotic vehicle will be equipped with the other two lasers LMS 221 to implement the safety and positioning modules. Indeed, the realization of this robotic vehicle prototype will serve to the achievement of the tunnel-profiling task, involving the generation of planes xy along the tunnel while the vehicle navigates autonomously in the underground mine.

8.4 Discussion

In applying the proposed method for synthesis of an Autonomous Vehicle configuration, the reached result is the systematic configuration of the robotic vehicle, a Mining Autonomous Vehicle (MAV) to perform the tunnel-profiling task (TPT). This configuration has been defined as a complete structure of interlinked components using embedded microprocessor units that implemented their actuation and sensing. These components fulfill the task specifications under the constraints of an underground mining environment, having the functionality derived by the analysis of the necessary motions specified as the Basic Configuration to carry out the task.

This instantiation of the Basic Configuration presents a complete configuration to perform the assigned task with certain level of autonomy, in comparison with the viable MAV configuration developed in the Chapter 5. Such degree of autonomy is essential issue in the synthesis process, since it involves fundamental actions of the robotic vehicle to produces an operational configuration, which can be then built and deploy. In this autonomy analysis, kinematic evaluation and simulation of positioning estimation are the analytical process used to detail the entire locomotion subsystem, specifying the necessary components to enhance actions of the robotic vehicle, such as positioning estimation, control, and perception functions, and the capability to recover from intrinsic propagation in the positioning uncertainty.

Although, this issue of autonomy was not addressed in the preliminary configuration (Chapter 5), the results obtained in the laboratory and real environment trials validated the performance of such prototype. Therefore, it is to be expected that the detailed configuration, defined by the overall systematic framework, improves the performance of the synthesized robotic vehicle to the effective achievement of the assigned task.

This detailed robotic vehicle configuration has been defined as follows:

- Identifying the task, convert the task specifications (e.g., accuracy and resolution) and the environment conditions (e.g., tunnel dimension and terrain geometry) into a list of Configuration Requirements and define their Geometric Description (i.e., an abstraction of what and where the tunnel-profiling task is to be achieve).

- Finding possible solutions, combine fundamental motions (i.e., prismatic and rotation) to produce compositions that cover the Geometric Description workspace.

- Analyze the motion compositions, evaluating their parametric formulation and C-space uniformity to quantify the simplicity of every composition in the Configuration Templates.

- Compare the Configuration Templates to select the simplest composition and define the Basic Configuration (i.e., the motion composition $P_1R_2P_3$) to solve the task, converting its specifications into a list of Configuration Parameters and the sequence of motion execution into the basic strategy to operate the robotic vehicle.

- Implementing the Basic Configuration, map the functionality of every motion to a subsystem into the robotic vehicle structure. The motion P_1 is analyzed as the Locomotion subsystem to move along the tunnel. The motion R_2 is the Deployment subsystem that heads the motion P_3. Finally, the motion P3 is the Tool subsystem to measure the tunnel profile.

- Analyze possible components to implement the subsystems, using the Configuration Parameters and Configuration Requirements as technical specifications and metrics to select proper components. Employ analytical expressions that relate the operation features of components (e.g., frequency and scanning range) to the motion parameters (e.g., the target range and resolution requirements related to a smaller spot diameter), lead the selection of a laser to be the Tool and Deployment subsystems.

- For the Locomotion subsystem, analyze the Configuration Parameter, using engineering principles (e.g., segmentation), determined that the type of mobile artifact is a feasible component to embody the motion P_1. Study the terrain properties (e.g., type of soil), identified that the selection is leveraged by a four-wheel

vehicle to navigate along the tunnels. Whereas, a geometric analysis to investigate the stability pose of the wheeled vehicle provides the vehicle dimensions, including the minimum wheel size to avoid obstacles (such as the expected rocks).

- Identify the kinematics requirements to improve the positioning estimation, the control performance, and the perception parameters, using a parametric comparison of different steering mechanisms (i.e., the Ackermann, Articulated, and Explicit vehicles) under the expected conditions of operation. This autonomy analysis defines the selection of an Ackermann vehicle.

- Define the sensor requirements to minimize the positioning uncertainty of the selected Ackermann vehicle, keeping the uncertainty propagation within certain boundaries. Simulate the expected sensor uncertainty to determine the type and number of sensors and landmarks needed for the achievement of the task.

- Instantiate the subsystems and modules of the robotic vehicle configuration, the laser LMS221 and the Super Truck vehicle are the selected components to implement the Basic Configuration $P_1R_2P_3$, their technical specifications are mapped into the Component Requirements.

- Analyze the Components Requirements for the actuation and sensing of the selected components to complete the Autonomous Vehicle configuration.

- Integrate the entire components for synthesis of the Autonomous Vehicle prototype to perform the assigned task with certain degree of autonomy.

Figure 8.6 shows, in broad terms, the employed systematic framework, summarizing the three gradual phases that compose it: System Abstraction, System Analysis, and System Design.

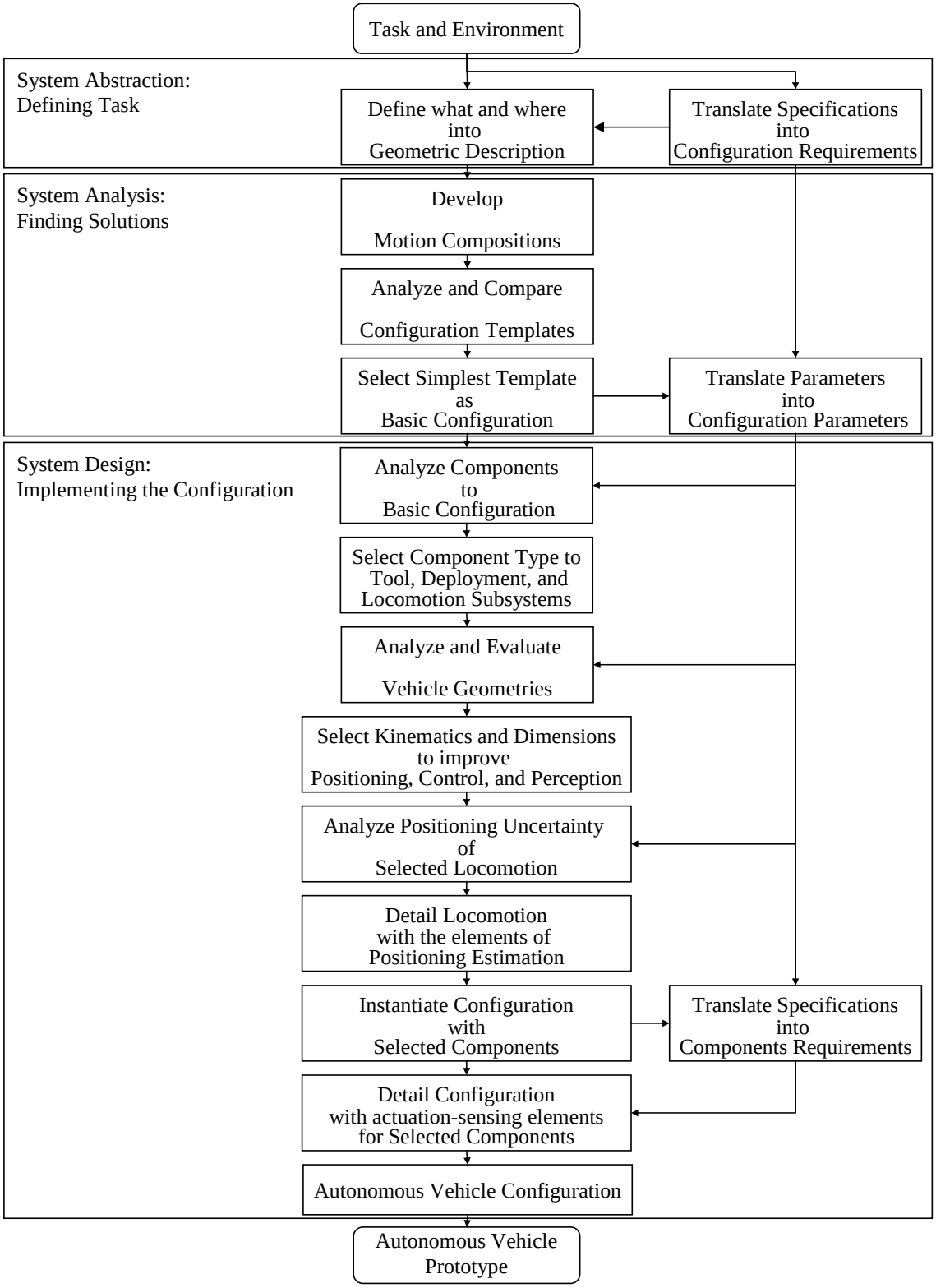

Figure 8.6: **The proposed framework for systematic synthesis of a Mining Autonomous Vehicle configuration to perform the tunnel-profiling task.**

Chapter 9

Conclusions

This research has formulated a systematic framework for synthesis of an Autonomous Vehicle configuration to perform an underground mining task. The framework assists to determine a suitable robotic vehicle configuration from the geometrical analysis of the task and the environment to the analytical selection of appropriate components, exploiting the vast inventory of technologies and products developed by Robotics and engineering. This chapter summarizes the main contributions and outlines the future directions of this research work.

9.1 Summary

A robotic vehicle configuration has been synthesized using the systematic framework. The model representing the configuration is a structure of interlinked components that fulfill the specifications to perform the assigned task under the constraints of the environment. Such structure constitutes a hierarchical and modular representation of the components to support the conceptual and physical implementation of the robotic vehicle system, through three essential subsystems: 1) Locomotion, to navigate and carry on the rest of components, 2) Deployment, to reach a particular location for the tool, and 3) Tool, to achieve the assigned task using the proper tool. The structure is integrated gradually with the results provided by the framework, following a general systematic procedure of first defining the task in geometric terms; second, finding possible solutions in terms of motions; and third, implementing the configuration through the components to build the robotic vehicle prototype.

The components realize the functionality of a fundamental composition of motions that solve the task. This motion composition is derived in a parametric comparison of rational solutions, which are formulated by the combination of elementary motions using the geometric abstraction of the task and the environment. Each motion of the basic composition becomes a subsystem into the hierarchical structure, embodied by components that are subjected the operation parameters of the motion and the task requirements.

To select the proper components, the framework uses robotic criteria and engineering principles, involving the autonomy analysis in the synthesis process to produce an operational robotic vehicle prototype that performs the task with certain degree of autonomy. This autonomy analysis includes analytical procedures to evaluate the kinematics and fundamental actions of the robotic vehicle, in order to detail entirely the configuration, specifying the necessary components that enhance the performance of the robotic vehicle prototype, such as the positioning estimation, control, and perception functions, and the essential capability to recover from uncertainty propagation in the positioning while the vehicle navigates.

The formulation of the systematic framework has been focused on the domain of underground mining. Particularly in active mines that compared to other demanding environments (outside of laboratories), the underground tunnels constitute a semi structured environment, in which the walls evidently define the limits of the space. This finite environment together with the safety and productivity requirements have motivated the attempt to automate the intensive tasks achieved in such application. The tunnel profiling task, a repetitive activity in the underground mining, has been the initial case to implement and evaluate the systematic framework proposed by this thesis.

The framework has assisted in the automatization of the tunnel profiling task, defining the configuration of a wheeled robotic vehicle with the complete components for supporting its implementation. The configuration is based on the use and the adaptation of a standard vehicle and a laser rangefinder as the work tool, as well as the adjustment with the rest of necessary sensors, actuators, electronics, and control schemes, to navigate and operate the tool. In this context, the systematic framework takes advantage of already existed products to synthesize a viable AV configuration, instead of the development of whole design of the vehicle (e.g., the mechanic design of the steering and traction mechanisms).

Nevertheless, it is important to observe that the systematic framework is a primitive approach, which should be tested and proved to be a mature approach and to gain generality, first of all in the underground mining domain with the development of challenger tasks, such as the extraction of samples, the perforation of walls for the insertion of explosives, and the ore transportation, among other tasks.

9.2 Contributions

The major result of this thesis is the validation of the proposed method as a suitable approach to systematically obtain the Autonomous Vehicle configuration.

The main thesis' contributions are outlined as follows:

- Formulation of a systematic framework to synthesize a wheeled Autonomous Vehicle. This design framework leads rational generation of the configuration: from concept to implementation, having the task and environment requirements as input.

- Definition of the fundamental configuration of the robotic system consisting in a functional structure, based on analytical and geometrical analysis, instead of a predefined configuration according to designer or design team experience. This basic configuration is an essential issue in the synthesis process to define the robotic vehicle functionality through the necessary degrees of freedom.

- Integration of autonomy analysis during the detailed configuration of the robotic vehicle. This analysis leads numerical generation of trade-offs for the positioning, control, and perception performance and evaluation of suitable configurations. An explicit analysis through parametric simulation is used to select the locomotion component and its actuation and sensing components, it is considered in the synthesis process as fundamental issue to produce reliable configurations.

- Introduction of a positioning error analysis for wheeled robotic vehicles. It is an aid to in-depth evaluation and comparison of steering geometries under equal operation conditions, while increasing the understanding on their fundamental differences. Analytical expressions derived from reformulated kinematic models are used to relate the performance of the robotic vehicle to the factors that impact this error.

- Implementation of control and perception analyses for wheeled robotic vehicles. The focus is the analytical evaluation and comparison among different steering geometries under equal operation conditions. Kinematic equations are derived to relate the performance of each steering mechanism to the tracking and heading errors and the estimated perception parameters.

- Development of a positioning uncertainty analysis for a wheeled robotic vehicle. It is an aid to investigate the positioning uncertainty evolution of an Ackermann steering geometry, while performing the assigned task. Analytical expressions derived from kinematic model are used to relate the performance of the vehicle to the expected sensor uncertainties.

- Formulation of a practical framework to develop operational and feasible Autonomous Vehicles from already existing components, capitalizing the extensive research and expertise inside of Robotics and traditional engineering. In particular, exploring the universality of conventional vehicles and the necessary sensors, actuators, and techniques produced during decades of engineering and research.
- Development of a computational toolkit encoded independent procedures that output both data and parametric graphs to allow their quantitative interpretation. The procedures integrate the vehicle kinematics, the task and environment model, and the component features in functions to:
  - model the geometric abstraction of the task and the environment, encoding solid modeling techniques (i.e., Constructive Solid Geometry and Straight Homogeneous Generalized Cylinder).
  - produce and analyze possible compositions of motions, computing the forward kinematics, C-space, and B-spline techniques.
  - evaluate the vehicle type and dimension (i.e., wheelbase and wheel) related to the environment conditions (i.e., terrain geometry and soil properties), implementing stability and terremechanics equations.
  - estimate the positioning and control errors for the Ackermann, Articulated, and Explicit vehicles, as well as to estimate the perception parameters, encoding the reformulated kinematic models with slip angles and Frenet frames.
  - simulate the positioning uncertainty of the Ackermann vehicle, encoding the uncertainty evolution and implementing the Extended Kalman Filter.
- Development of mechanical and electronic designs to purse the adaptation of the steering mechanism, the mounting of the selected lasers and sensors, and the implementation of the drive and steering controllers in embedded microprocessor units.

9.3 Observations

This investigation has provided the systematic framework to synthesize an AV configuration by assisting the derivation of configurations in concept and implementation. The fundamental approach is that reliable configurations can be defined by geometrical and analytical procedures involved in the processes of abstraction, analysis, and design of the robotic vehicle, rather than seeking in empiric manner or in-depth influenced by design experience.

The finite definition of task requirements and the precise description of environment conditions are essential elements in the synthesis process. In particular, the geometric abstraction is a significant aid to capture the needs and properties of the task and the

environment, specifying in a comprehensive representation what and where the task is to be performed. Moreover, it is used to estimate in a meaningful manner the robotic vehicle functionality through the generation of rationalized templates composed by fundamental motions. Therefore, it is important to observe that more detailed information on task and environment encapsulated on this geometric description, enable more accurate and detailed specification of the final configuration.

Although the generation and evaluation of configurations is based on kinematic analysis (rather than kinematic and dynamic), it is an effective means of deriving configuration templates, beyond traditional practice of brainstorms. The fundamental consideration is that the foundations of Robotics are geometrical. It is the analytical study of spatial motions to perform the task in the geometry of a 3-dimensional space. This parameterized composition of templates exploits the advantage of quantitative evaluation (i.e., kinematics and their configuration space) to address the trade-offs between alternative configurations. The idea is that the configuration should always aim at solving the task with minimum degrees of freedom and thus reduces the robotic vehicle complexity.

This parametric analysis is extended to detail the hierarchical functionality of the configuration while allowing the understanding about the robotic vehicle topology. The resulted parameters and the underlying behavior of each motion make explicit the definition and the scope of the essential functions of the robotic vehicle to be mapped as a subsystem into the AV structure. Furthermore, these motion parameters constitute the set of metrics to aid in the selection process of the proper components for each subsystem. Nevertheless, it is important to note that each essential function would be implemented by one or several components, but also a single component would embody more than a function.

The analytical processes used in the framework fill different levels of detail in the system design, related the robotic vehicle performance to the component characteristics and the environment properties through mathematical equations. Terramechanics expressions of robotic locomotion primarily influence the definition of the robotic vehicle type and the dimension range of the wheelbase and the wheels through an examination of the vehicle-terrain interaction and vehicle stability over the terrain geometry. The analytical comparison between alternative candidates and critical actions of the robotic vehicle (i.e., positioning, control, and perception) addresses the selection of the steering mechanism and the vehicle dimensions, and gives the direction to enhance the control and safeguarding capabilities. It is important to note that beyond the impact in the selection process, the numerical results of the performance for every candidate vehicle allow a quantitative interpretation of their advantages and drawbacks to perform the pursued task in the expected conditions of operation.

Additionally, the parametric simulations aids to improve the configuration derived through each analytical formulation, encoding the acceptable uncertainty of multiple

sensors that allow the robust implementation and reliable performance of the Autonomous Vehicle prototype. The demonstration has been performed by applying the systematic framework to a real underground mining application, generating the practical configuration, selecting the components, and providing the basic operation strategy. It shows that the framework is a viable approach completing a cycle of robotic vehicle synthesis. This observation arises from the framework focus to systematically identify the configuration, primarily with specific task and environment conditions that makes the problem of synthesis tractable.

To exploit the numerical and graphical information obtained from each analysis, all the analytical processes lead on individual procedures that are solved one by one rather than as a system. The procedures encode the mathematical expressions, which are derived from physics and geometry models that capture the relation among the vehicle kinematics, the task and environment model, and the component features. Although the attempt has been to support the mathematical based analyses for the tunnel profiling task, the general formulation of the equations can be easily be modified to accommodate case-based studies or what kind of information is available. In this context, it is important to address the packaging, documentation, and distribution of the computational procedures, whose current instantiation has been implemented in MATLAB language [MathWorks 03], as an analysis toolkit, making this proposed framework available, so that it can be put into use.

This research prototypes a primal example, and demonstrates the use of the systematic framework in only one AV configuration. Although this exercise has been a real-world application, the systematic framework is restricted in generality. This fact extends to two fundamental observations. First, it is evident the demand to test and prove the systematic framework with the development of several tasks, primarily in the underground mining domain to exploit its finite and semistructured environment, with regard to other applications. Second, the framework must increase its scope on wheeled robotic vehicles in other demanding applications. Applicable benchmarks that could be addressed by this framework are in real civil applications, such as agriculture, construction, forestry, mining, and transportation; since, the success of a robotic vehicle will eventually rest on availability and matureness of state-of-the-art on technology and components, which have bee generated successful by decades in such domains.

9.4 Future Directions

During the course of this work, some insights are leading to possible future research directions. In particular, the identified observations provide the need to evaluate the systematic framework primarily into the underground domain. Therefore, techniques to manipulate objects will need to be investigated, which will allow increasing the scope and usefulness of this proposed framework for related underground mining tasks. The chip sampling task is a possible application, which consists of extracting and collecting

mineral from tunnel ceiling. This task not only arises from the relative similarity to the tunnel profile tasks, but also it involves the manipulation of objects (i.e., the ore samples).

The framework is based on a kinematic analysis to develop the suitable configurations; however, the possible extension will be into the development of a dynamic analysis, following to the selection of components during the ultimate stage of the synthesis process. The knowledge of the features (such as mass, material, and load torque) and the performance parameters (such as power consumption, rate of response, torque, forces acting) of the instantiated components (e.g., actuators of the Locomotion subsystem), can be understood with this dynamic analysis to increase the reliability of the robotic configurations. This potential improvement can be seen to upgrade to the framework, using analysis mechanical software, such as [DYNAMechs 01, Model 03], and adapting simulation extension, such as ADAMS [MSCSoftware 03], and Darwin2k [Leger 99].

An important extension to this thesis would incorporate a control and computing architecture. Although the framework derives the basic strategy for controlling the robotic vehicle, dealing with a physical system must consider aspects of control such as actuator constraints, sensor response, and processing data (e.g., latency, operation rates). The architecture should lead the integration of the subsystems that compose the robotic vehicle configuration, connecting all the modules such as perception, drive, steering, and positioning; it is need to combine information from different sources (sensors, actuators) and to combine actions of the vehicle (navigation, obstacle avoidance). This architecture must provide the means by which the robotic vehicle performs its task efficiently. In this context, the research group in the Center for Intelligent Systems at Tecnológico de Monterrey, is addressed these issues; in particular, the focus is on sensor fusion by integrating multi-sensor information to develop hierarchical control architecture. As a result, it will bring detailed understanding for robotic vehicle navigation in natural environments.

9.5 Outlook

The configured Autonomous Vehicles for the underground mining application was an explicit request, expressed by an important mining company from México, Industrias Peñoles, S.A. de C.V. The research work has hence profited significantly from a real-world application to apply the framework for synthesis of Autonomous Vehicle configuration, to a complete and realistic concept-prototype, in addition to the academic and exciting effort to develop a robotic vehicle. It is hoped that this thesis motives the development of such correlations between industries and research centers, as well as itself will provide for new advances and directions and to be a useful reference in Robotics.

Chapter 5

Viable MAV Configuration

The structure, derived in the latter chapter, is used to the synthesis of the MAV configuration; to this aim, all subsystems should be instantiated with the proper components. This chapter addresses the selection of components by presenting the instantiation process, which is based on the Configuration Requirements and Configuration Parameters, in regard to the technical specifications and constraints that each selected component produces. These specifications and constrains are mapped to a table of Component Requirements, which are analyzed to avoid propagation of conflicts toward the rest of components.

A viable solution to configure the MAV is defined when the Configuration Requirements, the Configuration Parameters, and the Component Requirements have been fulfilled and the Basic Configuration is transformed into a complete structure that integrates hierarchically and modularly the choice components. In the following sections are developed the last stages of the System Design phase, involving the selection and the integration of the components to implement the MAV prototype. Finally an outline of the experimental results, which are used to validate this implementation, and observations are also presented.

5.1 Component Selection

Referring the MAV structure, shown in the Figure 4.36, the selection of components is derived considering the analysis order established in the section 4.5 (Components). In this stage, the framework uses an inventory of the available components, such as actuators, sensors, control elements, and mobile platforms, in addition to a searching in database sensors, actuators, and components, such as in online database (globalspec [GlobalSpec], laboratorytalk [Laboratorytalk], and specialized sites in the Internet).

Table 5.1: **Laser Technical Specifications**

Specification	Sentinel 100	C-ALS	LMS221	Configuration Requirement/Parameters
Range (m)	0.2 to 250	1.0 to 150	up to 80	d_3 and span_d_3
Accuracy (m)	± 0.05	± 0.20	± 0.06	accuracy_measured
Spot Diameter (m)	$\leq$ 0.016	$\leq$ 0.015	$\leq$ 0.009	sampling_resolution
Resolution (m)	0.01	0.01	0.01	resolution_measured
Measurement Rate (s)	1	0.2	0.013	sampling_time_interval
I/O Interface	RS232	RS232	RS232	digital
Power (VDC)	12	12-18	24	¬ fuel
Temperature (°C)	-10 to 45	-10 to 50	-30 to 50	temperature
Weight (kg)	0.6	10	9	P_3_weight
Dimension (mm)	167×260×324 (H×W×L)	100×700 (D×L)	352×195×266 (W×H×L)	

5.1.1 Tool Subsystem

A laser range finder should be the component that implements the motion P_3. Three possible lasers are identified and analyzed: laser Sentinel 100 made by Optech System [Optech], model C-ALS produced by MDL [MDL], and LMS221 made by Sick [SICK]. Table 5.1 lists the technical specifications of these laser range finders, respectively. The examination of each laser involves the Configuration Requirement and Parameters, such as the quantifiers d_3 and span_d_3 associated to the range and span of operation of the motion P_3.

The accuracy required is fulfilled by the model Sentinel 100; although, the laser LMS 221 presents better precision due to relation to the range d_3 and the spot diameter. The entire lasers satisfy the resolution and environmental temperature requirements, as well as the constraints of operation, i.e. the I/O interface to gather data (digital) and the power supply (¬ fuel). With respect to these technical specifications and the available of components the selection is the laser Sentinel 100. A second option can be the model LMS 221 since this laser shows a superior measurement rate, which should improve, together the minor spot diameter shown, the performance of the measurement process. The model C-ALS is limited by the required accuracy.

Thus, the laser Sentinel 100 instantiates the Tool subsystem, embodying the functionality of the motion P_3. The technical specifications of the selected laser are mapped as a list of Component Requirements for its actuation and sensing, such as a necessary serial port for serial transmission, and a power supply equal to 12 VDC, denoted by the quantifiers port_serial and power_laser, respectively. Table 5.2 shows these requirements. It is important noted that the quantifier P_3_weight is instantiated by the weight of the laser (P_3_weight $\leq$ 0.6 kg); hence, this specification is propagated to select the rest of the components.

Table 5.2: **Laser Component Requirements**

Technical Specification	Component Requirements
Sentinel 100	
I/O Interface RS232	port_serial_laser ≤ 1
Power 12 VDC	power_laser $\leq$ 12 VDC
Weight 0.6 kg	P_3_weight $\leq$ 0.6 kg
Dimension 167×260×324 (mm) (H×W×L)	height_laser $\leq$ 0.167 m
	width_laser $\leq$ 0.260 m
	length_laser $\leq$ 0.324 m

5.1.2 Deployment Subsystem

The selection of this component depends on the Configuration Requirements and Parameters, in addition the quantifier P_3_weight. Therefore, the following step is the evaluation of these specifications with the technical features of the possible component. In this case, the available component is a pant tilt unit model PTU 46-70 made by Direct Perception [DPerception]. Table 5.3 shows the technical features of this component.

The PTU satisfies the parameters of the motion R_2, the range of operation defined by the quantifier θ_2 is fulfilled by the pan range specification ($\pm$ 159°); i.e., a total range greater than the required range by the quantifier span_θ_2. Moreover, the constraint R_2_payload is satisfied since its load capacity is up to 2.72 kg to support the selected laser (P_3_weight $\leq$ R_2_payload). The resolution of the PTU reaches up to 0.0218°, which fulfills the value denoted by the quantifier $\Delta\theta_2$; whereas, the speed achieved by this PTU allows the deployment of the laser in a short period from established time, improving the time of the sampling (sampling_time_interval).

Table 5.3: **PTU Technical Specifications**

PTU 46-70 Specifications	Configuration Requirement/Parameters
Tilt Range 31 ° up and 47 ° down	
Pant Range ± 159 °	θ_2
Range 318 °	span_θ_2
Speed 60 °/s	sampling_time_interval
Resolution 0.0128 °	$\Delta\theta_2$
Rated Payload 2.72 kg	R_2_payload
I/O Interface RS232	digital
Power 11-37 VDC	¬ fuel
Weight 1.4 kg	R_2_weight
Dimension 228×130×108 mm (W×H×L)	

Table 5.4: **Laser Component Requirements**

Technical Specification	Component Requirements
PTU 46-70	
Payload 2.72 kg	R_2_payload $\leq$ 2.72 kg
I/O Interface RS232	port_serial_ptu $\leq$ 1
Power 12 VDC	power_ptu $\leq$ 12 VDC
Weight 1.4 kg	R_2_weight $\leq$ 1.4 kg
Dimension 228×130×108 mm (W×H×L)	height_ptu $\leq$ 0.228 m
	width_ptu $\leq$ 0.130 m
	length_ptu $\leq$ 0.108 m

The Deployment subsystem is, hence, instantiated by such PTU, implementing the functionality of the motion R_2 to carry and to orientate the Tool subsystem. The particular specifications are mapped to the table of the Component Requirements. In this case, the PTU is controlled via a RS232 serial port and supplied by an input voltage equal to 12 VDC, both requirements are denoted by the appropriate quantifier, as is shown in the Table 5.4.

5.1.3 Locomotion Subsystem

An initial configuration study that examined the requirements and parameters of the motion P_1 determined that a wheeled vehicle was feasible to implement its functionality. Several wheeled vehicle concepts have been investigated, which lead to the derivation and classification of kinematic, dynamic, and controllability models [Muir 87, Alexander 89, Dudzinski 89, Laumond 93, Murray 93, Samson 95, Campion 96]. Nevertheless, the selection of the wheeled vehicle is primarily based on task requirements and on the environment to traverse the expected terrain. During in this stage these requirements and parameters are studied to determine trends and trade offs to lead the selection of the component.

The selection is leveraged by a wheeled vehicle that navigates on the required terrain while carrying its payload and maintaining a stability position. To identify and derive the aforementioned wheeled vehicle features, the analysis explores the alternatives through the use of an analytical method that relates the Configuration Requirements and Parameters to the parametric features of the vehicle, such as the dimensions of the vehicle and wheels to navigate through the tunnel, which are expressed in terms of these requirements and parameters.

The analysis determines minimum values of the length and width of the wheeled vehicle and wheel dimensions that guarantee the navigation over the particular terrain, using analytical formulation of classical vehicle terrain system [Bekker 69, Wong 93] and its

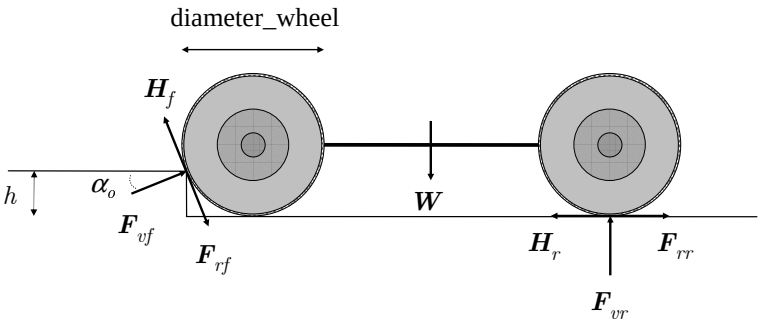

Figure 5.1: **Minimum wheel diameter through force analysis of discrete obstacle climbing that the four-wheel vehicle must perform.**

derivation for Robotics, developed by [Apostolopoulos 01]. In fact, based on the results of Apostolopoulos' analysis, a four-wheel vehicle will be analyzed to embody the Locomotion subsystem; since it offers greater advantages in a quantitative comparison between a four-wheel configuration and a six-wheel one under criteria of simplicity, control complexity, slope climbing, draw pull and traction [Apostolopoulos 01].

Due to the geometry of the terrain, the four-wheel vehicle must navigate while avoid the obstacles, including climbing obstacles; i.e., the quantifiers height_rock and distribution_rock imply that vehicle should climb this kind of obstacles. Consider for instance the case illustrated by the Figure 5.1, where the contact angle α_o can be expressed in term of the obstacle height h (associated to the quantifier height_rock) and the wheel diameter d_w [Apostolopoulos 01], given by

$$\sin \alpha_o = \frac{d_w - 2h}{d_w} \tag{5.1}$$

Thus, the minimum wheel diameter is at least two times the obstacle height h to allow the vehicle climbs a discrete obstacle on the compacted terrain (sandy_loam). This wheel diameter is denoted by the quantifier diameter_wheel, expressed as

$$\begin{aligned} 2\,\text{height\_rock} &\leq \text{diameter\_wheel} \\ 0.20\,\text{m} &\leq \text{diameter\_wheel} \end{aligned}$$

To determinate the dimensions of the wheeled vehicle, in terms of length and width, a geometric analysis based on equilibrium state of the vehicle referred to navigate through the tunnel. An initial convex hull is formed from the minimum diameter_-wheel and the selected components, the laser and the PTU. Over this convex hull is computed the center of gravity (CG), in order to obtain a stable position for supporting the components at different heights; thus, the dimensions of the wheelbase length and diameter of wheel are calculated, with the assumption of an equilibrium in the system forces acting on vehicle and a vertical moment of inertia equal to zero, as is shown in the Figure 5.2.

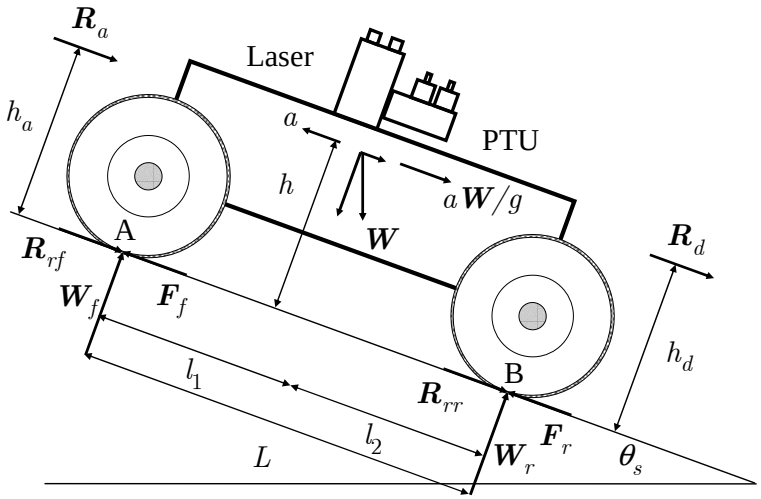

Figure 5.2: **Forces acting on a four-wheel Vehicle and the selected component(Laser and PTU). In the longitudinal direction, they include the aerodynamic resistance R_a, rolling resistance of the front and rear wheels R_{rf} and R_{rr}, drawbar load R_d, grade resistance R_g ($W \sin\theta_s$), and tractive effort of the front and rear wheels F_f and F_r. Whereas, a is linear acceleration of the vehicle along the longitudinal axis, g is acceleration due to gravity, and m and W are vehicle mass and weight, including the laser and PTU; L is the wheelbase, l_2 is the distance between the rear axle and the center of gravity (CG) of the vehicle, l_1 is the distance between the front axle and the center of gravity (CG) of the vehicle, h_a is the height of the point of application of the aerodynamic resistance, h is the height of CG, h_d is the height of drawbar hitch, and θ_s denotes the slope angle [Wong 93].**

The equation of motion along the longitudinal x-axis of the vehicle is expressed by

$$m\frac{d^2x}{dt^2} = aW/g = F_f + F_r - R_a - R_{rf} - R_{rr} - R_d - R_g \tag{5.2}$$

and by introducing the concept of inertia force, the above equation may be rewritten as

$$F = R_a + R_r + R_d + R_g + \frac{aW}{g} \tag{5.3}$$

where F is the total tractive effort and R_r is the total rolling resistance of the vehicle. By summing moments about A and B, the normal load on the front and rear axle W_f and W_r can be determined

$$W_f = \frac{Wl_2\cos\theta_s - R_a h_a - ahW/g - R_d h_d \mp Wh\sin\theta_s}{L} \tag{5.4}$$

$$W_r = \frac{Wl_1 \cos\theta_s - R_a h_a - ahW/g - R_d h_d \pm Wh \sin\theta_s}{L} \tag{5.5}$$

when the vehicle is at rest on level ground [Gillespie 92], the load equations simplify by static load on the axle as

$$W_f = \frac{Wl_2}{L} \tag{5.6}$$

$$W_r = \frac{Wl_1}{L} \tag{5.7}$$

The equilibrium assumption is expressed by $\Sigma\ F_n = 0$ and $\Sigma\ M_n = 0$; thus the $l_1 = l_2$ and the second moment of inertia on the vertical centroid axis is zero. The l_1 distance is calculated as a function of the height of the CG and the radius of the wheel r_w [Dixon 96] through the following expression

$$l_1 = h \tan\alpha_r + \frac{r_w}{\tan\alpha_r} \tag{5.8}$$

where α_r is the inclination angle, in this effort it has an experimental approximation equalt to 30°. A following stage computes different wheel diameters based on the PTU and Laser height-position (component height) and keeping a stable position for the new wheelbase long under these dimensions. The aforementioned process uses conventional static equations to find the convex hull centroid and the relation between wheel diameter and vehicle length. Further, these parametric data is utilized to find an approximation width dimensions for both the vehicle and the wheel, respectively.

The Figure 5.3 shows the initial condition; where the vehicle presents an unstable position since the orientation of the principal moments, represented by the dashed lines, are mismatched with respect to the horizontal and vertical axes. Whereas the Figures 5.4 shows the obtained results, where the minimum and maximum values are calculated for wheel and vehicle dimension as function of components height, having a stable position of the vehicle.

Similar process is developed to define the width dimensions of the vehicle and wheel, the results are depicted in the Figure 5.5. Figure 5.6 shows these results.

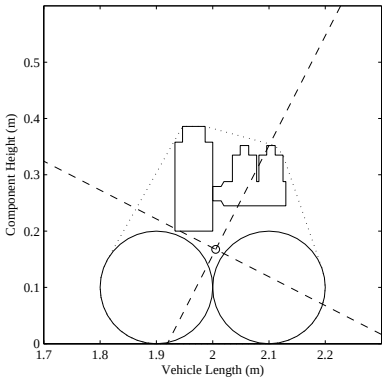

Figure 5.3: **Initial vehicle length (wheelbase) defines from the minimum wheel diameter and the dimensions of the Laser and PTU. The center of gravity presents an unstable position (dashed) under the convex hull (dotted).**

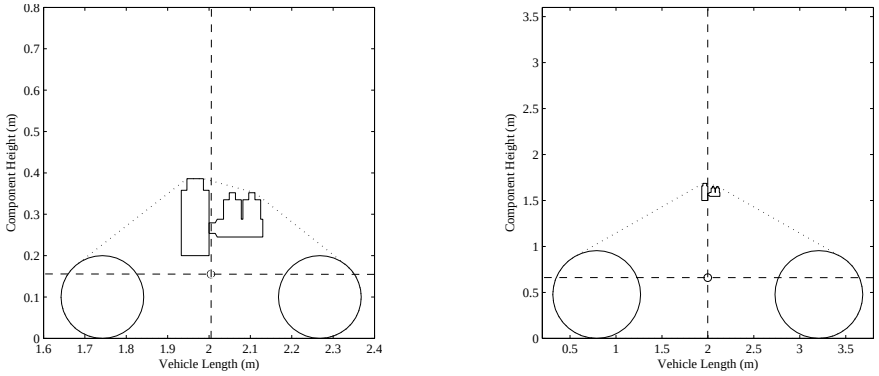

Figure 5.4: **Minimum vehicle length (left) and maximum vehicle length (right), which are defined by the convex hull of the wheel diameter the Laser and PTU dimensions, and the component height, considering a stable position.**

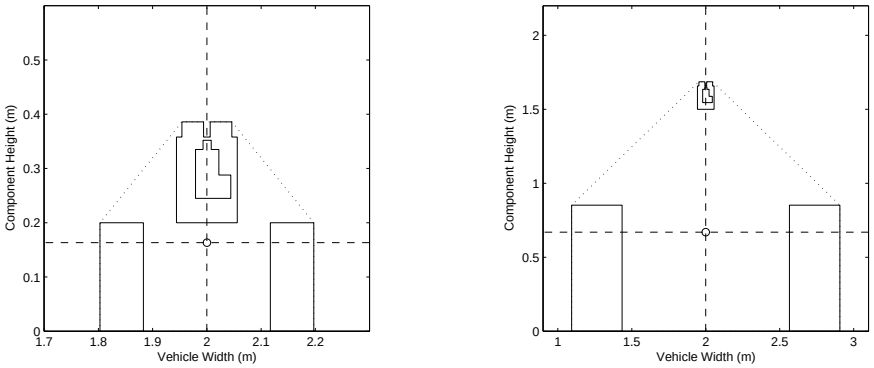

Figure 5.5: **Minimum vehicle width (left) and maximum vehicle width (right), which are defined by the convex hull to determinate a stable position.**

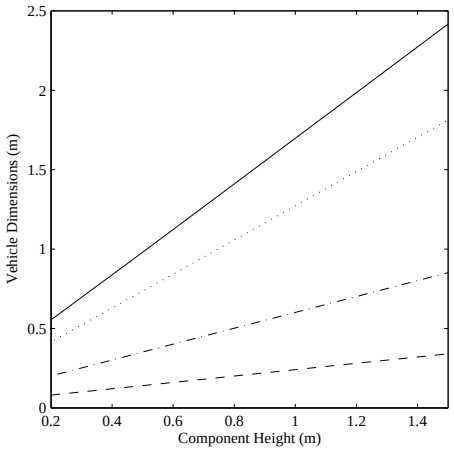

Figure 5.6: **Vehicle dimensions, wheelbase(solid), vehicle width (dotted), wheel diameter (dashdot) and wheel width (dashed).**

A wheeled vehicle traversing terrain is subject to sinkage, which depends on the properties of the terrain and the dimensions and loading of the wheel (weight distribution over each wheel). With the assumption of a maximum allowed sinkage by at least 1% of the wheel diameter for a solid or pneumatic wheel, under static loading as shown Figure 5.7, the estimated weight of the vehicle can be derived by

$$z_w = \left(\frac{3W_w \cos\theta_s}{(3-n)\,(k_c + k_\phi b_w)\,\sqrt{d_w}} \right)^{\frac{2}{(2n+1)}} \tag{5.9}$$

This equation expresses vehicle performance in terms of wheel sinkage as a function of soil parameters and properties of the terrain (Lean_Clay) under consideration: the exponent of soil deformation n, cohesive k_c and frictional k_ϕ moduli of soil defermotion and wheel dimensions, wheel diameter d_w (diameter_wheel) and wheel width b_w (width_wheel) [Wong 93, Apostolopoulos 01]. The results of the wheel weight are shown in the Figure 5.8, the soil parameters refer to the Table 4.9, in addition to the quantifier slope for the angle θ_s.

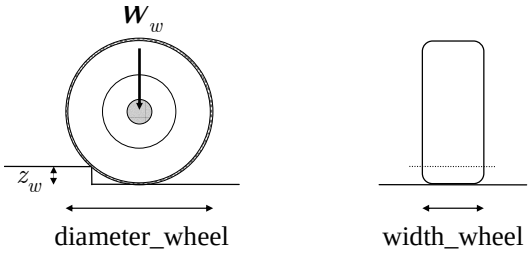

Figure 5.7: **Sinkage model as function of terrain properties and wheel dimension (diameter_wheel and width_wheel).**

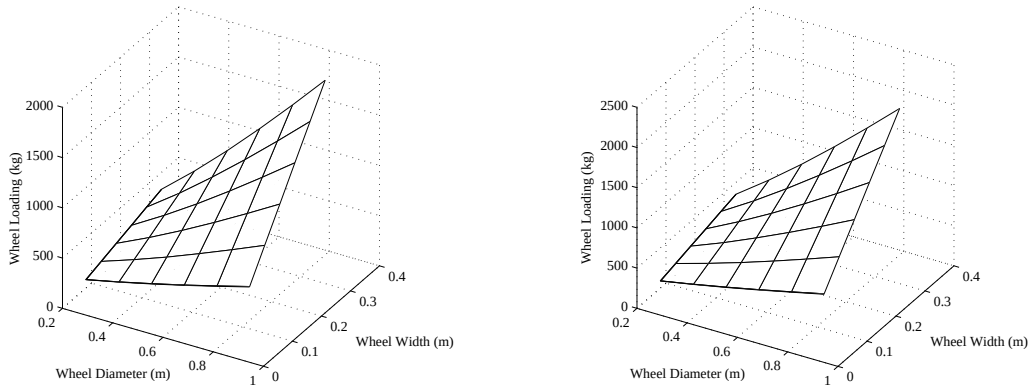

Figure 5.8: **Wheel loading as function of the terrain properties, the wheel dimension (diameter_wheel and width_wheel), and geometric of terrain: on level ground (left) and on terrain with slope $\theta_s = 20^\circ$ (right).**

Referring these results, it is noted that the minimum dimensions for the vehicle and wheel are well limited; therefore the vehicle must be fulfilled from these trade-offs (Table 5.5). The space of possible components is huge; nevertheless, by the extreme environmental conditions inside a mine, the search space is reduced to vehicles dedicated to perform mining task or the implementation and adaptation of some other vehicle, especially of kind electric as result to avoid fuel powered vehicles denoted by the constraint $\neg fuel$, such as all terrain vehicle (ATV), for instance a four-wheeled motorcycles or utility vehicles.

In the inventory, the vehicle type LHD model EST-2D Scooptram is available, which is facilitated by the Peñoles Company as partner of this effort. This LHD vehicle is an electric vehicle produced by Atlas Copco ([Atlas]). Table 5.6 shows its technical specifications. The vehicle satisfies the minimum dimensions found in the above geometric analysis; whereas the requirement on the payload is significantly filled (P_1_payload). An additional reason to select the LHD as the Locomotion subsystem, until this framework stage, it is the fact that it is a mining vehicle therefore its design involves the engineering and technological advances in the development of this kind of vehicles, i.e. an advantage that is taken by the framework for synthesis of the MAV configuration.

Table 5.5: **Vehicle dimension trade-offs**

Component	Vehicle		Wheel		
Height (m)	Wheelbase (m)	Width (m)	Diameter (m)	Width (m)	Loading (kg)
0.20	0.52	0.39	0.20	0.08	90
0.50	0.98	0.73	0.35	0.14	294
1.00	1.69	1.27	0.60	0.24	940
1.50	2.41	1.85	0.85	0.34	2000

Table 5.6: LHD Technical Specifications

LHD Specifications	Configuration Requirement/Parameters
Electric Motor 75 hp	¬ fuel
460-575 VAC, 3 Phase, 60 Hz	
Transmission:	d_1
3 speeds Forward/Reverse	span_d_1
Payload Capacity 3600 kg	P_1_payload
Steering Articulated	
Hydraulic power steering	
Empty Vehicle Weight 11385 kg	wheel_loading
Ground Clearance 229 mm	ground_clearance
	height_rock
Tire 12.00 × 24 L-5S	diameter_wheel
Diameter 1275 mm Width 325 mm	width_wheel
Vehicle Dimension 1549×1423×2540 mm (W×H×L)	wheelbase_vehicle
	width_vehicle
	height_tunnel
	width_tunnel
	length_tunnel

Therefore this LHD vehicle is selected to implement motion P_1, as same way, this selected vehicle is included in the structure of the MAV configuration, involving its Component Requirements that must be resolved for the actuation of the vehicle. These requirements depend directly on the kinematics behavior of the vehicle, which is defined by its mechanical elements. This model allows determining the number of required actuators to follow the functionality of the motion P_1, a straight-forward advance along the tunnel, avoiding collisions while the vehicle traverses it (requirement of safety).

The kinematics corresponds to an articulated vehicle, with a front and rear body that rotate relative to each other. The vehicle is supported by means of two parallel axles (rear axle and front axle) and four wheels. Steering is achieved by an articulation joint located midway between the two bodies; whereas the rear wheels are driven by a traction actuator (electric motor). Figure 5.9 shows the LHD vehicle geometry, its vehicle kinematic model is derived from this geometry, assuming rigid body and rolling motion constraints, this model is given by

$$\begin{aligned} \dot{x}_r &= V cos\theta \\ \dot{y}_r &= V sin\theta \\ \dot{\theta} &= \frac{V sin\gamma - l_1\dot{\gamma}}{l_1 + l_2 cos\gamma} \end{aligned} \tag{5.10}$$

where x_r and y_r denote the position of the vehicle relative to some fixed global frame

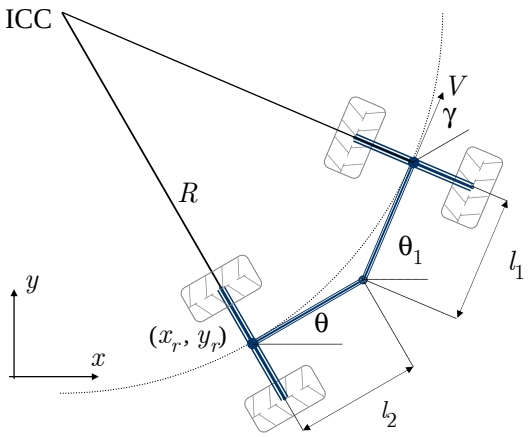

Figure 5.9: **Geometry of LHD Vehicle: an articulated vehicle is composed of a front and rear body which can rotate relative to each other. Each body has a single axle with two wheels which are fixed (non-steerable). The steering behavior is achieved by driving the articulation joint (yaw pivot) that connects both bodies.**

of reference, the subscript r denotes the rear axle. The angle θ is the orientation of the vehicle with respect to the x axis, while V represents the linear velocity of an imaginary wheel located midway between the real wheels (bicycle model), and the angle γ denotes the steering angle of the vehicle. L is the length of the vehicle, the wheelbase distance between the front and rear axle, defined by l_1 and l_2 respectively. R is the radius associated to the point $(x_r\ ,\ y_r)$ with respect to the ICC. Furthermore, based on the assumption that the vehicle develops a steady-state motion turning where γ is constant (i.e., $\dot{\gamma} = 0$), the kinematic model can be rewritten as

$$\begin{bmatrix} \dot{x_r} \\ \dot{y_r} \\ \dot{\theta} \\ \dot{\gamma} \end{bmatrix} = \begin{bmatrix} cos\,\theta \\ sin\,\theta \\ \frac{sin\,\gamma}{l_1 + l_2\,cos\,\gamma} \\ 0 \end{bmatrix} v_1 + \begin{bmatrix} 0 \\ 0 \\ 0 \\ 1 \end{bmatrix} v_2 \tag{5.11}$$

for the case $l_1 = l_2$

$$\begin{bmatrix} \dot{x_r} \\ \dot{y_r} \\ \dot{\theta} \\ \dot{\gamma} \end{bmatrix} = \begin{bmatrix} cos\,\theta \\ sin\,\theta \\ \frac{2\,tan\,\gamma/2}{L} \\ 0 \end{bmatrix} v_1 + \begin{bmatrix} 0 \\ 0 \\ 0 \\ 1 \end{bmatrix} v_2 \tag{5.12}$$

where v_1 and v_2 are the driving and the steering velocity inputs, respectively. Thus two controllers are required, one corresponds to linear velocity and other to steering angle, which are associated as the requirements control_drive and control_steering and mapped to the drive and steering modules into the AV structure. Table 5.7 shows then the Component Requirements for the selected LHD vehicle.

Table 5.7: **LHD Component Requirements**

Technical Specification	Component Requirements
LHD Vehicle	
Forward/Reverse Advance	control_drive
Steering	control_steering
Avoid Obstacles	safety
Payload 3600 kg	P_1_payload $\leq$ 3600 kg
Power 460-575 VAC, 3 Phase, 60 Hz	power_ldh $\leq$ 575 VAC 460 VAC $\leq$ power_ldh
Weight 11385 kg	P_1_weight $\leq$ 11385 kg weight_vehicle $\leq$ 11385 kg
Dimension 1549×1423×2540 mm (W×H×L)	height_lhd $\leq$ 1.423 m width_lhd $\leq$ 1.549 m length_lhd $\leq$ 2.540 m

Therefore the subsystems of the MAV structure are instantiated with the selected components to perform the TPT, as shown Figure 5.10. The complete fulfillment of the MAV structure must include the defined modules to provide the controlling and sensing of each subsystem: laser Sentinel 100, PTU 46-70, and the articulated vehicle. The following section outlines the integration of the components to synthesize the full configuration of the MAV.

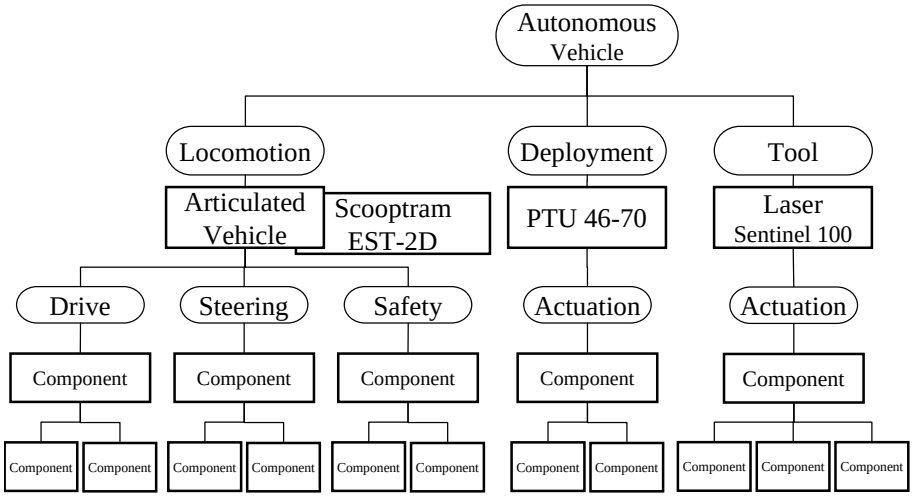

Figure 5.10: **MAV structure formulated by the articulated vehicle Scooptram model EST-2D, the PTU 46-70, and the laser rangefinder Sentinel 100.**

5.2 Component Integration

To make the fulfillment of the subsystems with specific components to control each module, the method continues with the integration, an iterative process to analyze the Component Requirements, resolving the constraints and avoiding technical conflicts with the Configuration Requirements and Parameters. This process behaves in accordance with the same order that were selected each component.

5.2.1 Tool Subsystem: Laser Sentinel 100

In normal operation the Sentinel 100 is programmed and controlled remotely via a serial communication link that requires a remote terminal equipped with a standard RS-232 port (quantifier port_serial_laser). The Sentinel 100 can receive remote commands at any time as soon as it is powered (quantifier power_laser).

To resolve the control and the data acquisition for this component a personal computer (PC) selected and mapped as the Processing Unit subsystem. This PC has the necessary hardware and software elements to operate the Sentinel 100. In this case, it is no necessary an extra sensor to feedback the control commands. Besides, the required power supply is implemented by a commercial battery at 12 VDC at 1.2 A to support the operation of the laser, such battery is mapped to the Power Unit subsystem, as shown the Figure 5.11.

5.2.2 Deployment Subsystem: PTU 46-70

The Component Requirements of the PTU specify a power supply (power_ptu) and a RS-232 communication link (port_serial_ptu) to operate and control the required rotational motion (pan motion). Hence the selected PC is upgraded with an additional serial interface. Since this PTU provides feedback of the pan and tilt position, returned by PTU commands, it is no necessary a feedback component. A battery 12 VDC satisfies the requirement of power.

Furthermore, the laser is attached to the top mounting plate on the PTU by means of a centered hole and standard #1/4-20 bolt and nut. These components are mapped to the Processing Unit and Power Unit subsystem respectively, as shown the Figure 5.11.

5.2.3 Locomotion Subsystem: LHD Vehicle

The mining vehicle should be adapted to navigate autonomously into the tunnel, implementing the motion P_1. Thus, in this experiment only the drive module is analyzed, assuming a straightforward steering, to resolve the components that perform its controlled actuation.

The selected LHD vehicle is driven by an electric motor via a pair of pedals; hence a simple adaptation is developed through these pedals. The drive module consists of two stepper motors mounted on the pedals to activate the traction actuator. Forward motion corresponds to the left stepper motor actuation, and backward displacement corresponds to the right stepper motor actuation. Stopping corresponds to the stepper motors neutral position or simultaneously actuation. To close the control-loop is necessary sensing the rotation or position of traction motor, which implies the vehicle displacement along the tunnel.

There are a number of different types of sensors, for robot applications optical encoders are a common means of sensing. A phase-quadrature incremental encoder made by Danaher Controls [Danaher], series 21/22 at 600 pulses per revolution is the feedback sensor, which is mounted to the transmission mechanism of the vehicle, having a dirt protection; this encoder constitutes the component to estimate the vehicle positioning using dead-reckoning technique. Therefore a parallel port is required to control the arrangement of stepper motors and to acquire the information from the encoder sensor.

An obstacle detector based on the sonar Polaroid 6500 achieves the safety function. This detector sends to Processing Unit a signal of stopping the vehicle whenever an obstacle appears in its course, via the above parallel port. Hence, the Processing Unit is upgrade with a parallel port. The necessary batteries are mapped to the Power Unit subsystem; whereas the power for the vehicle must be supplied by the facilities of the mine.

Figure 5.11 shows the complete structure with the integrated modules. In addition to the Locomotion, Deployment, Tool, Power Unit, and Processing Unit subsystem; the control panel is a remote PC (PC-IBM 386) where high-level commands are sent through a radio frequency (RF) link to the Processing Unit (PC-Pentium) to govern the MAV system. This link is a Communication Unit subsystem that consists of a RF modem own design, at 1200 bauds, to establish a radio channel half-duplex transmission, closing the control-loop to operate the vehicle. The Processing Unit controls the subsystems, synchronizing their actuations according to basic strategy. The control algorithms are implemented in the C++ programming language.

The Processing Unit is a personal computer PC-Pentium (PC-Local), 133 MHz, 32 MB RAM running on operating system Windows 95. The computer is configured with three serials ports and a parallel port to satisfy the Components Requirements. One serial is destined to control Tool subsystem, the second serial port controls Deployment subsystem and last one to Communication subsystem. The parallel port controls the Locomotion subsystem. The Control Panel is a computer PC-IBM-386 (PC-Remote), 66 MHz, 32 MB RAM, a serial port to communicate strategy commands.

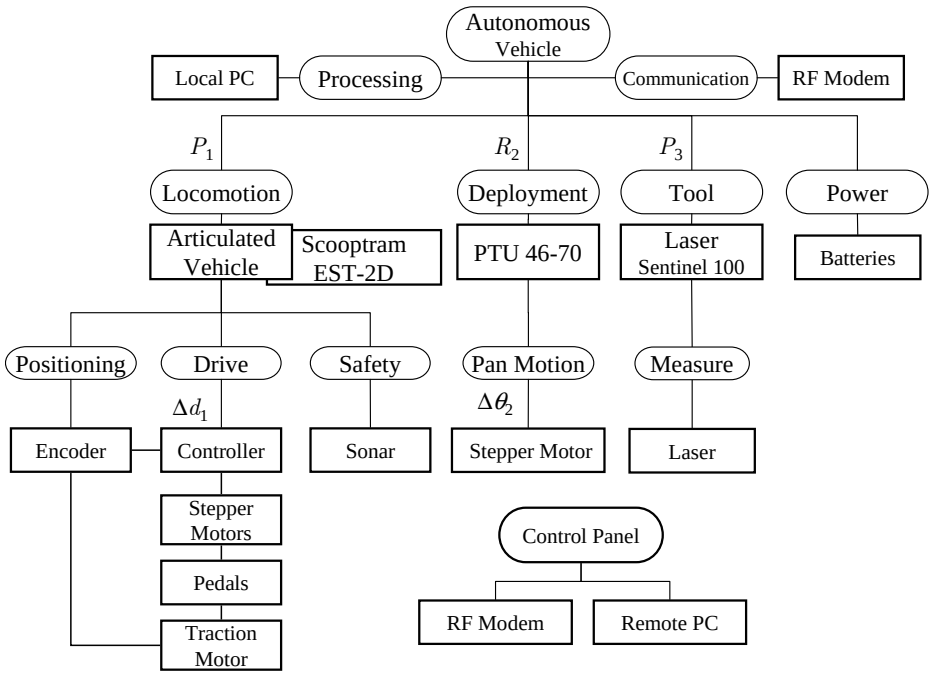

Figure 5.11: **MAV configuration to perform the tunnel profiling task. The Locomotion, Deployment and Tool subsystems are mapped from the Basic Configuration. The selected components satisfy the Configuration Requirements, Configuration Parameters, and Component Requirements. This structure presents the MAV as a system composed of hierarchical and modular interconnected components by means of Processing Unit to perform the TPT. Every subsystem is an integration of modules on the lowest hierarchical level, involving actuators, sensors, and controllers, which are combined to build up the subsystem functionality.**

5.3 Prototype

The MAV construction of prototype is the following stage of the framework, it was performed in the Robotics Laboratory at the Center for Intelligent Systems of the Tecnológico de Monterrey. Fig. 5.12 shows the distribution of the selected components to perform the tunnel-profiling task. An experimentation phase is used to improve the MAV configuration, which consisted of executing the assigned task in the real environment.

5.3.1 Experimental Results

The first trial ran on a flat surface as part of the indoor experimental effort to build the MAV. The vehicle traveled forward 21 meters while making several measurements along the way. The vehicle moved and stopped each 3 m to make three rotational translations with the sequence of angles: 60°, 90°, 120°, for each position the vehicle performed the measurements using the laser rangefinder.

Figure 5.12: **MAV prototype that integrates the components of the MAV configuration to perform the tunnel-profiling task.**

The recorded data was analyzed by the computational algorithm in the remote computer. The result is shown in the Figure 5.13. In the test, the robot forward/reverse motion was checked; the communication link and protocol were also evaluated. Finally, avoiding obstacles on vehicle was accomplished with the sonar module. The test purpose is to evaluate and debug every subsystem and module of the MAV configuration and to figure out the engineering problems, before it runs the test in real environment.

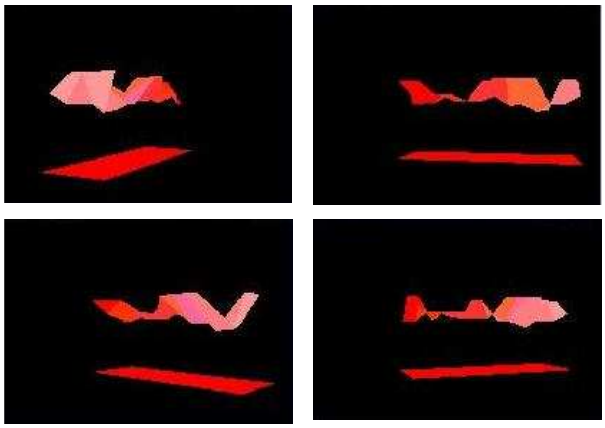

Figure 5.13: **Results of the indoor experiments, the inferior band represents the floor and the superior part represents the ceiling profile of the laboratory.**

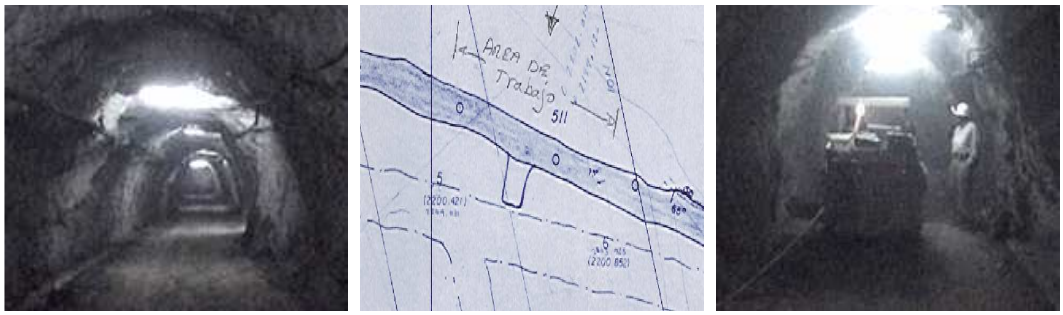

Figure 5.14: **Experimental trial in the "Las Golondrinas" mine (left), the work area with a 15 m long(middle), the MAV in operation (right).**

Real environment trial took place in the main tunnel of the mine "Las Golondrinas", which is the property of Peñoles Cia., and located in Guanajuato, México. During experimentation, initial conditions were fed to the control panel and transmitted to the MAV. The primitive commands dictated that at each meter (Δd_1) the vehicle stopped and carried out 15 measurements at equal intervals of 10° ($\Delta\theta_2$). The total distance traveled by the vehicle was 15 m.

Figure 5.14 shows the tunnel and the MAV in operation; whereas Figure 5.15 presents the resulting three-dimensional model of the mine tunnel, using the obtained measurements. The lower band represents the mine floor and the upper part represents the irregular ceiling of the tunnel profile. It is important to mention that resulting measures are approximate since it was considered a flat floor. The main outcomes of test analysis were an increase up to 20 % accuracy, in comparison to manual methods. This graphical representation is made using a graphic interface in Java 3-D.

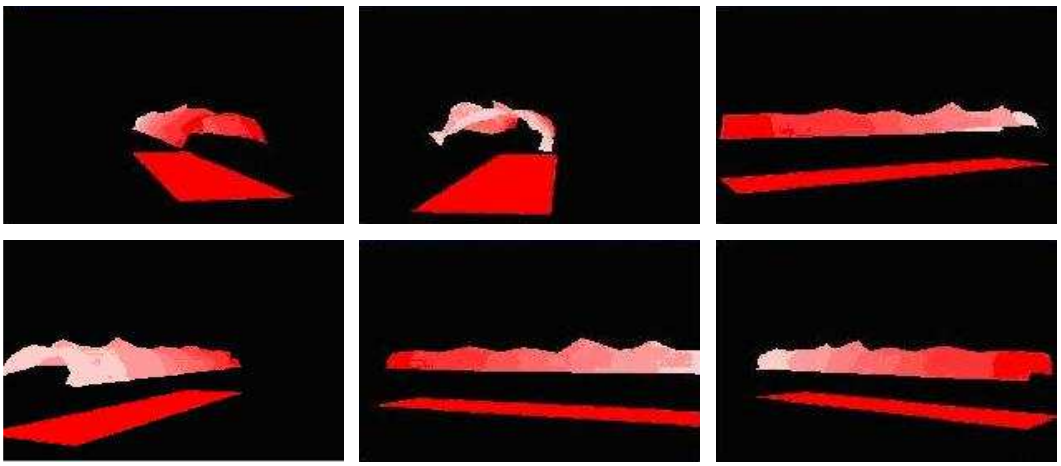

Figure 5.15: **Experimental results in the mine.**

5.3.2 Discussion

Although the results of the tunnel profiling task, obtained during the experimental trials, have demonstrated that the implemented robotic vehicle is a feasible solution for such task [Gutierrez 04]. The systematic procedure of the framework has not concluded for synthesis of a detailed AV configuration. However, the major result of this exercise is the validation of the systematic framework as a suitable approach to obtain the AV configuration from the effective specifications of the task and the environment; allowing the construction of the MAV that could be rapidly deployed, using available components that satisfies such specifications.

In applying the systematic framework for synthesis of the MAV configuration, several results are reached with the implementation of the MAV prototype that addresses the following observations:

- The MAV configuration has been derived with the assist of the systematic framework from the task and environment specifications.
- The MAV has been configured by identifying the fundamental composition of basic motions to perform the assigned task. This is the definition of the Basic Configuration, which represents the essential topology in terms of the functionality of such motions. Additionally, the sequential execution of the Basic Configuration provides the basic strategy of operation of the MAV.
- The MAV configuration has been fulfilled by selecting the components to implement the motion function of the Basic Configuration.
- In the synthesis of the MAV configuration, the system framework takes advantage of the inventory of components developed by decades of engineering. In particular, adapting an existing mining vehicle, which has been designed and optimized by the manufacturer for the required environment.
- The implementation of the MAV configuration has showed that is a suitable prototype to perform the assigned task (TPT), generating automatically the profile of a tunnel into the expected underground mine.

While the selected LHD mining vehicle is within the parametric specifications, which have founded by the framework and established in the Configuration Requirements and the Configuration Parameters, and represents an excellent option to perform the task, being a vehicle designed specifically for the conditions of the mine, other alternatives must be considered to deliver a MAV configuration using current technology and existing components within a reasonable cost, such as other vehicles with smaller dimensions. Moreover, the MAV configuration requests for an analysis of autonomy that allows the implementation of a robust and operational MAV prototype.

Therefore, the method integrates an analysis to provide a certain degree of autonomy that correlates the actions of the vehicle, such as accurate positioning, control, and perception. Such analysis is oriented to identify the kinematic requirements of the vehicle that improve position estimation, in addition to the control and perception requirements, as criteria in the synthesis process of the MAV configuration. The analysis involves a parametric comparison of different steering mechanisms under equal operation conditions to select then the proper vehicle that embody the Locomotion subsystem.

The next chapters recapture the procedure of the systematic framework, involving the development of a detailed MAV configuration for the tunnel profiling task.

Chapter 6

Autonomy Analysis

Many robotic vehicle actions require autonomy, as a function that correlates the perception, the control, and the positioning of the vehicle. A reliable degree of autonomy requires the vehicle be controlled by itself to navigate, following a given path and avoiding obstacles. Key to mobile robot autonomous performance is accurate positioning, which implicates that the vehicle positioning must be estimated to provide safe and effective control. In this chapter, the MAV configuration is discussed to improve positioning, control and perception from steering kinematics of the vehicle.

In Robotics, much research has been conducted about the position estimation, reporting numerous techniques; some techniques are excluded from specific environments (e.g., underground mining or planetary exploration), other schemes require complete knowledge or structure additional in the environment. A feasible and fundamental method to estimate the vehicle positioning is dead reckoning. It is based on the use of simple kinematic models and the integration of incremental motion information from internal sensors such as wheel and steer encoders to provide both low-level closed loop control and estimate the positioning of the vehicle. However, dead reckoning suffers from positioning error due to accumulation of sensor errors. Furthermore, this method is impacted by many factors that tend to involve a combination of vehicle parameters, environment conditions, and vehicle-environment interaction. A solution is to design the steering system to be less prone to positioning error.

To configure the AV, selecting the adequate vehicle kinematics that minimizes the position estimation error is fundamental criterion in the synthesis process of AVs, in addition to the control and perception requirements. Thus, it is necessary to conduct a systematic analysis to identify the kinematic requirements of the vehicle steering that improve the position estimation, control and perception of the robotic vehicle; since the kinematic model is derived propriety from Locomotion subsystem, which also is the physical interface between the environment and the robotic vehicle. The Figure 6.1 depicts the parametric analysis to obtain a configuration of the robot by integrating basic aspects of autonomy.

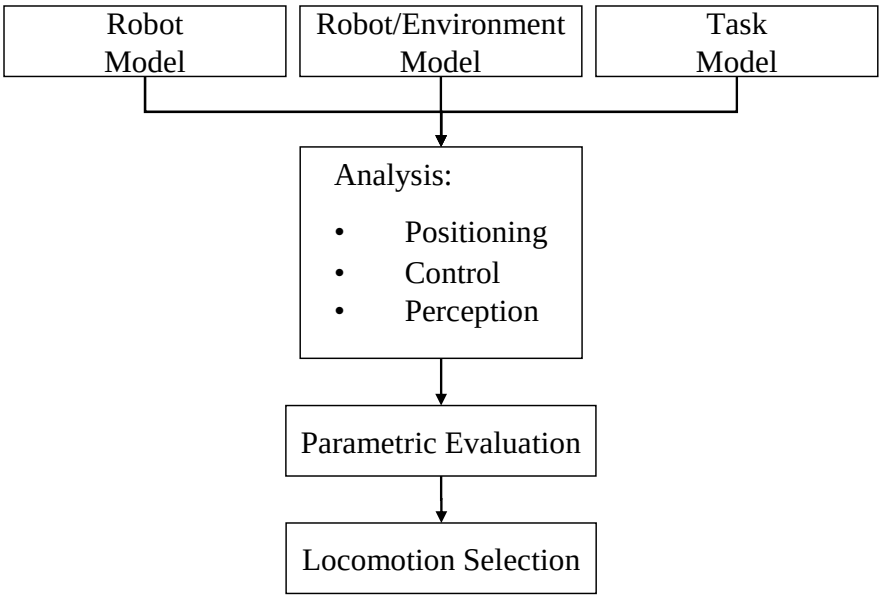

Figure 6.1: **Parametric analysis for configuration of the robot locomotion.**

The analysis establishes as input the task and environment requirements that the robotic vehicle must satisfy; it includes equations that capture the kinematic model and positioning, control and perception, allowing compare different parameters of feasible vehicles; by then select the Locomotion subsystem. The method works as follows:

1. The analysis uses simple steady-state models to estimate the generated error on vehicle positioning, considering the difference between a vehicle that navigates over ideal environment and other one that interacts with the expected environment. This calculated positioning error is used as a criterion for quantitative comparison of variant vehicles, involving steering mechanisms and vehicle dimensions.

2. The method leads a similar analysis to compare the requirements of control and perception for the vehicle locomotion. The comparison is conducted under equal and simpler conditions of operation, among the variant vehicles, to follow a path that incorporates the geometric constraints of the environment.

3. The quantitative results allow the definition of the Locomotion subsystem to complete the robotic vehicle configuration that performs the assigned task with the required degree of autonomy.

The following sections 6.1, 6.2, and 6.3 outline the proper method for the positioning, control, and perception analysis, respectively. Whereas, section 6.4 summarizes the obtained results to address the selection of the Locomotion subsystem, based on the parametric comparison of these results and the Configuration Requirements and the Configuration Parameters.

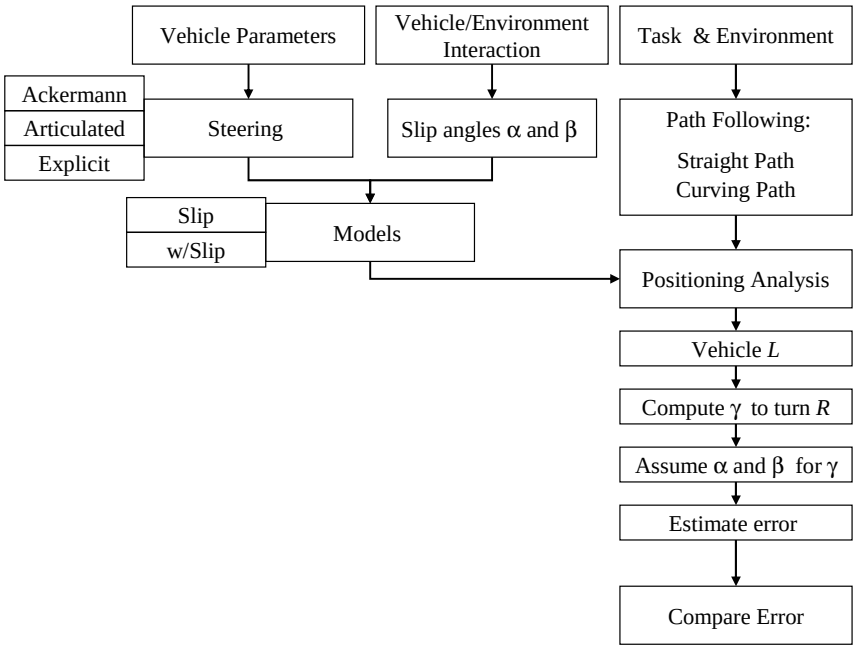

Figure 6.2: **Positioning analysis for steering kinematics.**

6.1 Steering Kinematics and Positioning

The key issue addressed in the synthesis process is that vehicle locomotion must minimize the error in the position estimation. The error is caused by many factors that are unpredictable and extremely difficult to model accurately, involving a combination of vehicle parameters (e.g., steering mechanism), environment conditions (e.g. terrain properties, confined space), and vehicle-terrain interaction. In the analysis for steering kinematics, the slip motion is chosen to represent the combination and impact of these factors; hence the error in the vehicle positioning is estimated for the case of kinematic model with explicit slip against ideal model without slip. Then, a quantitative comparison among the steering mechanisms is investigated as shown in Figure 6.2.

The analysis examines three widely-known vehicle steering schemes: Ackermann Steering (AS), aRticulated Steering (RS), and Explicit independent Steering (ES). Their kinematic models are derived, both including slip and ideal steering behavior. Two slip variables are introduced: slip angle α referenced to rear axle and slip angle β corresponding to front axle. The analysis considers steady state turning (R) for different vehicle length (L) to compute the steering angle γ. Then, the position error is theoretically estimated assuming equal magnitude of the slip angles for each steering schemes. The geometries of these steering mechanisms are shown in the Figures 6.3-6.5; Table 6.1 presents their kinematic models. The complete derivation of the kinematic models is developed in the Appendix B.

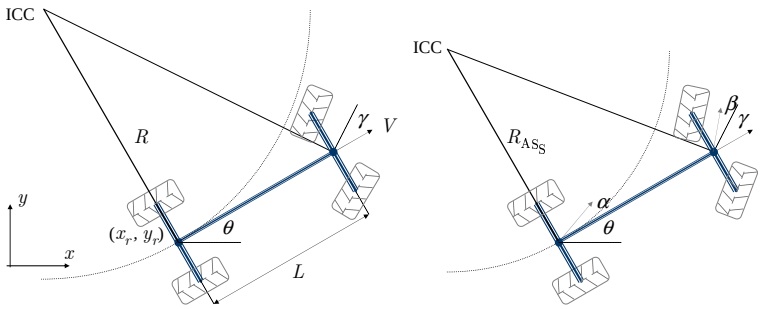

Figure 6.3: **Geometry of the Ackermann Steering (AS): (left) without slip angles and (right) including slip angles α and β. An ackermann vehicle consists of a front and rear axle. The wheels of the rear axle are commonly driven and their orientation is fixed, while the front axle wheels are steered through a kingpin axis.**

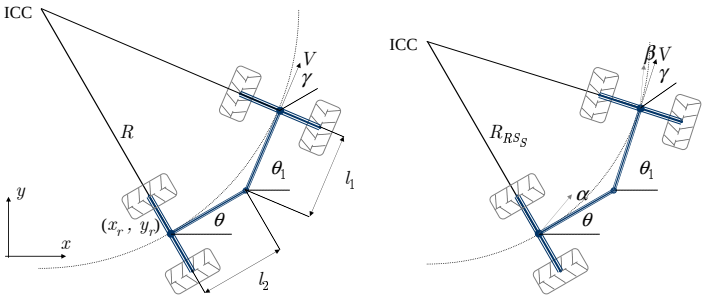

Figure 6.4: **Geometry of the Articulated Steering (RS): (left) without slip angles and (right) including slip angles α and β. An articulated vehicle is composed of a front and rear body which can rotate relative to each other. Each body has a single axle with two wheels which are fixed (non-steerable). The steering behavior is achieved by driving the articulation joint (yaw pivot) that connects both bodies.**

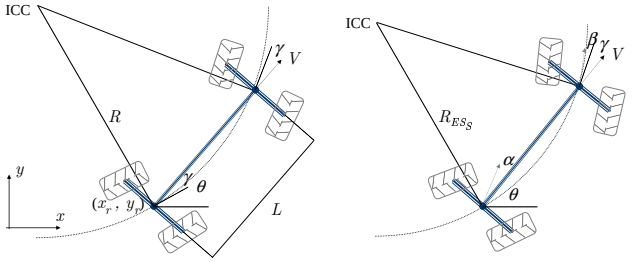

Figure 6.5: **Geometry of the Explicit Independent Steering (ES): (left) without slip angles and (right) including slip angles α and β. An explicit vehicle is designed so that all wheels can be driven and steered individually; however, considering the assumption of steady-state turning the ES becomes a bi-steerable vehicle (double ackermann steering) that has a linear relation between the front and rear steering angles (γ).**

Steering	**No Slip**	**Slip**
Ackermann	$\dot{x}_r = V cos\theta$ $\dot{y}_r = V sin\theta$ $\dot{\theta} = \frac{V sin\gamma}{L cos\gamma}$	$\dot{x}_r = V cos(\theta + \alpha)$ $\dot{y}_r = V sin(\theta + \alpha)$ $\dot{\theta} = \frac{V sin(\beta - \alpha + \gamma)}{L cos(\gamma + \beta)}$
Articulated	$\dot{x}_r = V cos\theta$ $\dot{y}_r = V sin\theta$ $\dot{\theta} = \frac{V sin\gamma - l_1\dot{\gamma}}{l_1 + l_2 cos\gamma}$	$\dot{x}_r = V cos(\theta + \alpha)$ $\dot{y}_r = V sin(\theta + \alpha)$ $\dot{\theta} = \frac{V sin(\beta - \alpha + \gamma) - l_1\dot{\gamma} cos\beta}{l_1 cos\beta + l_2 cos(\gamma + \beta)}$
Explicit	$\dot{x}_r = V cos(\theta + \gamma)$ $\dot{y}_r = V sin(\theta + \gamma)$ $\dot{\theta} = \frac{V sin2\gamma}{L cos\gamma}$	$\dot{x}_r = V cos(\theta + \gamma + \alpha)$ $\dot{y}_r = V sin(\theta + \gamma + \alpha)$ $\dot{\theta} = \frac{V sin(\beta - \alpha + 2\gamma)}{L cos(\gamma + \beta)}$

Table 6.1: **Kinematic Models of the steering mechanisms: where x and y denote the position of the vehicle relative to some fixed global frame of reference. The rear axle is denoted by a subscript r. The angle θ is the orientation of the vehicle with respect to the x axis, while V represents the linear velocity of an imaginary wheel located midway between the real wheels (bicycle model). The angle γ is defined as the steering angle of the vehicle, and L is the length of the vehicle, the distance between the front and rear axle; for the articulated steering l_1 denotes the front body length, while the rear body length is denoted by l_2.**

Observing these equations, particularly for kinematic models that incorporate slip; it can be seen that the vehicle motion depends not only on control inputs V and γ and vehicle length L, but also on the slip angles. The vehicle direction is given by the slip angle α and orientation angle θ, while the change rate of orientation $\dot{\theta}$ is function on steering angle γ and both slip angles α and β.

Furthermore, based on the assumption that the vehicle develops a steady-state motion turning where γ is a constant (i.e., $\dot{\gamma} = 0$), the rate of change of orientation depends propriety on driving radius R and it is given by $\dot{\theta} = \frac{V}{R}$; any change in the radius due to slip leads to an error in position estimation.

The effect of the slip angles in the vehicle motion is related to a deviation from the ideal performance; thus, the positioning error is computed as ratio of slip radius to ideal radius ($PositioningErrorRatio, PER = 1 - \frac{Radius_{Slip}}{Radius_{Ideal}}$). The ratio for the steering schemes are therefore developed in the following.

Ackermann ratio Referring to geometry of AS vehicle (Fig. 6.3), the radius without slip depends on the vehicle length L and γ

$$R_{AS} = \frac{Lcos\gamma}{sin\gamma}$$

solving for slip radius of AS vehicle,

$$R_{AS_S} = \frac{Lcos(\gamma + \beta)}{sin(\beta - \alpha + \gamma)}$$

thus, the ratio for ackermann steering (PER_{AS}) is denoted as:

$$PER_{AS} = 1 - \frac{cos(\gamma + \beta)sin\gamma}{cos\gamma sin(\beta - \alpha + \gamma)}$$

Articulated ratio Referring to geometry of RS vehicle (Fig. 6.4), the radius without slip depends on the both vehicle segments l_1 and l_2, and γ

$$R_{RS} = \frac{l_1 + l_2 cos\gamma}{sin\gamma}$$

slip radius is as

$$R_{RS_S} = \frac{l_1 cos\beta + l_2 cos(\gamma + \beta)}{sin(\beta - \alpha + \gamma)}$$

hence, the ratio for articulated steering (PER_{RS}) is formulated as:

$$PER_{RS} = 1 - \frac{[l_1 cos\beta + l_2 cos(\gamma + \beta)]\, sin\gamma}{(l_1 + l_2 cos\gamma) sin(\beta - \alpha + \gamma)}$$

Explicit ratio Referring to geometry of ES vehicle (Fig. 6.5), the radius without slip on the vehicle length L and γ

$$R_{ES} = \frac{Lcos\gamma}{sin2\gamma}$$

solving for slip radius,

$$R_{ES_S} = \frac{Lcos(\gamma + \beta)}{sin(\beta - \alpha + 2\gamma)}$$

hence, the ration for explicit steering (PER_{ES}) becomes:

$$PER_{ES} = 1 - \frac{cos(\gamma + \beta)sin2\gamma}{cos\gamma sin(\beta - \alpha + 2\gamma)}$$

To compute the ratio of each steering mechanism, the analysis assumes particular values of the slip angles. Scheding [Scheding 99] reports estimated values for the slip angles in experimental trails developed in underground mining on an articulated vehicle (Load, Haul and Dump truck - LHD). The values were estimated from real data using a statistical filter. The percentage for slip angle α is estimated as 66.19 % with respect to steering angle γ, whereas that it is 16.62 % for slip angle β. These estimated values are applied to PER equations under the disposition shown in Table 6.2, as a real reference to investigate the impact on the steering schemes.

Assuming that the slip angles are a percentage of the steering angle γ (i.e., $k_\alpha = \frac{\alpha}{\gamma}$ and $k_\beta = \frac{\beta}{\gamma}$) and by introducing the length ratio ($r = \frac{l_1}{l_2}$) for RS vehicle; the above equations of ratio result in

$$PER_{AS} = 1 - \frac{cos(\gamma\,[1 + k_\beta])sin\gamma}{cos\gamma sin(\gamma\,[k_\beta - k_\alpha + 1])} \tag{6.1}$$

$$PER_{RS} = 1 - \frac{[rcos(k_\beta\gamma) + cos(\gamma\,[1 + k_\beta])]\,sin\gamma}{[r + cos\gamma]sin(\gamma\,[k_\beta - k_\alpha + 1])} \tag{6.2}$$

$$PER_{ES} = 1 - \frac{cos(\gamma\,[1 + k_\beta])sin2\gamma}{cos\gamma sin(\gamma\,[k_\beta - k_\alpha + 2])} \tag{6.3}$$

Case	$k_\alpha(\%)$	$k_\beta(\%)$
(a) α	66.19	00.00
(b) β	00.00	16.62
(c) $\alpha > \beta$	66.19	16.62
(d) $\alpha = \beta$	16.62	16.62
(e) α	16.62	00.00

Table 6.2: **Percentages of the Slip Angles: k_α and k_β for the analysis cases.**

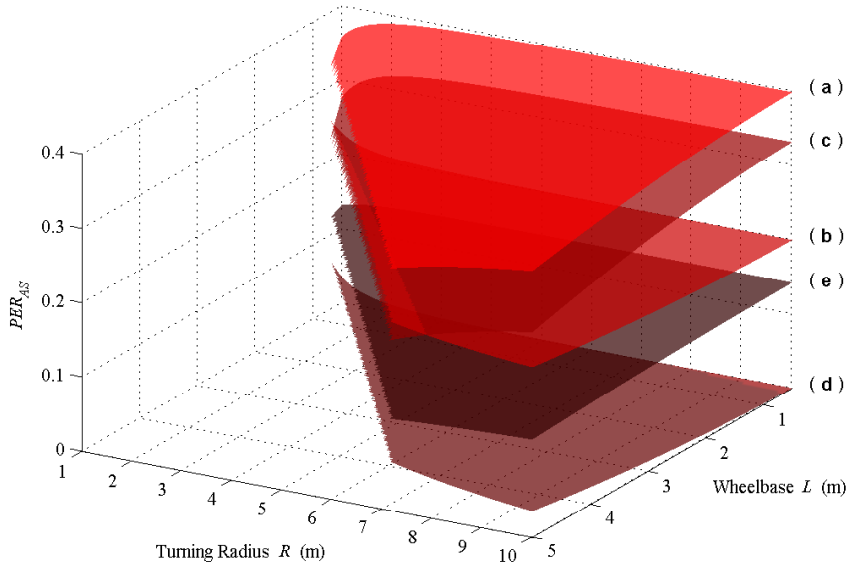

Figure 6.6: **Positioning error ratio for Ackermann steering.**

6.1.1 PER analysis for Ackermann steering

The ratio is computed for the AS vehicle to investigate relation between vehicle configuration and position estimation, using the aforementioned values at different proportion for k_α and k_β (Table 6.2) and varying the vehicle length while each vehicle performs a specific radius. The result is depicted in the Figure 6.6. Referring to this result several observations are made:

- The slip angle β produces a bigger error than the slip angle α. It can be observed in the plotted ratio for case (**b**) compared with the ratio produced by case (**e**).
- A combination of both slip angles produce smaller ratio than the ratio produced by the biggest slip angle of this combination; for instance, case (**c**) is smaller than case (**a**).
- When the slip angles are equal the effect is minor, both slip angles trend to cancel their effect on the performed radius of the case (**d**), that is clear in the term $(\beta - \alpha + \gamma)$; besides, the effect is minor at lower percentages.
- If $\alpha > \beta$, cases (**a**), (**c**), and (**e**), the ratio has the tendency to increase while the radius is increased and the vehicle length (wheelbase) is reduced, a behavior inversely proportional to the relation $\frac{L}{R}$. In the rest of cases where $\alpha \leq \beta$, cases (**b**) and (**d**), there is a proportional behavior to relation $\frac{L}{R}$.

These observations may be interpreted geometrically; Figure 6.7 shows the effect on radius induced by slip angles for two specific vehicles that perform an identical turn.

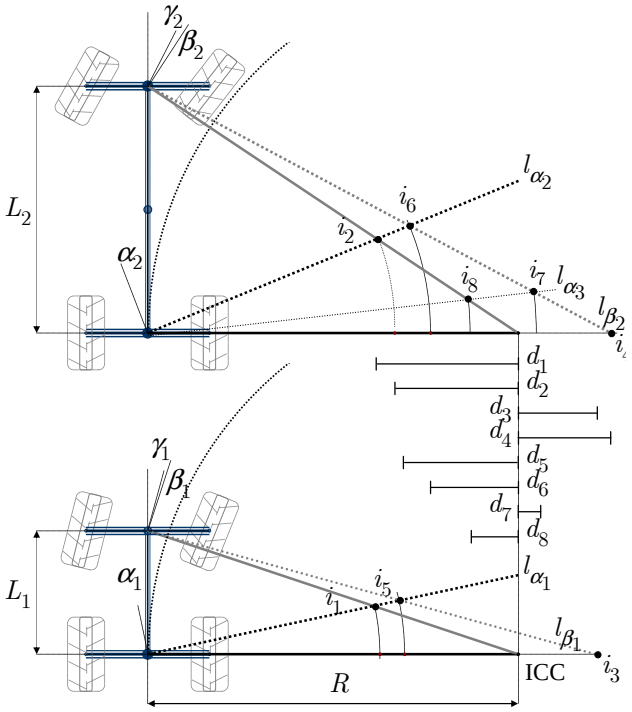

Figure 6.7: **Geometry of ratio induced by slip angles on AS vehicle.**

The wheelbases are $L_1 = 1$ m and $L_2 = 2$ m. The ideal radius R is 3 m, and the steering angles are derived as $\gamma_1 = atan(\frac{L_1}{R})$ and $\gamma_2 = atan(\frac{L_2}{R})$. The slip angle percentages are 66.19 % and 16.62 %, the slip effect is represented by perpendicular lines to the slip angles, which are denoted as l_{α_1}, l_{α_2}, l_{α_3}, l_{β_1}, and l_{β_2}. A intersection of two lines is denoted by a point i_i, which represent a new instantaneous center of curvature (ICC); its projection on the ideal radius allows observe the change of radius that the vehicle experiences due to the slip angles, it is the difference d_i between ideal radius and new radius. Table 6.3 summarizes key configuration results in relation to positiong error.

Wheelbase (m)	γ (°)	k_α (%)	k_β (%)	**Difference (m)**	PER_{AS}
$L_1 = 1$	18.43	66.19	00.00	$d_1 = 1.1384$	0.3794
$L_2 = 2$	33.69	66.19	00.00	$d_2 = 0.9925$	0.3308
$L_1 = 1$	18.43	00.00	16.62	$d_3 = 0.6379$	0.2126
$L_2 = 2$	33.69	00.00	16.62	$d_4 = 0.7474$	0.2491
$L_1 = 1$	18.43	66.19	16.62	$d_5 = 0.9169$	0.3056
$L_2 = 2$	33.69	66.19	16.62	$d_6 = 0.7097$	0.2366
$L_2 = 2$	33.69	16.62	16.62	$d_7 = 0.1809$	0.0602
$L_2 = 2$	33.69	16.62	00.00	$d_8 = 0.3722$	0.1240

Table 6.3: **PER results induced by slip angles on AS vehicle.**

Comparing separately the effect of the slip angles, it can be seen that both slip angles α and β produce opposed results under the disposition shown in Figure 6.7. The slip angle α decrease the radius, having an understeer vehicle when l_{α_1} intersects the ideal line from the front axle to original ICC on the point i_1, similar result is obtained in the vehicle L_2 on i_2 for l_{α_2}; although the percentages are equal to calculate α_1 and α_2, the positioning error ratio for the vehicle L_1 is bigger than the ratio for vehicle L_2 (i.e., $d_1 > d_2$).

The slip angle β increases the radius, generating an oversteer response of vehicles when l_{β_1} and l_{β_2} intersect the ideal line from the rear axle to original ICC on i_3 and i_4, respectively. In this case the ratio of vehicle L_1 is smaller than ratio of the vehicle L_2 (i.e., $d_3 < d_4$).

The combination of both slip angles at different percentages can be seen on the intersections points i_5 and i_6, for l_{β_1} with l_{α_1} and l_{β_2} with l_{α_2} respectively. The ratio of vehicle L_1 is bigger than the ration of vehicle L_2 (i.e., $d_5 > d_6$).

Assuming equal slip percentage for the rear and the front axle, the effect is less and tends to cancel the slip impact; for instance, the l_{α_3} is same percentage as l_{β_2}, the radius produced by both slip angles is denoted as i_7, which shows a ratio quite small (i.e., d_7). This assumption allows observe individually the effect produced by the slip angles. It is noted that the slip β produces a bigger ratio than slip α, as shown the differences d_4 and d_8, which assume same percentage of slip ($k_\alpha = k_\beta$) and the ratio is almost double for effect produced by front slip angle comparing with rear slip angle.

These results correspond with the aforementioned observations. Furthermore, when the radius increases the ratio $\frac{L}{R}$ is quite small, and the steering angle γ is small and the length of the vehicle can be negligible; to compute the error ratio assuming that $sin\gamma = \gamma$ and $cos\gamma = 1$ when the steering angle is expressed in radians, the ratio equation of AS vehicle can be simplified as:

$$PER_{AS_{\gamma \approx 0}} = 1 - \frac{1}{[k_\beta - k_\alpha + 1]}$$

Thus, if $R \gg L$ the positioning error ratio is only a function of the slip angles α and β.

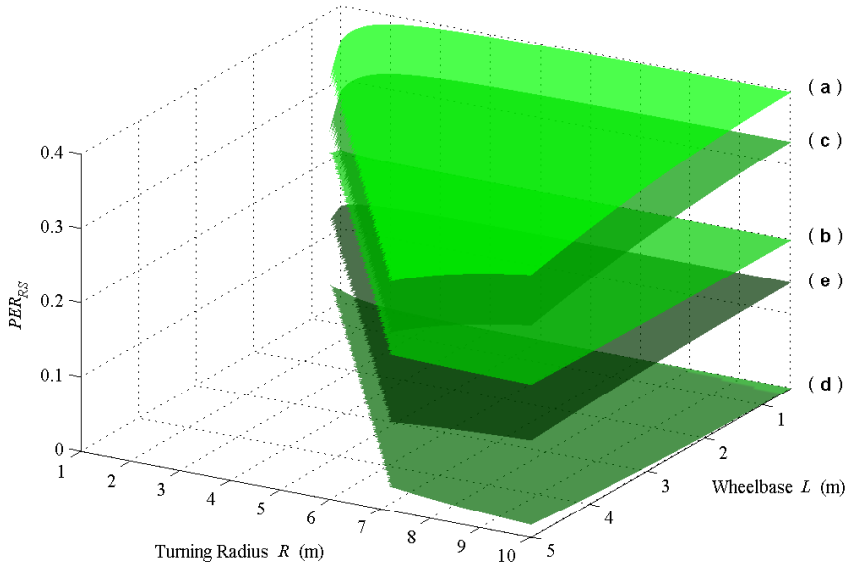

Figure 6.8: **Positioning error ratio for Articulated steering.**

6.1.2 PER analysis for Articualted steering

The ratio for the RS vehicle is computed as the AS vehicle, using the values for k_α and k_β shown in the Table 6.2 and varying the vehicle length while each vehicle steers at a specific radius. The result is depicted in the Figure 6.8. Referring to this result several observations are made:

- The slip angle β produces a bigger ratio than the slip angle α, as it can be seen in the plotted ratio for case (**b**) compared with case (**e**).
- Equal slip angles tend to cancel out error on the radius (**d**).
- In the relation $\alpha > \beta$, the ratio rises while the radius is increased and the vehicle length (wheelbase) is reduced, a behavior that is inversely proportional to the relation $\frac{L}{R}$. The behavior is proportional to relation $\frac{L}{R}$ at $\alpha \leq \beta$.

These observations are interpreted geometrically in the Figure 6.9, which shows the effect on radius induced by slip angles for two specific vehicles that perform identical turn. The vehicles perform an ideal radius R, as in AS case; the wheelbases are L_1 = 1m and L_2 = 2m and the length ratio $r = 1$, thus $l_1 = l_2$ in both vehicles. The obtained results are resumed in the Table 6.4.

These results correspond with the aforementioned observations and the ratio equation of RS vehicle for small steering angle γ is given as:

$$PER_{RS_{\gamma \approx 0}} = 1 - \frac{1}{[k_\beta - k_\alpha + 1]}$$

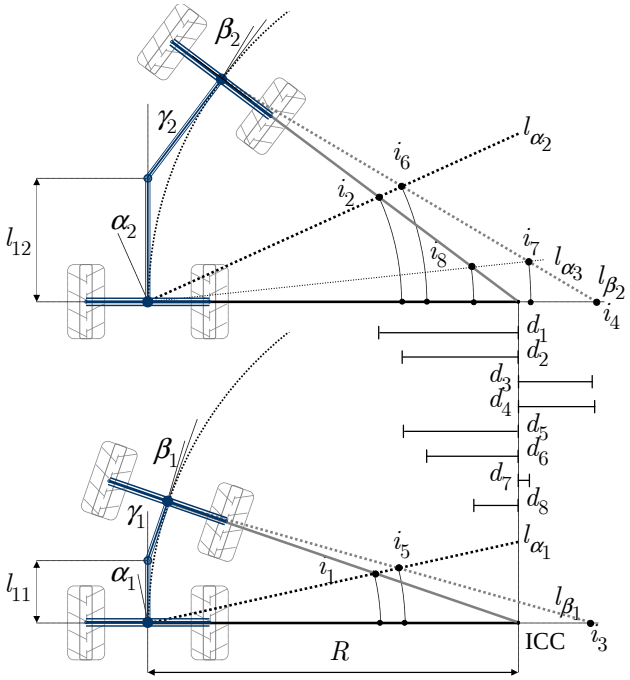

Figure 6.9: **Geometry of ratio induced by slip angles on RS vehicle. The slip effect is represented by perpendicular lines to the slip angles (l_{α_1}, l_{α_2}, l_{α_3}, l_{β_1}, and l_{β_2}). A intersection of two lines i_i represents a new instantaneous center of curvature (ICC); its projection on the ideal radius shows the difference d_i.**

Wheelbase (m)	γ (°)	k_α (%)	k_β (%)	**Difference (m)**	PER_{RS}
$L_1 = 1$	18.92	66.19	00.00	$d_1 = 1.1353$	0.3784
$L_2 = 2$	36.87	66.19	00.00	$d_2 = 0.9474$	0.3158
$L_1 = 1$	18.92	00.00	16.62	$d_3 = 0.6055$	0.2018
$L_2 = 2$	36.87	00.00	16.62	$d_4 = 0.6267$	0.2089
$L_1 = 1$	18.92	66.19	16.62	$d_5 = 0.9324$	0.3108
$L_2 = 2$	36.87	66.19	16.62	$d_6 = 0.7410$	0.2470
$L_2 = 2$	36.87	16.62	16.62	$d_7 = 0.0896$	0.0298
$L_2 = 2$	36.87	16.62	00.00	$d_8 = 0.3606$	0.1202

Table 6.4: **PER results induced by slip angles on RS vehicle.**

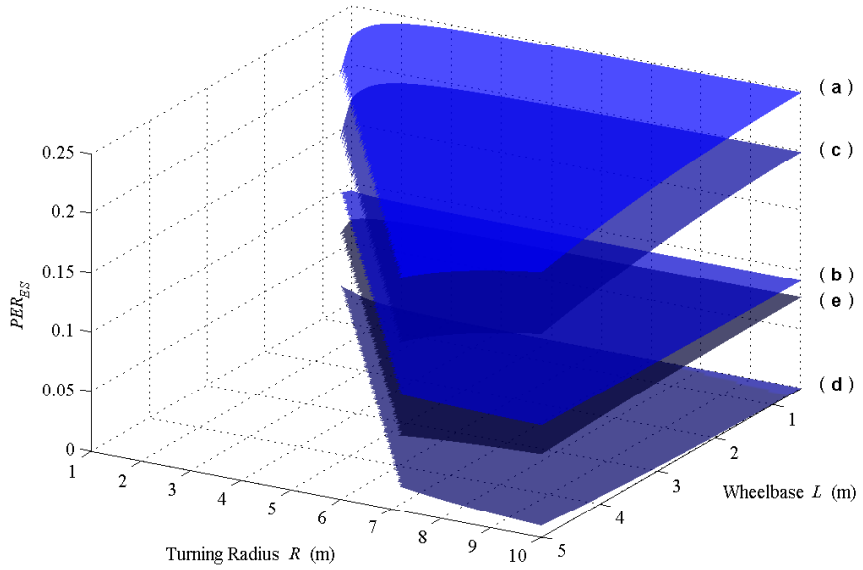

Figure 6.10: **Positioning error ratio for Explicit steering.**

6.1.3 PER analysis for Explicit steering

The ratio for the ES vehicle is computed as the AS vehicle, using the values for k_α and k_β shown in the Table 6.2 and varying the vehicle length while each vehicle performs a specific radius. The result is depicted in the Figure 6.10. Referring to this result several observations are made:

- The slip angle β produces a bigger ratio than the slip angle α, as it can be seen in the plotted ratio for case (**b**) compared with case (**e**).
- Equal slip angles produce a tendency to cancel their effect on the radius (**d**).
- In the relation $\alpha > \beta$, the ratio rises while the radius is increased and the vehicle length (wheelbase) is reduced, it is an inversely proportional behavior to the relation $\frac{L}{R}$. The behavior is proportional to relation $\frac{L}{R}$ at equal slip angles and $\alpha < \beta$.

These observations are interpreted geometrically in the Figure 6.11, which shows the effect on radius induced by slip angles for two specific vehicles that perform identical turn. The vehicles perform an ideal radius R, as in AS case; the wheelbases are $L_1 =$ 1m and $L_2 = 2$m. The obtained results are resumed in the Table 6.5.

These results correspond with the aforementioned observations and the ratio equation of ES vehicle for small steering angle γ is given as:

$$PER_{ES_{\gamma\approx 0}} = 1 - \frac{2}{[k_\beta - k_\alpha + 2]}$$

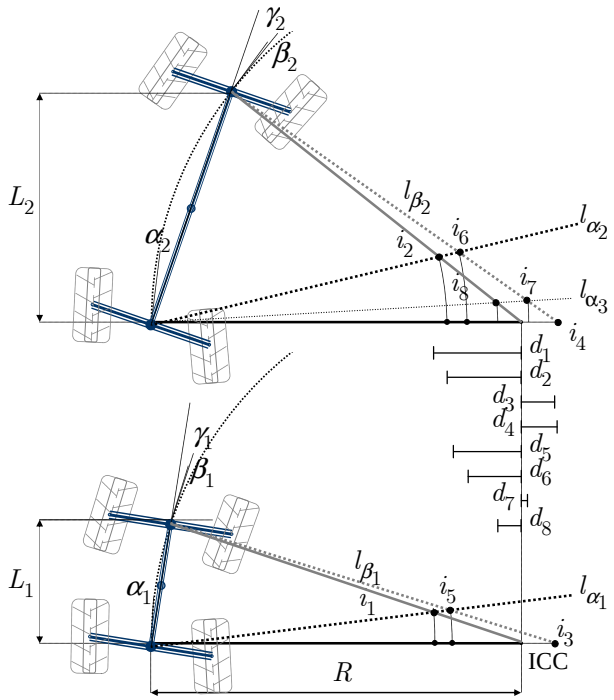

Figure 6.11: **Geometry of ratio induced by slip angles on ES vehicle. The slip effect is represented by perpendicular lines to the slip angles (l_{α_1}, l_{α_2}, l_{α_3}, l_{β_1}, and l_{β_2}). A intersection of two lines i_i represents a new instantaneous center of curvature (ICC); its projection on the ideal radius shows the difference d_i.**

Wheelbase (m)	γ (°)	k_α (%)	k_β (%)	**Difference (m)**	PER_{ES}
$L_1 = 1$	9.59	66.19	00.00	$d_1 = 0.7129$	0.2376
$L_2 = 2$	19.47	66.19	00.00	$d_2 = 0.6016$	0.2005
$L_1 = 1$	9.59	00.00	16.62	$d_3 = 0.2762$	0.0920
$L_2 = 2$	19.47	00.00	16.62	$d_4 = 0.2902$	0.0967
$L_1 = 1$	9.59	66.19	16.62	$d_5 = 0.5599$	0.1866
$L_2 = 2$	19.47	66.19	16.62	$d_6 = 0.4398$	0.1466
$L_2 = 2$	19.47	16.62	16.62	$d_7 = 0.0550$	0.0183
$L_2 = 2$	19.47	16.62	00.00	$d_8 = 0.1917$	0.0639

Table 6.5: **PER results induced by slip angles on ES vehicle.**

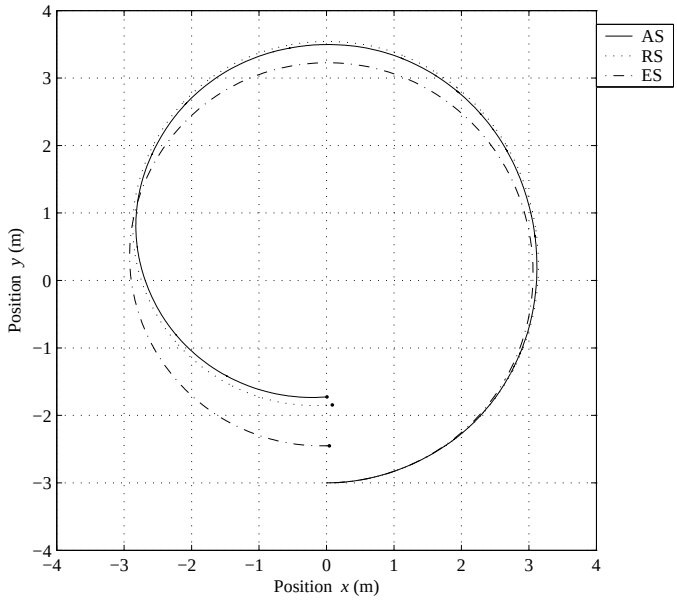

Figure 6.12: **Accumulated PER of Ackermann, Articulatedd and Explicit vehicles while performing a steady turn (R = 3 m).**

6.1.4 PER accumulation

It can be mentioned that although the error could be small, the impact in the vehicle positioning estimation is accumulated with the time. This can be seen from the kinematic models that are used to provide an estimate of the position and the orientation or heading of the vehicle with respect to some coordinate system. The deviation from the ideal performance of the radius impacts significantly the computation of the vehicle heading (θ), causing an error propagation to derive the vehicle position (x and y).

Figure 6.12 shows the estimated position of the vehicle, considering a certain percentage of the slip angles while the vehicles perform a complete turn. In particular, assume that the vehicles must perform a steady turn of radius R (3 m) and centered at the origin of coordinates. The circular trajectory must be traced counterclockwise at constant velocity (V = 1 m/s) starting with the rear axle midpoint of each vehicle located at point (0,-3), the length vehicle is 2 m.

The vehicle positioning estimation is calculated using the discrete kinematic models of the vehicles, which are derived from the previous kinematic models that include the slip angles (Table 6.1). The complete derivation of the models is developed in the Appendix B, whereas the slip angles are parameterized by a random process consisting of a sequence of discrete values of fixed length (Random walk or Brownian motion), as shown the Figure 6.13. Figure 6.14 shows the accumulated error, which is calculated as the distance between two points in the plane: the ideal position and the position that the vehicle experienced due to slip angles.

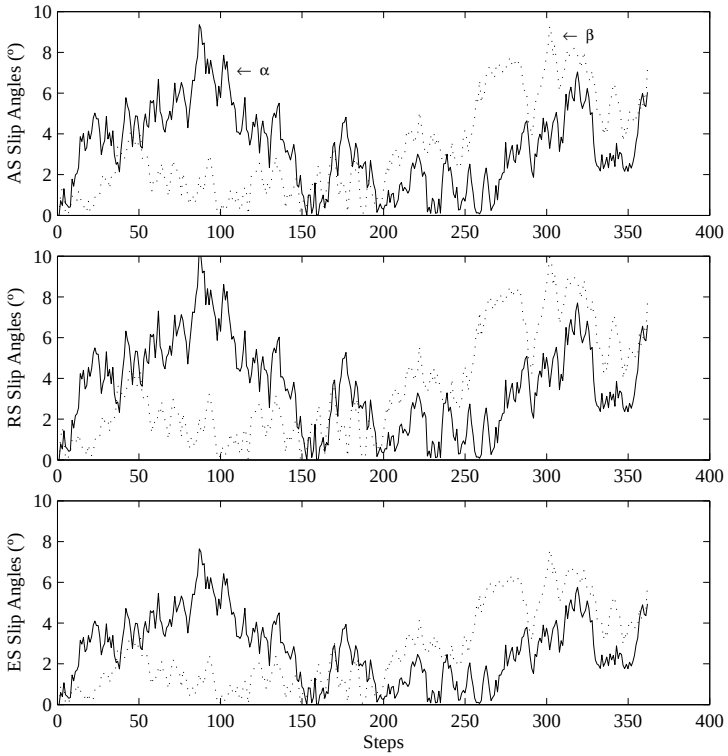

Figure 6.13: **Random estimation of the slip angles: 360 random values for slip angles α and β, respectively.**

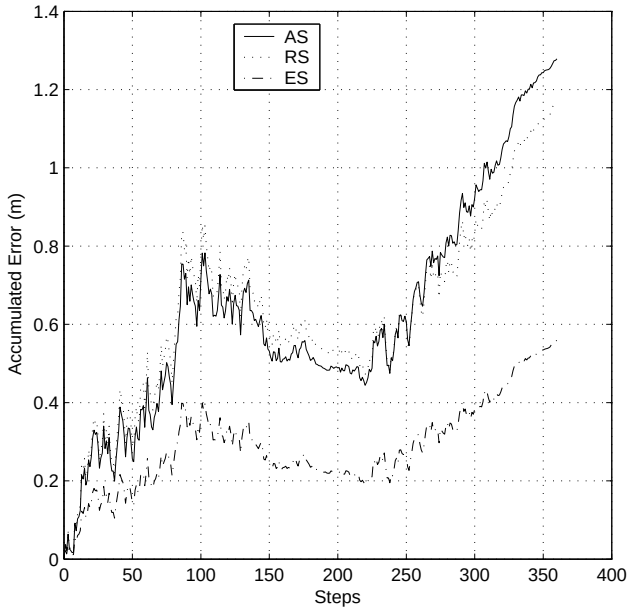

Figure 6.14: **Accumulated error of Ackermann, Articulatedd and Explicit vehicles while performing a steady turn. The error is calculated as the distance between the ideal position and the position that the vehicle experienced due to slip angles.**

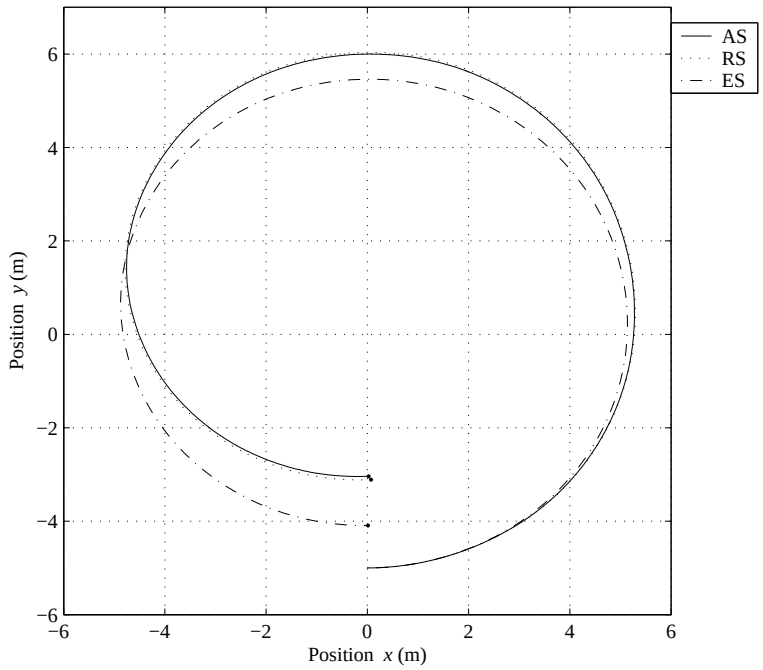

Figure 6.15: **Accumulated PER of AS, RS and ES vehicles at $R = 5$ m.**

Figure 6.15 and Figure 6.16 show the accumulated error for a steady turn 5 m and 10 m, respectively.

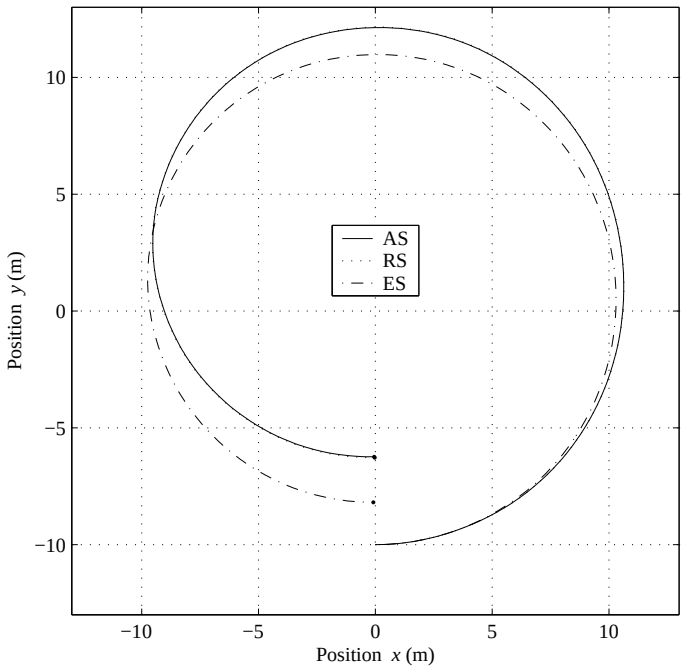

Figure 6.16: **Accumulated PER of AS, RS and ES vehicles at $R = 10$ m.**

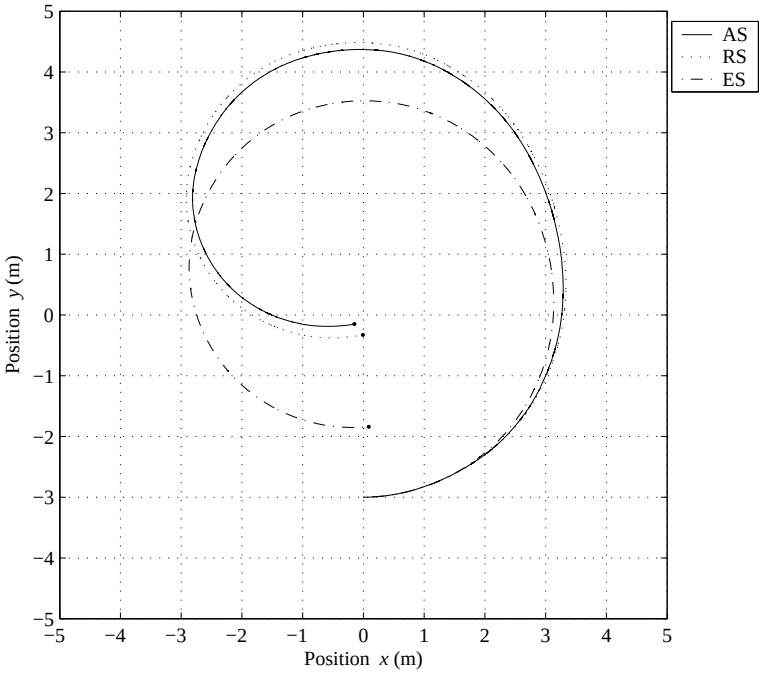

Figure 6.17: **Accumulated PER of AS, RS and ES vehicles at $R = 3$ m and $V = 4$ m/s.**

Figure 6.17 shows the accumulated error for a turn 3 m at vehicle velocity $V = 4$ m/s. As it is expected the accumulated error in the positioning estimation of the ES vehicle is smaller than the error of the AS and RS vehicles by a factor superior to 50 %; whereas the AS error and RS error are similar. Therefore, the results in the analysis the vehicle positioning should be taken into account at the selection of the locomotion configuration.

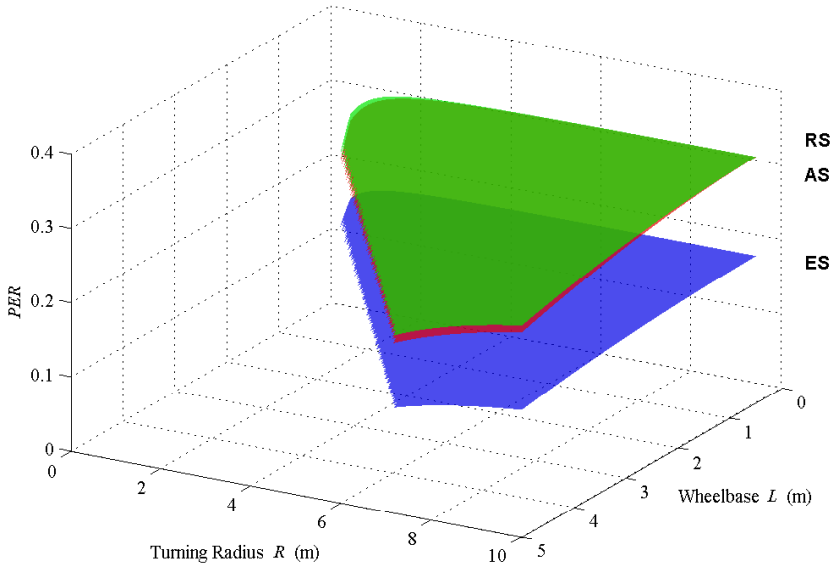

Figure 6.18: **PER comparison of Ackermann, Articulated and Explicit steering:** $k_\alpha =$ **66.19** % **and** $k_\beta =$ **16.62** %**.**

6.1.5 Discussion and Comparison

The error of vehicle positioning has been estimated for Ackermann, Articulated, and Explicit independent vehicles. The error is calculated as ratio between an ideal and a slip turning radius. The ratio of these vehicles, in the context of same conditions, addresses the following comparisons:

1. The results show an advantage for the ES vehicles to minimize the error of the vehicle positioning. The ES ratio presents an improvement superior to 60 % in comparison with the AS and RS ratios (as seen in Figure 6.18 and Figure 6.19). Therefore, it can be expected a better accuracy for the vehicle positioning estimation through the dead-reckoning.

2. The AS and RS vehicles present similar ratios. A 10 % improvement margin is presented by AS vehicle compared with RS ratio at small turning radius; whereas this improvement trends to be negligible at large turning radius, where the AS and RS vehicle produce equal ratios. Therefore, it can be expected comparable accuracy for vehicle positioning estimation between Ackermann and Articulated vehicle.

3. The results in the three steering mechanisms present a tendency to minimize the ratio when the wheelbase is increased; although this advance is negligible when the turning radius is increased. Therefore, it can be expected an improvement that is proportional to relation $\frac{L}{R}$.

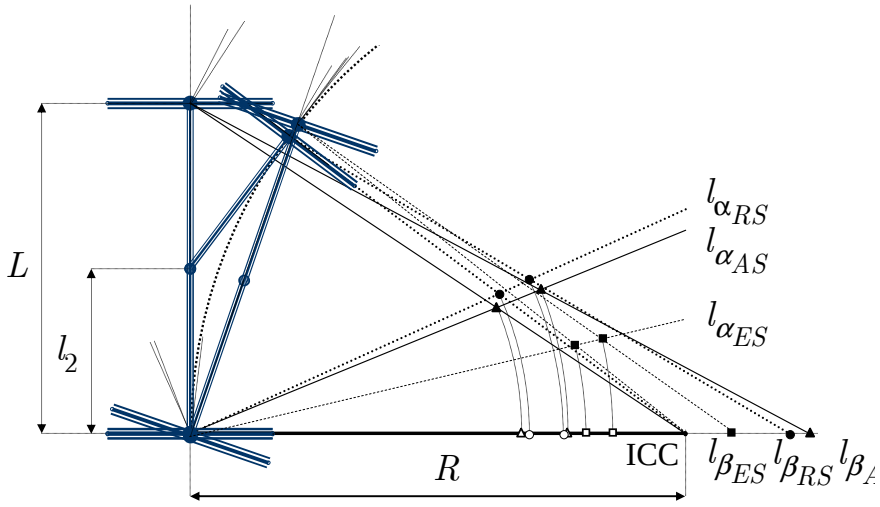

Figure 6.19: **Geometric positioning error comparison for Ackermann, Articulated and Explicit vehicles. The slip effect is represented by perpendicular lines to the slip angles ($l_{\alpha_{AS}}$, $l_{\alpha_{RS}}$, $l_{\alpha_{ES}}$, $l_{\beta_{AS}}$, $l_{\beta_{RS}}$ and $l_{\beta_{ES}}$). The intersection of these lines for AS (△), RS (○), and ES(◇) represents a new instantaneous center of curvature and its projection on the ideal radius shows the difference.**

It has to be noted that the ES vehicle requires minor steering angle γ to perform a specific turning radius in comparison with AS and RS vehicles; however, the behavior also is maintained when these vehicles are compared to perform a specific steering angle γ, as shown in Figure 6.20. Therefore, it may be argued that this advantage is correlated to the relation $\frac{L}{R}$ and the number of degrees of freedom required to steer the vehicle, which is captured in the kinematic model. The ES vehicle, actuating as a double Ackermann steering, is considered with a rear steering angle and a front steering angle (2 DOF's); whereas the both vehicles AS and RS consist of only one degrees of freedom to steer the vehicle.

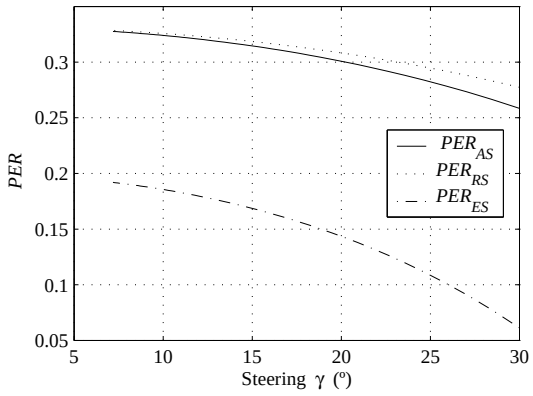

Figure 6.20: **Positioning error ratio for Ackermann, Articulatedd and Explicit steering while turning a specific steering angle γ at k_α = 66.19 % and k_β = 16.62 %.**

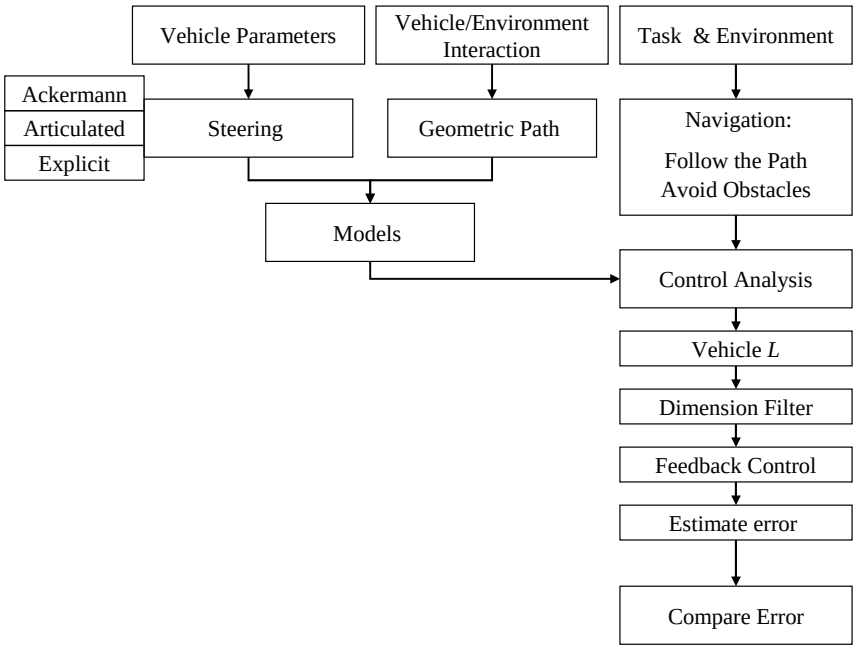

Figure 6.21: **Control analysis for steering kinematics.**

6.2 Steering Kinematics and Control

The key issue of the autonomous navigation performance is to follow a path while regarding safety requirements (avoid obstacles). It is to control the vehicle motion in terms of the path, which may be specified as a series of way-points linked by lines or smooth splines. The path incorporates the geometric constraints of the environment, whereas the controller converts ideal plans into actual motion execution, inputs variables for motion are derived from vehicle kinematics, through a tracking criterion. Thus, in the synthesis process is essential to investigate the steering kinematics that minimizes the tracking error. Figure 6.21 shows the control analysis, in which a parametric comparison is investigated among the steering schemes and the tracking performance.

The analysis examines the three steering schemes: Ackermann Steering (AS), aRticulated Steering (RS), and Explicit independent Steering (ES) while following a path, which is based on the Geometric Description of the environment; in particular, path of constant curvature are considered. In the following, the error is the distance of vehicle from their orthogonal projections on the path. The error measurement is accomplished by means of a local frame, known as Frenet frame, moving along the path as a function of the curvilinear abscissa. Two different Frenet frames are used on the midpoints of both axles of the vehicles as discussed by Altafini [Altafini 99], to investigate the tracking error around the path assuming a stable control. Local asymptotic stability to path is achieved by means of a conventional linear-state feedback, in the context of similar and minimal control for the steering schemes.

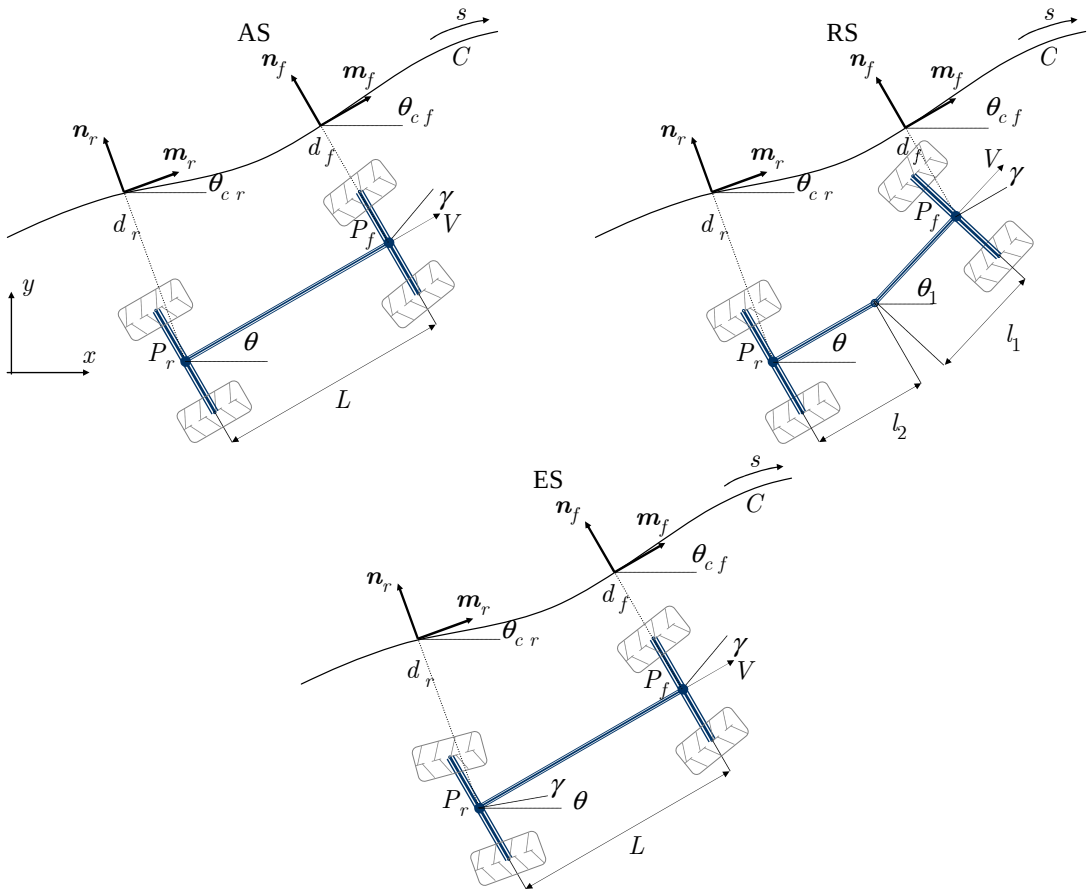

Figure 6.22: **Path coordinates for the steering kinematics.**

6.2.1 Modelling path coordinate

This analysis concerns only with the geometric displacement of the vehicle in the environment, where the vehicle must follow the path in terms of the arc length along the environment while avoiding obstacles. With reference to Figure 6.22, the kinematic models to describe the motion of two points (P_r and P_f) relative to the curve (C) are derived.

Two Frenet frames moving on the curve correspond to the orthogonal projections on c of the both point P_r and P_f, where each frame is represented by the unitary vectors $\mathbf{n}$ and $\mathbf{m}$ (normal and tangent to the oriented curve). Let d_r and d_f be the distance between the axle midpoints and the path (origin of each Frenet frame) respectively. Denote by θ_{cr} and θ_{cf} the angles between the current tangent to the path and the x axis of the fixed frame, and $s \rightarrow [0, 1]$ is the curvilinear abscissa of the curve C. The curvature along the path is defined as

$$c(s) = \frac{\dot{\theta}_c}{\dot{s}}$$

Assuming that $c(\cdot)\,\epsilon\,C^1$ and that the path satisfies some technical conditions, discussed by Samson [Samson 95]. The without slip kinematic models of the steering schemes of Table 6.1 are expressed in terms of the path coordinates $q_p = (s, d, \theta_p, \gamma)$:

$$\begin{pmatrix} \dot{s} \\ \dot{d} \\ 0 \end{pmatrix} = \mathbf{R} \begin{pmatrix} \dot{x} \\ \dot{y} \\ 0 \end{pmatrix} + \begin{pmatrix} c(s)\, d\, \dot{s} \\ 0 \\ 0 \end{pmatrix}$$

where $\theta_p = \theta - \theta_c$ is the relative orientation angle between the vehicle and the tangent to the path. $\mathbf{R}$ denotes the transfer rotation matrix from the fixed frame to the Frenet frame,

$$\mathbf{R} = \begin{pmatrix} cos\theta_c & sin\theta_c & 0 \\ -sin\theta_c & cos\theta_c & 0 \\ 0 & 0 & 1 \end{pmatrix}$$

and thus, the path coordinates $\mathbf{q_{pAS}}$ for the Ackermann steering is given by

$$\dot{\mathbf{q}}_{\mathbf{pAS}} = \begin{bmatrix} \dot{s_f} \\ \dot{s_r} \\ \dot{d_f} \\ \dot{d_r} \\ \dot{\theta_{pf}} \\ \dot{\theta_{pr}} \\ \dot{\gamma} \end{bmatrix} = \begin{bmatrix} \frac{cos\,\theta_{pf}}{cos\,\gamma\,[1 - d_f\,c(s_f)]} \\ \frac{cos\,\theta_{pr}}{[1 - d_r\,c(s_r)]} \\ \frac{sin\,\theta_{pf}}{cos\,\gamma} \\ sin\,\theta_{pr} \\ \frac{sin\,\gamma}{L\,cos\,\gamma} - \frac{cos\,\theta_{pf}\,c(s_f)}{cos\,\gamma\,[1 - d_f\,c(s_f)]} \\ \frac{sin\,\gamma}{L\,cos\,\gamma} - \frac{cos\,\theta_{pr}\,c(s_r)}{[1 - d_r\,c(s_r)]} \\ 0 \end{bmatrix} v_1 + \begin{bmatrix} 0 \\ 0 \\ 0 \\ 0 \\ 1 \\ 0 \\ 1 \end{bmatrix} v_2 \tag{6.4}$$

whereas the path coordinates $\mathbf{q_{pRS}}$ for the Articulated steering is given as:

$$\begin{aligned} \dot{\mathbf{q}}_{\mathbf{pRS}} = \begin{bmatrix} \dot{s_f} \\ \dot{s_r} \\ \dot{d_f} \\ \dot{d_r} \\ \dot{\theta_{pf}} \\ \dot{\theta_{pr}} \\ \dot{\gamma} \end{bmatrix} &= \begin{bmatrix} \frac{l_2 + l_1\,cos\,\gamma}{l_1 + l_2\,cos\,\gamma}\,\frac{cos\,\theta_{pf}}{[1 - d_f\,c(s_f)]} \\ \frac{cos\,\theta_{pr}}{[1 - d_r\,c(s_r)]} \\ \frac{l_2 + l_1\,cos\,\gamma}{l_1 + l_2\,cos\,\gamma}\,sin\,\theta_{pf} \\ sin\,\theta_{pr} \\ \frac{sin\,\gamma}{l_1 + l_2\,cos\,\gamma} - \frac{l_2 + l_1\,cos\,\gamma}{l_1 + l_2\,cos\,\gamma}\,\frac{cos\,\theta_{pf}\,c(s_f)}{[1 - d_f\,c(s_f)]} \\ \frac{sin\,\gamma}{l_1 + l_2\,cos\,\gamma} - \frac{cos\,\theta_{pr}\,c(s_r)}{[1 - d_r\,c(s_r)]} \\ 0 \end{bmatrix} v_1 \\ &+ \begin{bmatrix} \frac{l_2\,l_1\,sin\,\gamma}{l_1 + l_2\,cos\,\gamma}\,\frac{cos\,\theta_{pf}}{[1 - d_f\,c(s_f)]} \\ 0 \\ \frac{l_2\,l_1\,sin\,\gamma\,sin\,\theta_{pf}}{l_1 + l_2\,cos\,\gamma} \\ 0 \\ \frac{l_2\,cos\,\gamma}{l_1 + l_2\,cos\,\gamma} + \frac{l_2\,l_1\,sin\,\gamma}{l_1 + l_2\,cos\,\gamma}\,\frac{cos\,\theta_{pf}\,c(s_f)}{[1 - d_f\,c(s_f)]} \\ \frac{l_2}{l_1 + l_2\,cos\,\gamma} \\ 1 \end{bmatrix} v_2 \end{aligned} \tag{6.5}$$

and the path coordinates $\mathbf{q_{pES}}$ for the Explicit steering is given as:

$$\dot{\mathbf{q}}_{\mathbf{pES}} = \begin{bmatrix} \dot{s_f} \\ \dot{s_r} \\ \dot{d_f} \\ \dot{d_r} \\ \dot{\theta_{pf}} \\ \dot{\theta_{pr}} \\ \dot{\gamma} \end{bmatrix} = \begin{bmatrix} \frac{cos\,(\theta_{pf}+\gamma)}{[1-d_f\,c(s_f)]} \\ \frac{cos\,(\theta_{pr}-\gamma)}{[1-d_r\,c(s_r)]} \\ sin\,(\theta_{pf}+\gamma) \\ sin\,(\theta_{pr}-\gamma) \\ \frac{sin\,2\gamma}{L\,cos\,\gamma} - \frac{cos\,(\theta_{pf}+\gamma)\,c(s_f)}{[1-d_f\,c(s_f)]} \\ \frac{sin\,2\gamma}{L\,cos\,\gamma} - \frac{cos\,(\theta_{pr}-\gamma)\,c(s_r)}{[1-d_r\,c(s_r)]} \\ 0 \end{bmatrix} v_1 + \begin{bmatrix} 0 \\ 0 \\ 0 \\ 0 \\ 0 \\ 0 \\ 1 \end{bmatrix} v_2 \tag{6.6}$$

where v_1 is the vehicle velocity V and v_2 is the steer velocity $\dot{\gamma}$. These previous equation systems may be rewritten as:

$$\dot{\mathbf{q}}_{\mathbf{pAS}} = \mathcal{A}(\mathbf{q}_{\mathbf{pAS}}) + \mathcal{B}(\mathbf{q}_{\mathbf{pAS}})\, v_2 \tag{6.7}$$

$$\dot{\mathbf{q}}_{\mathbf{pRS}} = \mathcal{A}(\mathbf{q}_{\mathbf{pRS}}) + \mathcal{B}(\mathbf{q}_{\mathbf{pRS}})\, v_2 \tag{6.8}$$

$$\dot{\mathbf{q}}_{\mathbf{pES}} = \mathcal{A}(\mathbf{q}_{\mathbf{pES}}) + \mathcal{B}(\mathbf{q}_{\mathbf{pES}})\, v_2 \tag{6.9}$$

The above systems are nonlinear; however, these systems can be locally asymptotically stabilized to a path of constant curvature by means of the Lyapunov linearization method, how was proven for an Articulated vehicle by Altafini [Altafini 99]: for a path of constant curvature C, the equilibrium point $\mathbf{q_{pe}}$ is calculated from the geometry between the vehicle and the path. The control objective consists in regulating the lateral distances or errors d_f and d_r and the relative orientation angles θ_{pf} and θ_{pr} to zero. The solution consists in choosing an appropriate gain K for the closed-loop state matrix $\mathbf{A} - v_1\, K\, \mathbf{B}$, i.e. if all eigenvalues have negative real parts. Where the Jacobian matrix has the form:

$$\mathbf{A} = \left.\frac{\partial \mathcal{A}}{\partial \mathbf{q_p}}\right|_{\mathbf{q_p}=\mathbf{q_{pe}}}$$

and

$$\mathbf{B} \stackrel{\triangle}{=} \mathcal{B}(\mathbf{q_{pe}})$$

The tracking errors, composing by the lateral displacements and the relative orientation angles of both points from the path, are then simulated to compare the three steering schemes for a given task; in particular, following a line-arc-line path at steady state. A path that may be found in a wide range of possible Autonomous Vehicle applications, such as the corridors in the underground mining: the walls limit the workspace and the tunnels are connected by tight corners. Figure 6.23 depicts the geometric constraint of an underground mining environment.

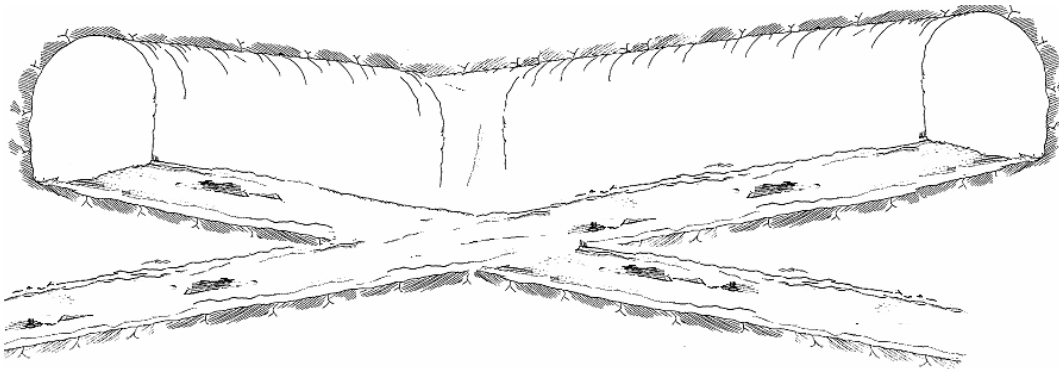

Figure 6.23: **Tunnel interconnection for an underground mining environment.**

A previous analysis serves as physical filter to reduce the vehicle dimension space to simplify the control analysis. The filtering process begins by avoiding obstacles, in particular the walls of the environment while turning at a unique steering command, i.e. steering angle γ is constant. There is a parametric variation of both length and width of the vehicle, recognizing the set of vehicle candidates to perform the task. Only successful vehicle dimensions need to be considered by the following path test. The filter is derived from the task requirements and the environment constraints: the tunnel width is 3.5 m, considering the middle of the tunnel as the initial position (*start*) before to turn. Figure 6.24 depicts the geometry of the vehicle and the environment. The steering γ is permitted to up 35°; whereas the range of dimensions are from 1.0 m to 3.5 m for the length and width of the vehicle.

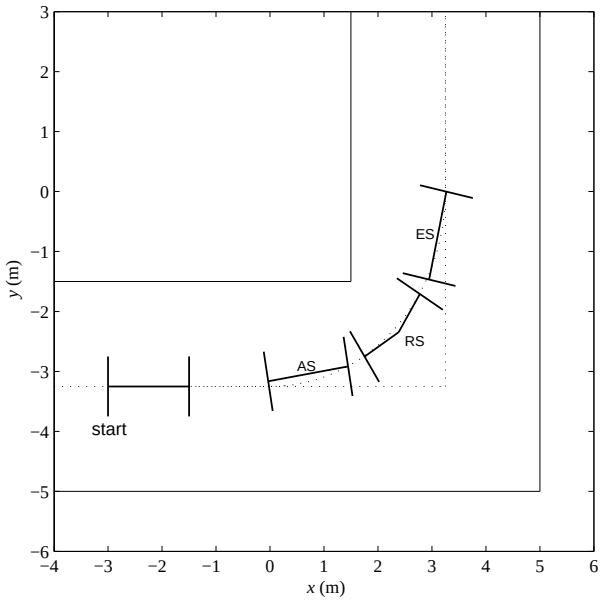

Figure 6.24: **Vehicles avoid obstacles.**

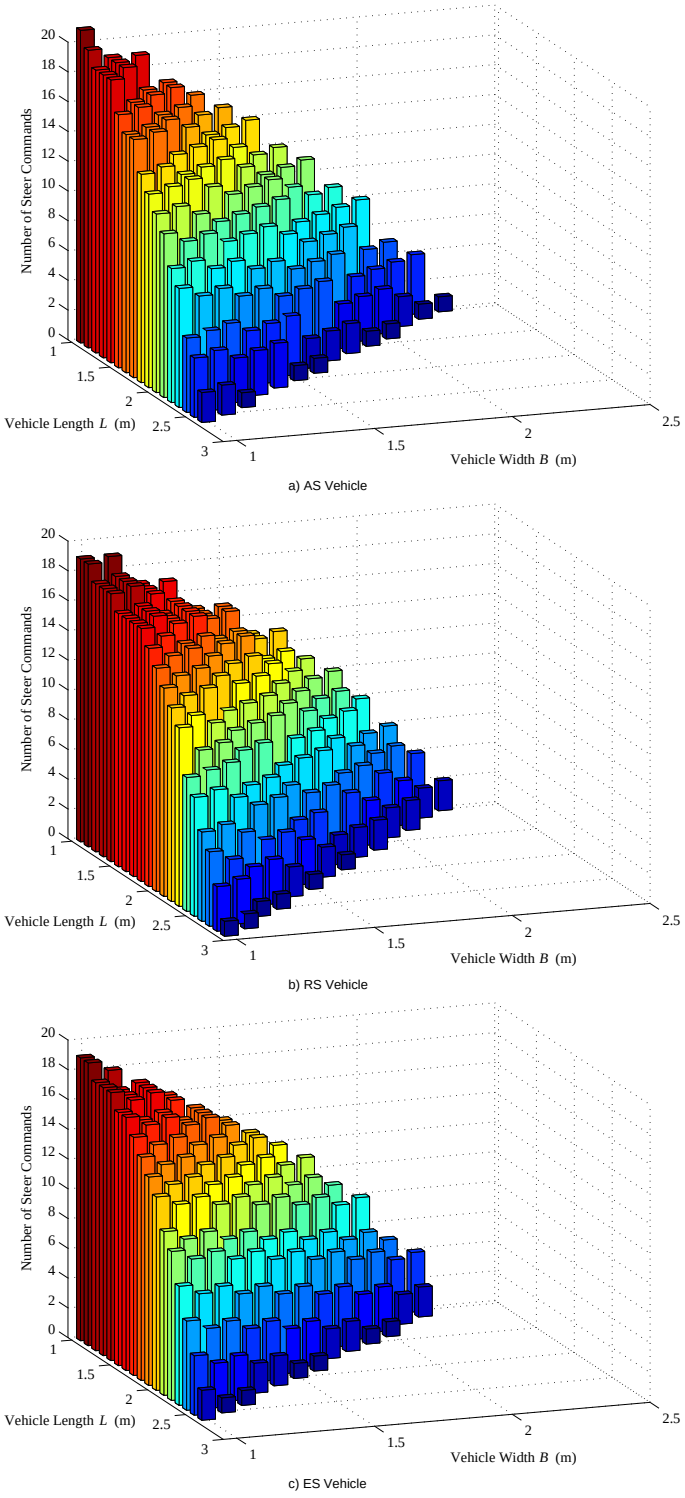

Figure 6.25: **Vehicle dimensions that avoid obstacles while turning at steady state.**

The results of the filter are shown in Figures 6.25-6.26, in terms of the number of

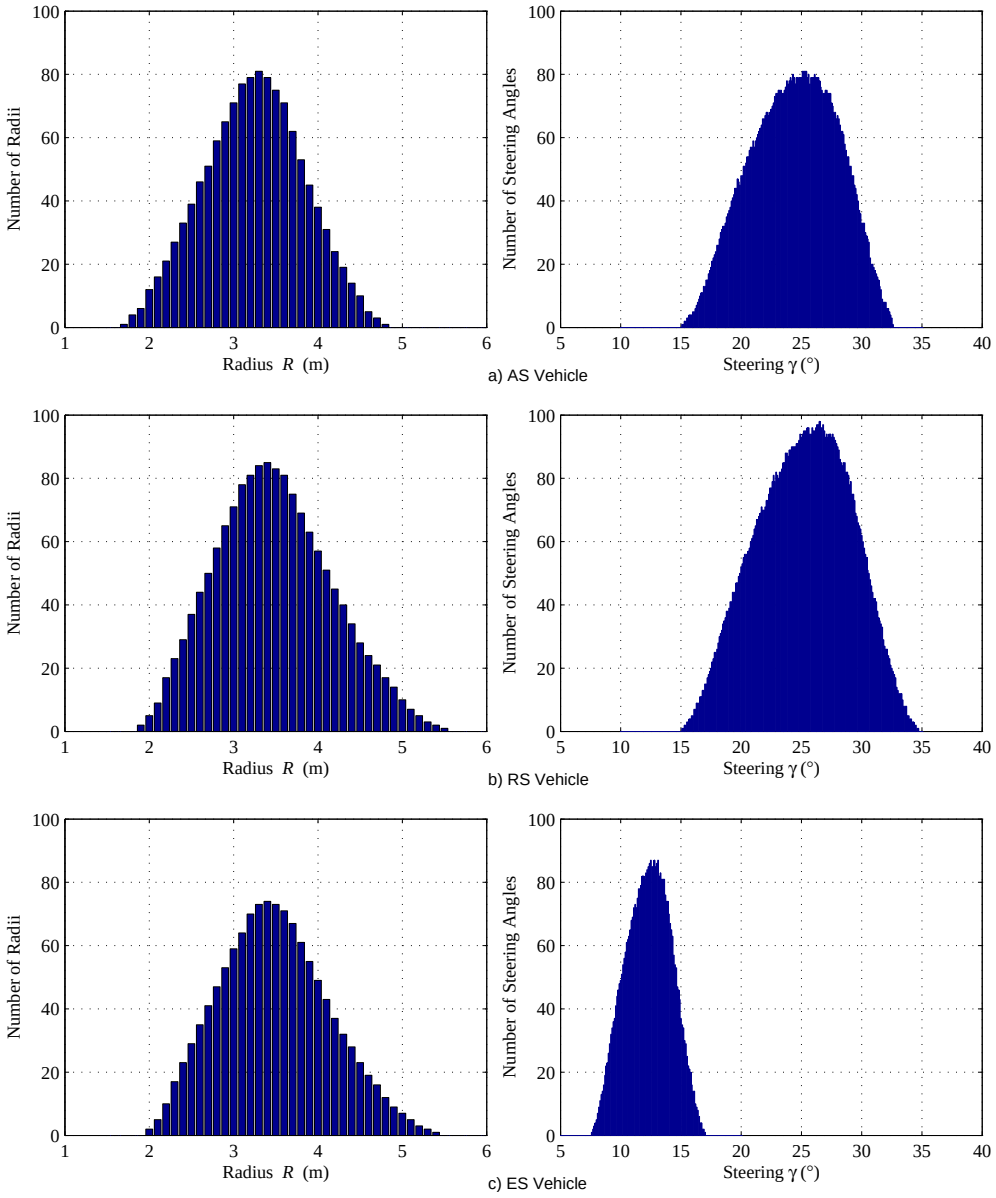

Figure 6.26: **Radius and steering histograms for the AS, RS, and ES vehicles.**

steer commands that represents the frequency of successful steering angles to turn avoiding the walls at the particular dimensions, vehicle length L and vehicle width B respectively. The histograms show the number of radii and steering angles γ for every successful vehicle. The results lead to following observations. The RS scheme allows the largest vehicle, since the vehicle can reach up to 3 m long; whereas the AS and ES reach about 2.5 m long. The lesser dimensions have the greater number of successful instantiations, which the AS schemes presents the greater number of steer commands. Besides, the ES scheme needs the lowest steering range to fill the same radius range as the AS and RS schemes.

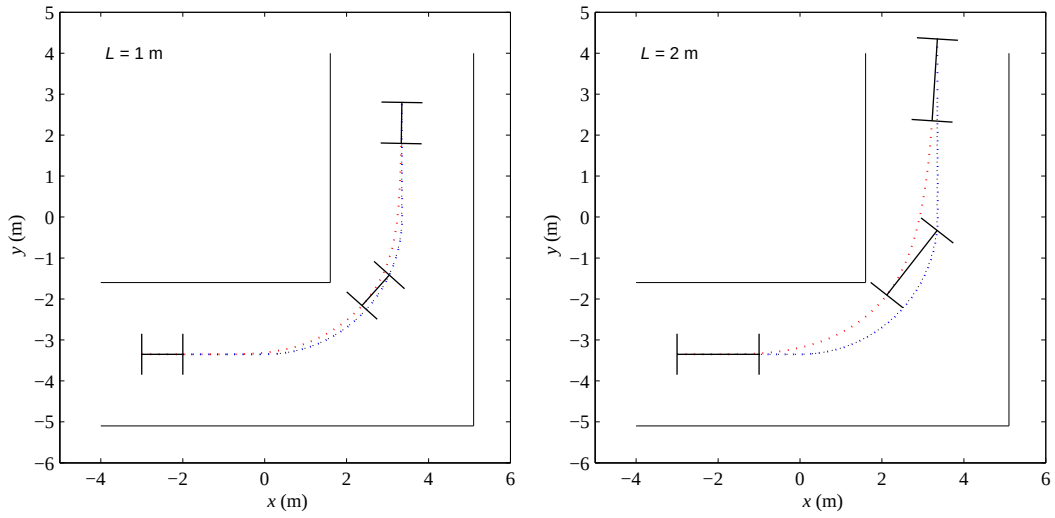

Figure 6.27: **Tracking a line-arc-line path with linear state feedback:** $v_1 = 1$ **m/s, and curvature** $c = 1/3.35$ **for both AS vehicles** $L = 1$ **m and** $L = 2$ **m.**

6.2.2 Control analysis for Ackermann steering

The tracking errors are computed for the AS vehicle to investigate the relation between vehicle configuration and control, using the aforementioned linear-state feedback while following a path. With respect to the previous results, the range of the allowable vehicle length is between 1 m and 2 m, with a vehicle width at 1 m. The path consists of a straight line, an arc of a circle, and a straight line. The radius of the circle arc is 3.35 m as the average of the maximum allowable radius, i.e. a constant curvature $c = \frac{1}{3.35}$. For the following purpose, the translational velocity v_1 of the vehicle is considered as a constant value (an open-loop).

Figure 6.27 shows the performance for the path tracking with a linear state feedback control. The obtained results are shown in Figure 6.28, in terms of both the tracking errors d_f and d_r and the heading errors θ_{pf} and θ_{pr}, with respect to the steering angle γ and the control input v_2 ($\dot{\gamma}$). Referring to these results several observations are made:

- The vehicle dimension $L = 2$ m produces a bigger tracking error than the lower vehicle $L = 1$ m. It can be observed in the plotted error for the rear axle midpoints (d_r), and interpreted as an upper area to turn, the off-tracking bounds between the rear and the front trajectories. The off-tracking increases in the transition from the straight line to the circle arc, and it decreases on the transition from the circle arc to the straight line. There is a proportional behavior to relation between the curvature and the vehicle length cL for the maximum off-tracking.

- A similar behavior can be observed for the heading errors (θ_{pr}), the bigger dimension produces a bigger error than the error produced by the smaller vehicle.

- The bigger configuration has a slower convergence, the control simulation follows

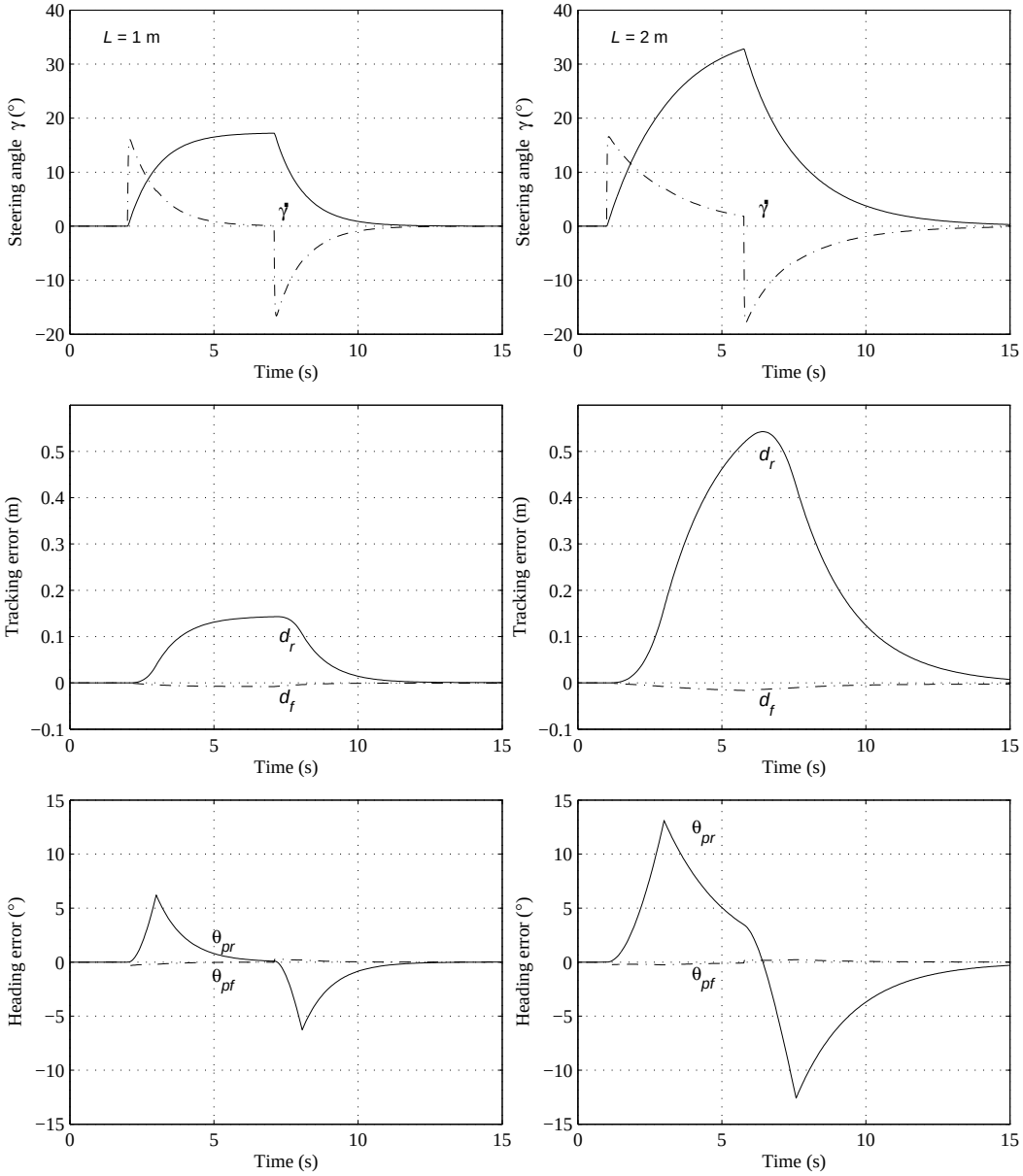

Figure 6.28: **Errors of tracking and heading for the AS vehicles: d_f, d_r, θ_{pf} and θ_{pr}, for both vehicles $L = 1$ m and $L = 2$ m, respectively.**

the given path, than the lower configuration. It can be observed in the plotted for the state of the steering angle γ, which steps-up and decays faster for the smaller vehicle. It becomes a steady state behavior with $\dot{\gamma}$ constant (approximately zero) for the following of both the straight lines and of the circle arc, beyond the transitions: line-arc and arc-line.

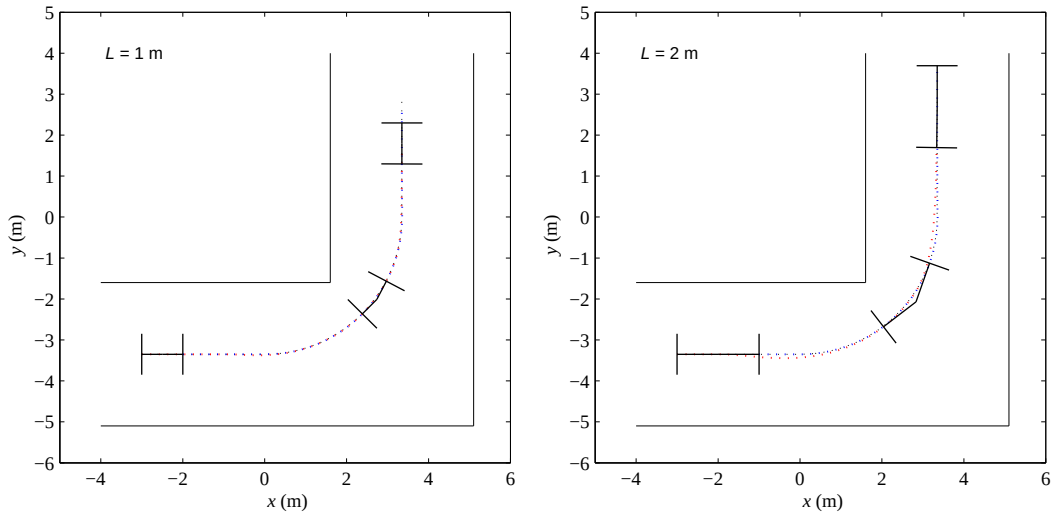

Figure 6.29: **Tracking a line-arc-line path with linear state feedback:** $v_1 = 1$ **m/s, and curvature** $c = 1/3.35$ **for both RS vehicles** $L = 1$ **m and** $L = 2$ **m.**

6.2.3 Control analysis for Articulated steering

The tracking errors are computed for the RS vehicle to investigate the relation between vehicle configuration and control, using the aforementioned linear-state feedback while following a path. As in the AS vehicle case, two vehicle lengths are simulated ($L = 1$ m and $L = 2$ m). The path is a line-arc-line, with the arc of a circle of radius 3.35 m, i.e. a curvature $c = \frac{1}{3.35}$. In this analysis, there is a length ratio $r = 1$, thus $l_1 = l_2$ in both vehicles.

Figure 6.29 shows the performance for the path tracking with a linear state feedback control. The obtained results are shown in Figure 6.30, in terms of both the tracking errors d_f and d_r and the heading errors θ_{pf} and θ_{pr}, with respect to the steering angle γ and the control input v_2 ($\dot{\gamma}$). These results lead to the following observations:

- The upper dimension $L = 2$ m produces a bigger tracking error than the lower vehicle $L = 1$ m. It can be observed in the plotted error for the rear axle midpoints (d_r). In particular, the off-tracking is approximately zero for the smaller vehicle, having minimum values on the transitions: line-arc and arc-line. However, there is a proportional behavior to relation between the curvature and the vehicle length cL for the maximum off-tracking.

- A similar behavior can be observed for the heading errors (θ_{pr}), the bigger dimension produces a bigger error than the error produced by the smaller vehicle.

- The bigger configuration has a slower convergence than the lower vehicle. It can be observed in the plotted for the state of the steering angles γ for both vehicles; furthermore, the lower RS vehicle presents a more explicit steady state behavior than the smaller AS vehicle.

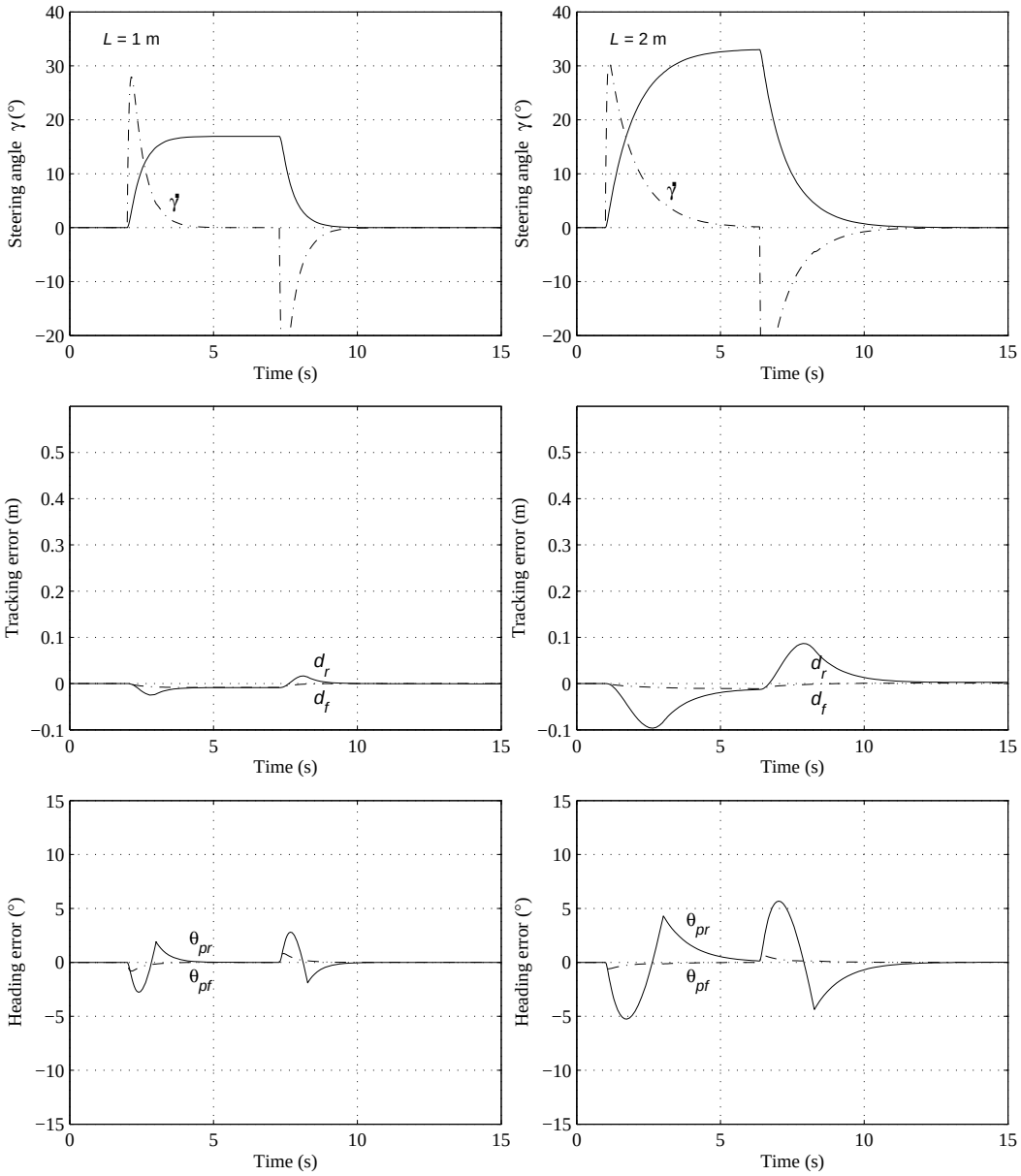

Figure 6.30: **Errors of tracking and heading for the RS vehicles: d_f, d_r, θ_{pf} and θ_{pr}, for both vehicles L = 1m and L = 2m.**

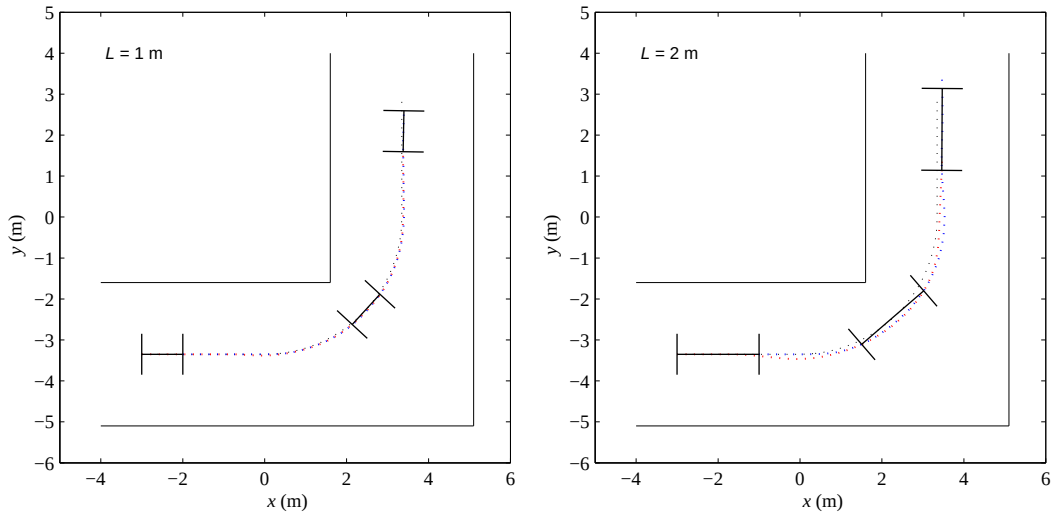

Figure 6.31: **Tracking a line-arc-line path with linear state feedback:** $v_1 = 1$ **m/s, and curvature** $c = 1/3.35$ **for both ES vehicles** $L = 1$ **m and** $L = 2$ **m.**

6.2.4 Control analysis for Explicit steering

The tracking errors are computed for the ES vehicle to investigate the relation between vehicle configuration and control, using the aforementioned linear-state feedback while following a path as in the AS and RS vehicles. Two vehicle lengths are simulated (L = 1 m and L = 2 m). The path is a line-arc-line, with a curvature $c = \frac{1}{3.35}$.

Figure 6.31 shows the performance for the path tracking with a linear state feedback control. The obtained results are shown in Figure 6.32, in terms of both the tracking errors d_f and d_r and the heading errors θ_{pf} and θ_{pr}, with respect to the steering angle γ and the control input v_2 ($\dot{\gamma}$). Referring to these results several observations are made:

- Although the off-trackings are lesser than AS vehicle, the errors present an oscillatory behavior that tends to increase. The upper wheelbase $L = 2$ m produces a bigger tracking error than the smaller vehicle $L = 1$ m, as shown in the plotted error for the rear axle midpoints (d_r).

- An instable behavior can be observed for the heading errors (θ_{pr}), the bigger dimension produces a bigger error than the error produced by the smaller vehicle.

- The bigger configuration has a slower convergence than the smaller vehicle. It can be observed in the plotted for the state of the steering angles γ for both vehicles. A particular control strategy must be derived, possible by an exact feedback linearization as the Lyapunov second method.

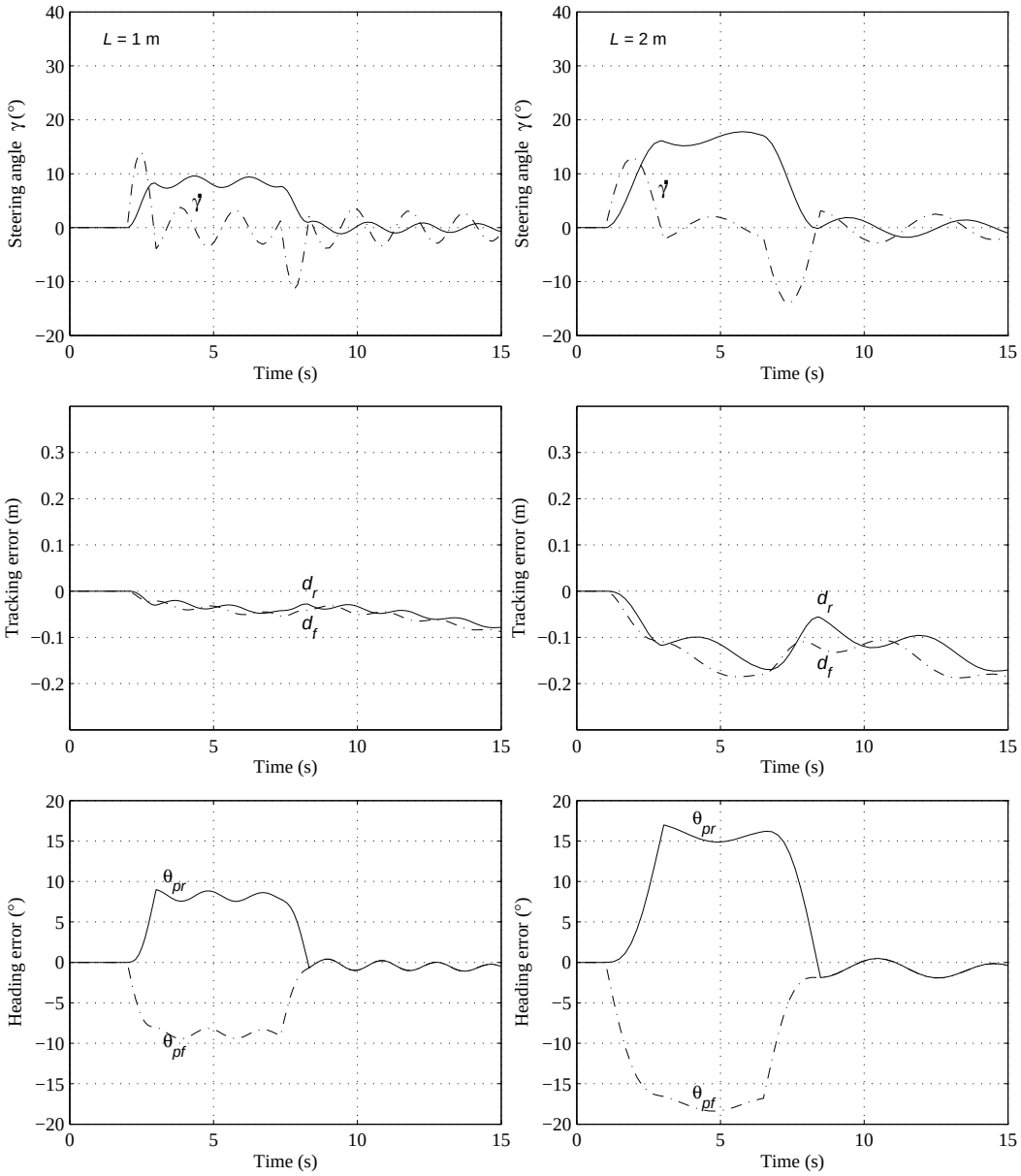

Figure 6.32: **Errors of tracking and heading for the ES vehicles: d_f, d_r, θ_{pf} and θ_{pr}, for both vehicles L = 1m and L = 2m.**

6.2.5 Discussion and Comparison

The tracking error and heading error of vehicle control has been estimated for the Ackermann, Articulated, and Explicit vehicles. The errors are calculated in the following of a given path: line-arc-line with linear state feedback. The errors of these vehicles, in the context of same conditions, address the following comparisons:

1. The results show an advantage for the RS vehicles to minimize the errors of the tracking and heading. The RS vehicles present an improvement superior to follow a line-arc-line path in comparison with the AS and ES schemes. The tracking error may be considered approximately zero for a length ratio $r = 1$, where $l_1 = l_2$. Therefore, it can be expected a better accuracy for the vehicle control, which should impact the estimation of the vehicle positioning through the dead-reckoning.

2. The AS vehicles present an off-tracking, which may be a disadvantage for possible applications in confined environments. However, this off-tacking tends to decrease as a function to the relation between the curvature and the vehicle length cL. Therefore, it can be expected comparable accuracy for vehicle control for relations $L \ll R$, where $c = \frac{1}{R}$.

3. The results in the three steering mechanisms present a tendency to minimize the errors when the wheelbase L decreases; although this advance is negligible when the circle radius of the curvature R is increased. Therefore, it can be expected a improvement that is a proportional function to relation $\frac{L}{R}$.

It has to be noted that the RS vehicle requires a minor area to perform a specific turning radius in comparison with AS and RS vehicles; which converts an Articulated vehicle more deployed in confined environments such as the underground mining. Furthermore, it may be argued that this advantage is correlated to the relation $\frac{L}{R}$ and the number of degrees of freedom required to steer the vehicle, which is captured in the kinematic model.

The ES vehicle, actuating as a double Ackermann steering, is considered to be provided with a rear steering angle and a front steering angle; whereas the both vehicles AS and RS consist of only one degrees of freedom to steer the vehicle. Therefore, the ES schemes requests a particular control strategy for achieving a given path and improving the vehicle performance, such as a Lyapunov-oriented approach.

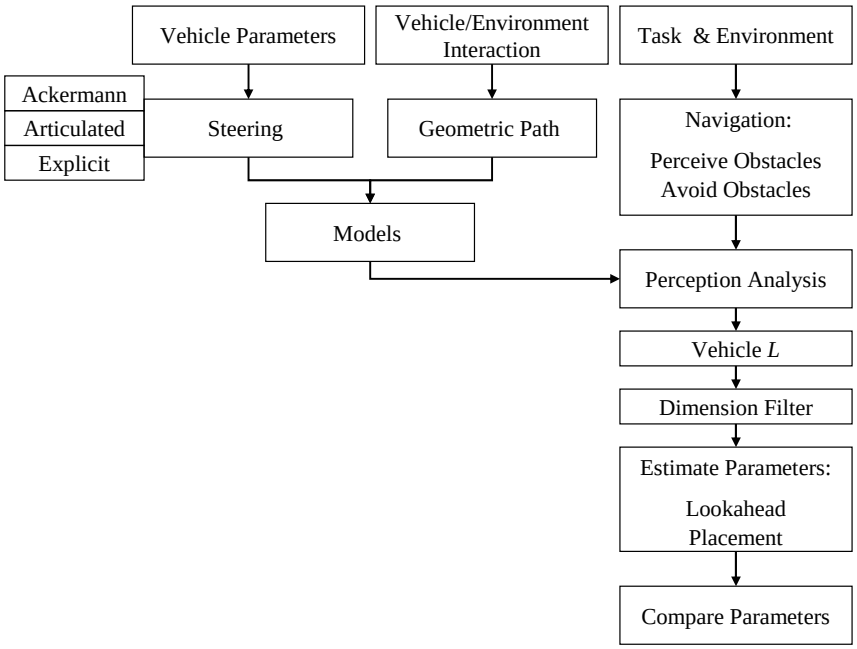

Figure 6.33: **Perception analysis for steering kinematics.**

6.3 Steering Kinematics and Perception

The key issue of the autonomous navigation performance is to perceive and avoid obstacles together with the position estimation and the control, while performing a given task in a particular environment. This involves information from sensors regarding of the surrounding environment, by allowing the control of the vehicle motions as reactive responses to avoid obstacles. A reactive behavior consists of predefined motions, such as panic stop or steady turning, which is based on sensor information and the kinematic vehicle model. Thus, in the synthesis process is essential to investigate the relation between the steering kinematics and the parameters of perception. Figure 6.33 depicts the perception analysis, in which a parametric comparison is investigated among the steering schemes and the perception parameters.

The analysis examines the three steering schemes: Ackermann Steering (AS), aRticulated Steering (RS), and Explicit independent Steering (ES) while following a maneuver to avoid obstacles: steady state turn, i.e. $\dot{\gamma} = 0$. This involves the physical parameters defining the vehicle performance and the perception parameters defining the performance of external sensors. In the perception analysis, a physical filter serves to reduce the vehicle dimension space to simplify the analysis, similar to the control section. Then, a parametric variation of both length and width of the vehicle is developed, following by an estimation of the perception parameters at different sensor placements, to investigate the relation between the vehicle steering configuration and perception requirements.

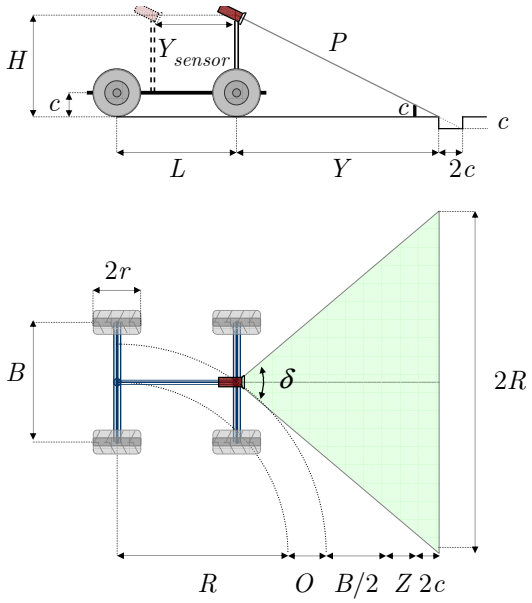

Figure 6.34: **Perception parameters to perceive positive and negative obstacles.**

Figure 6.34 shows the geometric relation between the physical parameters and perception parameters, since the physical parameters are composed by: the length of the vehicle L, the vehicle width B, R denoting the radius to avoid the obstacles; whereas the wheel radius r, and the required clearance c, defined as the height of undercarriage above the terrain. The perception parameters are defined by: the height of the sensor H, the lookahead distance Y, which includes the offset placement of the sensor Y_{sensor}, the angle of the field of view δ, and the measured range P.

The kinds of maneuvers, as minimal abilities, are stop and turning to allow avoiding the obstacles. This perception analysis considers that the vehicle actions respond immediately once the surrounding is perceived, which involves the time of response $T_{response}$ from the time to take the sensor information, the generation of commands, to the time of the actuator response. Hence, the response distance D, the product of the vehicle velocity V and the time of response $T_{response}$, is assumed here approximately zero ($D = V\,T_{response} \approx 0$).

The field of view δ of the vehicle must have a sufficient effective range to sense objects within an area, and to avoid the tunnel vision constraint, discussed by [Kelly 98]. This area is not only on straight line navigation, but also it must consider while turning for avoiding the obstacles. For robots that can point turn is a simple function, such as holonomic vehicles: Explicit Steer; however, in this analysis the ES is analyzed as double Ackermann.

Therefore, the minimum effective field of view must sense obstacles within an area as double as the minimum radius or maximum steering angle γ, according to [Wagner 02];

this perception parameter leads to the following expression:

$$\delta = 2\,atan\left(\frac{R}{P}\right) = 2\,atan\left(\frac{R}{\sqrt{H^2 + Y^2}}\right)$$

To perceive negative obstacles as a hole, the ratio, derived by [Kelly 98], of sensor height H to the lookahead distance Y has to satisfy,

$$\frac{H}{Y} = \frac{r}{2r} = \frac{1}{2}$$

since the minimum allowable value of the wheel radius is constrained for the environment conditions, considering in particular $c = r$, implicates c as the minimum height of positive obstacles, such as rocks. Furthermore, the lookahead distance Y is given as

$$Y = R + O + \frac{B}{2} + Z + 2\,c + Y_{sensor} - L$$

a function of the physical parameters and of the placement of the sensor Y_{sensor}, where Z denotes a zone of safety as a threshold that includes the chassis width and the wheel width, O is the off-tracking bound between the rear and the front trajectories while the vehicle turning by avoiding the obstacles. These equations allow estimate the perception parameters to perceive positive and negative obstacles. Then the perception parameters Y, H, and δ are estimated to compare the three steering schemes. Following a safety maneuver: the vehicle must turn to avoid the obstacles as in a wide range of possible Autonomous Vehicle applications. For instance in the underground mining, the walls represent positive obstacles, which is shown in Figure 6.35.

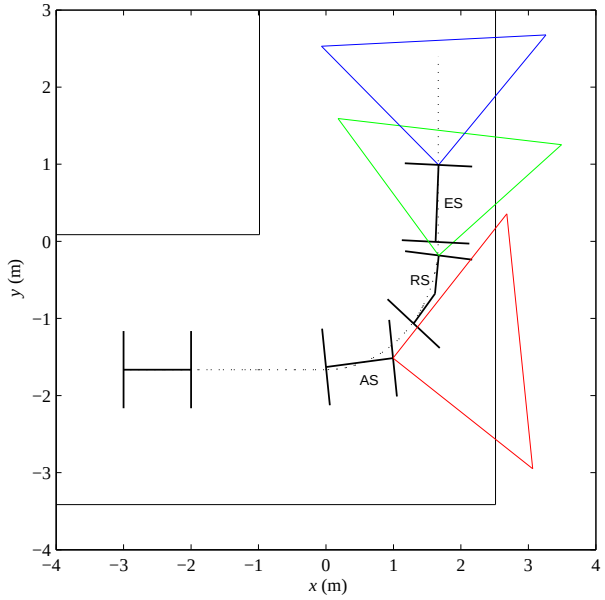

Figure 6.35: **Vehicles avoid walls: as positive obstacles.**

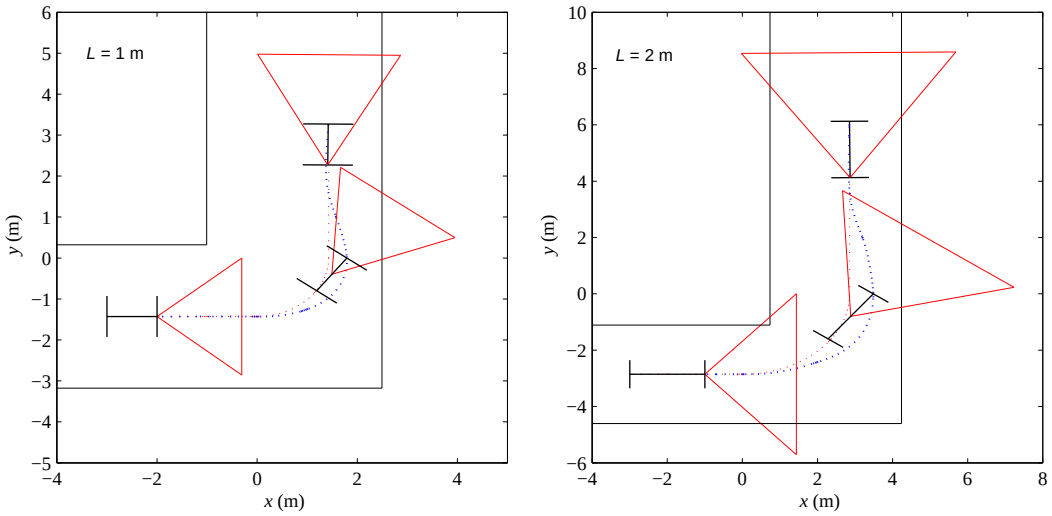

Figure 6.36: **Perception for the AS vehicles while avoiding walls: $L = 1$ m and $L = 2$ m at different placement Y_{sensor} (0, $L/2$, and L).**

6.3.1 Perception analysis for Ackermann steering

The perception parameters are computed for the AS vehicle to investigate the relation between vehicle configuration and perception, using the aforementioned equations. With respect to the previous results, the range of the allowable vehicle length is between 1 m and 2 m, with a vehicle width at 1 m, as is shown in Figure 6.36. The allowable steering angle γ is 35° as maximum; the safety zone Z is 0.25 m. Table 6.6 shows the results obtained and Figure 6.37 shows the trajectory of the field of view projected onto the lookahead distance Y, i.e. the maximum perception line onto the groundplane. Referring to these results several observations are made:

- An increment of the wheelbase L produces a increment of the perception parameters: Y, H, and δ. It is a function of both: the placement of the sensor Y_{sensor} and the off-tracking O generated by the AS vehicle.
- The effective angle δ of the field of view is smaller when the sensor placement is on the rear axle ($Y_{sensor} = L$). Nevertheless, the lookahead distance Y increases by this factor Y_{sensor} and thus the height to place the sensor increases.
- Since the sensor must see the distance P required without being obstructed by the vehicle parts or other components, the sensor placement on the front axle ($Y_{sensor} = 0$) presents a minor gap of this parameter. In particular the lower wheelbase has the smallest value.
- Considering a perception line onto the distance Y, the sensor is limited to see all terrain that the vehicle reaches in the maneuver to avoid the obstacles. This is the problem of tunnel vision which is smaller for the lower vehicle.

Y_{sensor} (m)	Wheelbase (m)			Perception Parameter
	$L = 1.00$	$L = 1.50$	$L = 2.00$	
0	1.69	2.07	2.44	Y (m)
$L/2$	2.19	2.82	3.44	
L	2.69	3.57	4.44	
0	0.85	1.03	1.22	H (m)
$L/2$	1.10	1.41	1.72	
L	1.35	1.78	2.22	
0	1.89	2.31	2.72	P (m)
$L/2$	2.45	3.15	3.84	
L	3.01	3.99	4.96	
0	74.05	85.71	92.71	$\delta(^\circ)$
$L/2$	60.43	68.48	73.25	
L	50.75	56.51	59.87	
Radius (m)	1.43	2.14	2.86	
Off-tracking (m)	0.31	0.47	0.63	

Table 6.6: **Perception Parameters for the AS vehicle: the lookahead distance Y, the height of the sensor H, the distance measured P, and the angle of the field of view δ, which are calculated from the offset placement of the sensor Y_{sensor}, and the steering angle $\gamma = 35^\circ$ for three different wheelbases L, respectively.**

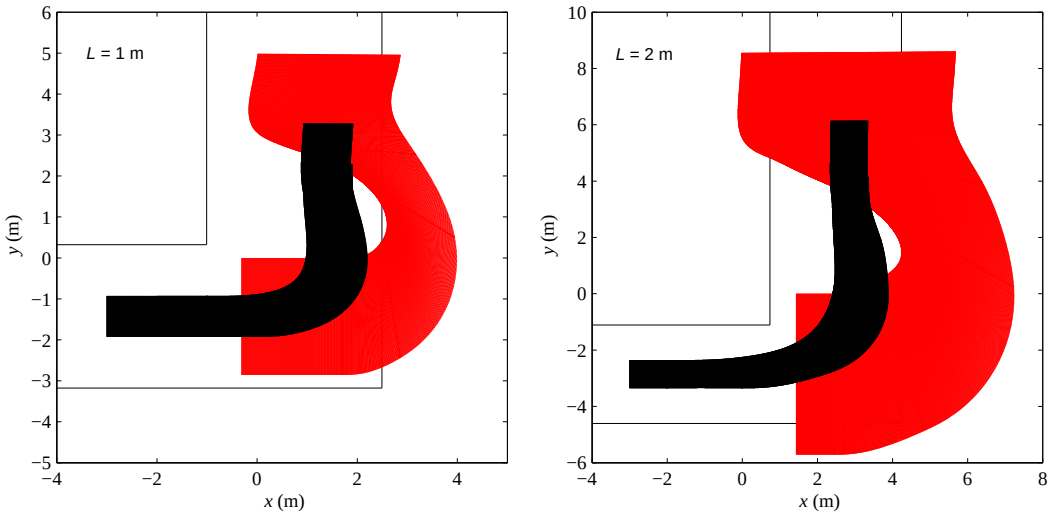

Figure 6.37: **Trajectories of AS vehicle (black) and the projected field of view onto a lookahead distance Y for: $L = 1$ m and $L = 2$ m at $Y_{sensor} = 0$.**

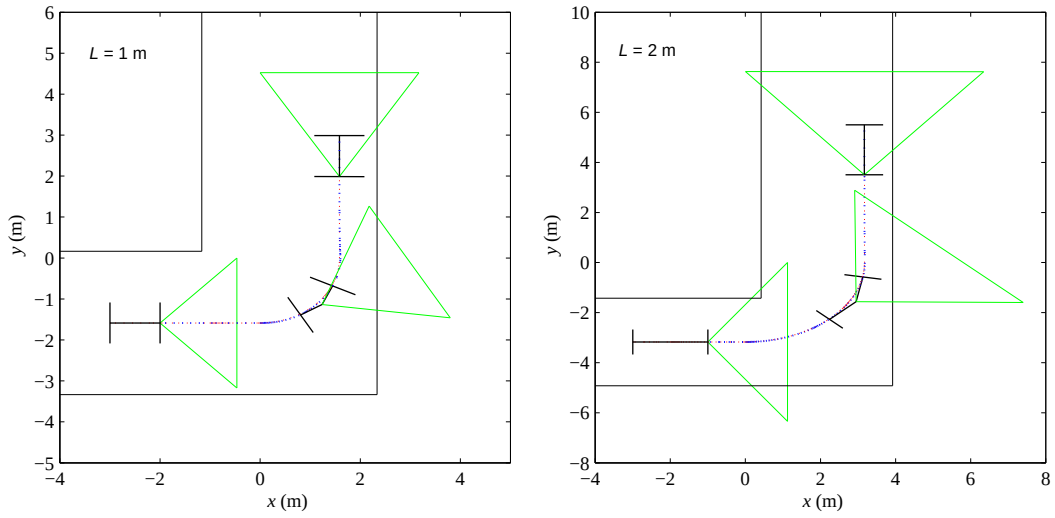

Figure 6.38: **Perception for the RS vehicles while avoiding walls: $L = 1$ m and $L = 2$ m at different placement Y_{sensor} (0, $L/2$, and L).**

6.3.2 Perception analysis for Articulated steering

The perception parameters are computed for the RS vehicle, to investigate the relation between vehicle configuration and perception, using the aforementioned equations and same values: the allowable steering angle γ is 35°, the safety zone Z is 0.25 m, and the range of the wheelbase is between 1 m and 2 m, as is shown in Figure 6.38. Table 6.7 shows the results obtained and Figure 6.39 shows the trajectory of the field of view projected onto the lookahead distance Y, i.e. the maximum perception line onto the groundplane. Referring to these results several observations are made:

- The increment of the perception parameters Y, H, P and δ is a function of both: the placement of the sensor Y_{sensor} and of the wheelbase L.
- The field of view δ decreases if the sensor placement increase up to on the rear axle position ($Y_{sensor} = L$). Although the lookahead distance Y increases by this factor Y_{sensor}, thus the height H to place the sensor increases, a similar behavior as the AS vehicle.
- A minor gap of the parameter P is presented by the smaller wheelbase ($L = 1$ m), if the sensor placement is on the front axle ($Y_{sensor} = 0$) to see this required distance P without being obstructed.
- The tunnel vision problem decrease if the wheelbase L is increased, assuming the projected perception line onto the lookahead distance Y. For a wheelbase $L = 2$ m the sensor can see all terrain that the vehicle will reach in its maneuver to avoid the obstacles.

Y_{sensor} (m)	Wheelbase (m)			Perception Parameter
	$L = 1.00$	$L = 1.50$	$L = 2.00$	
0	1.54	1.83	2.12	Y (m)
$L/2$	2.04	2.58	3.12	
L	2.54	3.33	4.12	
0	0.77	0.91	1.06	H (m)
$L/2$	1.02	1.29	1.56	
L	1.27	1.66	2.06	
0	1.72	2.04	2.37	P (m)
$L/2$	2.28	2.88	3.49	
L	2.84	3.72	4.61	
0	85.45	98.64	106.41	$\delta(^\circ)$
$L/2$	69.73	79.05	84.53	
L	58.44	65.17	69.08	
Radius (m)	1.59	2.38	3.17	
Off-tracking (m)	0.00	0.00	0.00	

Table 6.7: **Perception Parameters for the RS vehicle: the lookahead distance Y, the height of the sensor H, the distance measured P, and the angle of the field of view δ, which are calculated from the offset placement of the sensor Y_{sensor}, and the steering angle $\gamma = 35^\circ$ for three different wheelbases L, respectively.**

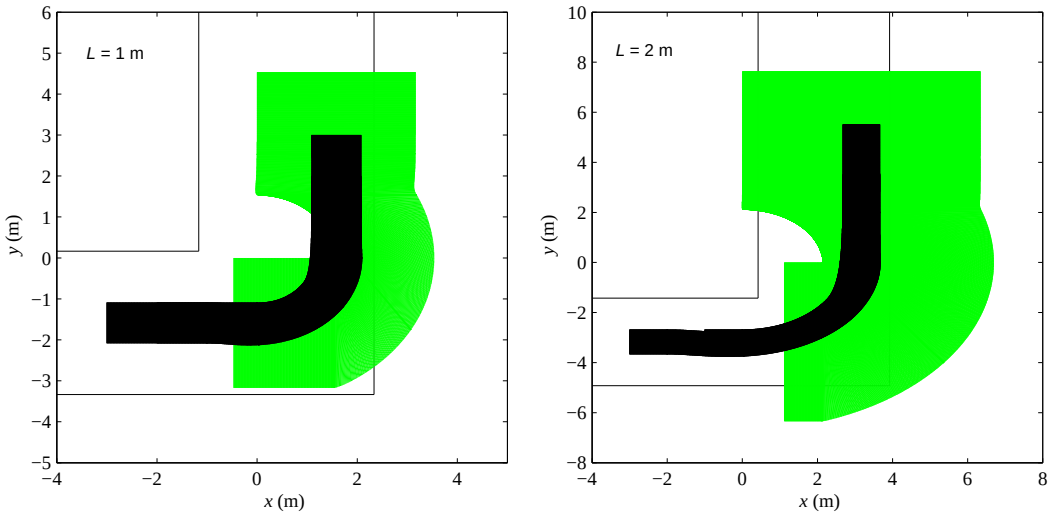

Figure 6.39: **Trajectories of RS vehicle (black) and the projected field of view onto a lookahead distance Y for: $L = 1$ m and $L = 2$ m at $Y_{sensor} = 0$.**

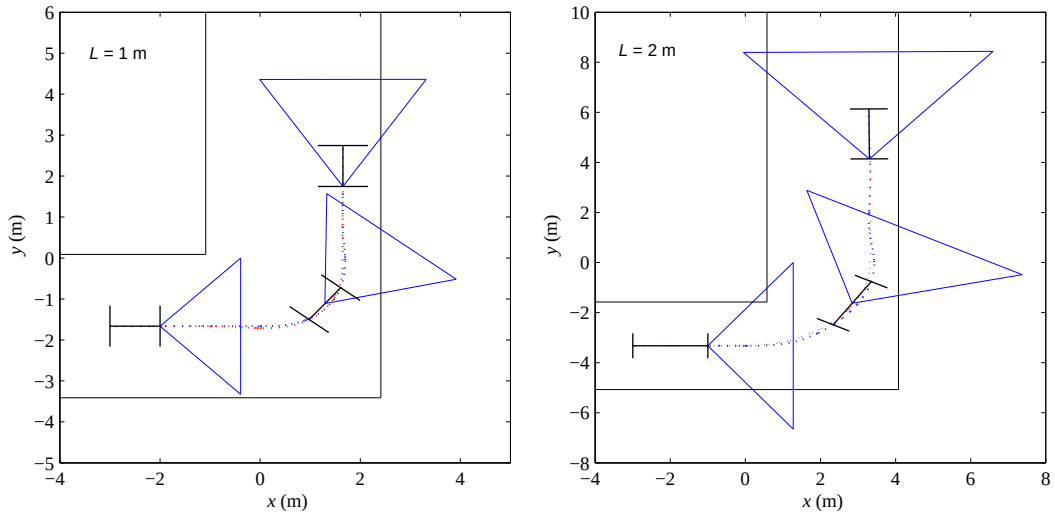

Figure 6.40: **Perception for the ES vehicles while avoiding walls: $L = 1$ m and $L = 2$ m at different placement Y_{sensor} (0, $L/2$, and L).**

6.3.3 Perception analysis for Explicit steering

To investigate the relation between vehicle configuration and perception, the perception parameters are computed for the ES vehicle, using the equations derived in previous section and assuming the same allowable values as in the cases of the AS and RS vehicles. Figure 6.40 depicts the analyzed wheelbases: $L = 1$ m and $L = 2$ m. Table 6.8 shows the results and Figure 6.41 shows the trajectory of the field of view projected onto the lookahead distance Y on the groundplane. These results lead to the following observations:

- The perception parameters Y, H, P and δ are related to the placement of the sensor Y_{sensor} and of the wheelbase L, since the off-tracking is approximately zero, thus it can be a negligent parameter similar to the RS vehicle.

- The height H to place the sensor is a function of the offset placement Y_{sensor}; i.e., when it is on the rear axle ($Y_{sensor} = L$) the angle δ of the field of view decreases and the lookahead distance Y increases by this factor, similar behavior as the AS and RS vehicles.

- To fill the requirement where the sensor must see the distance P without being obstructed, the better sensor placement is on the front axle ($Y_{sensor} = 0$), presenting a gap of this parameter that is directly proportional to the wheelbase L.

- The tunnel vision problem defined by the ES vehicle is comparable to RS vehicle, which decrease if the wheelbase L is increased, assuming the projected perception line onto the lookahead distance Y.

Y_{sensor} (m)	Wheelbase (m)			Perception Parameter
	$L = 1.00$	$L = 1.50$	$L = 2.00$	
0	1.61	1.94	2.28	Y (m)
$L/2$	2.11	2.69	3.28	
L	2.61	3.44	4.28	
0	0.81	0.97	1.14	H (m)
$L/2$	1.06	1.35	1.64	
L	1.31	1.72	2.54	
0	1.80	2.17	3.66	P (m)
$L/2$	2.36	3.01	3.84	
L	2.92	3.85	4.78	
0	85.36	97.86	105.17	$\delta(^\circ)$
$L/2$	70.29	79.25	84.48	
L	59.30	65.86	69.65	
Radius (m)	1.66	2.49	3.33	
Off-tracking (m)	0.00	0.00	0.00	

Table 6.8: **Perception Parameters for the ES vehicle: the lookahead distance Y, the height of the sensor H, the distance measured P, and the angle of the field of view δ, which are calculated from the offset placement of the sensor Y_{sensor}, and the steering angle $\gamma = 35^\circ$ for three different wheelbases L, respectively.**

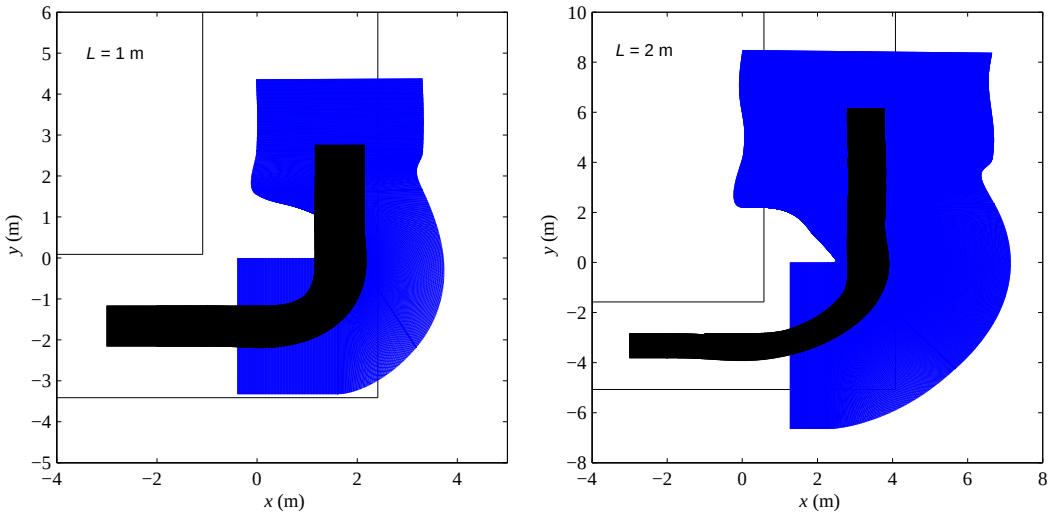

Figure 6.41: **Trajectories of ES vehicle (black) and the projected field of view onto a lookahead distance Y for: $L = 1$ m and $L = 2$ m at $Y_{sensor} = 0$.**

6.3.4 Discussion and Comparison

The perception parameters have been estimated for the Ackermann, Articulated, and Explicit vehicles. These parameters are calculated in the following of a maneuver to avoid obstacles: turning at minimum allowable radius performance. The parametric results of these vehicles, in the context of same conditions, address the following comparisons:

1. The results show an advantage for the RS vehicles to minimize the perception parameters: the lookahead distance Y, the height of the sensor H, and the distance measured P. The RS vehicles present a minor margin in comparison with the AS and ES schemes.

2. The AS vehicles tend to minimize the effective angle δ of the field of view; however, the AS vehicles present the tunnel vision problem with a margin superior than the RS and ES. This problem tends to decrease while the wheelbase is increased, which may be a disadvantage for lower wheel dimensions, such as $L = 1$ m. In particular, the tunnel vision problem can affect the accuracy for the vehicle control, which should impact the integrity of the vehicle.

3. The results in the three steering mechanisms present a tendency to minimize the parameters when the wheelbase L is decreased and there is a relation proportional to distance of the sensor placement Y_{sensor}.

It has to be noted that the ratio $\frac{L}{R}$ for ES vehicle is a smallest to perform a minimum turning radius in comparison with AS and RS vehicles; Table 6.9 shows the estimated result at same ratio $\frac{L}{R}$ and $Y_{sensor} = 0$ for the three steering schemes. In particular all schemes perform identical radius. The results show a similar behavior and calculated parameters for the RS and ES vehicles, in addition the tunnel vision problem is minimize for these vehicles, in comparison whit the obtained for the AS vehicle.

This characteristic can be argued as advantage for the RS and ES vehicles, where the sensor physically points all reachable terrain by the vehicle, since the RS and ES vehicles present a natural panning while the vehicles follow a path or maneuver to avoid obstacles. The RS and ES vehicles use the steering action to point the sensor with the orientation to follow the curvature, this is due to the sensor is on front axle.

A possible approach to minimize the tunnel vision problem, it is increased the effective width that covers the sensor or that sensor panning. A time-of-flight laser may become available to cover up to 180 ° of the field of view onto the calculated lookahead distance Y. Figure 6.42 shows the diminution of the tunnel vision problem for the three steering schemes while avoiding obstacles.

	Wheelbase (m)			Perception Parameter
	$L = 1.00$	$L = 1.50$	$L = 2.00$	
AS Vehicle	1.89	2.37	2.84	Y (m)
RS Vehicle	1.62	1.95	2.28	
ES Vehicle	1.62	1.95	2.28	
AS Vehicle	0.95	1.18	1.42	H (m)
RS Vehicle	0.81	0.97	1.14	
ES Vehicle	0.81	0.98	1.14	
AS Vehicle	2.12	2.64	3.17	P (m)
RS Vehicle	1.81	2.18	2.55	
ES Vehicle	1.81	2.18	2.55	
AS Vehicle	76.42	86.78	92.84	$\delta(^\circ)$
RS Vehicle	85.36	97.82	105.11	
ES Vehicle	85.36	97.82	105.11	
Radius (m)	1.67	2.50	3.33	
AS Off-tracking (m)	0.28	0.42	0.55	

Table 6.9: **Perception Parameters for the AS, RS, and ES vehicles: the lookahead distance Y, the height of the sensor H, the distance measured P, and the angle of the field of view δ, which are calculated from the offset placement of the sensor $Y_{sensor} = 0$, and the relation $\frac{L}{R} = 0.60$ for three different wheelbases L, respectively.**

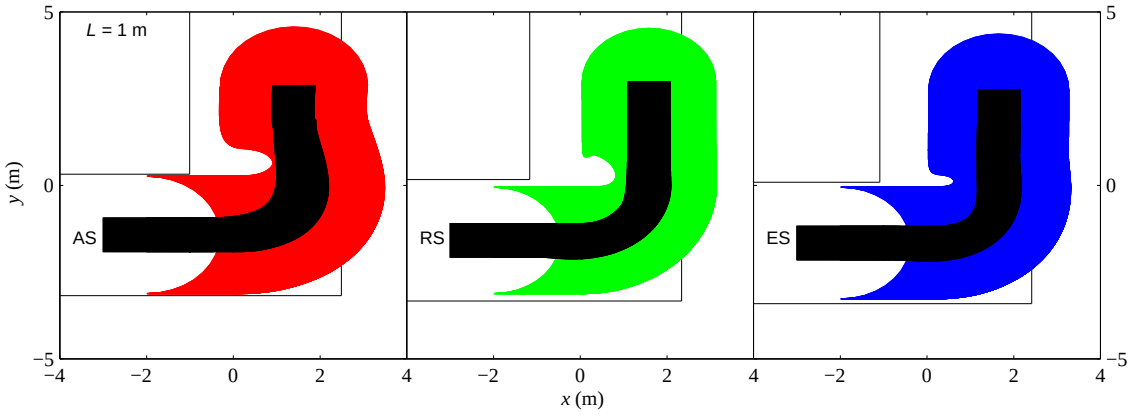

Figure 6.42: **Trajectories for the AS, RS, and ES vehicles and the projected field of view angle $\delta = 180^\circ$ onto the lookahead distance Y: $L = 1$m and $Y_{sensor} = 0$, respectively. The gap of tunnel vision problem is reduced for the three steering schemes. In particular the AS behavior is improved, which guarantee the integrity and the accuracy of the vehicle control.**

6.4 Selection

A parametric comparison of the Ackermann, Articulated, and Explicit steering schemes, in terms of positioning, control, and perception performance, has been developed under same conditions. The advantages and disadvantages of these three steering schemes have been examined in each case.

In this analysis, the Explicit scheme provides the best advantages to minimize the error of the position estimation rather than Ackermann and Articulated schemes. This scheme has also a better performance to minimize the tunnel vision problem against the Ackerman vehicle; however, the Explicit steering mechanism shows a disadvantage in the issues of actuation complexity and coordination control to perform the desired driving and heading, due to the greater number of necessary DOF to steer the vehicle.

The Ackermann scheme includes better position estimation than Articulated vehicle, due to less impact of slip, but the Articulated scheme provides advantages to maneuver a path in confined environments with efficient driving and steering; i.e., Articulated schemes minimize the tracking error versus both Explicit and Ackermann vehicles. This vehicle has also the advantage over the Ackermann and Explicit (in minor degree) schemes to reduce the tunnel vision problem, due to the intrinsic panning of the sensor while it is placed on the front axle.

These trade-offs must be considered in the synthesis process to select the vehicle scheme for the Locomotion subsystem, which must meet the task and environment requirements, determining the components that minimize the downsides of each steering scheme to support autonomous performance of the given task.

Therefore the selection of the Locomotion subsystem for the tunnel profiling task (TPT) will be based on these obtained results. In addition to the Configuration Requirements and Configuration Parameters defined through the proposed method and analyzed in the chapters 4 and 5. This is done in the following section, to proceed with the remainder of the systematic framework for synthesis of the MAV configuration in the next chapter.

6.4.1 Locomotion subsystem

An initial configuration study examined the basic motions to perform the tunnel profile task determined that a mobile platform must navigate along of the mine corridors to gather the tunnel profile at equidistant intervals. The Configuration Requirements and the Configuration Parameters being to leverage on a wheeled vehicle to traverse the desired terrain while maintaining an efficient autonomous mobility: accurate position estimation and simplicity required to control through the expected tunnels.

Steering Schemes	Autonomy		
	$\frac{L}{R}$ for $R_{min} \leq R \leq 8\,m$	$\frac{L}{R}$ for $L \ll R$	Positioning
AS	10	0	Slip Angles
RS	0	0	Minimize PER (%)
ES	60	60	wrt the RS vehicle
	$\frac{L}{R_{min}}$	$\frac{L}{R}$ for $L \ll R$	Control
AS	Off-tracking	0	Path Following:line-arc-line
RS	0	0	Tracking Error (m)
ES	> 0	0	Curvature $c = \frac{1}{R}$
	FoV width $2R_{min}$	FoV = 180°	Perception
AS	$f(\frac{L}{R})$	0	Avoid Obstacle: turn R_{min}
RS	$f(\frac{R}{L})$	0	Tunnel Vision Problem
ES	$f(\frac{R}{L})$	0	
AS	Off-tracking	Off-tracking	Avoid Obstacle: turn R_{min}
RS	0	0	Y, H, and P Parameters
ES	0	0	wrt the RS vehicle
AS	0	0	Avoid Obstacle: turn R_{min}
RS	15	0	δ Parameter (%)
ES	15	0	wrt the AS vehicle

Table 6.10: **Comparison of results for the AS, RS, and ES steering schemes under positioning, control, and perception analysis.**

Despite the advantages provides by the ES and RS steering schemes, the Ackermann scheme is selected, since it has advantage of allowing the vehicle to be significantly simpler control required than the ES mode, and more accurate position estimation than the RS scheme as is shown in Table 5.10.

Mainly, the selection is a small wheelbase dimension, because the vehicle must steer at minimum radius (R_{min}) to follow path commands. Therefore an Ackermann vehicle with wheelbase $L = 1$ m has a control advantage over ES scheme of same dimension, considering a tracking error equivalent to the off-tracking that develops the Ackermann vehicle but a better and efficient steering at steady state, i.e. minimum control commands.

Furthermore, the AS wheelbase $L = 1$ m provides better positioning than RS mode, due to AS scheme minimizes a 10 % the effect of the factors that tend to increase the error to estimate the vehicle positioning with reference to the obtained results for the RS scheme at same conditions of evaluation.

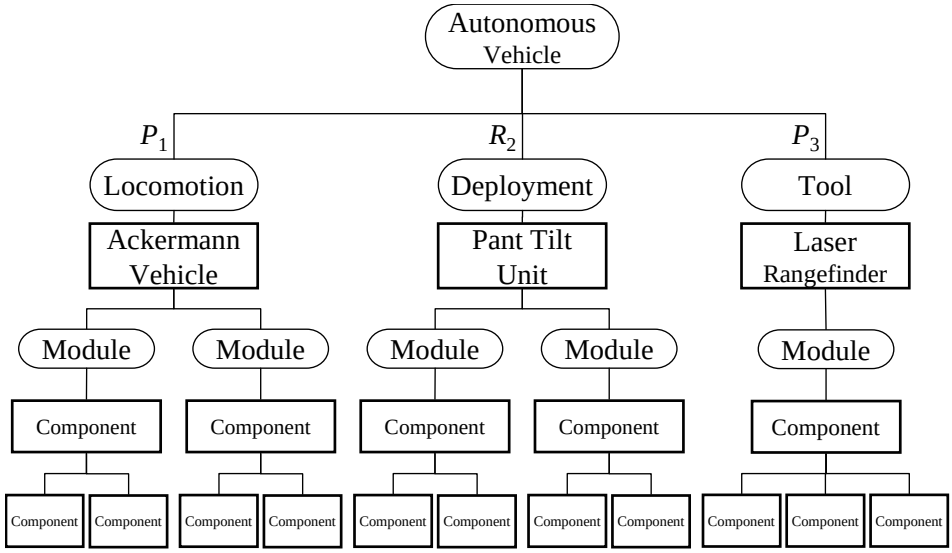

Figure 6.43: **Mining Autonomous Vehicle structure formulated by a Ackermann vehicle, a pant tilt unit, and a laser rangefinder.**

Therefore, the robotic vehicle configuration is updated with the selection of an Ackermann vehicle, which is mapped into the MAV structure as the Locomotion subsystem to perform the tunnel-profiling task. Figure 6.43 shows such MAV structure, composed by the Ackermann vehicle and the rest of components to implement the motions $P_1R_2P_3$ of the Basic Configuration.

However, the fulfillment the Configuration Parameters of the motion P_1 implies the estimation of the vehicle positioning for the achievement of the task at least a distance equivalent to 50 m, which corresponds to the minimum long of the tunnel (50 m $\leq$ length_tunnel). The estimation must be solved from the kinematics of the Locomotion subsystem and the use of multiple sensors. But the estimation of the vehicle position and orientation presents an error caused by many factors that involve the interaction among the vehicle, the sensors, and the environment; moreover, such error is accumulative, i.e., an uncertainty of the vehicle positioning which increases with the traveled distance by the robotic vehicle.

The following point of the systematic framework is an analysis to investigate the quantitative sensor requirements that minimize the positioning uncertainty. The analysis uses a generic architecture that assumes the existence of an absolute sensor and landmarks to update the vehicle positioning, estimated by the sensors of velocity and steering. In the next chapter, the theoretical propagation of positioning uncertainty is estimated to evaluate and bound the expected uncertainty of such sensors and the number of landmarks for allowing the successful execution of the task.

Bibliography

[Alexander 89] J.C. Alexander and J.H. Maddocks. *On the Kinematics of Wheeled Mobile Robots*. International Journal of Robotics Research, Vol. 8, No. 5, pp. 15–27, October 1989.

[Altafini 99] C. Altafini. *A Path-Tracking Criterion for an LHD Articulated Vehicle*. The International Journal of Robotics Research, Vol. 18, No. 5, pp. 435–441, May 1999.

[Altshuller 01] G. Altshuller. *And Suddenly the Inventor Appeared : TRIZ, the Theory of Inventive Problem Solving*. Technical Innovation Center, 2001.

[Ambrose 94] R. Ambrose and D. Tesar. *The Optimal Selection of Robot Modules for Space Manipulators*. In Proceedings of the ASCE Space 94 Conference, February 1994.

[Antonsson 01] E.K. Antonsson and J. Cagan. *Formal Engineering Design Synthesis*. Cambridge University Press, New York, NY, 1st edition, 2001.

[Apostolopoulos 96] D. Apostolopoulos. *Systematic Configuration of Robotic Locomotion*. Thechnical Report CMU-RI-96-30, The Robotics Institute, Carnegie Mellon University, 1996.

[Apostolopoulos 01] D. Apostolopoulos. *Analytical Configuration of Wheeled Robotic Locomotion*. Ph.D. Thesis, The Robotics Institute, Carnegie Mellon University, 2001.

[Atlas] Atlas. *Atals Copco Wagner Inc: LHD EST-2D*. Available at `http://www.atlascopcowagner.com/`.

[Bares 91] J. Bares. *Configuration of Walkers for Extreme Terrain*. Ph.D. Thesis, Civil Engineering, Carnegie Mellon University, 1991.

[Bekker 56] M.G. Bekker. *Theory of Land Locomotion: The Mechanics of Vehicle Mobility*. University of Michigan Press, Ann Arbor, MI, 1956.

[Bekker 69] M.G. Bekker. *Introduction to Terrain-Vehicle Systems*. University of Michigan Press, Ann Arbor, MI, 1969.

[Bickel 82] J.O. Bickel and T.R. Kuesel. *Tunnel Engineering Handbook*. Van Nostrand Reinhold Co., 1982.

[Borenstein 97] J. Borenstein, H.R. Everett, L. Feng and D. Wehe. *Mobile Robot Positioning and Sensors and Techniques*. Journal of Robotic Systems, Special Issue on Mobile Robots, Vol. 14, No. 4, pp. 231–249, April 1997.

[Brooks 81] R.A. Brooks. *Symbolic Reasoning Among 3-D Models and 2-D Images*. Artificial Intelligence Journal, Vol. 17, No. 1-3, pp. 285–348, 1981.

[Campion 96] G. Campion, G. Bastin and B. D'Andra-Novel. *Structural Properties and Classification of Kinematic and Dynamic Models of Wheeled Mobile Robots*. IEEE Transactions On Robotics and Automation, Vol. 12, No. 1, pp. 47–62, February 1996.

[Cannon 99] H.N. Cannon. *Extended Earthmoving with an Autonomous Excavator*. M.S. Thesis, The Robotics Institute Carnegie Mellon University, 1999.

[Chedmail 96] P. Chedmail and E. Ramstein. *Robot Mechanism Synthesis and Genetic Algorithms*. In Proceedings of the IEEE International Conference on Robotics and Automation, volume 4, pp. 3466–3471, 22-28 April 1996.

[Chen 95] I-M. Chen and J.W. Burdick. *Determining Task Optimal Modular Robot Assembly Configurations*. In Proceedings of the IEEE International Conference on Robotics and Automation, volume 1, pp. 132–137, 21-27 May 1995.

[Chen 97] I-M. Chen and G. Yang. *Automatic Generation of Dynamics for Modular Robots with Hybrid Geometry*. In Proceedings of the IEEE International Conference on Robotics and Automation, volume 3, pp. 2288–2293, 20-25 April 1997.

[Chironis 96] N.P. Chironis and N. Sclater. *Mechanisms and Mechanical Devices Sourcebook*. McGraw-Hill, 1996.

[Chocron 97] O. Chocron and P. Bidaud. *Evolutionary Algorithms in kinematic Design of Robotic System*. In Proceedings of the IEEE/RSJ International Conference on Intelligent Robots and Systems, volume 2, pp. 1111–1117, 7-11 September 1997.

[Chocron 99] O. Chocron and P. Bidaud. *Evolving Walking Robots for Global Task Based Design*. In Proceedings of the Congress on Evolutionary Computation, volume 1, pp. 405–412, June 1999.

[Chun 87] W. Chun. *Ground Vehicle Options*. SPIE The International Society of Optical Engineering: Mobile Robots, Vol. 852, pp. 188–194, 1987.

[Clarke 92] T.A. Clarke and N.E. Lindsey. *Profiling Methods Reviewed*, 1992. Tunnels and Tunnelling.

[Corke 99] P. Corke, G. Winstanley, J. Roberts, E. Duff and P. Sikka. *Robotics for the Mining Industry: Opportunities and Current Research*. In Proceedings of the Int. Conf. Field and Service Robotics, pp. 208–219, 29-31 August 1999.

[Craig 86] J.J. Craig. *Introduction to Robotics : Mechanics and Control*. Addison-Wesley, Reading, MA, 2nd edition, 1986.

[Danaher] Danaher. *Danaher Industrial Controls: Seris 21/22*. Available at `http://www.dancon.com/`.

[De-Boor 78] C. De-Boor. *A Practical Guide to Splines*. Springer-Verlag, New York, NY, 1st edition, 1978.

[Dixon 96] J.C. Dixon. *Tires, Suspension, and Handling*. Society of Automotive Engineers, 1996.

[DPerception] DPerception. *SICK AG: LMS 221 Outdoor*. Available at `http://www.sick.de/`.

[Dudzinski 89] P.A. Dudzinski. *Design Characteristics of Steering Systems for Mobile Wheeled Earthmoving Equipment*. Journal of Terramechanics, Vol. 26, No. 1, pp. 25–82, 1989.

[Durrant-Whyte 96] H. Durrant-Whyte. *An Autonomous Guided Vehicle for Cargo Handling Applications*. The International Journal of Robotics Research, Vol. 15, No. 5, pp. 407–440, October 1996.

[Durrant-Whyte 01] H. Durrant-Whyte. *A Critical Review of the State-of-the-Art in Autonomous Land Vehicle Systems and Technology*. Thechnical Report SAND2001-3685, Sandia National Laboratories, 2001.

[DYNAMechs 01] DYNAMechs. *Dynamics of Mechanisms: A Multibody Dynamic Simulation Library*, 2001. Available at `http://dynamechs.sourceforge.net/`.

[Everett 95] H.R. Everett. *Sensors for Mobile Robots : Theory and Application*. A.K. Peters, Wellesley, MA, 1995.

[Farritor 96] S. Farritor, S. Dubowsky, N. Rutman and J. Cole. *A Systems-Level Modular Design Approach to Field Robotics*. In Proceedings of the IEEE International Conference on Robotics and Automation, volume 4, pp. 2890–2895, 22-28 April 1996.

[Farritor 98] S. Farritor. *On Modular Design and Planning for Field Robotic Systems*. Ph.D. Thesis, Department of Mechanical Engineering, Massachusetts Institute of Technology, 1998.

[Farritor 01] S. Farritor and S. Dubowsky. *On Modular Design of Field Robotic Systems*. Autonomous Robots, Vol. 10, No. 1, pp. 57–65, January 2001.

[Fiorini 00] P. Fiorini. *Ground Mobility Systems for Planetary Exploration*. In Proceedings of the IEEE International Conference on Robotics and Automation, volume 1, pp. 908–913, 24-28 April 2000.

[Fong 03] T.W. Fong, C. Thorpe and B. Glass. *PdaDriver: A Handheld System for Remote Driving*. In Proceedings of the IEEE International Conference on Advanced Robotics, July 2003.

[Fraichard 98] Th. Fraichard and R. Mermond. *Path Planning with Uncertainty for Car-Like Robots*. In Proceedings of the IEEE International Conference on Robotics and Automation, volume 1, pp. 27–32, 16-20 May 1998.

[Fukuda 90] T. Fukuda and Y. Kawauchi. *Cellular Robotic System as One of the Realization of Self-Organizing Intelligent Universal Manipulator*. In Proceedings of the IEEE International Conference on Robotics and Automation, volume 1, pp. 662–667, 13-18 May 1990.

[Gage 95] D.W. Gage. *Unmanned Ground Vehicle (UGV) Development Efforts*. Special Issue on Unmanned Ground Vehicles, Unmanned Systems Magazine, 1995.

[Gambao 02] E. Gambao and C. Balaguer. *Robotics and Automation in Construction*. IEEE Robotics and Automation Magazine, Vol. 9, No. 1, pp. 4–6, March 2002.

[Gelb 74] A. Gelb. *Applied Optimal Estimation*. The MIT Press, Cambridge, MA, 1st edition, 1974.

[Gillespie 92] T.D. Gillespie. *Fundamentals of Vehicle Dynamics*. Society of Automotive Engineers, 1992.

[GlobalSpec] GlobalSpec. *Online Product and Service Database*. Available at `http://www.globalspec.com/`.

[González 04] F.G. González. *Automatización de la Dirección de un Vehículo Autónomo*. M.S. Thesis, Tecnológico de Monterrey, 2004.

[Gutierrez 04] J. Gutierrez, J.L. Gordillo and I. Lopez. *Configuration and Construction of an Autonomous Vehicle for a Mining Task*. In Proceedings of the IEEE International Conference on Robotics and Automation, volume 2, pp. 2010–2016, 26 April-1 May 2004.

[Han 97] J. Han, W.K. Chung, Y. Youm and S.H. Kim. *Task Based Design of Modular Robot Manipulator Using Efficient Genetic Algorithm*. In Proceedings of the IEEE/RSJ International Conference on Intelligent Robots and Systems, volume 1, pp. 507–512, 20-25 April 1997.

[Hayati 97] S. Hayati, R. Volpe, P. Backes, J. Balaram, R. Welch, R. Ivlev, G. Tharp, S. Peters, T. Ohm, R. Petras and S. Laubach. *The Rocky 7 Rover: A Mars Sciencecraft Prototype*. In Proceedings of the IEEE International Conference on Robotics and Automation, volume 3, pp. 2458–2464, 20-25 April 1997.

[Hornby 01] G.S. Hornby, H. Lipson and J.B. Pollack. *Evolution of Generative Design Systems for Modular Physical Robots*. In Proceedings of the IEEE International Conference on Robotics and Automation, volume 4, pp. 4146–4151, 21-26 May 2001.

[Hoschek 93] J. Hoschek and D. Lasser. *Fundamentals of Computer Aided Geometric Design*. A. K. Peters, 1st english edition, 1993.

[Huang 90a] C.L. Huang. *Contour Generation and Shape Restoration of the Straight Homogeneous Generalized Cylinder*. In Proceedings of the 10th IEEE International Conference on Pattern Recognition, volume 1, pp. 409–413, 16-21 June 1990.

[Huang 90b] M.Z. Huang and K.J. Waldron. *Relationship Between Payload and Speed in Legged Locomotion Systems*. IEEE Transactions On Robotics and Automation, Vol. 6, No. 5, pp. 570–577, October 1990.

[Hurteau 92] R. Hurteau, M. St-Amant, G. Laperrire and G. Chevrette. *Optical Guidance System for Underground Mine Vehicle*. In Proceedings of the IEEE International Conference on Robotics and Automation, volume 1, pp. 639–644, 12-14 May 1992.

[Ivanov 94] G.I. Ivanov. *The Formules of Creativity or How to Learn to Invent*. Prosveschenie, 1994.

[Joskowicz 94] L. Joskowicz and E.Sacks. *Configuration Space Computation for Mechanism Design*. In Proceedings of the IEEE International Conference on Robotics and Automation, volume 2, pp. 1080–1087, 8-13 May 1994.

[Katragadda 99] L. Katragadda. *Synergy: A Language and Framework for Robot Design*. Ph.D. Thesis, The Robotics Institute, Carnegie Mellon University, 1999.

[Kelly 98] A. Kelly and A. Stentz. *Rough Terrain Autonomous Mobility - Part 1: A Theoretical Analysis of Requirements*. Autonomous Robots, Vol. 5, No. 2, pp. 129–161, May 1998.

[Kelmar 88] L. Kelmar and P. Khosla. *Automatic Generation Of Kinematics for A Reconfigurable Modular Manipulator System*. In Proceedings of the IEEE International Conference on Robotics and Automation, volume 2, pp. 663–668, 24-29 April 1988.

[Kim 93] J-O. Kim and P. Khosla. *Design of Space Shuttle Tile Servicing Robot: An Application of Task-Based Kinematic Design*. In Proceedings of the IEEE International Conference on Robotics and Automation, volume 3, pp. 867–874, 2-6 May 1993.

[Kotay 97] K.D. Kotay and D.L. Rus. *Task-Reconfigurable Robots: Navigators and Manipulators*. In Proceedings of the IEEE/RSJ International Conference on Intelligent Robots and Systems, volume 2, pp. 1081–1089, 7-11 September 1997.

[Laboratorytalk] Laboratorytalk. *Online Product and Service Database*. Available at `http://www.laboratorytalk.com/`.

[Latombe 91] J-C. Latombe. *Robot Motion Planning*. Kluwer Academic Publishers, Boston, 1st edition, 1991.

[Laumond 93] J.P. Laumond. *Controllability of a Multibody Mobile Robot*. IEEE Transactions On Robotics and Automation, Vol. 9, No. 6, pp. 755–763, December 1993.

[Leger 98] P.C. Leger and J. Bares. *Automated Synthesis and Optimization of Robot Configurations*. In Proceedings of the Proceedings of the 1998 ASME Design Engineering Technical Conferences, 1998.

[Leger 99] P.C. Leger. *Automated Synthesis and Optimization of Robot Configurations: An Evolutionary Approach*. Ph.D. Thesis, The Robotics Institute, Carnegie Mellon University, 1999.

[Lozano-Perez 83] T. Lozano-Perez. *Spatial Planning: a Configuration Space Approach*. IEEE Transactions on Computers, Vol. 2, No. 2, pp. 108–120, February 1983.

[MathWorks 03] MathWorks. *The MathWorks: MATLAB*, 2003. Available at `http://www.mathworks.com/`.

[Matsumaru 95] T. Matsumaru. *Design and Control of the Modular Robot System: TOMMS*. In Proceedings of the IEEE International Conference on Robotics and Automation, volume 2, pp. 2125–2131, 21-27 May 1995.

[McCarthy 00] J.M. McCarthy. *Mechanism Synthesis Theory and the Design of Robot*. In Proceedings of the IEEE International Conference on Robotics and Automation, volume 1, pp. 55–60, 24-28 April 2000.

[McCormac 99] J.C. McCormac. *Surveying*. Prentice Hall, 1999.

[McCrea 97] A. McCrea. *Genetic Algorithm Performance in Parametric Selection of Bridge Restoration Robot*. In Proceedings of the 14th International Symposium on Automation and Robotics in Construction, pp. 437–441, 1997.

[MDL] MDL. *Measurement Devices Ltd: LaserAce1000 and C-ALS*. Available at `http://www.mdl.co.uk/`.

[Meyrowitz 96] A.L. Meyrowitz, D.R. Blidberg and R.C. Michelson. *Autonomous Vehicles*. In Proceedings of the IEEE, volume 84, pp. 1147–1164, August 1996.

[Model 03] Working Model. *MSC Software: Working Model*, 2003. Available at `http://www.krev.com/`.

[Moore 89] H.J. Moore and B.M. Jakosky. *Viking Landing Sites, Remote-Sensing Observations, and Physical Properties of Martian Surface Materials*. International Journal of Solar System Studies, Vol. 81, pp. 164–184, September 1989.

[MSCSoftware 03] MSCSoftware. *MSC Software Corporation: ADAMS*, 2003. Available at `http://www.mscsoftware.com/`.

[Muir 87] P.F. Muir and C.P. Neuman. *Kinematic Modeling of Wheeled Mobile Robots*. Journal of Robotic Systems, Vol. 4, No. 2, pp. 281–329, April 1987.

[Murata 98] S. Murata, H. Kurokawa, E. Yoshida, K. Tomita and S. Kokaji. *A 3-D Self-Reconfigurable Structure*. In Proceedings of the IEEE

International Conference on Robotics and Automation, volume 1, pp. 432–439, 16-20 May 1998.

[Murray 93] R.M. Murray and S.S. Sastry. *Nonholonomic Motion Planning: Steering Using Sinusoids*. IEEE Transactions On Automatic Control, Vol. 38, No. 5, pp. 700–716, May 1993.

[Nordlund 96] M. Nordlund. *An Information Framework for Engineering Design Based on Axiomatic Design*. Ph.D. Thesis, Royal Institute of Technology (KTH), 1996.

[Norton 04] R.L. Norton. *Design Of Machinery : An Introduction To The Synthesis And Analysis Of Mechanisms And Machines*. McGraw-Hill, 2004.

[Ogata 02] K. Ogata. *Modern Control Engineering*. Prentice Hall, 2002.

[Optech] Optech. *Optech Incorporated: Sentinel 100*. Available at `http://www.optech.on.ca/`.

[Palacios 00] G.J. Palacios. *Control de Dirección de un Vehículo Autónomo*. M.S. Thesis, Tecnológico de Monterrey, 2000.

[Pamecha 96] A. Pamecha and G.S. Chirikjian. *A Useful Metrics for Modular Robot Motion Planning*. In Proceedings of the IEEE International Conference on Robotics and Automation, volume 1, pp. 442–447, 22-28 April 1996.

[Paredis 93] C.J.J. Paredis and P.K. Khosla. *Synthesis Methodology for Task Based Reconfiguration of Modular Manipulator Systems*. In Proceedings of the 6th International Symposium on Robotics Research, 2-5 October 1993.

[Paredis 96a] C.J.J. Paredis. *An Agent-Based Approach to the Design of Rapidly Deployable Fault Tolerant Manipulators*. Ph.D. Thesis, Department of Electrical and Computer Engineering, Carnegie Mellon University, 1996.

[Paredis 96b] C.J.J. Paredis and P.K. Khosla. *Designing Fault Tolerant Manipulators: How Many Degrees-of-freedom?* The International Journal of Robotics Research, Vol. 15, No. 6, pp. 611–628, December 1996.

[Paul 81] R.P. Paul. *Robot Manipulators : Mathematics, Programming, and Control*. MIT Press, Cambridge, MA, 1981.

[Peñoles 04] Industrias Peñoles. *S.A. de C.V., Mining Division*, 2004. Available at `http://www.penoles.com.mx/`.

[Pettersson 98] L. Pettersson. *Terrain Analysis as a Design Tool for Autonomous Vehicles in Difficult Terrain.* In Proceedings of the NordDesign'98, June 1998.

[Pilarski 99] T. Pilarski, M. Happold, H. Pangels, M. Ollis, K. Fitzpatrick and A. Stentz. *The Demeter System for Automated Harvesting.* In Proceedings of the 8th International Topical Meeting on Robotics and Remote Systems, April 1999.

[Pilarski 02] T. Pilarski, M. Happold, H. Pangels, M. Ollis, K. Fitzpatrick and A. Stentz. *The Demeter System for Automated Harvesting.* Autonomous Robots, Vol. 13, No. 1, pp. 9–20, July 2002.

[Potvin 01] Y. Potvin, P. Nodin, M. Sandy and K. Rosengren. *Towards the Elimination of Rockfall Fatalities in Australian Mines.* Thechnical Report MERIWA M341, Australian Centre for Geomechanics, 2001.

[Requicha 92] A.A.G. Requicha and J.R. Rossignac. *Solid Modeling and Beyond.* IEEE Computer Graphics and Applications, Vol. 12, No. 5, pp. 31–44, September 1992.

[Rollins 98] E. Rollins, J. Luntz, A. Foessel, B. Shamah and W. Whittaker. *Nomad: A Demonstration of the Transforming Chassis.* In Proceedings of the IEEE International Conference on Robotics and Automation, volume 1, pp. 611–617, 16-20 May 1998.

[Roston 94] G. Roston. *Genetic Methodology for Configuration Design.* Ph.D. Thesis, Mechanical Engineering, Carnegie Mellon University, 1994.

[Samson 95] C. Samson. *Control of Chained Systems Application to Path Following and Time-Varying Point-Stabilization of Mobile Robots.* IEEE Transactions On Automatic Control, Vol. 40, No. 1, pp. 64–77, January 1995.

[Scheding 97] S. Scheding, E. Nebot, S. Stevens, H. Durrant-Whyte, J. Roberts, P. Corke, J. Cunningham and B. Cook. *Experiments in Autonomous Underground Guidance.* In Proceedings of the IEEE International Conference on Robotics and Automation, volume 3, pp. 1898–1903, 20-25 April 1997.

[Scheding 99] S. Scheding, E. Nebot, S. Stevens, H. Durrant-Whyte, J. Roberts, P. Corke, J. Cunningham and B. Cook. *An Experiment in Autonomous Navigation of an Underground Mining Vehicle.* IEEE Transactions On Robotics and Automation, Vol. 15, No. 1, pp. 85–95, February 1999.

[Selig 00] J.M. Selig. *Geometrical Foundations of Robotics*. World Scientific Pub Co, 1st edition, 2000.

[SICK] SICK. *SICK AG: LMS 221 Outdoor*. Available at `http://www.sick.de/`.

[Solleiro 02] E. Solleiro, D. Flores, J. Gama and S. Sergey. *Tepetates of Central Mexico*. In Proceedings of the 17th WCSS, 14-21 August 2002.

[Song 88] S. Song and K. Waldron. *Machines that Walk: The Adaptive Suspension Vehicle*. MIT Press, 1988.

[Steele 93] J. Steele, C. Ganesh and A. Kleve. *Control and Scale Model Simulation of Sensor-Guided LHD Mining Machines*. IEEE Transactions on Industrial Applications, Vol. 29, No. 6, pp. 1232–1238, November-December 1993.

[Stentz 98] A. Stentz, J. Bares, S. Singh and P. Rowe. *A Robotic Excavator for Autonomous Truck Loading*. In Proceedings of the IEEE/RSJ International Conference on Intelligent Robotic Systems, volume 3, pp. 1885–1893, 13-17 October 1998.

[Stentz 99] A. Stentz, M. Ollis, S. Scheding, H. Herman, C. Fromme, J. Pedersen, T. Hegadorn, R. McCall, J. Bares and R. Moore. *Position Measurement for Automated Mining Machinery*. In Proceedings of the International Conference on Field and Service Robotics, pp. 299–304, August 1999.

[Stentz 01] A. Stentz. *Robotic Technologies for Outdoor Industrial Vehicles*. In Proceedings of the SPIE AeroSense, 2001.

[Stroupe 01] A. Stroupe, S. Singh, R. Simmons, T. Smith, P. Tompkins, V. Verma, R. Vitti-Lyons and M.D. Wagner. *Technology for Autonomous Space Systems*. Thechnical Report CMU-RI-TR-00-02, The Robotics Institute, Carnegie Mellon University, 2001.

[Sukhatme 97] G.S. Sukhatme. *On The Evaluation Of Autonomous Mobile Robots*. Ph.D. Thesis, Faculty Of The Graduate School, University Of Southern California, 1997.

[Tesar 89] D. Tesar. *A Generalized Architecture for Robot Structures*. ASME Transaction on Manufacturing Review, Vol. 2, No. 2, pp. 91–118, June 1989.

[Thorpe 91a] C. Thorpe, M. Hebert, T. Kanade and S. Shafer. *Toward Autonomous Driving: The CMU Navlab: Part II: Architecture and Systems*. IEEE Expert, Vol. 6, No. 4, pp. 44–52, August 1991.

[Thorpe 91b] C. Thorpe, M. Hebert, T. Kanade and S. Shafer. *Toward Autonomous Driving: The CMU Navlab: Part I:Perception.* IEEE Expert, Vol. 6, No. 4, pp. 31–42, August 1991.

[Thorpe 97] C. Thorpe. *Mobile Robots and Smart Cars.* In Proceedings of the First International Conference on Field and Service Robotics, December 1997.

[Thrun 03] S. Thrun, D. Haehnel, D. Ferguson, M. Montemerlo, R. Triebel, W. Burgard, C. Baker, Z. Omohundro, S. Thayer, and W.L. Whittaker. *A System for Volumetric Robotic Mapping of Abandoned Mines.* In Proceedings of the IEEE International Conference on Robotics and Automation, volume 3, pp. 4270–4275, 14-19 September 2003.

[Todd 85] D. Todd. *Walking Machines: An Introduction to Legged Robots.* Chapman and Hall, New York, NY, 1985.

[Trebi-Ollennu 99] A. Trebi-Ollennu and J.M. Dolan. *An Autonomous Ground Vehicle for Distributed Surveillance: CyberScout.* Thechnical Report ICES-04-09-99, The Robotics Institute, Carnegie Mellon University, 1999.

[Ulrich 00] K.T. Ulrich and S.D. Eppinger. *Product Design and Development.* Irwin/McGraw-Hill, 2000.

[Ulupinar 95] F. Ulupinar and R. Nevatia. *Shape from Contour: Straight Homogeneous Generalized Cylinders and Constant Cross Section Generalized Cylinders.* IEEE Transaction on Pattern Analysis and Machine Intelligence, Vol. 17, No. 2, pp. 120–135, February 1995.

[Unsal 00] C. Unsal and P. Khosla. *Mechatronic Design of a Modular Self-Reconfiguring Robotic System.* In Proceedings of the IEEE International Conference on Robotics and Automation, volume 2, pp. 1742–1747, 24-28 April 2000.

[Vazquez 02] D.J. Vazquez. *Control de Dirección de un Vehículo Autónomo con Retroalimentación Visual.* M.S. Thesis, Tecnológico de Monterrey, 2002.

[Wagner 02] M.D. Wagner, D. O'Hallaron, D. Apostolopoulos and C. Urmson. *Principles of Computer System Design for Stereo Perception.* Thechnical Report CMU-RI-TR-02-01, Robotics Institute, Carnegie Mellon University, 2002.

[Waldron 85] K.J. Waldron. *The Mechanics of Mobile Robots.* In Proceedings of the IEEE International Conference on Advanced Robotics, volume 1, pp. 533–544, September 1985.

[Waldron 95] K.J. Waldron. *Terrain Adaptive Vehicles*. Transactions of the ASME, Journal of Mechanical Design: Special 50th Anniversary Design Issue, Vol. 117, No. 3, pp. 107–112, June 1995.

[Wong 93] J.Y. Wong. *Theory of Ground Vehicles*. John Wiley and Sons, New York, NY, 3rd edition, 1993.

[Yim 00] M. Yim, D.G. Duff and K.D. Roufas. *PolyBot:A Modular Reconfigurable Robot*. In Proceedings of the IEEE International Conference on Robotics and Automation, volume 1, pp. 514–520, 24-28 April 2000.

[Yim 02] M. Yim, Y. Zhang and D. Duff. *Modular Robots*. IEEE Spectrum, Vol. 39, No. 2, pp. 30–34, Febraury 2002.

[Yoshida 97] E. Yoshida, S. Murata, K. Tomita, H. Kurokawa and S. Kokaji. *Distributed Formation Control for a Modular mechanical System*. In Proceedings of the IEEE/RSJ International Conference on Intelligent Robots and Systems, volume 2, pp. 1090–1097, 7-11 September 1997.

Appendix A

Constructive Solid Geometry

This appendix outlines the derivation of the Geometric Description for the Tunnel Profiling Task through the Constructive Solid Geometry (CSG) technique. In CSG a solid is represented as a set-theoretic Boolean expression of primitive solid objects.

Primitives

In the strict sense, CSG is a method of representation and a certain standard set of primitive objects. A CSG object is built from the standard primitive, using regularized Boolean operations and rigid motions. The CSG standard primitives are the parallelepiped (box), the triangular prism, the sphere, the cylinder, the cone, and the torus (bounden primitive solids).

The primitives are generic in the sense that they represent shapes that must be instantiated by user to chosen dimensions. All standard primitives have a finite domain. For example, the cylinder always has a finite radius and a finite length. With each primitive object there is associated a local coordinate frame. These different local coordinate frames must be related to one another, by placing them with respect to a common world coordinate frame.

A solid design is usually created in several steps that begin with and existing design and modify it, or create a new design from primitive objects. Primitive objects are selected from a universe of possible shapes. A shape is instantiated by assigning values to certain parameters.

- Each primitive is selected from a set of solid shapes and is instantiated by choosing values for certain dimensioning parameters that control the final shape. For instance, a CSG modeler may use boxes, cylinders, spheres, cones, and torus. The parameters in this case include the side lengths of boxes, the diameter and length of cylinders.

- A primitive is created by sweeping a contour along a space curve. Both the shape of the contour and the shape of the space curve are defined by parameters. For instance, it can sweep a disk of radius r along a line segment of length l, thus creating a solid cylinder. This approach lends itself to generating and verifying cutting paths for numerically controlled machining.

- All primitives are algebraic halfspaces; that is, point sets defined as

$$\{(x, y, z)|f(x, y, z)\, 0\}$$

  where f is an irreducible polynomial. The coefficients of the polynomial can be considered the shape parameters.

Straight Homogeneous Generalized Cylinder

Another potentially useful addition is the inclusion of sweeping primitives, modeling primitives of the sweeping model approach to solid modeling. Sweeping and object along a trajectory through space defines a new object, called a sweep. The simplest kind of sweep is defined by a 2-D area (cross section) swept along a linear path normal to the plane of the area to create a volume. General sweeps of 2-D cross sections are known as generalized cylinders in computer vision. For example, a cylinder is defined by a Straight Homogeneous Generalized Cylinder (SHGC), which is specified by four tuples (A, C, r, α). A is the axis, which is a curve in space defined in parametric form by $A(s) = (x_a, y_a, z_a)\,(s)$. At each point $A(s)$ on the axis, the cross section is described in a $U - V$ plane, with $A(s)$ at the origin, and defined by constant angle α. The U-axis will be in the direction of the steepest descent of the $U - V$ plane from the tangent to the axis.

In SHGCs, the straight attribute implies that $A(s)$ is a linear function. The axis is a line segment, and all $U - V$ planes are parallel. The $u - v - s$ coordinate system is used to define all the SHGC. On $u - v$ cross section plane for each value of s, the cross section is the set of point $r(s)C(t)$ for values of t from 0 to 1. The cross section function $C(t) = (U_c(t), V_c(t))$ describes the shape of cross section; the radius function $r(s)$ describes its size. So, the cross sections have the same shape of the SHGC.

Regularized Boolean Operations

After instantiation, primitive objects can be combined using regularized Boolean operations. The operations are the regularized union, denoted $\cup^*$; regularized intersection, denoted $\cap^*$; and regularized difference, denoted $-^*$. They differ from corresponding set theoretic operations in that the result is the closure of the operation on the interior of the two solids, and they are used to eliminate dangling lower-dimensional structure.

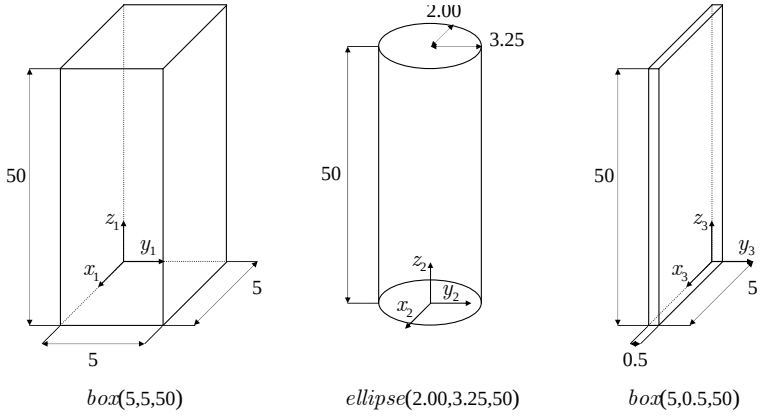

Figure A.1: **Standard primitives for the Tunnel Profiling Task:** $box(5, 5, 50)$**,** $ellipse(2, 3.25, 50)$**, and** $box(5, 0.5, 50)$**, and their local coordinate frames respectively.**

Before the two objects are intersected, united or differenced, they must be positioned appropriately with respect to each other. This is done by translation, rotation and scaling, as needed. To make this positioning meaningful, we must establish a relationship between the local coordinate frames of the objects. A simple is to identify the local frames with a single, universal coordinate frame.

Construction of a Generic Mining Tunnel

The abstraction of Tunnel Profiling Task requires representing the shape of physical objects, and such representations and basic operations on them can be provided by solid modeling. Three standard primitives are needed to represent the generic tunnel, two boxes and an ellipse. The boxes and ellipse are specified as $box(5, 5, 50)$, $box(5, 0.5, 50)$, and $ellipse(2, 3.25, 50)$, as shown the Figure A.1, these dimensions correspond to the tunnel dimension.

The three primitives are associated to universal coordinate frame (x,y,z), instead of their local frames (x_i,y_i,z_i), for $i = 1, 2, 3$. Then, the $box(5, 5, 50)$ is translated on the x-axis by a range equal to 2.5, which is expressed as

$$x\_translate(box(5, 5, 50), -2.5)$$

whereas the $box(5, 0.5, 50)$ is translated on the x-axis by a range equal to 2.5, and by a range equal to -0.5 on y-axis, given by

$$y\_translate(x\_translate(box(5, 0.5, 50), -2.5), -0.5)$$

The result of these transformations are shown in Figure A.2.

A Boolean subtraction is done on the $box(5, 5, 50)$ and $ellipse(2, 3.25, 50)$, the Figure

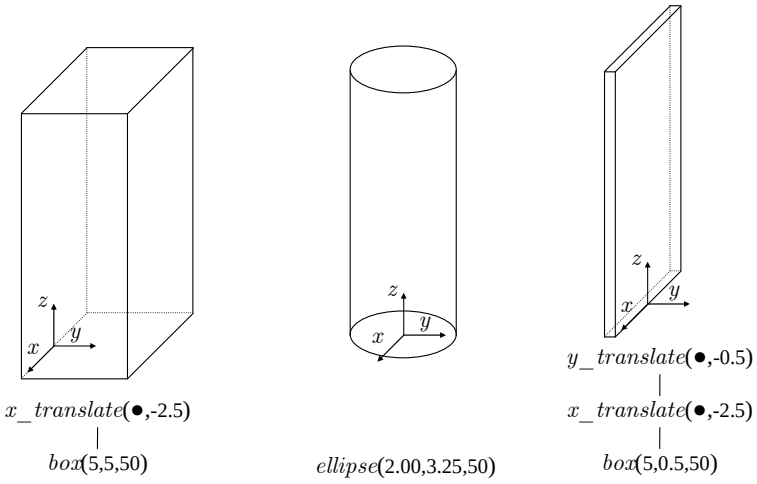

Figure A.2: **Transformations developed to the** $box(5, 5, 50)$**, and** $box(5, 0.5, 50)$**.**

A.3 depicts the result, which has the following expression

$$x\_translate(box(5, 5, 50), -2.5) \quad -^* \quad ellipse(2, 3.25, 50)$$

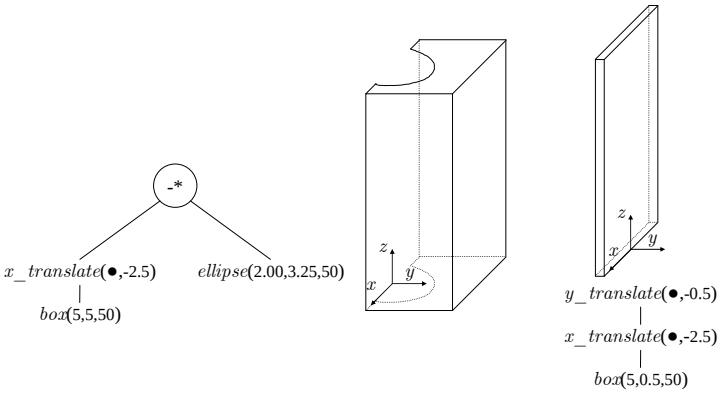

Figure A.3: **Regularized Boolean difference** $-^*$ **between the** $box(5, 5, 50)$ **and the** $ellipse(2, 3.25, 50)$**.**

Finally, the tunnel representation is done by union operation between the latter result and the $box(5, 0.5, 50)$, resulting in the next expression and shown in the Figure A.4.

$$\begin{gathered}(x\_translate(box(5, 5, 50), -2.5) \ -^* \ ellipse(2, 3.25, 50)) \\ \cup^* \\ (y\_translate(x\_translate(box(5, 0.5, 50), -2.5), -0.5))\end{gathered}$$

Due to the real tunnel has no even walls is need to include this characteristic in its

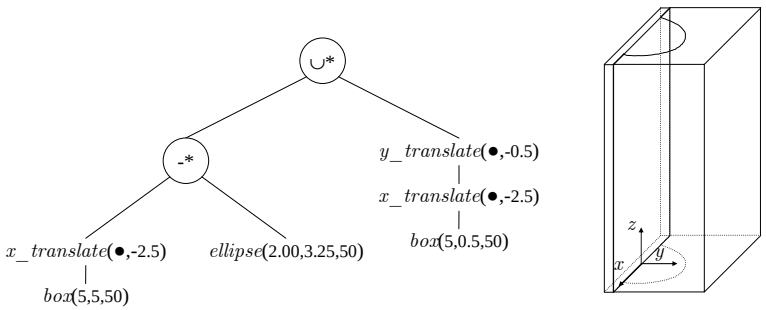

Figure A.4: **Geometric Description of the Tunnel Profiling Task through the CSG model.**

geometric description; therefore, the standard primitives are generated by RSHGC models, introducing an error factor ε to the $U - V$ cross function $C(t)$ to produce the variations on the solid superficies. This error is generated randomly, and added in the function of the cross section 2-D area (cross section), which is swept along a linear path normal to the plane of the area to create the standard primitive, given as:

$$\begin{aligned} A(s) &= sin(2\,\pi\,s) \\ C(t) &= (U_c(t), V_c(t)) \\ C(t) &= (\varepsilon + cos(2\,\pi\,t), \varepsilon + sin(2\,\pi\,t)) \end{aligned}$$

The result is shown in the Figure A.5.

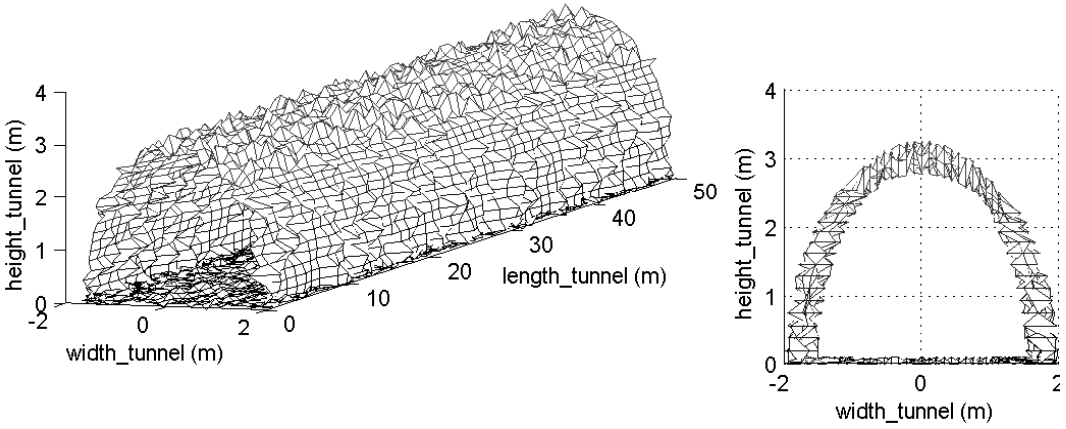

Figure A.5: **Geometric Description of the tunnel with no even walls.**

Appendix B

Kinematic Models

This appendix summarizes the derivation of kinematic models for the schemes: Ackermann Steering (AS), aRticulated Steering (RS), and Explicit independent Steering (ES), which are incorporated in Section 6.1.

Ackermann Steering Model

The AS kinematics is shown in Figure 6.3, this scheme is also known as kingpin steering and mostly used in the automobile industry. In the scheme AS, the vehicle has a front and a rear pair of wheels. The rear wheels are commonly driven and their orientation is fixed, while the front wheels are steered, each wheels rotate different amounts to point at the instantaneous center of curvature (ICC), during a turn the inner front wheel must turn through a larger than outer one, thus, the inner wheel travels a shorter distance that the outer wheel.

The model derivation is on the assumption that the both front and rear wheels collapse into a single wheel located at the midpoint of each axle (bicycle model), where x and y denote the position of the vehicle relative to some fixed coordinate system. The subscripts r and f denote the rear and the front axle, respectively. The angle θ is the orientation of the vehicle with respect to the x axis, whereas V represents the linear velocity of the vehicle. The angle γ denotes the steering angle of the vehicle, and L is the vehicle length, the distance between the front axle and rear one. Furthermore, it is assumed that the vehicle develops a steady-state motion turning where γ is a constant, i.e., $\dot{\gamma} = 0$.

- **AS Model without Slip**

The kinematic model of the vehicle derived from rigid body is given by

$$\dot{x}_r = V\cos(\theta) \tag{B.1}$$
$$\dot{y}_r = V\sin(\theta) \tag{B.2}$$

and using the rigid body constraint that relates the front and rear axles as

$$x_r + L\cos(\theta) = x_f \quad \text{(B.3)}$$
$$y_r + L\sin(\theta) = y_f \quad \text{(B.4)}$$

The AS scheme is subject to the nonholonomic constraint on rolling without slipping, that is

$$\dot{x}_r \sin(\theta) - \dot{y}_r \cos(\theta) = 0 \quad \text{(B.5)}$$
$$\dot{x}_f \sin(\theta + \gamma) - \dot{y}_f \cos(\theta + \gamma) = 0 \quad \text{(B.6)}$$

Differentiating B.3 and B.4 with respect to time

$$\dot{x}_r - L\dot{\theta}\sin(\theta) = \dot{x}_f \quad \text{(B.7)}$$
$$\dot{y}_r + L\dot{\theta}\cos(\theta) = \dot{y}_f \quad \text{(B.8)}$$

Substituting B.1 and B.2 in B.7 and B.8 respectively, to obtain

$$V\cos(\theta) - L\dot{\theta}\sin(\theta) = \dot{x}_f \quad \text{(B.9)}$$
$$V\sin(\theta) + L\dot{\theta}\cos(\theta) = \dot{y}_f \quad \text{(B.10)}$$

Substituting B.9 and B.10 in B.6, where $C_{\theta+\gamma} = \cos(\theta + \gamma)$, $S_{\theta+\gamma} = \sin(\theta + \gamma)$, $C_\theta = \cos(\theta)$, and $S_\theta = \sin(\theta)$, that is

$$(V C_\theta - L\dot{\theta}S_\theta)S_{\theta+\gamma} = (V S_\theta + L\dot{\theta}C_\theta)C_{\theta+\gamma} \quad \text{(B.11)}$$

Simplifying B.11

$$V C_\theta S_{\theta+\gamma} - L\dot{\theta}S_\theta S_{\theta+\gamma} = V S_\theta C_{\theta+\gamma} + L\dot{\theta}C_\theta C_{\theta+\gamma}$$
$$V(S_{\theta+\gamma}C_\theta - C_{\theta+\gamma}S_\theta) - L\dot{\theta}(C_{\theta+\gamma}C_\theta + S_{\theta+\gamma}S_\theta) = 0$$

using the trigonometric identities

$$\sin(a - b) = \sin(a)\cos(b) - \cos(a)\sin(b)$$
$$\cos(a - b) = \cos(a)\cos(b) + \sin(a)\sin(b)$$

then

$$V\sin(\theta + \gamma - \theta) - L\dot{\theta}\cos(\theta + \gamma - \theta) = 0$$

to obtain

$$\dot{\theta} = \frac{V\sin(\gamma)}{L\cos(\gamma)} \quad \text{(B.12)}$$

▪ AS Model with Slip

In practice, the constraint of zero velocity in the direction of the axles (nonholonomic constraint) is a factor that must be considered to estimate the position of the vehicle. Thus, a kinematic model that introduces the slip factor is formulated. The kinematic model of the vehicle derived from rigid body is given by

$$\dot{x}_r = V\cos(\theta + \alpha) \tag{B.13}$$
$$\dot{y}_r = V\sin(\theta + \alpha) \tag{B.14}$$

and using the rigid body constraint that relates the front and rear axles as

$$x_r + L\cos(\theta) = x_f \tag{B.15}$$
$$y_r + L\sin(\theta) = y_f \tag{B.16}$$

The AS scheme is subject to the constraints, where $\theta_1 = \theta + \gamma$, that is

$$\dot{x}_r\sin(\theta + \alpha) - \dot{y}_r\cos(\theta + \alpha) = 0 \tag{B.17}$$
$$\dot{x}_f\sin(\theta_1 + \beta) - \dot{y}_f\cos(\theta_1 + \beta) = 0 \tag{B.18}$$

Differentiating B.15 and B.16 with respect to time

$$\dot{x}_r - L\dot{\theta}\sin(\theta) = \dot{x}_f \tag{B.19}$$
$$\dot{y}_r + L\dot{\theta}\cos(\theta) = \dot{y}_f \tag{B.20}$$

Substituting B.13 and B.14 in B.19 and B.20 respectively, to obtain

$$V\cos(\theta + \alpha) - L\dot{\theta}\sin(\theta) = \dot{x}_f \tag{B.21}$$
$$V\sin(\theta + \alpha) + L\dot{\theta}\cos(\theta) = \dot{y}_f \tag{B.22}$$

Substituting B.21 and B.22 in B.18, where $C_{\theta+\alpha} = \cos(\theta + \alpha)$, $S_{\theta+\alpha} = \sin(\theta + \alpha)$, $C_{\theta_1+\beta} = \cos(\theta_1 + \beta)$, $S_{\theta_1+\beta} = \sin(\theta_1 + \beta)$, $C_\theta = \cos(\theta)$, and $S_\theta = \sin(\theta)$, that is

$$(V\,C_{\theta+\alpha} - L\dot{\theta}S_\theta)S_{\theta_1+\beta} = (V\,S_{\theta+\alpha} + L\dot{\theta}C_\theta)C_{\theta_1+\beta} \tag{B.23}$$

Simplifying B.23 to obtain

$$\dot{\theta} = \frac{V\sin(\beta - \alpha + \gamma)}{L\cos(\gamma + \beta)} \tag{B.24}$$

Articulated Steering Model

Figure 6.4 shows the typical geometry of the RS scheme, the vehicles that use this kind of steering are mostly used into applications with confined environment, such as the Load-Haul-Dump (LHD) trucks in mining applications. An articulated vehicle is composed of two bodies connected by a kingpin hitch, a front and a rear body which can rotate relative to each other. Each body has a single axle with two wheels which are fixed (non-steerable). The steering behavior is achieved by driving the articulation joint (actuator) located midway between the front and rear axles.

The model derivation is on the assumption that the both front and rear wheels collapse into a single wheel located at the midpoint of each axle (bicycle model), where x and y denote the position of the vehicle relative to some fixed coordinate system. The subscripts r and f denote the rear and the front axle, respectively.The angles θ and θ_1 denote the orientation of the vehicle bodies with respect to the x axis of the coordinate system; V represents the linear velocity. The angle γ denotes the steering or articulation angle of the vehicle and presents the relation $\gamma = \theta_1 - \theta$. l_1 denotes the length of the front body of the vehicle and l_2 denotes the length of the rear body, thus the distance between the front axle and rear axle is $L = l_1 + l_2$. Furthermore, it is assumed that the vehicle develops a steady-state motion turning where γ is a constant, i.e., $\dot{\gamma} = 0$.

▪ RS Model without Slip

The kinematic model of the vehicle derived from rigid body is given by

$$\dot{x}_r = V\cos(\theta) \tag{B.25}$$
$$\dot{y}_r = V\sin(\theta) \tag{B.26}$$

and using the rigid body constraint that relates the front and rear axles as

$$x_r + l_2\cos(\theta) + l_1\cos(\theta_1) = x_f \tag{B.27}$$
$$y_r + l_2\sin(\theta) + l_1\sin(\theta_1) = y_f \tag{B.28}$$

The RS vehicle is subject to the nonholonomic constraints, assumption of rolling without slipping, that is

$$\dot{x}_r\sin(\theta) - \dot{y}_r\cos(\theta) = 0 \tag{B.29}$$
$$\dot{x}_f\sin(\theta_1) - \dot{y}_f\cos(\theta_1) = 0 \tag{B.30}$$

Differentiating B.27 and B.28 with respect to time

$$\dot{x}_r - l_2\dot{\theta}\sin(\theta) - l_1\dot{\theta}_1\sin(\theta_1) = \dot{x}_f \tag{B.31}$$
$$\dot{y}_r + l_2\dot{\theta}\cos(\theta) + l_1\dot{\theta}_1\cos(\theta_1) = \dot{y}_f \tag{B.32}$$

Substituting B.25 and B.26 in B.31, and B.32 respectively, to obtain

$$V\cos(\theta) - l_2\dot{\theta}\sin(\theta) - l_1\dot{\theta}_1\sin(\theta_1) = \dot{x}_f \quad \text{(B.33)}$$
$$V\sin(\theta) + l_2\dot{\theta}\cos(\theta) + l_1\dot{\theta}_1\cos(\theta_1) = \dot{y}_f \quad \text{(B.34)}$$

Substituting B.33 and B.34 in B.30, and then simplifying to obtain

$$\dot{\theta} = \frac{V\sin(\gamma) - l_1\dot{\gamma}}{l_1 + l_2\cos(\gamma)} \quad \text{(B.35)}$$

- **RS Model with Slip**

The kinematic model of the vehicle derived from rigid body is given by

$$\dot{x}_r = V\cos(\theta + \alpha) \quad \text{(B.36)}$$
$$\dot{y}_r = V\sin(\theta + \alpha) \quad \text{(B.37)}$$

and using the rigid body constraint that relates the front and rear axles as

$$x_r + l_2\cos(\theta) + l_1\cos(\theta_1) = x_f \quad \text{(B.38)}$$
$$y_r + l_2\sin(\theta) + l_1\sin(\theta_1) = y_f \quad \text{(B.39)}$$

The RS scheme is subject to the constraints, that is

$$\dot{x}_r\sin(\theta + \alpha) - \dot{y}_r\cos(\theta + \alpha) = 0 \quad \text{(B.40)}$$
$$\dot{x}_f\sin(\theta_1 + \beta) - \dot{y}_f\cos(\theta_1 + \beta) = 0 \quad \text{(B.41)}$$

Differentiating B.38 and B.39 with respect to time

$$\dot{x}_r - l_2\dot{\theta}\sin(\theta) - l_1\dot{\theta}_1\sin(\theta_1) = \dot{x}_f \quad \text{(B.42)}$$
$$\dot{y}_r + l_2\dot{\theta}\cos(\theta) + l_1\dot{\theta}_1\cos(\theta_1) = \dot{y}_f \quad \text{(B.43)}$$

Substituting B.36 and B.37 in B.42 and B.43 respectively, to obtain

$$V\cos(\theta + \alpha) - l_2\dot{\theta}\sin(\theta) - l_1\dot{\theta}_1\sin(\theta_1) = \dot{x}_f \quad \text{(B.44)}$$
$$V\sin(\theta + \alpha) + l_2\dot{\theta}\cos(\theta) + l_1\dot{\theta}_1\cos(\theta_1) = \dot{y}_f \quad \text{(B.45)}$$

Substituting B.44 and B.45 in B.41, and then simplifying to obtain

$$\dot{\theta} = \frac{V\sin(\beta - \alpha + \gamma) - l_1\dot{\gamma}\cos(\beta)}{l_1\cos(\beta) + l_2\cos(\gamma + \beta)} \quad \text{(B.46)}$$

Explicit Steering Model

Figure 6.5 shows the typical geometry of the ES kinematics, the vehicle structure is designed so that all four wheels can be driven and steered individually. This kind of vehicle is referred to as a Four-Wheel-Steering vehicle which is used in several research laboratories and for different application with cluster space such as airport terminals. Under the assumption of steady-state turning the ES model becomes a bi-steerable vehicle (double Ackermann Steering) that has a linear relation between its front steering angle and rear steering angle: front steering angle γ is equal to rear steering angle γ in opposite direction. This model can be approximated using a bicycle model.

The model derivation is on the assumption that the both front and rear wheels collapse into a single wheel located at the midpoint of each axle (bicycle model), where x and y denote the position of the vehicle relative to some fixed coordinate system. The subscripts r and f denote the rear and the front axle, respectively. The angle θ denotes the orientation of the vehicle with respect to the x axis of the coordinate system; V represents the linear velocity. The angle γ denotes the steering angle of the vehicle. L denotes the length of the vehicle, the distance between the front axle and rear axle. Furthermore, it is assumed that the vehicle develops a steady-state motion turning where γ is a constant, i.e., $\dot{\gamma} = 0$.

▪ ES Model without Slip

The kinematic model of the vehicle derived from rigid body is given by

$$\dot{x}_r = V\cos(\theta - \gamma) \tag{B.47}$$
$$\dot{y}_r = V\sin(\theta - \gamma) \tag{B.48}$$

and using the rigid body constraint that relates the front and rear axles as

$$x_r + L\cos(\theta) = x_f \tag{B.49}$$
$$y_r + L\sin(\theta) = y_f \tag{B.50}$$

The RS vehicle is subject to the nonholonomic constraints, assumption of rolling without slipping, that is

$$\dot{x}_r\sin(\theta - \gamma) - \dot{y}_r\cos(\theta - \gamma) = 0 \tag{B.51}$$
$$\dot{x}_f\sin(\theta + \gamma) - \dot{y}_f\cos(\theta + \gamma) = 0 \tag{B.52}$$

Differentiating B.49 and B.50 with respect to time

$$\dot{x}_r - L\dot{\theta}\sin(\theta) = \dot{x}_f \tag{B.53}$$
$$\dot{y}_r + L\dot{\theta}\cos(\theta) = \dot{y}_f \tag{B.54}$$

Substituting B.47 and B.48 in B.53, and B.54 respectively, to obtain

$$V\cos(\theta-\gamma)-L\dot{\theta}\sin(\theta) = \dot{x}_f \quad \text{(B.55)}$$
$$V\sin(\theta-\gamma)+L\dot{\theta}\cos(\theta) = \dot{y}_f \quad \text{(B.56)}$$

Substituting B.55 and B.56 in B.52, and then simplifying to obtain

$$\dot{\theta} = \frac{V\sin(2\gamma)}{L\cos(\gamma)} \quad \text{(B.57)}$$

- **ES Model with Slip**

The kinematic model of the vehicle derived from rigid body is given by

$$\dot{x}_r = V\cos(\theta-\gamma+\alpha) \quad \text{(B.58)}$$
$$\dot{y}_r = V\sin(\theta-\gamma+\alpha) \quad \text{(B.59)}$$

and using the rigid body constraint that relates the front and rear axles as

$$x_r+L\cos(\theta) = x_f \quad \text{(B.60)}$$
$$y_r+L\sin(\theta) = y_f \quad \text{(B.61)}$$

The RS scheme is subject to the constraints, that is

$$\dot{x}_r\sin(\theta-\gamma+\alpha)-\dot{y}_r\cos(\theta-\gamma+\alpha) = 0 \quad \text{(B.62)}$$
$$\dot{x}_f\sin(\theta+\gamma+\beta)-\dot{y}_f\cos(\theta+\gamma+\beta) = 0 \quad \text{(B.63)}$$

Differentiating B.60 and B.61 with respect to time

$$\dot{x}_r-L\dot{\theta}\sin(\theta) = \dot{x}_f \quad \text{(B.64)}$$
$$\dot{y}_r+L\dot{\theta}\cos(\theta) = \dot{y}_f \quad \text{(B.65)}$$

Substituting B.58 and B.59 in B.64 and B.65 respectively, to obtain

$$V\cos(\theta-\gamma+\alpha)-L\dot{\theta}\sin(\theta) = \dot{x}_f \quad \text{(B.66)}$$
$$V\sin(\theta-\gamma+\alpha)+L\dot{\theta}\cos(\theta) = \dot{y}_f \quad \text{(B.67)}$$

Substituting B.66 and B.67 in B.63, and then simplifying to obtain

$$\dot{\theta} = \frac{V\sin(\beta-\alpha+2\gamma)}{L\cos(\gamma+\beta)} \quad \text{(B.68)}$$

Appendix C

Extended Kalman Filter

This appendix summarizes the derivation of a discrete Extended Kalman Filter (EKF)to provide an estimate of the vehicle positioning, which is considered in Section 7.2. This EKF quantifies the performance of Ackermann Steering (AS) locomotion configuration under certain sensor uncertainties, where information from various sensors is fused via EKF equations. The EKF consists of two basic steps: prediction and update, as is shown in Figure C.1. Prediction is performed when absolute sensor information is unavailable to predict the next discrete time-step. An update occurs when absolute sensor information is available to estimate and to improve both the position and the orientation, minimizing statistically the uncertainty of the vehicle positioning. Following the notation used in [Gelb 74] and the description in [Durrant-Whyte 96], the prediction and update step are defined from the vehicle model.

Discrete Vehicle Model

The selected AS locomotion uses a steering sensor and a velocity sensor to provide positioning and orientation by means of continuous vehicle model that is expressed as

$$\begin{aligned} \dot{x}(t) &= V(t)\, cos(\theta(t)) \\ \dot{y}(t) &= V(t)\, sin(\theta(t)) \\ \dot{\theta}(t) &= \frac{V(t)\, tan(\gamma(t))}{L} \end{aligned} \tag{C.1}$$

This model is converted into discrete model, assuming that the both control inputs V and γ are approximately constant over a sample interval ΔT. All the derivates are approximated by first-order forward differences, replacing the continuous time t with discrete time index k ($t = \Delta T\, k \stackrel{\triangle}{=} k$). Then the motion model is given by state

variables $[x,\ y,\ \theta]$ at the instant k

$$\begin{aligned} x(k+1) &= x(k) + \Delta T[V(k)\, cos(\theta(k))] \\ y(k+1) &= y(k) + \Delta T[V(k)\, sin(\theta(k))] \\ \theta(k+1) &= \theta(k) + \Delta T\left[\frac{V(k)\, tan(\gamma(k))}{L}\right] \end{aligned} \tag{C.2}$$

The velocity $V(k)$ is equal to rotational wheel speed measured $\omega(k)$ multiplied by the wheel radius $r(k)$ of the rear wheel, according the bicycle model and the approach presented in (Durrant-Whyte, 1996). Hence, the discrete model is rewritten as

$$\begin{aligned} x(k+1) &= x(k) + \Delta T[r(k)w(k)\, cos(\theta(k))] \\ y(k+1) &= y(k) + \Delta T[r(k)w(k)\, sin(\theta(k))] \\ \theta(k+1) &= \theta(k) + \Delta T\left[\frac{r(k)w(k)\, tan(\gamma(k))}{L}\right] \\ r(k+1) &= r(k) \end{aligned} \tag{C.3}$$

The discrete state vector at a time $k+1$ is defined as

$$\mathbf{x}(k+1) = \mathbf{f}\left(\mathbf{x}(k), \mathbf{u}(k)\right)$$

where $\mathbf{x}(k)$ denotes the state vector and $\mathbf{u}(k)$ is the control vector at a time k.

$$\begin{aligned} \mathbf{x}(k) &= [x(k), y(k), \theta(k), r(k)]^T \\ \mathbf{u}(k) &= [\omega(k), \gamma(k)]^T \end{aligned}$$

Prediction Step

The prediction of state is obtained using the previous state and current control state. This estimate state of the state $\mathbf{x}(k)$ is computed as

$$\hat{\mathbf{x}}^+(k) = \left[\hat{x}^+(k), \hat{y}^+(k), \hat{\theta}^+(k), \hat{r}^+(k)\right]^T$$

let

$$\bar{\mathbf{u}}(k) = [\bar{\omega}(k), \bar{\gamma}(k)]^T$$

be the mean measured from velocity sensor and steering sensor of the control vector $\mathbf{u}(k)$, generating a prediction at time-step $(k+1)$ which is defined as

$$\begin{aligned} \hat{\mathbf{x}}^-(k+1) &= \mathbf{f}\left(\hat{\mathbf{x}}^+(k), \bar{\mathbf{u}}(k)\right) \\ \hat{\mathbf{x}}^-(k+1) &= \left[\hat{x}^-(k+1), \hat{y}^-(k+1), \hat{\theta}^-(k+1), \hat{r}^-(k+1)\right]^T \end{aligned}$$

Error Model: Errors are included in the discrete model by two primary sources (steering noise and velocity noise).

- The steering error is modeled as a combination of additive disturbance error $\delta\gamma_a(k)$ and multiplicative error $\delta\gamma_m(k)$:

$$\gamma(k) = \bar{\gamma}(k)\,[1 \,+\, \delta\gamma_a(k)] + \delta\gamma_m(k)$$

  where $\bar{\gamma}(k)$ is mean measured from the steering sensor and $\gamma(k)$ denotes the true mean steering angle.

- The velocity error is modeled as a combination of additive disturbance error $\delta\omega_a(k)$ and multiplicative error $\delta\omega_m(k)$:

$$\omega(k) = \bar{\omega}(k)\,[1 \,+\, \delta\omega_a(k)] + \delta\omega_m(k)$$

  where $\bar{\omega}(k)$ is mean measured from the velocity sensor and $\omega(k)$ denotes the true mean velocity.

- Further, the wheel radius error is integrated as an additive disturbance which is modeled as random walk noise:

$$r(k) = \hat{r}^{+}(k) \,+\, \Delta T\,\delta r(k)$$

These source errors are modeled as constant, zero mean, uncorrelated white sequence, with standard deviation $\sigma_{\gamma a}$, $\sigma_{\gamma m}$, $\sigma_{\omega a}$, $\sigma_{\omega m}$, and σ_r respectively.

Hence, there is an error between the nominal (error-free or ideal) state and estimated state, an error between the nominal state and the prediction state, and a difference between the nominal and the measured control input given respectively by

$$\delta\mathbf{x}^{+}(k) \;=\; \mathbf{x}(k) - \hat{\mathbf{x}}^{+}(k)$$

$$\delta\mathbf{x}^{-}(k+1) \;=\; \mathbf{x}(k+1) - \hat{\mathbf{x}}^{-}(k+1)$$

$$\delta\mathbf{u}(k) \;=\; \mathbf{u}(k) - \bar{\mathbf{u}}(k)$$

Then, the error propagation model is defined as

$$\begin{aligned}
\delta\mathbf{x}^{-}(k+1) &= \mathbf{x}(k+1) - \hat{\mathbf{x}}^{-}(k+1) \\
&= \mathbf{f}\left(\mathbf{x}(k), \mathbf{u}(k)\right) \,-\, \mathbf{f}\left(\hat{\mathbf{x}}^{+}(k), \bar{\mathbf{u}}(k)\right) \\
&= \mathbf{f}\left(\hat{\mathbf{x}}^{+}(k) \,+\, \delta\mathbf{x}^{+}(k), \bar{\mathbf{u}}(k) \,+\, \delta\mathbf{u}(k)\right) \,-\, \mathbf{f}\left(\hat{\mathbf{x}}^{+}(k), \bar{\mathbf{u}}(k)\right)
\end{aligned}$$

The error transfer model can be written in state vector notation denoted as

$$\delta\mathbf{x}^-(k+1) \;=\; \mathbf{F}(k)\delta\mathbf{x}^+(k) \,+\, \mathbf{G}(k)\delta\mathbf{w}(k)$$

where

$$\begin{aligned}
\delta\mathbf{w}(k) &= [\delta\Omega(k), \delta\Gamma(k), \delta r(k)]^T \\
\delta\Omega(k) &= \hat{r}^+(k)\bar{\omega}(k)\delta\omega_a(k) \,+\, \hat{r}^+(k)\delta\omega_m(k) \\
\delta\Gamma(k) &= \hat{r}^+(k)\bar{\omega}(k)\bar{\gamma}(k)\delta\gamma_a(k) \,+\, \hat{r}^+(k)\bar{\omega}(k)\delta\gamma_m(k)
\end{aligned}$$

$\mathbf{F}(k)$ defines the state error transfer matrix that represents the gradient or Jacobian of $\mathbf{f}(\cdot)$ with respect to the states

$$\mathbf{F}(k) = \begin{bmatrix}
1 & 0 & -\Delta T\hat{r}^+(k)\bar{\omega}(k)\sin\hat{\theta}^+(k) & \Delta T\bar{\omega}(k)\cos\hat{\theta}^+(k) \\
0 & 1 & \Delta T\hat{r}^+(k)\bar{\omega}(k)\cos\hat{\theta}^+(k) & \Delta T\bar{\omega}(k)\sin\hat{\theta}^+(k) \\
0 & 0 & 1 & \dfrac{\Delta T\bar{\omega}(k)\tan\bar{\gamma}(k)}{L} \\
0 & 0 & 0 & 1
\end{bmatrix}$$

Likewise the source error transfer matrix $\mathbf{G}(k)$ is the Jacobian of $\mathbf{f}(\cdot)$ with respect to the noise sources

$$\mathbf{G}(k) = \begin{bmatrix}
\cos\hat{\theta}^+(k) & -\sin\hat{\theta}^+(k) & 0 \\
\sin\hat{\theta}^+(k) & \cos\hat{\theta}^+(k) & 0 \\
\dfrac{\tan\bar{\gamma}(k)}{L} & \dfrac{\sec^2\bar{\gamma}(k)}{L} & 0 \\
0 & 0 & 1
\end{bmatrix}$$

on the definition

$$\begin{aligned}
\mathbf{P}^-(k+1) &= \mathrm{E}\left[\delta\mathbf{x}^-(k+1)\delta\mathbf{x}^-(k+1)^T\right] \\
\mathbf{P}^+(k) &= \mathrm{E}\left[\delta\mathbf{x}^+(k)\delta\mathbf{x}^+(k)^T\right] \\
\mathbf{\Sigma}(k) &= \mathrm{E}\left[\delta\mathbf{w}(k)\delta\mathbf{w}(k)^T\right]
\end{aligned}$$

where $\mathbf{\Sigma}(k)$ is the noise strength matrix, on the assumption that the source errors are uncorrelated and

$$\mathrm{E}\left[\delta\mathbf{x}^+(k)\delta\mathbf{w}(k)^T\right] = 0$$

thus $\mathbf{\Sigma}(k)$ is given by

$$\mathbf{\Sigma}(k) = \begin{bmatrix} [\hat{r}^{+}(k)]^2([\bar{\omega}(k)]^2\sigma_{\omega a}^2 \ + \ \sigma_{\omega m}^2) & 0 & 0 \\ 0 & [\hat{r^{+}}(k)\bar{\omega}(k)]^2([\bar{\gamma}(k)]^2\sigma_{\gamma a}^2 \ + \ \sigma_{\gamma m}^2) & 0 \\ 0 & 0 & \sigma_r^2 \end{bmatrix}$$

Then, the prediction covariance is expressed by

$$\mathbf{P}^{-}(k+1) = \mathbf{F}(k)\mathbf{P}^{+}(k)\mathbf{F}(k)^T \ + \ \mathbf{G}(k)\mathbf{\Sigma}(k)\mathbf{G}^T(k)$$

To update the vehicle positioning, the next step in the filter is to combine information from the sensors to estimate the vehicle positioning.

Update Step

Referring to Figure 6.8, each observation from the absolute sensor is converted into the range and the bearing observation referenced to the vehicle coordinate system. This observation is converted into base-coordinates, and then it is matched to the known landmark locations in the path. The matched landmark is transformed back into vehicle coordinate system, which is used to correct the vehicle positioning, using the EKF equations.

Hence the observation $\mathbf{z}_v(k)$, on assumption that the measurements are made by the sensors at a time-step k, in cartesian coordinates referred to vehicle frame are given by

$$\mathbf{z}_v(k) = \begin{bmatrix} z_{vx}(k) \\ z_{vy}(k) \end{bmatrix} = \begin{bmatrix} r_{sensor}(k)\cos\phi(k) - d \\ r_{sensor}(k)\sin\phi(k) \end{bmatrix}$$

The observation variance $\Sigma_z(k)$ is approximated in terms of the observations $\mathbf{z}_v(k)$, assuming that the errors in the absolute sensor are modeled as a gaussian uncorrelated with sequence with constant standard deviation $\sigma_{r_{sensor}}$ and σ_ϕ respectively, to obtain the variance $\Sigma_v(k)$ as

$$\mathbf{\Sigma}_v(k) = \begin{bmatrix} \sigma_{r_{sensor}}^2 & 0 \\ 0 & r_{sensor}^2\sigma_\phi^2 \end{bmatrix}$$

whereas the observation variance $\Sigma_z(k)$ in vehicle coordinates is obtained as

$$\mathbf{\Sigma}_z(k) = \begin{bmatrix} \cos\phi(k) & -\sin\phi(k) \\ \sin\phi(k) & \cos\phi(k) \end{bmatrix} \begin{bmatrix} \sigma_{r_{sensor}}^2 & 0 \\ 0 & r_{sensor}^2\sigma_\phi^2 \end{bmatrix} \begin{bmatrix} \cos\phi(k) & \sin\phi(k) \\ -\sin\phi(k) & \cos\phi(k) \end{bmatrix}$$

This observation is associated with the base coordinates of the landmark location

$\mathbf{b} = [x_b(k), y_b(k)]^T$ that has been made. The vehicle positioning is updated by transforming the matched landmark from base coordinates back through the predicted vehicle positioning $\mathbf{x}^-(k)$ according to

$$\hat{\mathbf{z}}_v(k) = \begin{bmatrix} \hat{z}_{vx}(k) \\ \hat{z}_{vy}(k) \end{bmatrix} = \begin{bmatrix} \cos\hat{\theta}^-(k) & \sin\hat{\theta}^-(k) \\ -\sin\hat{\theta}^-(k) & \cos\hat{\theta}^-(k) \end{bmatrix} \begin{bmatrix} x_b(k) - \hat{x}^-(k) \\ y_b(k) - \hat{y}^-(k) \end{bmatrix}$$

Then the innovation or observation prediction error covariance $\mathbf{S}(k)$ is calculated by

$$\mathbf{S}(k) = \mathbf{H}(k)\mathbf{P}^-(k)\mathbf{H}^T(k) + \mathbf{\Sigma}_z(k)$$

where $\mathbf{H}(k)$ denotes the Jacobian of the matrix with respect to the $\hat{\mathbf{z}}_v(k)$

$$\mathbf{H}(k) = \begin{bmatrix} -\cos\hat{\theta}^-(k) & -\sin\hat{\theta}^-(k) & -[x_b(k) - \hat{x}^-(k)]\sin\hat{\theta}^-(k) & 0 \\ & & +[y_b(k) - \hat{y}^-(k)]\cos\hat{\theta}^-(k) & \\ \sin\hat{\theta}^-(k) & -\cos\hat{\theta}^-(k) & -[x_b(k) - \hat{x}^-(k)]\cos\hat{\theta}^-(k) & 0 \\ & & -[y_b(k) - \hat{y}^-(k)]\sin\hat{\theta}^-(k) & \end{bmatrix}$$

and the Kalman gain is calculated by

$$\mathbf{W}(k) = \mathbf{P}^-(k)\mathbf{H}^T(k)\mathbf{S}^{-1}(k)$$

The vehicle positioning can be computed from

$$\hat{x}^+(k) = \hat{x}^-(k) + \mathbf{W}(k)[\mathbf{z}_v(k) - \hat{\mathbf{z}}_v(k)]$$

and the covariance can be updated from

$$\mathbf{P}^+(k) = \mathbf{P}^-(k) - \mathbf{W}(k)\mathbf{S}(k)\mathbf{W}^T(k)$$

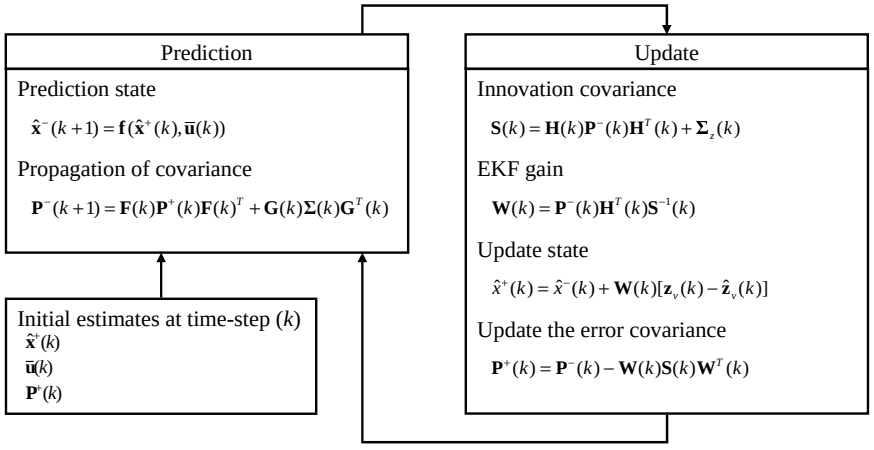

Figure C.1: **Extended Kalman Filter operation: prediction and update steps.**